STUDIES OF ^{152}Gd, ^{152}Sm and ^{182}W NUCLEI USING A DUAL-PARAMETER ENERGY-TIME SPECTROMETER

by

MOHAMMED SHUHADEH SULEIMAN EL-DAGHMAH
B.Sc., M.Sc.

A thesis submitted for the Degree of
Doctor of Philosophy
at the
University of London

Physics Department
Bedford College
London

1982

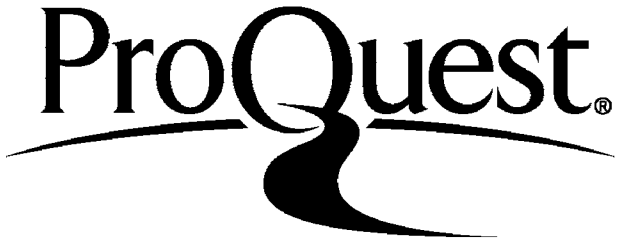

في ذكرى والدي

ولأمي الحنـــون

To The Memory of My Father

And to

My Mother ...

بسم الله الرحمن الرحيم

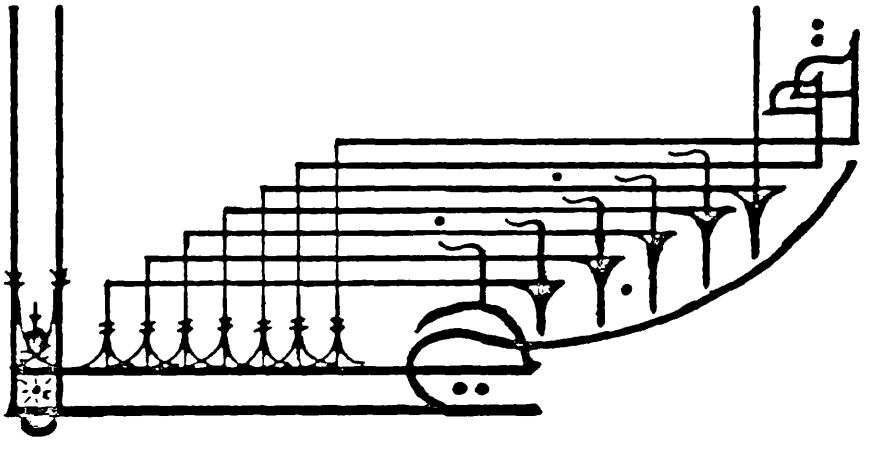

But Say 'O my Lord
Advance me in
Knowledge.'

114 - Ta - Ha
Qur'ān.

ABSTRACT

The decay schemes of three intermediate mass nuclei, ^{152}Gd, ^{152}Sm and ^{182}W were studied using a dual-parameter energy-time spectrometer employing Ge(Li) detectors for γ- γ coincidence measurements.

The applicability of current nuclear models to the properties of these nuclei were investigated. In particular these nuclei were chosen to test the interacting boson model as they spanned the vibrational SU(5) limit (^{152}Gd), through the transitional SU(5) to SU(3) limit (^{152}Sm), to the rotational SU(3) limit (^{182}W).

The half-lives of four nuclear states which lie in the nanosecond range were measured using the technique of delayed coincidence with plastic-Ge(Li) detectors. These values were used to calculate the absolute reduced transition probabilities for transitions depopulating these nuclear states.

New energy levels have been suggested as a result of the observation of new transitions in singles spectra, and their existence confirmed from coincidence data. The energy level schemes were constructed; nuclear properties of the levels deduced and compared with model predictions.

CONTENTS

LIST OF FIGURES

ACKNOWLEDGEMENTS

I wish to acknowledge my indebtedness to Dr. N.M. Stewart for his supervision and constant help with this work. I would like to thank Dr. T.D. Macmahon, the Director, and the staff at the University of London Reactor Centre for their assistance in enabling me to make use of the facilities there. I would also wish to extend my acknowledgement to Professor Dobbs who as head of the Physics Department provided additional funds for this work, and my thanks are similarly due to the staff and members of this Department. My thanks are due to Dr. A. Shaban for his help.

I am grateful to Dr. W. Abdur Rahman and Mr. S. Younis for their encouragement. I wish to acknowledge the assistance from the Research Student Support Scheme given by the British Council.

Additionally I want to thank Ms. S. Khaled for her help, and my thanks are due to Ms. Helen Abbott who patiently typed this work.

CHAPTER 1.

INTRODUCTION

1.1. General:

Gamma-ray spectroscopy is one of the most important means for investigating nuclear structure by building up the decay schemes of nuclei.

Recent advances in gamma-ray spectroscopy have been enhanced by the rapid development of semiconductor detectors. These have replaced the scintillation counters because of their superior energy resolution with respect to these high efficiency scintillation counters. However, by increasing the sensitive volume of the semiconductor detectors, their efficiency can be increased. The principles and the general properties of these solid-state detectors are given in many review articles.[1-4]

As improvements in the semiconductor detectors continue, the high resolution measurements have been greatly aided by the developments in nuclear electronics such as multi-channel pulse-height analysers, time-pick off and timing filter amplifiers.

The conventional fast-slow coincidence systems which have been used to build decay schemes and to study the angular correlation of the gamma-rays, are now being improved by more sophisticated data handling methods such as Dual-paramater data collection systems (DPDC).

A Dual-parameter data collection system was used to record gamma-ray coincidence data from Ge(Li) detectors to enable the decay scheme of the three nuclei ^{152}Gd, ^{152}Sm and ^{182}W to be constructed. At the same time the DPDC system enabled the half-lives of four nuclear states

in ^{152}Sm and ^{182}W to be measured using plastic scintillator and Ge(Li) detectors.

Plastic scintillators provide fast timing signals necessary for the lifetime measurements.

The results will be given and discussed in Chapters 4,5 and 6.

1.2. Radioactivity:

The radioactive materials decay according to the following equation:-

$$A = A_o e^{-\lambda t} \qquad (1.1)$$

where

A is the activity at time t.

A_o is the activity at time t = o

t is the time in seconds

λ is the decay constant of the radioisotope.

The time required for the activity to fall to half of its initial value is called the "half-life" (T). T is given by:-

$$T = -\frac{\log_e 0.5}{\lambda} = \frac{0.693}{\lambda} \qquad (1.2)$$

Then equation (1.1) can be written in the form:

$$A = A_o e^{-0.693\ t/T} \qquad (1.3)$$

The activity of the isotope per gramme is called the specific activity. The maximum specific activity ($S_{max.}$) of the isotope can be derived as follows[5]:-

The one gramme of a pure radioisotope contains

$$\frac{6.02 \times 10^{23}}{W} \quad \text{atoms}$$

where, W is the atomic mass of the isotope, then:

$$S_{max.} = \frac{6.02 \times 10^{23}}{W} \times \lambda \qquad (1.4)$$

Since one curie is 3.7×10^{10} disintegrations/second, then:

$$S_{max.} = \frac{6.02 \times 10^{23}}{3.7 \times 10^{10}} \times \frac{\lambda}{W} \quad \text{curies} \qquad (1.5a)$$

or

$$S_{max.} = \frac{6.02 \times 10^{23}}{3.7 \times 10^{10}} \times \frac{0.693}{W \times T} \quad \text{curies} \qquad (1.5b)$$

1.3. Neutron activation:

Radioactive isotopes can be produced by neutron bombardment. The nuclear reactors can be used as a source of neutrons, where the radioactive isotope is produced by neutron irradiation.

When neutrons interact with target nuclei, radioactive nuclei can be produced by several different nuclear processes.

The notation used to denote these reactions is:

A(n,x)B

where

A is the initial nucleus.

n is the number of captured neutrons.

x could be a photon or particles emitted.

B is the final (produced) nucleus.

If x is a photon, then we call the reaction an (n,γ) reaction, this was used to produce the radioisotopes used in this work.

When nuclei are irradiated in the reactors, a number of processes go on concurrently.[5] Neutrons are captured by nuclei of the target element, they give rise - directly or through an intermediate beta decay - to the desired radioisotope. The nuclei of the product radioisotope may be destroyed by the capture of additional neutrons, and in the same time they undergo radioactive decay. The number of target nuclei present will be reduced by the primary neutron catpure process. The rate of the build-up of the required radioisotope is the result of all these factors.

If no intermediate beta decay is involved, or if the half-life of such decay is short, the activity of the product radioisotope is given by the equation:-

$$A = \frac{N_o \ \sigma_1 \ \phi \ \lambda_1}{\lambda_1 + \sigma_2 \phi - \sigma_1 \phi} \ (e^{-\sigma_1 \phi t} - e^{-(\lambda_1 + \sigma_2 \phi) t}) \qquad (1.6)$$

where

A is the activity in transformations/second.

N_o is the number of target nuclei originally present.

σ_1 is the cross-section of the target nuclei,
σ_2 is the cross-section of the product nuclei } for neutron capture.

λ_1 is the decay constant of the product radiosotope.

ϕ is the neutron flux in the reactor. ($n \ cm^{-2} \ s^{-1}$)

t is the time of irradiation. (s)

For a short irradiation time and low fluxes, the burn up of the target nuclei can be neglected, and frequently the neutron absorption cross-section of the product isotope is negligible. Then equation (1.6) can be written as:-

$$S = \frac{0.6 \ \sigma \ \phi \ (1 - e^{-0.693 \times t/T})}{3.7 \times 10^{10} \ W} \qquad (1.7)$$

where:

S is the specific activity of the product radioisotope in curies per gramme of the target material.

σ is the activation cross-section of the target material in barns.

W is the atomic weight of the target material.

t is the irradiation time.

T is the half-life of the product radioisotope.

The above equation was used to calculate the activities of the sources used in this work. (See Chapter 3).

The specific activity reaches its saturation value $S_{max.}$ at large values of irradiation time (t), thus:-

$$S_{max.} = \frac{0.6\ \sigma\ \phi}{3.7 \times 10^{10}\ W} \qquad Ci\ g^{-1} \qquad (1.8)$$

It was noticed that the activity reaches half of its saturation value in an irradiation time equal to one half-life. Furthermore, the saturation activity is directly proportional to the neutron flux, hence if a high specific activity is required, the irradiation should be carried out in the highest possible flux.

1.4. Electromagnetic Radiation:-

Electromagnetic radiation is emitted from the nuclei as a result of changes in the current and charge of distribution.

The quantum theory of the gamma-radiations are given in several texts (e.g. Blatt and Weisskopf[6]). It is convenient to classify electromagnetic radiation by multiple orders L, according to the angular momentum L (in units of $\hbar$) carried off by each quanta.

Suppose that we have an initial nuclear state with spin J_i, its component in Z direction m_i and with parity π_i. If it decays to a lower state with J_f, m_f and π_f by emitting a gamma-radiation carrying angular momentum (eigen-value L), its component μ and parity π, then according to the conservation laws, we have[7]:-

$$J_i = J_f + L \tag{1.9}$$

$$\pi_f = \pi_i \times \pi \tag{1.10}$$

These will impose the selection rules:-

$$| J_i - J_f | \leq L \leq | J_i + J_f | \tag{1.11}$$

$$,\pi_i \times \pi_f = (-)^L \text{ For electric multipole transition (EL)} \tag{1.12}$$

$$,\pi_i \times \pi_f = (-)^{L+1} \text{ For magnetic multipole transition (ML)} \tag{1.13}$$

The electromagnetic radiation is proportional to $(R/\lambda)^2$, where R is the nuclear radius and λ is the wave length of the emitted radiation.

For most known γ-radiation $R \leq \lambda$, this is related to the fact that, the transition probability decrease rapidly with increasing the multipole order.

These multipole orders are limited to the lowest one or two orders.

The relative probability of emitting a magnetic multipole radiation is smaller than that of the electric multipole radiation of the same order. Mixing transitions could occur, where both electric and magnetic types are presented. The mixing ratio (δ^2) for these mixed (non-pure) transitions is given by:-

δ^2 = intensity of (L + 1) component/intensity of L component.

If J_i or $J_f = 0$, then only electric or magnetic multipole is allowed (i.e. we have pure transition).

If $J_i = 0$ and $J_f = 0$, then no radiation can occur by a single photon emission.

The transition probability for the gamma-ray is given by[7]:-

$$T(L,J_i \rightarrow J_f) = \frac{8\pi(L+1)}{L\,[(2L+1)!!]^2} \quad \frac{1}{\hbar} \quad \left(\frac{w}{c}\right)^{2L+1} \quad B(L,J_i \rightarrow J_f) \qquad (1.14)$$

where

w is the transition frequency.

B is the reduced transition probability, given by:-

$$B(EL) = 4.57 \times 10^{-20} \times \frac{L[(2L+1)!!]^2}{8\pi(L+1)} \times \left(\frac{197}{E\ (\text{in MeV})}\right)^{2L+1} \times$$

$$\left[T(EL) \text{ in sec.}^{-1}\right] \text{ in } e^2 fm^{2L} \qquad (1.15)$$

and

$$B(ML) = 4.15 \times 10^{-20} \times \frac{L\,[(2L+1)!!]^2}{8\pi(L+1)} \times \left(\frac{197}{E\ (\text{in MeV})}\right)^{2L+1} \times$$

$$\left[T(ML) \text{ in sec.}^{-1}\right] \text{ in } \mu_N^2 \; f_m^{2L-2} \qquad (1.16)$$

where

1 fm = 10^{-13} cm.

μ_N is the nuclear magneton ($e\hbar/2M_nC = 5.05 \times 10^{-24}$ erg. gauss^{-1}).

A useful relationship between T and B is given by[7]:-

$$\begin{aligned} T(E1) &= 1.59 \times 10^{15} \quad E^3 \quad B(E1) \\ T(E2) &= 1.22 \times 10^{9} \quad E^5 \quad B(E2) \\ T(M1) &= 1.76 \times 10^{13} \quad E^3 \quad B(M1) \\ T(E3) &= 5.67 \times 10^{2} \quad E^7 \quad B(E3) \\ T(M2) &= 1.35 \times 10^{8} \quad E^5 \quad B(M2) \end{aligned} \qquad (1.17)$$

These relations will be used in relative branching ratios for the

transition probabilities as given in Chapters 4,5 and 6.

The experimental absolute transition probability (T^{γ}) is given as follows[8]:-

Suppose that we have the transitions a,b,c and d depopulating a nuclear state whose half-life is measured experimentally, then T^{γ} is given by:-

$$T^{\gamma}(a) = T(\text{Expt.}) \left[1 + \alpha_{\text{Tot.}}(a) \right] \sum_{x=a}^{d} I_{\text{Tot.}}(x) / I_{\text{Tot.}}(a) \qquad (1.18)$$

where

T(expt.) is the half-life of the nuclear state in seconds.

$$, I_{\text{Tot.}}(x) = I(x) \left[1 + \alpha_{\text{Tot.}}(x) \right] \qquad (1.19)$$

where

I (x) is the relative intensity of the gamma-ray (x) determined experimentally.

$\alpha_{\text{Tot.}}$ is the total internal conversion coefficient determined experimentally, and given by:

$$\alpha_{\text{Tot.}} = \alpha_K(x) + \alpha_L(x) + \alpha_M(x) + \ldots \qquad (1.20)$$

$, \alpha_K, \alpha_L, \alpha_M, \ldots$ are the partial coefficients for K.L,M.....electrons (see next section).

Then the reduced transition probability B (σL) is given by:-

$$B(\sigma L) = C(\sigma L) / E^{2L+1} \; T^{\gamma}(\sigma L) \qquad (1.21)$$

where

σ stands for the type of the transition, i.e., electric (E) or magnetic (M).

$C(\sigma L)$ is a constant given in Table 1.1. for L = 1,2,3,4 and 5.

E is the energy of the gamma transition in (keV).

The units of $B(\sigma L)$ are e^2b^L for the electric transition or $\mu_N^2 b^{L-1}$ for the magnetic transition. ($1b = 10^{-24}$ Cm^2, μ_N is the nuclear magneton).

TABLE 1.1.

Values for the Constant $C(\sigma L)$

(Numbers on the right are the powers of 10 by which we multiply numbers on the left)

Multipolarity (σL)	$C(\sigma L)$	
E1	4.40	- 9
E2	5.63	+ 1
E3	1.21	+ 12
E4	4.06	+ 22
E5	1.97	+ 33
M1	3.96	- 5
M2	5.12	+ 5
M3	1.09	+ 16
M4	3.65	+ 26
M5	1.77	+ 37

1.5. Internal Conversion:

The internal conversion coefficients (α) provide important means for determining γ-ray transition multipolarities.

The internal conversions were discovered in 1924[9] and observed as a line spectrum in magnetic spectrometers.

Whenever a nucleus is in an excited state, with excitation energy insufficient for nuclear particle emission, the nucleus de-excites either by emitting gamma-radiation, or by losing this energy directly by internal conversion to an orbiting electron, which results in the ejection of the electron from its orbit.

The internal conversion coefficient (α) is the ratio of the electron emission rate (N_e) to the gamma emission rate (N_γ), i.e.,

$$\alpha = N_e/N_\gamma \quad ; \tag{1.22}$$

partial internal-conversion coefficients are used in connection with electron emission from specific shells, e.g.:

$\alpha_K = N_{e_K}/N_\gamma$ is the coefficient for ejection of the electron from the K-shell, α_{L_1} is the coefficient for ejection of the electron from L_1 shell.

The sum of the partial coefficients is α_{Total} where:

$$\alpha_{Tot.} = \alpha_K + \alpha_{L_1} + \alpha_{L_2} + \ldots\ldots \tag{1.22a}$$

The theoretical calculations[10] were based on the coupling of the nucleus with the electromagnetic field, but many modifications have been made by Rose et al.[11,12], Sliv and Band[13] and Green and Rose[14] to obtain better results.

Also, the assumption of "penetration" of the shell electrons into the nucleus[15], has helped in providing more accurate and complete tables of the internal conversion coefficients as computed by Hager and Seltzer[16,17], and by Pauli and Alder[18]. For further details, see texts[19,20]. The tables reported in Ref. 21 were used in this work to determine the transitions multipolarities as given in Chapters 4,5 and 6.

CHAPTER 2.

THEORY

2.1. Nuclear Shell Model.

It was known that the nuclear separation energies showed discontinuities of the same type as those observed in the atomic ionization potentials.[22] The evidence of the shell structure became overwhelming after sufficient accumulating of experimental facts.[23,24] The discontinuities in the nuclear binding energies occur at nucleon numbers 2,8,20,28,50,82 and 126, known as "magic numbers". These numbers are similar to the atomic numbers (Z = 2,10,18,36,54 and 86) of the noble gases. In atomic physics, these numbers correspond to the closing shells.

The shell model was able to interpret the magic numbers by the suggestion of the spin-orbit coupling as given in Ref. 25.

By introducing a connection between the representation of the nucleus as a group of particles in a spherical symmetric potential well plus residual interactions, and representing it as a non-interacting particles in a potential well having quadrupole deformation, one can correlate the single particle motion of the shell model and the collective motion, as was done by Nillson[26] and Elliott[27].

The nuclear shell model has different versions: the independent particle model, the shell model, the single particle model and the extreme single particle model.

In the independent particle model, the nucleons are considered to move freely in a single particle potential which depends on the nucleon's spatial, spin and charge coordinates, i.e., we have a system of independent

noninteracting fermions with appropriate density.[28]

In the nuclear shell model, we start from the above point, but we consider the fact that the motion of a nucleon is not entirely independent of the motion of the other particles.[28]

In the single particle model, the nucleus is considered as a core of completely filled closed shells containing the maximum allowed number of nucleons and unfilled shells containing the remaining number of nucleons.

The single particle model estimates the half-lives for the gamma-ray emission as given in the work of Wapstra et. al.[29]

In the extreme single-particle model, the excitation is mainly due to the single unpaired nucleon.

The reduced transition probability $B(\sigma L)$ for the gamma-rays was estimated, using this model by Weisskopf[30] and the relations are:-

$$B(EL) = \frac{(1.2)^{2L}}{4\pi} \left(\frac{3}{L+3}\right)^2 A^{2L/3} \text{ in } e^2 fm^{2L} \qquad (2.1)$$

$$B(ML) = \frac{10}{\pi} \left(\frac{3}{L+3}\right)^2 (1.2)^{2L-2} A^{(2L-2)/3} \text{ in } \mu_N^2 (fm)^{2L-2} \qquad (2.2)$$

where

L is the angular momentum carried off by the photon.

A is the atomic number of the nucleus.

μ_N is the nuclear magneton.

These expressions are independent of the energy of the transition and they are crude estimates giving an order of magnitude.[7]

However, there is significant interaction with the independent particle motion, this interaction arises due to the nuclear pairing effect.

For heavy nuclei ($A \gtrsim 100$), these interaction energies are measured by the odd-even mass difference (Δ), which is of the order of one MeV.

This pair-correlated system can be described in terms of generalized one-particle excitation referred to as quasiparticle. The low-lying states of odd-A nuclei could have single-quasiparticle states[31], while for even-even nuclei, we have two-quasiparticle states.

2.2. Collective vibrations:

For many-body system, it is possible to describe the excitation spectra in terms of elementary modes of excitation representing the different, approximately independent, fluctuations about equilibrium[31,32].

The correlation between the collective vibrations and the shell model could be established if we considered that the collective vibrations may occur as a result of interactions between the particles giving rise to correlations in the particles motion and associated oscillation in the average density and field, i.e., relating the collective motion to the degrees of freedom of the individual particles. The spherical nuclei are supposed to undergo vibrations about the equilibrium shape.

The variation of the density associated with a vibrational mode can be characterized by an amplitude α which represents the displacement from equilibrium.

For small values of α, the vibrational energy can be expressed in powers of α and its time derivative $\dot{\alpha}$, then the vibrational energy $E(\alpha,\dot{\alpha})$ is given by[31]:-

$$E(\alpha,\dot{\alpha}) = \frac{1}{2} C \alpha^2 + \frac{1}{2} D \dot{\alpha}^2 \qquad (2.3)$$

where

C is the restoring force paramater.

D is the mass parameter.

This equation represents a harmonic oscillator, where the first term represents the potential energy of deformation and the second term represents the kinetic energy.

The energy spectra for the familiar harmonic oscillator can be written in the form:-

$$E(n) = n\, E_1 \qquad (2.4)$$

where

n is the degree of the phonon excitation

E_1 is the energy of the first excited state.

The first excited state ($J^{\pi} = 2^+$) is called one-phonon excitation, the second excited state ($J^{\pi} = 4^+$) is the two-phonon excitation, ...etc. The second excited state (4^+) would have three degenerates with spins 0,2 and 4, while the third excited state (6^+) would have degenerates with spins 0,2,3,4 and 6 (Ref. 22).

Thus, the energy spectrum takes the sequence

$E_1, 2E_1, 3E_1, \ldots$.

Nuclei with $N \leq 88$ follow this rule for the low-lying states (e.g. ^{152}Gd, see Chapter 4).

The above rule may not hold for higher spins. As the angular momentum takes higher values, the equilibrium shape of the nucleus becomes nonspherical as a result of the centrifugal forces.[31]

The spectrum may take a form of a rotational spectrum in addition to the vibrational spectra, in this case the rotational degrees of freedom appear as special superpositions of the vibrational modes.

(We will discuss this point in views of the experimental data on ^{152}Gd in Chapter 4).

In the intrinsic coordinate system, the deformation amplitudes are denoted by $a_{\lambda\nu}$(λ is the multipole order, $\nu = 0$ or ± 2) and the quadrupole deformations are expressed in terms of the deformation parameters β and γ [31], where $\alpha = \sum_{\lambda\nu} |a_{\lambda\nu}|^2$.

The spheroidal equilibrium shape has $\gamma = 0$ (prolate)or $\gamma = \pi$ (oblate); we have for $\lambda = 2$,

$$a_{20} = \beta \cos\gamma \qquad (2.4.a.)$$

$$a_{22} = \frac{1}{\sqrt{2}} \beta \sin\gamma = a_{2-2} \qquad (2.4.b.)$$

When $\nu = 0$, we have axial symmetry, i.e., we have β vibrations.
When $\nu = \pm 2$ (γ- vibration), the axial symmetry is broken and we have nuclear shape of ellipsoidal type.

2.3. Collective Rotation:

The deformed nuclei show rotational spectra. It was known that nuclei having $155 < A < 185$ and $A > 225$ are deformed nuclei, therefore having rotational like spectra.[31,32]

In the deformed nuclei, there are two different modes of excitations, rotational excitations and intrinsic excitations. The rotational excitations are associated with a collective motion of the nucleons, which affects only the orientation of the nucleus in space, while preserving the internal structure of it.

The second type of excitation - the intrinsic excitation - is associated with the excitation of the individual particles or with the

collective vibrations of the nuclear shape.[33]

The rotational spectrum depends on the nuclear equilibrium shape and it is simple for the axially symmetric nuclei, then the rotational motion can be characterized by the quantum numbers J, M and K, where J is the angular momentum, M its component in the Z direction and K is its component along the nuclear symmetry axis.

The spectrum is given by the simple formula:-

$$E(J) = AJ(J+1) \qquad (2.5)$$

where

A is constant proportional to the moment of inertia (I),

$(A \propto \frac{1}{I})$.

In the axially symmetric deformation, there is no vibration-rotation interaction. However, if the deformation is decreased and rotational frequency is increased, then the intrinsic nuclear structure is excited by the rotational motion and the quantum number K is no longer constant of motion, i.e., we have some sort of vibration - rotation interaction.[34]

The simple formula (2.5) should be modified by introducing another term proportional to $J^2(J+1)^2$.

Then, formula (2.5) takes the form:-

$$E(J) = E_o + AJ(J+1) + BJ^2(J+1)^2 \qquad (2.6)$$

where

E_o is the energy scale constant.

A and B are normalizing parameters which can be determined by fitting the experimental values of the first and the second excited states of the ground state band. Here, B is small, but plays an important role as the spin increases.

Equation (2.5) implies the following ratios between the energies of the excited states of the ground band:-

$$E(4^+)/E(2^+) = 10/3$$

$$E(6^+)/E(2^+) = 7$$

In Bohr-Mottelson collective model[31,32] the reduced transition probability B(E2) for K = 0 bands is given by:

$$B(E2, J \rightarrow J-2) = \frac{15}{32\pi} \frac{J(J-1)}{(2J-1)(2J+1)} Q_o^2 e^2 b^2 \qquad (2.7)$$

where

Q_o is the intrinsic quadrupole momemt, given by:

$$Q(J) = - \frac{J}{(2J+3)} Q_o \quad e\,b \qquad (2.8)$$

where

Q(J) is the quadrupole moment.

In general, if the transition operator $\mu(\sigma L)$ is given for the transition, then $B(\sigma L)$ is given by[7,32]:

$$B(\sigma L, J_i \rightarrow J_f) = \frac{1}{2J_i+1} | \langle f || \mu(\sigma L) || i \rangle |^2 \qquad (2.9)$$

where

$\langle f || \mu(\sigma L) || i \rangle$ is the reduced matrix element.

If the nuclear state is excited by Coulomb excitation, then we have reduced upward transition propability $B(\sigma L, J_f \rightarrow J_i)$ which is given by:

$$B(\sigma L, J_f \rightarrow J_i) = \frac{2J_i+1}{2J_f+1} B(\sigma L, J_i \rightarrow J_f) \qquad (2.10)$$

The coupling between the rotational and the intrinsic motion resulting from Coriolis and centrifugal forces.

These effects manifest themselves in band mixing between the different rotational bands.[31]

(Some of these effects will be discussed in the case of ^{152}Sm nucleus in Chapter 5).

2.4. The interacting boson model (IBM):

The interacting boson model has been introduced recently as an alternative algebraic model[35,36] to the geometric model of Bohr and Mottelson[31,37,38], to describe the properties of medium-mass and heavy nuclei. The spectra of these nuclei were assumed to arise from a collective quadrupole motion of the nucleons.

The collective quadrupole states in nuclei were described in terms of the concept of shape and of its deformation as described by Bohr and Mottelson.[38] This description was used for nuclei with a stable deformation of axial symmetry. Afterwards, this has been extended to other situations either in a purely phenomenological fashion[39] or in a more microscopic way.[40]

In the IBM the collective nuclear motion is described in terms of a system of interacting bosons. The neutrons and the protons are taken in pairs, the paired protons are called proton bosons (N_π) and the paired neutrons are called neutron bosons (N_ν). Each pair could be coupled either to angular momentum $L = 0$ (called s-boson) or to $L = 2$ (called d-boson).[41,42,43,44] The total number of the interacting bosons (N) is equal to $N_\pi + N_\nu$.

Other modes of excitations are expected to occur, of particular importance is the collective octupole modes.

Therefore, we consider a system of two different kinds of interacting bosons which could be coupled to angular momentum L = 0(s - boson) or to L = 3 (f - boson).

When no distinction between the proton and the neutron pairs is made, then the IBM is referred to as IBM-1. If proton and neutron bosons are explicitly introduced then the model is IBM-2.

The calculations performed for the IBM in the following chapters are based on IBM-1 and shortly referred to as IBM.

2.4.1. Interacting boson model (IBM-1):

In this model, the even-even nucleus is treated as a system of interacting proton (N_π) and neutron (N_ν) bosons outside the closed shell. The total number of bosons N equals $N_\pi + N_\nu$.

These bosons can occupy two levels, a ground state level with angular momentum L = 0 (s-bosons) and an excited level with angular momentum L = 2 (d-bosons).[42]

For these bosons, the only allowed representations are the totally symmetric ones, belonging to the partition [N] of SU(6) group. In the absence of interaction and for zero splitting, all states belonging to [N] are degenerate.

The energy difference ($\epsilon = \epsilon_d - \epsilon_s$) and the boson-boson interaction lift the degeneracy and give rise to a definite spectrum. For quadrupole states, the general model Hamiltonian is written as[42]:-

$$H = \epsilon_s s^\dagger s + \epsilon_d \sum_m d_m^\dagger d_m + \sum_{L=0,2,4} \frac{1}{2}\sqrt{2L+1}\; C_L \times \left[(d^\dagger d^\dagger)^{(L)} \quad (dd)^{(L)}\right]^{(0)} + \text{other terms} . \qquad (2.11)$$

where

ϵ_s and ϵ_d are the energies of the s and d bosons.

, m = L, L-1,....,-1

, (L),(O) are the generators of the SU(6) group.

$d^\dagger$(d), $s^\dagger$(s) are the creation (annihilation) operators of the d and the s bosons, the parantheses denote angular momentum coupling.

The first two terms in equation (2.11) denote the single boson energies. The other terms denote the two-body interaction.

Thus the above Hamiltonian can be written in simpler form which contains only one-body and two-body terms:-

$$H = \sum_{i=1}^{N} \epsilon_i + \sum_{i,j}^{N} V_{ij} \qquad (2.12)$$

It is possible to find an analytical solution to the eigenvalue problem for the Hamiltonian (equation 2.11). Analytical solutions correspond to dynamical symmetries of the Hamiltonian H, where it is possible to write this Hamiltonian in terms of invariant operators (Casimir operators) of a complete chain of subgroups of SU(6)[45,46,47].

This means that for different choices of the parameters ϵ, C_L,... the Hamiltonian can produce both vibrational and rotational spectra. When the energy ϵ is much larger than the interaction terms C_L, then we have the vibrational limit of the model (SU(5)).

The other limit arises when ϵ is small and of the same order of magnitude as the two-body matrix element C_L. In particular if both energies ϵ_s, ϵ_d and the two-body matrix elements correspond to those of quadrupole-quadrupole interaction, then we have the rotational limit (SU(3)).

The transitional limit from SU(5) to SU(3) arises for nuclei with

spectra intermediate between these two limits. These limits will be discussed in detail as follows:-

- The vibrational limit SU(5)[42]:

States in this limit are characterized by the number of bosons occupying the L = 2 states (d-bosons). The Hamiltonian (equation 2.11) reduced to:-

$$H = \epsilon \sum_m d_m^\dagger d_m + \sum_L \frac{1}{2} \sqrt{2L+1} \; C_L \; [(d^\dagger d^\dagger)^{(L)} (dd)^{(L)}]^{(o)} \qquad (2.13)$$

where

The second term denotes the boson-boson interaction.

The interacting d-boson Hamiltonian (equation 2.13) can be diagonalized and the eigenvalues are given by[42,48,49]:-

$$E(n_d, v, n_\Delta, L, m) = \epsilon n_d + \frac{1}{2}\alpha n_d(n_d-1) + \beta (n_d-v)(N_d+v+3) + \gamma[L(L+1) - 6n_d] \qquad (2.14)$$

where,

ϵ, α, β and γ are parameters determined by fitting experiment to theory.

α, β and γ are related to C_o, C_2 and C_4, by considering states with $n_d = 2$, one has:-

$$\left.\begin{aligned} C_o &= \alpha + 10\beta - 12\gamma \\ C_2 &= \alpha - 6\gamma \\ C_4 &= \alpha + 8\gamma \end{aligned}\right\} \qquad (2.15)$$

In general, n_d could have any value from 0 up to N (total number of interacting bosons).

v is the boson seniority, this quantum number is related to n_d by the formula:

$$v = n_d - 2n_\beta \qquad (2.16$$

where

n_β is the quantum number that counts the number of boson pairs coupled to zero angular momentum.

n_Δ is another quantum number that accounts for the boson triplets coupled to zero angular momentum.

L,m are the angular momentum and its projection in the z axis.

The spectra of equation (2.14) are arranged into "bands" defined as follows:-[42]

$$\begin{aligned}
&\text{Y-band} && |n_d, n_d, o, L = 2\,n_d, m\rangle \\
&\text{X-band} && |n_d, n_d, o, L = 2\,n_d-2, m\rangle \\
&\text{Z-band} && |n_d, n_d, o, L = 2\,n_d-3, m\rangle \\
&\beta\text{-band} && |n_d, n_d-2, o, L = 2n_d-4, m\rangle
\end{aligned} \tag{2.17}$$

The reduced transition probability B(E2) can be deduced from the reduced matrix element (F) given by:[42]

1. For transitions within the Y-band:

$$F = \sqrt{(n_d+1)(4n_d+5)} \quad \text{for } (L' = 2\,n_d + 2 \rightarrow L = 2\,n_d) \tag{2.18}$$

2. For interband transitions:

$$\begin{aligned}
&Z \rightarrow Y,\ (L' = 2n_d - 1 \rightarrow L = 2n_d),\ F = \sqrt{\frac{(2n_d-2)(4n_d+1)}{(2n_d-1)}} \\
&Z \rightarrow X,\ (L' = 2n_d - 1 \rightarrow L = 2n_d-2),\ F = \sqrt{\frac{3(2n_d+1)}{n_d-1}}
\end{aligned} \tag{2.19}$$

Then

$$B(E2, J_i \rightarrow J_f) = \frac{1}{2J_i+1} F^2 \tag{2.20}$$

It was noticed that nuclei away from closed shells and regions of large deformations are characterized by vibrational spectra but with large splitting between members of the two-phonon triplets 0^+, 2^+ and 4^+ and relatively large quadrupole moments of the first excited state 2^+.

In this limit, the ground band should have states with the energy ratio $E(4^+)/E(2^+) \simeq 2$.

- The rotational limit (SU(3))[44]:

In this limit ϵ is small and the boson-boson interaction term of the form $V_{ij} = -k\, Q_i.Q_j$ is important, then the Hamiltonian (equation 2.11) becomes:

$$H = -k \sum_{i,j}^{N} Q_i.Q_j = -k\sum_i Q_i^2 - 2k \sum_{i,j} Q_i.Q_j \qquad (2.21)$$

where

Q_i is the quadrupole operator of the ith boson.

k is the strength of the interation.

The transition operator can be written in this limit as:

$$T^{(E2)} = \alpha_2 \sum_i Q_i \qquad (2.22)$$

where

α_2 is an effective E2 charge.

The Hamiltonian (equation 2.21) can be diagonalized with eigenvalues given by:-[44]

$$E([N](\lambda,\mu)\ KLm) = k\left[\frac{3}{4}L(L+1) - C(\lambda,\mu)\right] \qquad (2.23)$$

where

$C(\lambda,\mu)$ is the quadratic Casimir operator of the SU(3) subgroup, given by:-[47]

$$C(\lambda,\mu) = \lambda^2 + \mu^2 + \lambda\mu + 3(\lambda+\mu) \qquad (2.24)$$

where

[N] labels the totally symmetric irreducible representations of SU(6) group.

(λ,μ) labels the representation of SU(3) subroup.

$$, L = \lambda, \lambda+1, \lambda+2, \ldots, 2\lambda-2, 2\lambda \qquad (2.25)$$

Equation (2.21) may be written in more general form, namely:

$$H = -k \sum_{i,j} Q_i . Q_j - k' \sum_{i,j} L_i . L_j \qquad (2.26)$$

where

L_i is the angular momentum of the ith boson.

k' is the strength of the L.L. interaction.

The eigenvalue of equation (2.26) is:-

$$E([N](\lambda,\mu)\ KLm) = \alpha\, L(L+1) - \beta\, C(\lambda,\mu) \qquad (2.27)$$

where

$\alpha = \frac{3}{4} k - k'$ and $\beta = k$

The energy difference between (2N,O) representation and next to the lowest (2N-4,2) representation is $(12N-6)\beta$.

Using equation (2.22), the reduced transition probability between members of the ground state band can be calculated, and is given by[44]:-

$$B(E2,\ L+2 \longrightarrow L) = \frac{3}{4} \alpha_2 \frac{(L+2)(L+1)}{(2L+3)(2L+5)} (2N-L)(2N+L+3)\ e^2 b^2 \qquad (2.28)$$

The quadrupole moment (Q) is given by:

$$Q(L) = -\alpha_2 \left(\frac{16\pi}{40}\right)^{\frac{1}{2}} \frac{L}{2L+3} (4N+3)\ e\ b \qquad (2.29)$$

Here, α_2 can be determined by fitting experiment to theory.

Nuclei performing rotational spectra (SU(3) Limit) should have ground band with states having energies proportional to L(L+1) (i.e. small β). This implies the ratios:-

$E(4^+)/E(2^+) = 10/3$

$,E(6^+)/E(2^+) = 7$

(see section 2.3).

The IBM expects that the transitions between the β and the γ bands and the ground state band is absolutely forbidden.[44]

- The transitional limit from SU(5) to SU(3):[43]

Some nuclei show spectra between the vibrational (SU(5)) and the rotational (SU(3)) limits, to explain this situation, the Hamiltonian in equation (2.11) is written in the form:-

$$H = \epsilon n_d - k\, Q.Q - k'\, L.L. \qquad (2.30)$$

The first term represents the SU(5) limit, while the last two terms representing the SU(3) limit.

Equation (2.30) can be written as:-[50]

$$H = (\epsilon_c - \Theta \hat{N}_\nu)\, n_d + k\, \hat{Q}^2 \qquad (2.31)$$

where

$$\hat{Q}^2 = \hat{G} - \frac{3}{4}\hat{L}(\hat{L}+1)$$

$\hat{G}$ is the Casimir operator of SU(3) limit.

$\hat{L}$ is the angular momentum operator.

ϵ_c and Θ are constants determined by fitting experiment to theory.

$\hat{N}_\nu$ is the number of neutron boson operators.

The first term in equation (2.31) represents the single boson energy. The second term represents a correction to this term resulting from the quadrupole-quadrupole interaction between the bosons.

For few bosons outside the closed shell, the first term (the effective single particle term) gives rise to the vibrational spectra (SU(5) limit).

As $\hat{N}_\nu$ increases, $\hat{Q}^2$ takes over until rotational spectra arise (SU(3) limit).

It is important here to study the behaviour of the branching ratios from states of the β- and γ- bands to the ground state band, the ratio:

$$R = \frac{B(E2,\ 2_2^+ \longrightarrow 0_g^+)}{B(E2,\ 2_2^+ \longrightarrow 2_g^+)} \tag{2.32}$$

In the SU(5) limit R = 0 and for SU(3) limit R = 7/10, this is according to the group structure of the IBM. This ratio will be checked in Chapters 4,5 and 6.

- Connection to the collective model:

The boson Hamiltonian can be related to the collective model of Bohr & Mottelson qualitatively as follows:-[51]

The collective Bohr-Hamiltonian is given by:

$$H = H_I(\beta, \gamma) + H_{rot.}. \tag{2.33}$$

where

$$H_{rot.} = \sum_{k=1}^{3} \hbar^2 L_k^2 / 2I_k \tag{2.34}$$

where

L_k is the component of the angular momentum with respect to the intrinsic axis.

I_k is the moment of inertia given by:-

$$I_k = 4 B^2 \beta^2 \sin^2 (\gamma - \tfrac{2}{3}\pi k) \tag{2.35}$$

where

B is constant,

, β and γ are the deformation parameters (see sec.2.2.)

$$H_I = H_\beta + H_\gamma + H_{\beta\gamma} + V \tag{2.36}$$

H_I represents the vibrational spectra.

If H_I is large compared to $H_{rot.}$, then the rotational energy is small, i.e., the quadrupole-quadrupole interaction between the bosons will be negligible, hence we reach to the vibrational limit (SU(5)).

The other two limits, i.e., the rotational (SU(3)) and the transitional from SU(5) to SU(3) limits occur when the quadrupole-quadrupole interaction is large compared to the single boson energies ϵ_s and ϵ_d (equation 2.11).

Thus one can write down the energy function in terms of the parameters of the two models (i.e., collective Bohr model and the IBM).

In SU(5) limit of the IBM, the energy function is given by the formula:-[52]

$$E(N;\beta) = \epsilon \frac{N\beta^2}{1+\beta^2} + f_1 N(N-1) \frac{\beta^4}{(1+\beta^2)^2} \qquad (2.37)$$

where

$$f_1 = \frac{1}{10} C_o + \frac{1}{7} C_2 + \frac{9}{35} C_4 \qquad (2.38)$$

where

C_o, C_2 and C_4 are given by equation (2.15)

ϵ, N are given in equation (2.14).

β is the deformation parameter (equation 2.4.a.)

When β is small, then equation (2.37) reduces to:

$$E(N) = \epsilon N \qquad (2.39)$$

which is exactly like equation (2.4), i.e., we have collective vibration as given by Bohr and Mottelson model.

In SU(3) limit of the IBM, the energy function is given by

$$E(N,\beta,\gamma) = -k \left[\frac{N}{1+\beta^2} (5 + \frac{11}{4}\beta^2) + \frac{N(N-1)}{(1+\beta^2)^2} X \left(\frac{\beta^4}{2} + 2\sqrt{2^7}\beta^3 \cos 3\gamma + 4\beta^2 \right) \right] - k' \frac{6N\beta^2}{1+\beta^2} \qquad (2.40)$$

where,

k and k' are belonging to SU(3) limit and given in equation (2.26).

β and γ are given in equation (2.4.a.)

From equation (2.37) we notice that the SU(5) limit is γ independent, i.e. we have β-vibration.

Equation (2.40) shows that when $\gamma = o$ and $\beta = \sqrt{2}$, then we have sharp minimum i.e., we have axial symmetry and prolate shape.

Thus we conclude that:-

1. The SU(5) limit corresponds to aspherical shape of the nucleus (harmonic vibrator).
2. The SU(3) limit corresponds to an axially deformed shape (axial rotor).

2.4.2. The interacting boson model (IBM-2):

In this version of the IBM we assume that the structure of the low-lying collective quadrupole states in the nuclei are dominated by the excitation of the valence particles, i.e., particles outside the major closed shells.[52] The neutrons and the protons are paired together and these pairs are called bosons, as mentioned in IBM-1 version. Here we distinguish the proton bosons from the neutron bosons.

The number of pairs is counted from the nearest closed shell, i.e., the number of pairs is counted from the beginning to the middle of the shell, while the number of hole-pairs is counted from the middle to the end of the shell.[41]

Then the general Hamiltonian is written as:

$$H = H_{\pi} + H_{\nu} + V_{\pi\nu} \qquad (2.41)$$

where

H_{π} and H_{ν} are the proton (neutron) boson Hamiltonians and like the Hamiltonian given in equation (2.11). $V_{\pi\nu}$ is the proton-neutron boson interaction.

- Connection with the shell model:

If the s and the d bosons are assumed to correspond to S and D fermion pairs, one can relate the two Hamiltonians of the shell model and the IBM - 2 as follows:-[52]

First, we truncate the shell-model space from the complete valence space to the subspace spanned by S and D pairs. Second, we map this space into a boson space.

Otsuka[53] replaced the realistic shell between nucleon numbers 50 and 82 by a single large shell with j = 31/2. One can write the boson Hamiltonian as:-[54]

$$H = \epsilon (n_{d_\pi} + n_{d_\nu}) - k\, Q_\pi^{(2)} \cdot Q_\nu^{(2)} + \text{residual terms}. \qquad (2.42)$$

where

$Q^{(2)}$ is the quadrupole boson operator.

The shell model Hamiltonian can be written as:

$$H = H_\pi + H_\nu + H_{\pi\nu} \qquad (2.43)$$

where

H_π and H_ν are the energies of the proton and neutron respectively.

$H_{\pi\nu}$ is the strong attractive proton-neutron interaction which is given by:-

$$H_{\pi\nu} = -k\, T_\pi^{(2)} \cdot T_\nu^{(2)} \qquad (2.44)$$

where

$T^{(2)}$ is the quadrupole fermion operator.

In the boson space equation (2.44) can be written as:-

$$H_{\pi\nu} = -k\, Q_\pi^{(2)} \cdot Q_\nu^{(2)} \qquad (2.45)$$

which shows the proton-neutron boson interaction which rises from

the proton-neutron interaction.

Thus the shell model Hamiltonian (equation 2.43) can be written in a form similar to equation (2.42).

2.5. Other models:

1. Variable moment of inertia (VMI):

In this model, the energy levels of the ground-state bands in even-even nuclei can be interpreted on the bases of a semiclassical term in which, the energy contains, in addition to the usual rotational term, a potential energy term which depends on the difference of the moment of inertia I_J (for the state of angular momentum J) from that of the ground state I_o.

Each nucleus is then characterized by the two parameters I_o and σ where σ is the "softness parameter".

The energy spectrum can be given by the formula:-[55]

$$E(J) = [J(J+1)/2I_J] \left\{1 + [J(J+1)/4C\ I_J^3]\right\} \qquad (2.46)$$

where

The moment of inertia I_J is given by:-

$$I_J = I_o / \left\{1-[J(J+1)/2C\ I_J^3]\right\} \qquad (2.47)$$

where

C is the restoring force constant (see equation 2.3)

Equation (2.46) can be written in terms of I as follows:-

$$E_J(I) = \tfrac{1}{2}C(I-I_o)^2 + \tfrac{1}{2}[J(J+1)/I] \qquad (2.48)$$

The softness parameter can be written in terms of C and I_o as follows:-

$$\sigma_o = 1/2C\ I_o^3 \qquad (2.49)$$

Here, σ can be defined as the percentage increase of the moment of inertia per unit change of angular momentum ($\Delta I/I\Delta J$). The increase of the moment of inertia can be explained as a result of the increase of the deformation parameter β at higher angular momentum[56] or due to the decrease of the pairing energy for neutrons and protons with increasing J.[57]

The limits of validity of the model can be explained as follows:-

When $\sigma = o$, i.e., $I_J = I_o$, then C is very large and the energy spectrum (equation 2.46) becomes:-

$$E_J(\sigma = o) = \frac{1}{2I_o} J(J+1) \qquad (2.50)$$

which is the well-known form given by equation (2.5), i.e., the nucleus is rigid, and we have strong coupling or adiabatic limit. In this limit, the energy ratio $R_J = E_J/E_2$ is

$$R_J(\sigma = o) = \frac{1}{6} J(J+1) \qquad (2.51)$$

Then

$$R_4(\sigma = o) = 10/3 \simeq 3.33$$

This is the same ratio of energies in the rotational spectra.

In the limit of very soft nuclei, i.e., when $\sigma \to \infty$, then equation (2.46) becomes:-

$$E_J(\sigma \to \infty) = \frac{3}{4}[J(J+1)/I_J] \qquad (2.52)$$

The ratio R_J in this limit is given by the formula:-

$$R_J(\sigma \to \infty) = \left[\frac{1}{6} J(J+1)\right]^{2/3} \qquad (2.53)$$

and

$$R_4(\sigma \to \infty) = (10/3)^{2/3} \simeq 2.23$$

This ratio approaches the spherical region of nuclei. Thus the limits of the model lie in the range:

$$\left[\frac{1}{6}J(J+1)\right]^{2/3} \leq R_J \leq \frac{1}{6}J(J+1) \qquad (2.54)$$

We conclude that this model agrees very well with the rotational model (axial rotor) and at the same time approaches the vibrational model of nuclei.

2. Pairing plus quadrupole model (PPQM):

In this model, the collective Hamiltonian is written in terms of the potential and inertial functions of deformation. Depending on the shape of the potential energy of deformation, this Hamiltonian can describe both the vibrational limit, in which the nucleus undergoes harmonic vibrations about the spherical shape, and the rotational limit, in which the low excitations consist of rotations of a nearly rigid deformed nucleus.

The Hamiltonian can be written in the form:-[58]

$$H = V(\beta,\gamma) + H_{rot.} + H_{vib.} \qquad (2.55)$$

where

$V(\beta,\gamma)$ is the potential energy of deformation.

$H_{rot.}$ is the rotational kinetic energy which depends on the moment of inertia in addition to β and γ parameters.

$H_{vib.}$ is the vibrational kinetic energy which depends on β and γ parameters.

In this model, the parameters of the model are determined microscopically, then the Hamiltonian is quantized and the resulting Schrodinger equations can be solved numerically.[58]

3. General Collective Model (GCM)[59]:

In this model, the Hamiltonian is written in terms of collective degrees of freedom and quadrupole operator. The collective Hamiltonian is given by:[59]

$$H = T + V \tag{2.56}$$

where

T is the kinetic energy.

V is the potential energy surface.

In deriving the quadrupole operator, the following assumptions were made:-

1. Constant charge distribution.
2. Incompressibility of nuclear matter.
3. No distinction between protons and neutrons.
4. Expansion of the irreducible quadrupole tensor only up to second order.

Then the Hamiltonian can be diagonalized and the eigenvalues can be derived.

The collective properties are determined as in the case of the old models by the mass paramaters and by the potential energy surface (PES) which gives a vivid representation of the dynamical collective properties of the nucleus.

4. Boson Expansion Technique (BET):[60]

In this model, the Hamiltonian is given as a sum of:-

1. Single particle Hamiltonian
2. A particle - hole type quadrupole quadrupole interaction.
3. A pairing interaction of both monopole and quadrupole types.[61,62]

By taking first the single-particle Hamiltonian and the monopole-type pairing interaction, the original shell-model type single-particle system is replaced by a system of quasiparticles.

Then the Hamiltonian is written in a form which is quadratic in the quasiparticle pair creation and scattering operators. An orthogonal transformation is made so as to isolate a collective particle-hole operator.[62]

These fermion-pair operators are expanded in an infinite series of boson operator products.

The coefficients of this expansion are then determined so that all the comutation relations satisfied by the fermion pairs are satisfied by their boson-expanded form as well.

After the expansion coefficients are obtained, the fermion-pair operators in the Hamiltonian are replaced by their boson-expanded forms and, thus the boson Hamiltonian emerges. Thus fourth or sixth order Hamiltonian can be used in the calculations:

$$H = H_{s.p.} + H_{ph} + H_{pair} \tag{2.57}$$

$$H = H_{s.p.} + \sum_{\lambda} H_{\lambda\text{-ph}} + \sum_{\lambda} H_{\lambda\text{-pair}}$$

, $H_{s.p.}$ is the single particle Hamiltonian.

$H_{\lambda\text{-ph}}$ is the λ-pole particle-hole Hamiltonian.

$H_{\lambda\text{-pair}}$ is the λ-pole pairing Hamiltonian.

CHAPTER 3.

EXPERIMENTAL ARRANGEMENTS.

3.1. Single spectra measurements:

A pure germanium detector was used to measure soft gamma-ray energies up to about 200 keV, while large volume true coaxial Ge(Li) detectors were used for extensive measurements of higher energy gamma-rays.

The high mobility of Lithium ions in Germanium is used to increase the semiconductor resistivity and produce a large sensitive volume detectors.[63]

The specifications of these detectors together with the pure germanium detector used in this work are shown in Table (3.1.). The Ge(Li) detectors were equipped with liquid N2 cooled FETs low noise preamplifiers whose output pulses were fed into a spectroscopy amplifier (ORTEC - 572). To optimize the signal-to-noise ratio, the shaping time constant is set at 2μsec. and the baseline restorer (BLR) is set at automatic mode (AUTO). The signals were taken to the analoge-to-digital converter (ADC) (Northern Scientific - 628), then to the memory unit (Northern Scientific - 630) with 4096 channels.

A block diagram of the simple energy spectrometer is shown in Fig. (3.1).

The source activity was chosen to achieve count rates below 2000 counts/second at a 25 cm source-to-detector distance. This enables pile-up effects[64] to be avoided and no coincidence summing corrections have to be made as suggested by Debertin and Schotzig.[65]

The recorded spectra were analysed using the computer program SAMPO.[66]

Table (3.1.)

Specifications of the detectors

No.	Detector	Approximate Volume	Relative Efficiency	Resolution (keV) 1332 keV (^{60}Co)	Photopeak/Compton 1332 keV (^{60}Co)
1	ORTEC Ge (Li)	70 CC	12%	2.21 (05)	35
2	ORTEC Ge (Li)	60 CC	10%	1.94 (04)	35
3	Princeton Ge(I)	200mm^2 X 5mm		225,500 ev*	

* The FWHM of 5.9 keV and 122 keV gamma ray lines, respectively

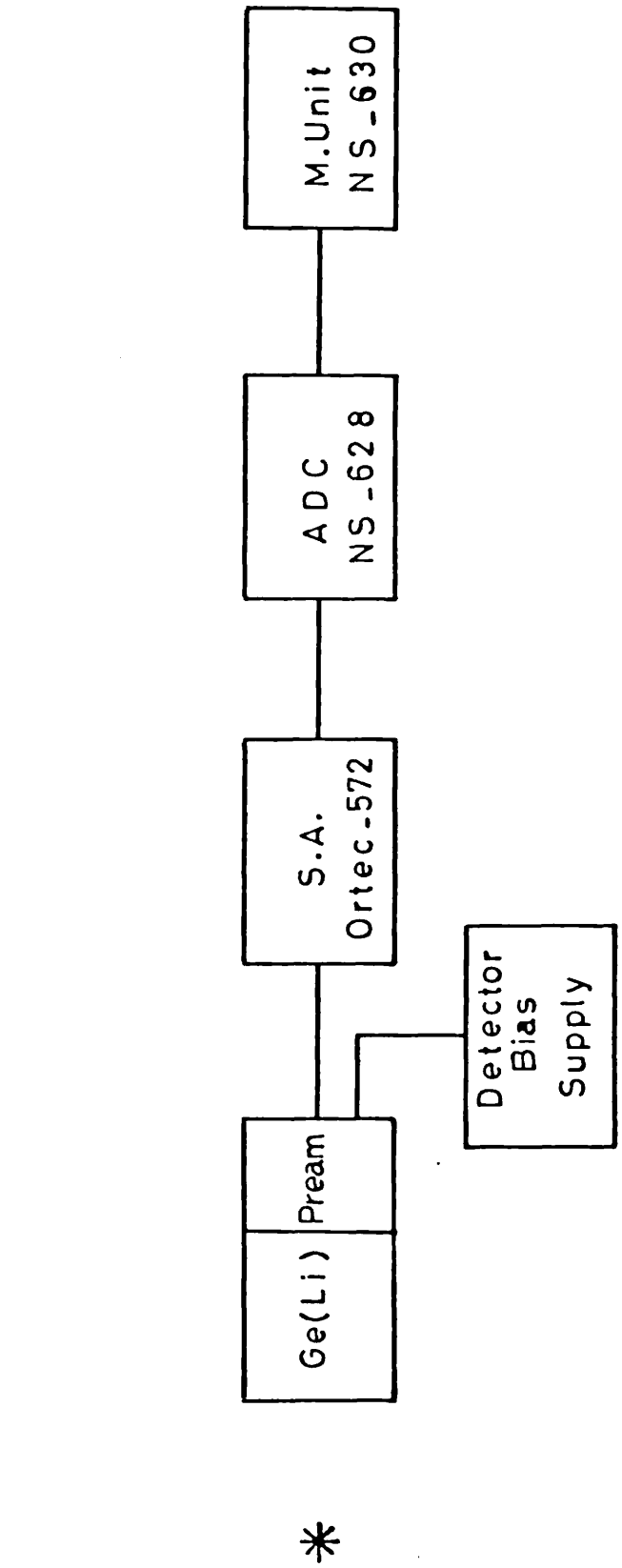

Fig. (3.1.) Block diagram for the single measurements arrangement.

3.2. Energy and Efficiency Calibrations:

The energy calibration was determined by a least square fit to an nth degree polynomial[66] to the most prominent gamma-rays from the decay of the particular isotopes under consideration. These energies were taken from Ref. 67. The peaks were fitted by the program SAMPO[66,68]. The error in energy was related to the shift in the peak centroid and the third order polynomial was considered to give a satisfactory fitting. The errors reported in this work were ranging from about 10 to 30 eV.

The efficiency calibration of the detectors was done using the chemical standards sources set[69] consisting of the isotopes ^{241}Am, ^{133}Ba, ^{57}Co, ^{60}Co, ^{137}Cs, ^{54}Mn and ^{22}Na. The energies range of these isotopes are from 30 keV up to 1332 keV, the energy calibrations for these isotopes were taken from Ref. 67.

The relation between the efficiency (ε) of the Ge(Li) detectors and the energy of the gamma-rays (E) is given by:-[68]

$$\varepsilon = P_1 \left[E^{P2} + P_3 \exp. (P_4 E) \right] \qquad (3.1)$$

where

P_1, P_2, P_3 and P_4 are parameters determined by the least square method as carried out by the program SAMPO[66] modified to run on the University of London CDC - 6600 computer.

The efficiency curve for the 12% Ge(Li) detector (detector number 1, Table 3.1) is shown in Fig. (3.2.).

The efficiency curve for the 10% Ge(Li) detector (detector number 2, Table 3.1) is similar to that in Fig. (3.2.)

The efficiency curve for the pure germanium detector (detector number 3, Table 3.1) is shown in Fig. (3.3.). The relative intensity

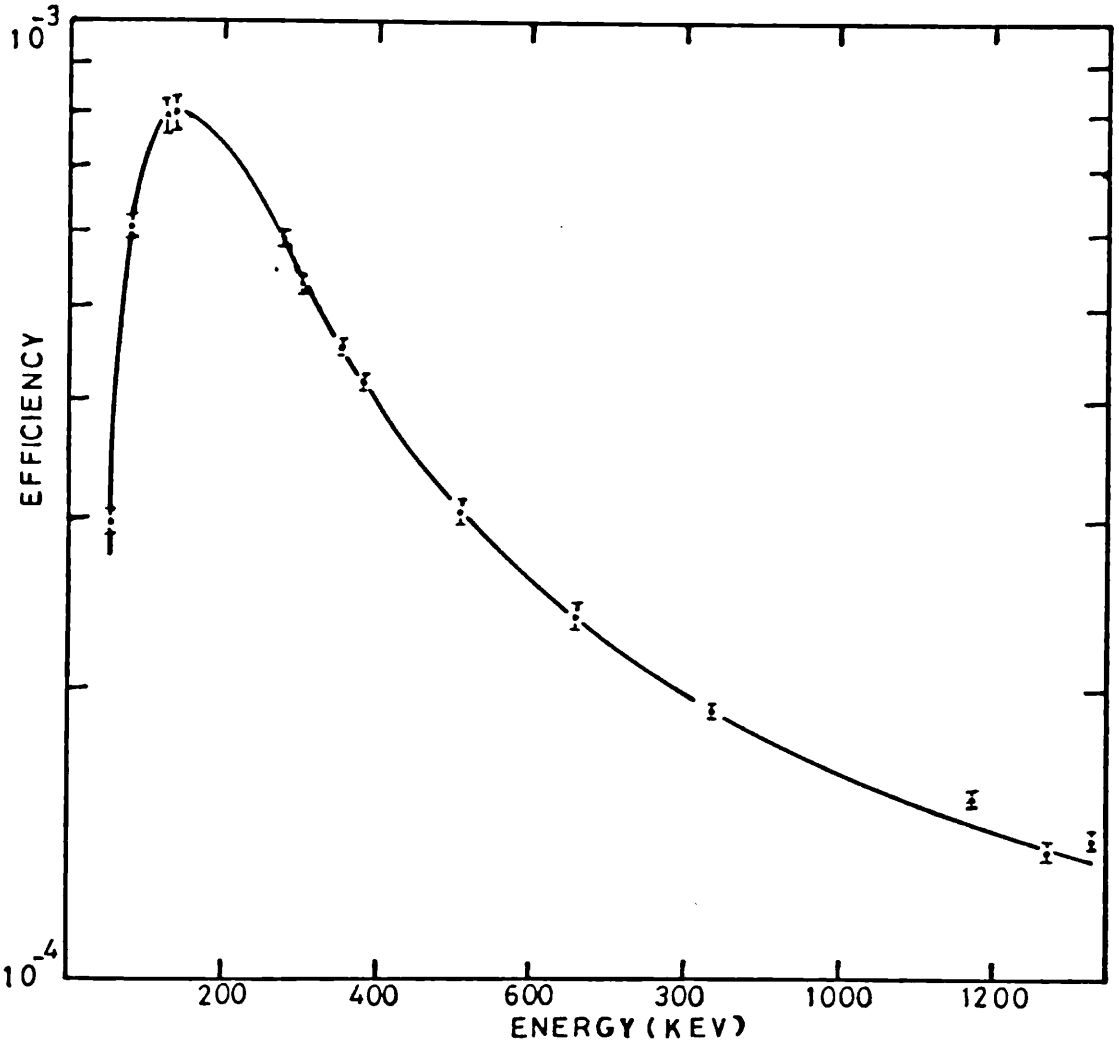

Fig. (3.2.) Efficiency calibration of the 12% Ce(Li) detector.

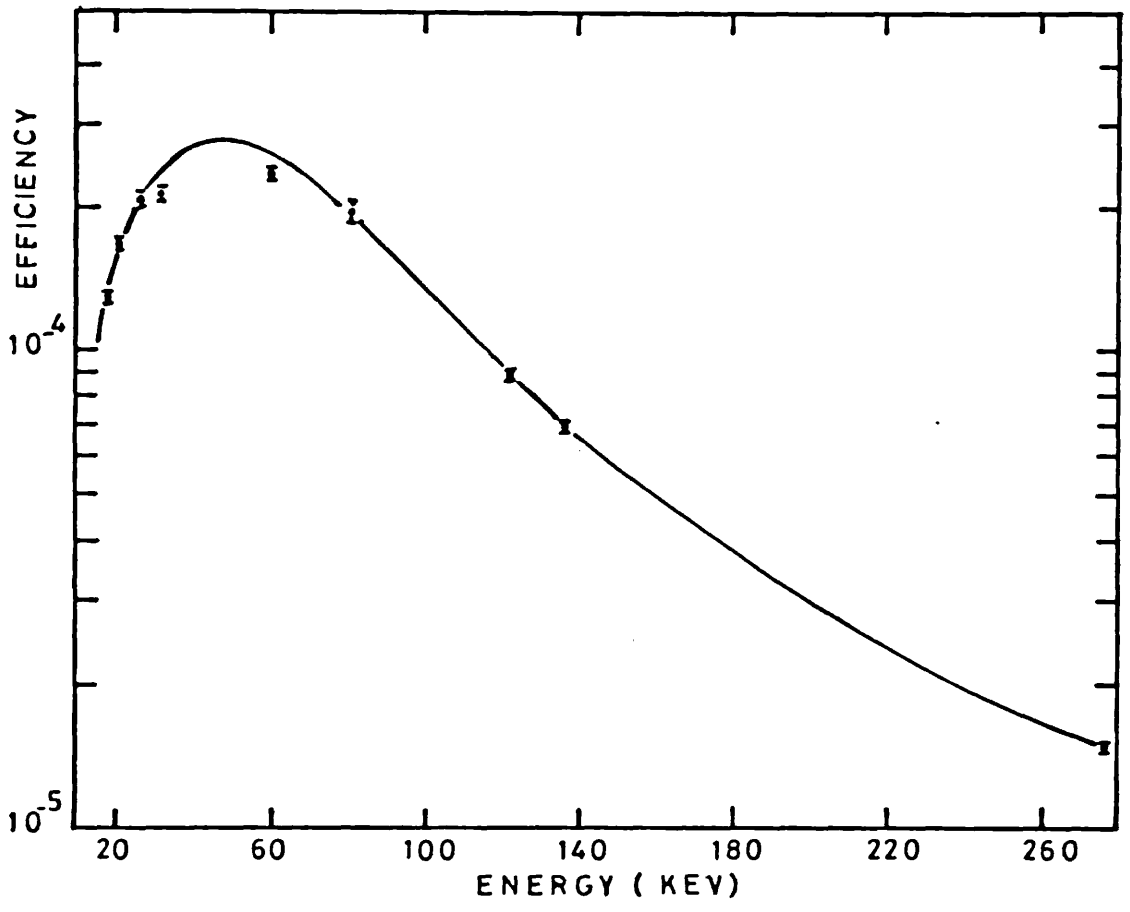

Fig. (3.3.) Efficiency calibration of the pure Ge detector.

measured by this detector (energies ~ 200 keV) were calculated by hand, because no good fitting for this curve is obtained.

The errors in the relative intensities are due to two major factors: the errors in the peak area which is higher for weak peaks and the error in the efficiency calibration. The errors in the peak area are extremely small especially for the prominent peaks, this results from the excellent fitting carried out by SAMPO[66].

The efficiency calibration errors are of the order of 1% for Ge(Li) detectors and about 2% for the pure germanium (Ge) detector.

3.3. Time Spectroscopy:

1. Timing with Scintillators:

In scintillation counters the incident photon is first converted to light in the scintillator, which has optical contact to the photon detector through a light guide. The ionising gamma-radiation loses its energy to electrons released by the photo-effect, the Compton process or by pair production. Thus, the incident radiation excites the scintillator with the resulting energy emitted in the form of visible or ultra-violet light.

The photomultiplier is used as photon detector, thus the external photoelectric effect is utilized to convert light to an electrical signal. Amplification is usually handled through secondary emission, with the primary electrons emanating from the photocathode focussed on the first dynode by an electron-optical system.[70] Every impinging primary electron releases secondary electrons. An electrical signal will be obtained at the anode on the end of a subsequently located dynode stages.

This signal will be used for timing information, i.e., current signal, while signal used for energy information (relatively slower than the anode signal) is taken from one of the dynode stages of the photomultiplier, this is voltage pulse.

The scintillation counters have very high efficiency, i.e., most of the energy dissipated in the crystal is converted into electrical signals. But the energy resolution of these detectors is generally poor.

This is due to the statistical frequency functions of five separate processes in cascade:

(a) light production in the scintillator itself.

(b) light collection at the photocathode.

(c) production of electrons at the photocathode.

(d) collection of the photoelectrons on the first dynode.

(e) multiplication in the photomultiplier dynode structure.[71]

These detectors are useful for fast timing if we use the anode output pulses for triggering a fast discriminator, since these pulses have a decay time constant of a few nanoseconds (in case of plastic scintillators).

The poor energy resolution of the scintillation detectors can be compensated if a high resolution Ge(Li) detectors were used in conjunction with the formers. Thus by employing a system consisted of a plastic - Ge(Li) detectors, one can construct good lifetime spectrometer by making use of their superior characteristics, i.e., fast timing signals of the plastic detectors and high energy resolution of the Ge(Li) detectors.

The average form, i.e., the rise time and decay time of the output

pulses is usually the same for all pulses obtained from the scintillation detectors.[72]

For a phosphor of decay time τ, the number of the photoelectrons (n(t)) produced at the photocathode of the photomultiplier is distributed as:[70]

$$n(t) = \frac{R}{\tau} \quad e^{-t/\tau} \qquad (3.2)$$

where

R is the total photoelectron yield.

Then, the best timing is produced when τ is small (in the case of plastic scintillator, τ equals about 2 nsec.[7])

All detectors and auxiliary electronics show statistical fluctuations in the timing pulses used to derive timing analysers. Thus, even for radiations emitted strictly simultaneously, e.g., two 511 keV positron annihilation quanta or the 1332 KeV quanta of ^{60}Co, there are time fluctuations in the detectors. This results in a finite time resolution obtained when using these detectors.

When ^{60}Co isotope is used to measure the system resolution, the timing spectrum obtained is called the prompt time distribution which can be characterized by the two quantities:-

(a) The full width at half maximum (FWHM) which is called the time resolution.

(b) The slope which is exponential and can be expressed as apparent half-life. Instead of the slope, sometimes the full width at a tenth ($\frac{1}{10}$) of the maximum (FWTM) is quoted.

The finite width of the prompt time distribution or the time resolution is affected by the following quantities, in addition to the parameters affecting energy resolution:[72]

(a) Variation of the light path length from the scintillator to

the photocathode.

(b) Finite decay time of the light emitting states in the scintillator.

(c) Noise of the photomultiplier.

(d) Jitter and uncertainty in the triggering of the associated electronics.

The fast signal (current pulse) produced at the anode of the photomultiplier usually used to trigger a constant fraction discriminator working in either leading edge technique (LET) or in a constant fraction technique (CFT). These techniques will be discussed in the following sections.

2. Timing with semiconductor detectors:[7,72,73]

The semiconductor detector system consists of a semiconductor element, a cryostat, a liquid-nitrogen dewar and a charge-sensitive preamplifier. The detector element is a single crystal of germanium made into a p-i-n diode. The cryostat assembly is designed to maintain a vacuum for the detector element to establish a cryogenic temperature and to hold the detector concentrically in the endcap. The dewar serves as a reservoir for the liquid nitrogen. The detector is designed to operate at nearly liquid nitrogen temperature, so as to lower the leakage current and hence the noise of the system and to maintain the lithium compensation of Ge(Li) detectors.[74] A charge-sensitive preamplifier is mechanically mated to the cryostat and electrically connected to the detector element via vacuum-tight feedthrough. Coaxial detectors were used because of their excellent performance, since it is easy to manufacture them in the form of single crystal.[75]

The thin dead layers of these detectors minimize scattering and absorption of the incoming photon beam, it optimizes the electric field

for the best peak shape which is very important when computer-fitting the data, and it enhances high-resolution-timing performance.

The performance parameters of the Ge(Li) detectors are the energy resolution, the peak-to-Compton ratio and the efficiency (Table 3.1).

The absolute efficiency of the detector is defined as the number of recorded counts divided by the number of photons emitted by the source.

The absolute efficiency (ε_a) is the product of the geometrical efficiency (ε_g), i.e., the fraction of emitted particles which actually strike the detector, and the intrinsic efficiency (ε_i), then:

$$\varepsilon_a = \varepsilon_g \times \varepsilon_i$$

The efficiency of the Ge(Li) detectors is referenced to the 3" x 3" NaI(Tl) detector. The measurements are made using the 1.33 MeV line of a ^{60}Co source positioned at 25 cm from the detector. The counts are taken for a fixed-time and the absolute efficiency is then determined by dividing the total number of counts in the photopeak by the number of disintegrations that actually occurred in the source during the same period of time. This efficiency is divided by 1.2×10^{-3}, which is the absolute efficiency of the 3" x 3" NaI(Tl) crystal at 25 cm from the source.

If the energy of the particle must be measured, the sensitive depth must exceed the range of the particle, in this case ε_i is essentially 100%.[74]

For energy spectroscopy, the detector's sensitive depth must be sufficient to completely absorb all the radiation energy. However, by increasing this sensitive depth, the detector sensitive volume is increased

and this may increase the detector noise contribution.

The peak-to-Compton ratio is obtained by dividing the height of the 1.33 MeV peak by the average Compton plateau between 1.040 and 1.096 MeV.

This ratio is a measure of the detector's ability to distinguish low energy peaks in the presence of high energy sources.

The Compton plateau results from Compton interaction in the crystal in which the resulting photon, reduced in energy, escapes from the sensitive volume of the detector.

The energy resolution of the detector is a measure of its ability to distinguish between closely spaced energy lines in a spectrum. A lower limit of the energy resolution (FWHM) for the detector is determined by the noise-broadening effect. However, factors such as statistical effects, imperfect charge collection and variations in energy lost in the dead layer of the source and the detector can cause additional broadening of the peak.

In high resolution-timing applications where the rise time of the pulses from the detector must be very short, the charge transit distance has to be kept as small as possible and large electric field maintained. In these cases, the sensitive depth may be restricted by the need for very precise timing information.[74]

The energy lost by ionising radiation in the Ge(Li) detectors results in the creation of electron-hole pairs. The average energy necessary to create an electron-hole pair in a given semiconductor at a given temperature is independent of the type and the energy of the radiation.

This energy is 2.95 eV in germanium at 80 K.

The forbidden energy gap for germanium at this temperature is 0.73 eV, thus it is clear that not all the energy of the radiation is spent in breaking covalent bonds. Some of it is released to the lattice under the form of phonons. At 80 K electrons and holes velocities are the same and they drift to the contacts of the opposite polarity, following the lines of force of the electric field established by the applied voltage. Hence a current signal is delivered by the detector to the charge sensitive preamplifier which integrates on its feedback capacitance this signal and feeds the resulting voltage signal to the filter amplifier. The rise time of the pulse generated by the detector can be measured at the output of the charge-sensitive preamplifier. If the preamplifier is sufficiently fast, then the rise time is determined by: the charge collection time (T), the rise time of the detector equivalent circuit (negligible quantity in most cases) and the plasma zone (in case of heavy ionizing particles).

Always the collection time is the dominant factor. The order of magnitude of this time is given by the following formula:[74]

$$T \simeq W \times 10^{-8} \text{ sec.} \qquad (3.3)$$

where W is the thickness of the depletion region measured in mm. This formula holds for Ge(Li) detectors operating at 80 K. The rise time decreases with increasing the bias voltage of the detector.

Generally, solid state detectors have a finite charge collection time which depends on the shape of the detector and the applied voltage.

The charge collection time depends on the location where the electron-hole pairs were created, this means that different pulse heights as well as different rise times for these pulses will be obtained.

It was found that gamma rays interacting near the centre of the detector yield pulses with minimum rise time, while those interacting near the electrode will produce pulses with rise time equal to approximately twice as long (see Fig. 3.5.). ($T \sim 100$ n sec.)

3.4. Timing Problems:

1. Jitter:

Jitter is the timing uncertainty of the pick-off signal that is caused by noise in the system and by statistical fluctuations of the signals from the detector. Thus, jitter denotes the time spread characterized by the full width at half maximum (FWHM). When using these pulses for triggering a discriminator, jitter will cause the discriminator to respond either sooner or later than would occur if no noise were presented (Fig. 3.4.a.).

When using the scintillation detectors, it was found that pulses with higher amplitudes yield less jitter.[72] Hence, the discriminator level of the constant fraction discriminator (CFD) should be kept above the noise level (> 0.1 V).

In the semiconductor detectors, jitter is reduced drastically by cooling the FETs of the preamplifiers and the Ge(Li) crystal to the liquid Nitrogen temperature.

2. Walk:

Walk is the time variation in the generating time caused by signal amplitude (Fig. 3.4.b.) or rise time (Fig. 3.4.c.) variations.

Since nearly all signals have amplitude variation, walk is a major source of time inaccuracy.

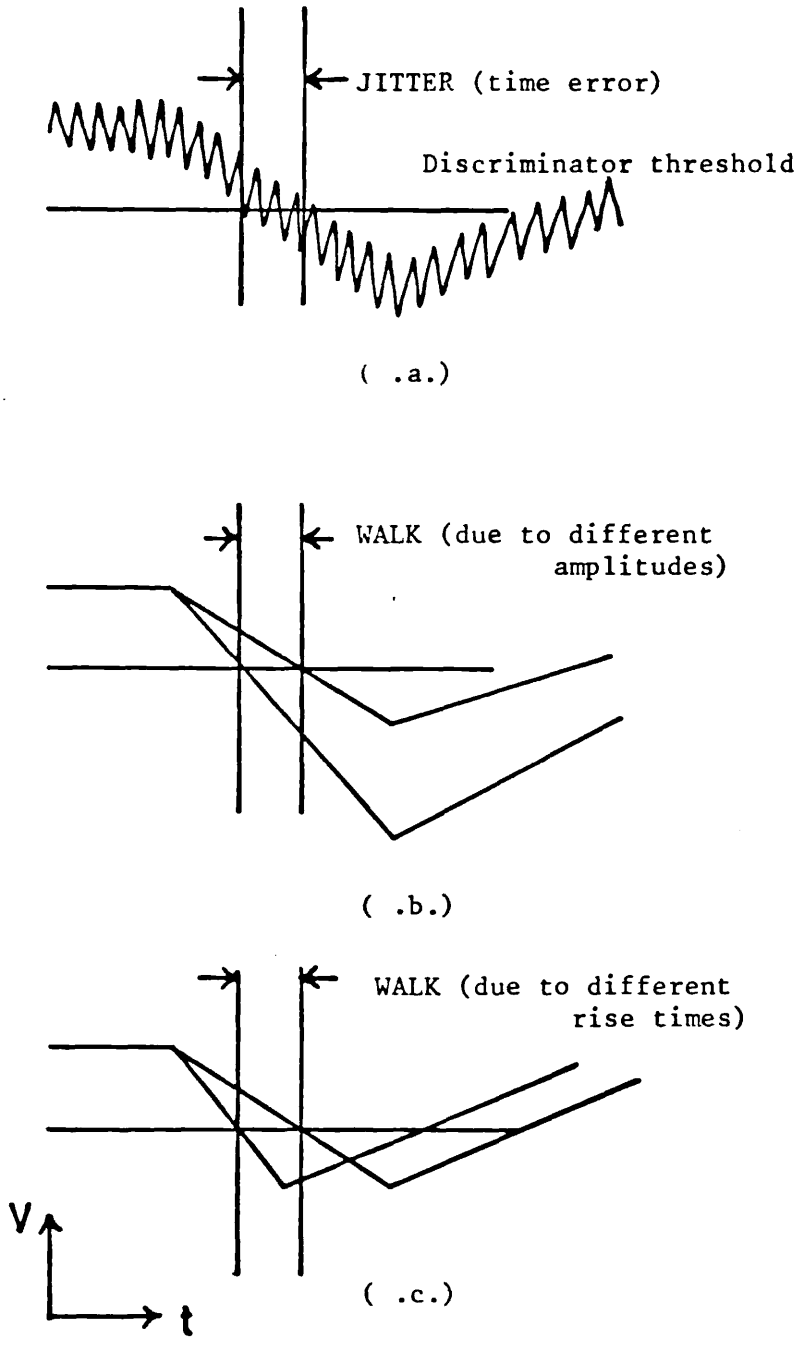

Fig. (3.4.) Jitter and Walk in Leading-Edge Time deviation

Walk can be seen as the shift of the prompt time distribution as a function of the pulse height.[70]

In the case of semiconductor detectors, walk is caused by both amplitude and rise-time variations. The solid-state detectors have a finite charge collection time which depends on the location where the electron-hole pair was produced, thus different pulse height and rise-time distribution were expected.

There are three timing techniques to eliminate walk. These are: the leading edge timing (LET), the constant fraction timing (CFT) and the amplitude-and-rise time compensated timing (ARC).

The simplest and familiar one is the (LET), which is suitable for scintillation counters, since only the dependence on the amplitude variation affects the prompt time distribution.[70]

Many authors have used this method[75,77,78] for timing measurements (see Fig.3.4.).This method is unsuitable for timing with Ge(Li) detectors.

The (CFT) method provides a first-order correction for amplitude dependent time walk. This was reported by Chase[79] and Bengtson & Moszynski.[80]

In this method, the input pulse is first attenuated by a pre-determined factor (f_v = 20% of the original height). The full amplitude pulse which is delayed by some time (t_d), is inverted, and is then added to the attenuated pulse.

The timing signal is derived at the zero-crossing point of the total pulse.

The zero-crossing point will be the same for all pulses regardless of their heights (See Fig. 3.5.).

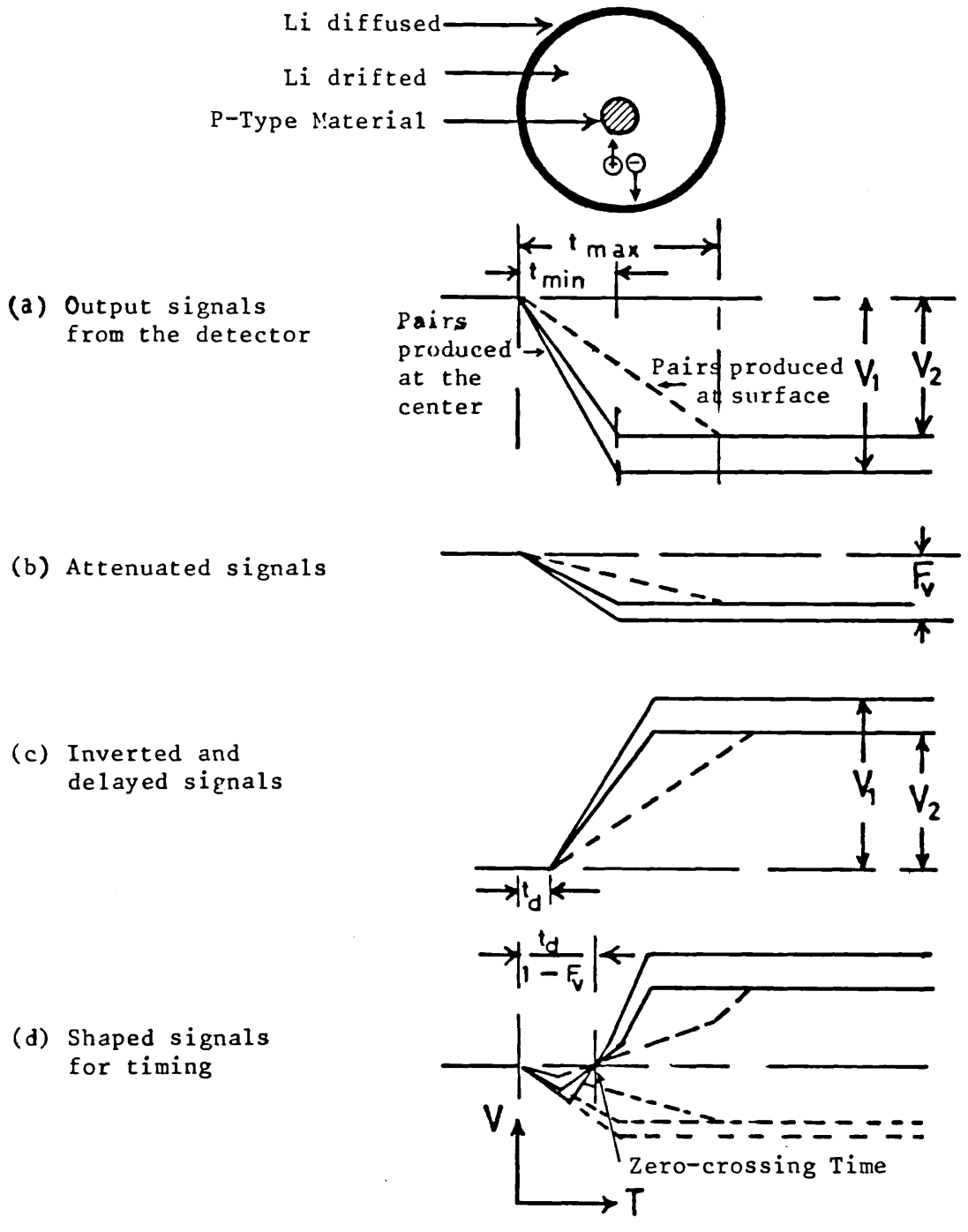

Fig. (3.5.) Time distributions of pulses produced in a coaxial Ge(Li) detector and the signal formation in a Constant-Fraction Discriminator for ARC Timing.

Gedcke & McDonald[81,82] have developed such fast discriminators working on (CFT). These discriminators were suitable for both Ge(Li) and scintillator detectors.

The (ARC) timing is a special case of the (CFT). It provides a first-order correction for both amplitude and rise-time walk.[75]

The principle is shown in Fig. (3.5.) which provides the best timing techniques.

3.5. Time Spectrometer:

The delayed coincidence method was used to measure the half-lives of the nuclear states reported in this work.[71,83,84]

The general principle of this method is to measure the time difference between the population and the depopulation of a nuclear state. These two events are detected by two separate detectors, the population of the nuclear state is corresponding to the "BIRTH" of the state (START) pulse, while the depopulation of the state is the "DEATH" of the state (STOP) pulse.

By measuring the time distribution of the delay of the STOP pulses with regard to the related START pulses, the half-life of the nuclear level can be measured.

The START pulse was taken from the plastic scintillator 1" x 1" NE 102 which was connected to an RCA 8575 fast photomultiplier with an (ORTEC - 265) base.

The rise-time of the anode pulses was about 2 n sec. with amplitude of about 7 volts. This pulse was suitable for triggering the CFD (ORTEC - 473A) operating in CFT mode. The CF mode gives better time resolution

than the LE mode (see Sec. 3.4.).

The output pulse of the CFD was fed into the START of the time-to-pulse height converter (TPHC) (ORTEC - 467).

The pulse from the Ge(Li) detector (detector no. 2, Table 3.1.) was used as the STOP signal for the TPHC.

This pulse was first fed to a timing filter amplifier (TFA) (ORTEC - 474) which shapes the pulse and at the same time provides certain amplification to it.

The differentiation and integration time constants of the (TFA) were adjusted to obtain the best performance using the isotopes ^{60}Co and ^{22}Na, the values were 100 n sec. and 20 n sec. respectively.

The gain of the TFA was adjusted so that the CFD level (ORTEC - 463)was set above the noise level. The output pulses were fed into the CFD input, which was operating in the CFT mode (see Section 3.4.).

The output pulses from the CFD were fed into a nanosecond delay unit (ORTEC-425A), then into the STOP input of the TPHC.

The output of the TPHC was fed into the high level of the multi-channel analyser (MCA), where the timing spectrum was displayed.

The shape of the spectrum and the time resolution (FWHM) depend on the combination of all the functions mentioned above in addition to the range of the TPHC.

Special care should be paid to the geometry of the detectors. They were fixed at 180^{o} to minimize any effect of the $\gamma - \gamma$ angular correlation.

This set-up is called the fast part of the time spectrometer.

To obtain the time distribution of a certain excited nuclear state, the fast timing spectrum should be gated by the energy of a transition which depopulates this excited state.

The energy selection arms (from both detectors) were fed into a slow coincidence unit (ELSCINT), where the output was used to gate the fast timing spectrum on the (MCA).

A block diagram of the spectrometer is shown in Fig. (3.6).

Fig. (3.7.) shows a block diagram of the time calibration of the (MCA) using a pulse generator. Fig. (3.8.) shows the time calibration of the (MCA) at different (TPHC) ranges.

The time calibration of the (MCA) as a function of the (TPHC) ranges at different (ADC) conversion gains of the (MCA) is shown in Fig. (3.9.), the expected linearity between the time calibration of the (MCA) and the (TPHC) ranges is obvious. For analysing the spectrum, the slope method[70] was employed and the least square method was used to fit the data.

In the slope method the half-life is the time taken by the count rate to drop from a certain value to half this value.

The timing spectrum shows a statistical distribution due to the distribution of the delayed STOP signals with regard to the related START signals.

The coincidence count rate (N_t) between two detectors is given by:[83]

$$N_t = \frac{N_1 N_2}{N} \qquad (3.4)$$

where

N_1 is the count rate of the detector counting the START pulses.

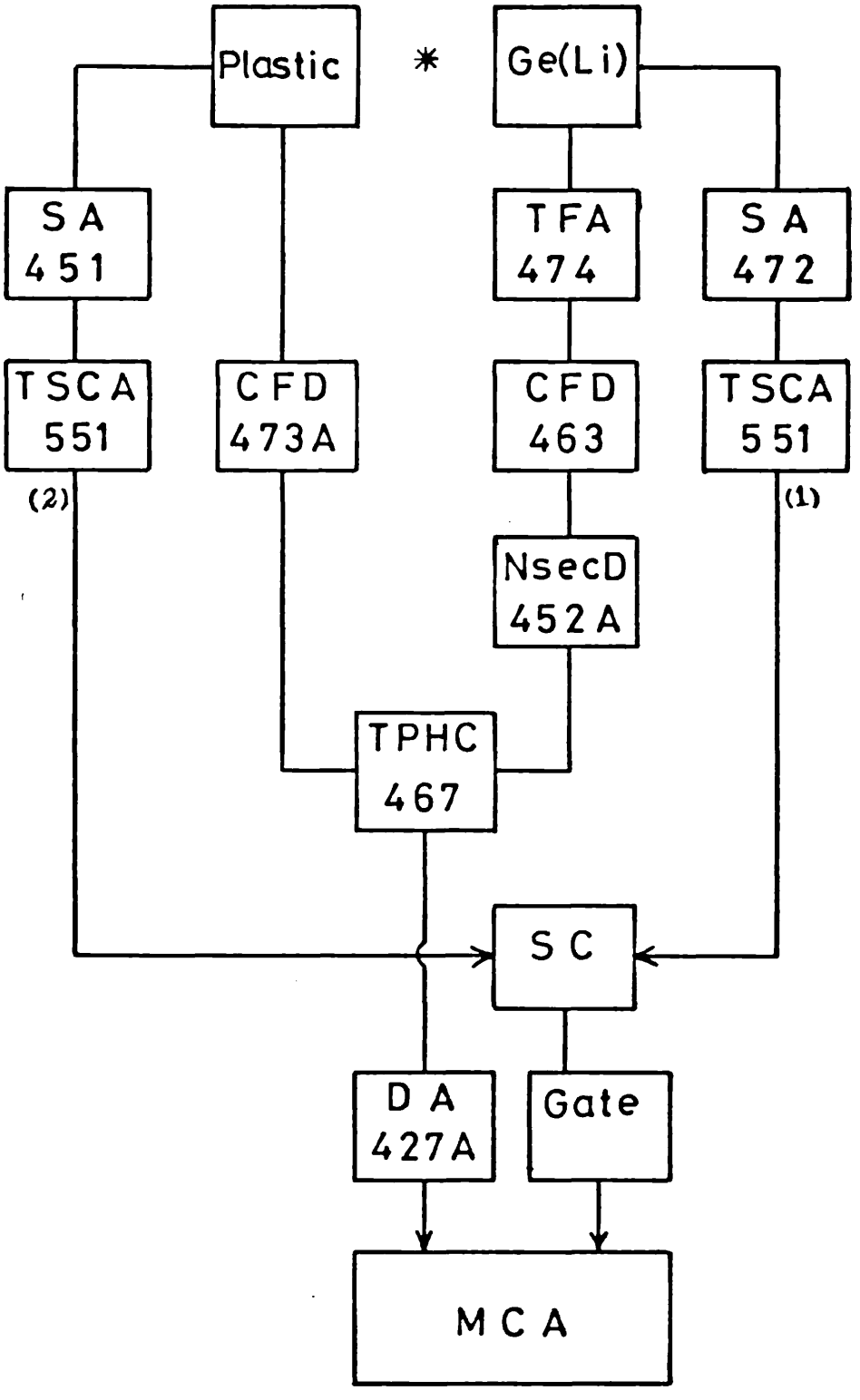

Fig. (3.6.) Block diagram of the Timing Spectrometer.

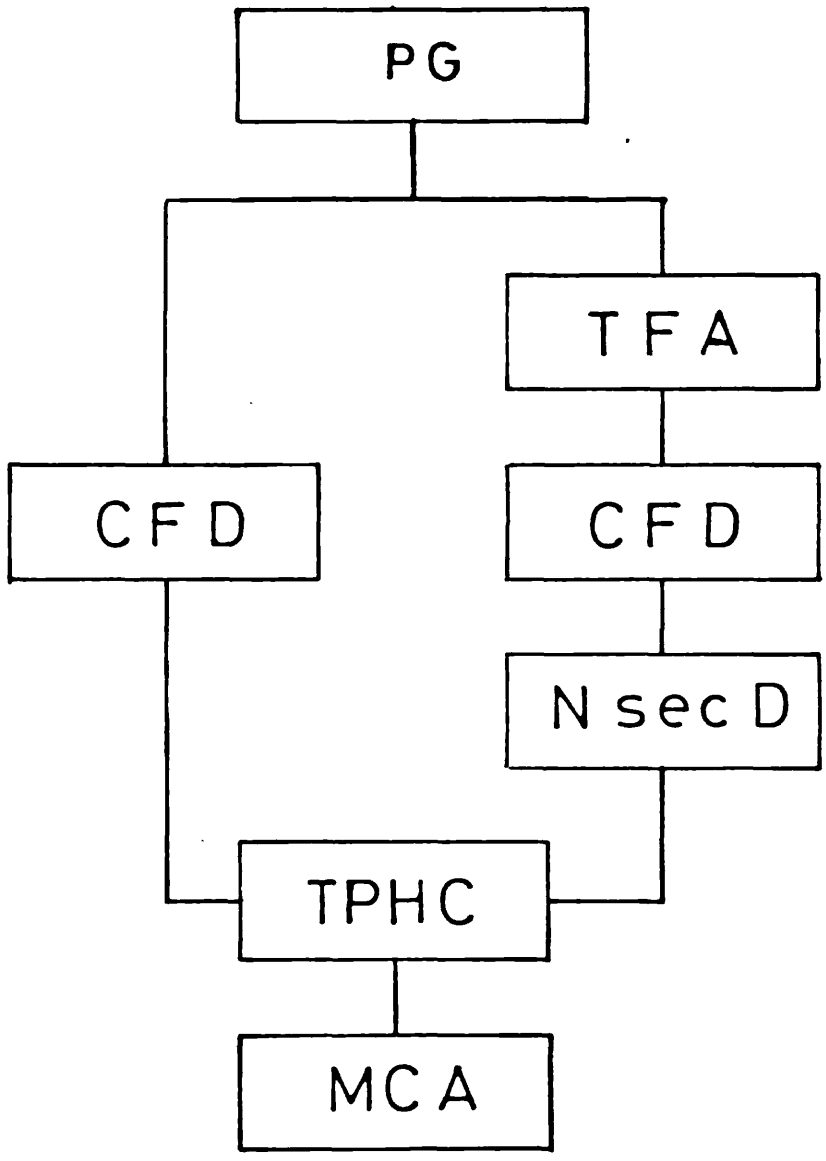

(Fig. 3.7.) Block diagram for the Time Calibration of the MCA.

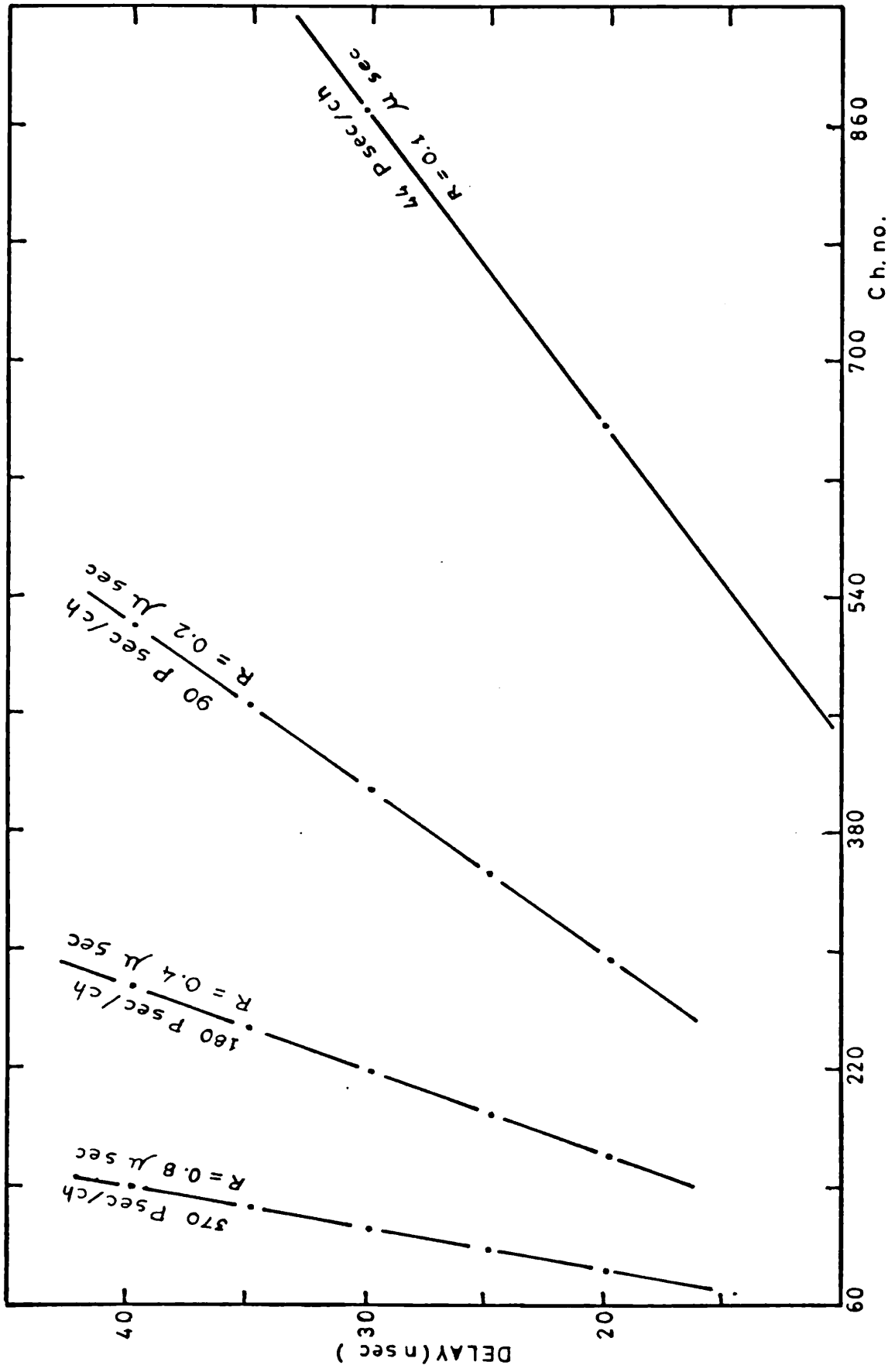

Fig. (3.8.) The time calibration of the MCA at different TPHC ranges.

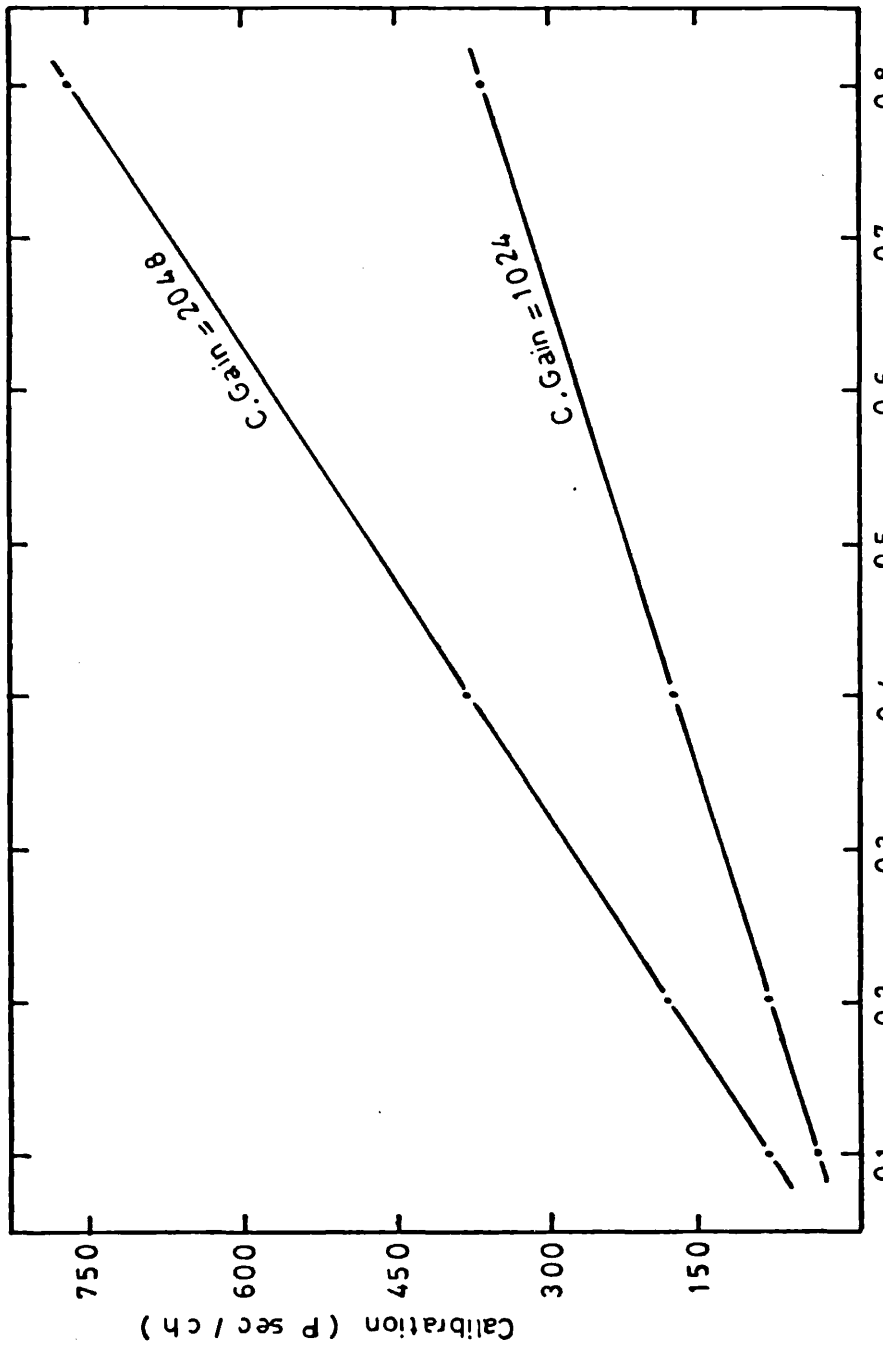

Fig.(3.9.) Time Calibration of the MCA as a function of the TPHC ranges at different ADC conversion gains.

N_2 is the count rate of the detector counting the STOP pulses.

N is the source activity.

Equations (3.4) & (3.5) show that a higher N_{true} count rate is produced if the source strength is small (few microcuries).

The coincidence circuit recognizes the two pulses as "coincident" if the time interval between them is smaller than a certain given value τ, i.e., the circuit resolving time.

However, there is possibility for uncorrelated events occuring during the resolving time to be accepted as coincident. These are called chance coincidences.

The relation between the true coincidence (N_t) and the chance coincidence (N_c) is given by:[71]

$$\frac{N_t}{N_c} = \frac{1}{2\tau N} \qquad (3.5)$$

where

$\frac{N_t}{N_c}$ is the true-to-chance ratio which is increased as the source activity is small and the resolving time is low.

2τ is called the system resolution which is determined by the full width at half-maximum (FWHM) of the timing spectrum.

3.6. Energy-time Spectroscopy:

1. Fast-slow coincidence system:

For establishing the nuclear decay schemes, the gamma-gamma coincidence should be measured.[85] To determine the coincidences of events or to measure the time intervals between them if they are correlated in time, the fast-slow principle was introduced.[85]

A block diagram of the system is shown in Fig. (3.10). The fast part of the system is exactly the same as that in Section (3.5), but the "START" detector is the Ge(Li) detector (detector number 2, Table 3.1.). This detector was chosen as a "START" because it is less efficient than detector number 1 (Table 3.1).

The two detectors were set at 90°. This is to minimize crystal-to-crystal scattering.

The accuracy of the coincidence measurements depends on the system resolution which is the FWHM of the fast part timing spectrum. The resolution of our system was about 30 n seconds.

Because of the statistical distribution of the timing spectrum, a timing single channel analyser (TSCA - 1) is used to select the true part of the spectrum, i.e., the window is set on the peak of the timing spectrum. The energy information (the gate) is chosen by another (TSCA - 2) at the gating detector arm. The outputs of these analysers were fed to a slow coincident unit, the output of which is used to gate the MCA. The high level of the MCA is fed by pulses coming from the spectrum detector (detector number 1, Table 3.1.).

2. The Dual Parameter Data Collection System (DPDC):

The conventional fast-slow coincidence system is insufficient for extensive measurements especially when complex decay schemes with many transitions are involved.

The dual parameter energy-time spectrometer[87] provides a large amount of data in a considerably short time compared to the conventional fast-slow coincidence system. The data is written on large capacity magnetic tapes in one single run which can then be analysed quickly and efficiently.

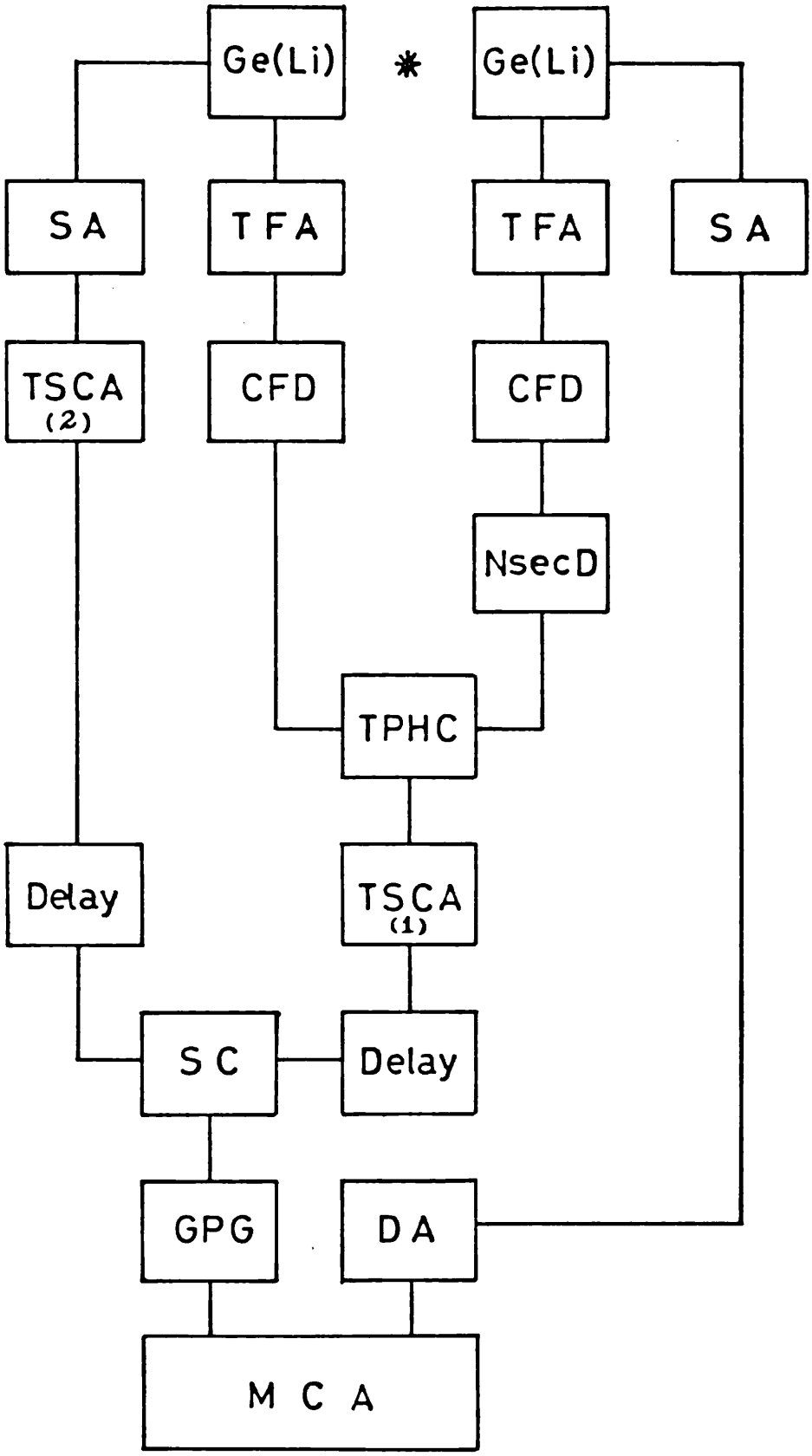

Fig. (3.10.) Block diagram of the Fast-Slow Coincidence System

A block diagram of the energy-time spectrometer is shown in Fig. (3.11).

The two Ge(Li) detectors were coupled to a 4096 x 4096 Dual-paramater system.

The time spectrometer was discussed in Section (3.5.) but the start signals are initiated from the Ge(Li) detector (no. 2 in Table 3.1.). The stop signals are initiated from Ge(Li) detector (no. 1 in Table 3.1.). The two detectors are set at 90^{o} to minimize detector-to-detector scattering.

The signals of the fast part of the two Ge(Li)detectors are fed into two TSCA (ORTEC - 551), one of which is used to select the total timing spectrum which equals to the true and the chance parts of the spectrum.

The other TSCA (ORTEC - 551) is set on the chance part of the total timing spectrum. The outputs of these two TSCAs are used to trigger the gate pulse generator, the output of which is used to gate the two ADCs and at the same time is coupled to the WRITE interface of the DPDC system.

Ge(Li) detector (no. 1, Table 3.1.) is used as the spectrum detector and the energy output signals are fed into a spectroscopy amplifier (ORTEC - 572). The output of the amplifier is fed into the delay amplifier (ORTEC - 427A), the output of which is then fed into the high level of the spectrum ADC(NS - 628).

Detector no. 2 (Table 3.1.) is used as the gating detector, the energy output signals are fed into another spectroscopy amplifier (ORTEC - 472). The output of the amplifier is fed into the delay amplifier (ORTEC - 427A), the output of which is then fed into the high level of the gating

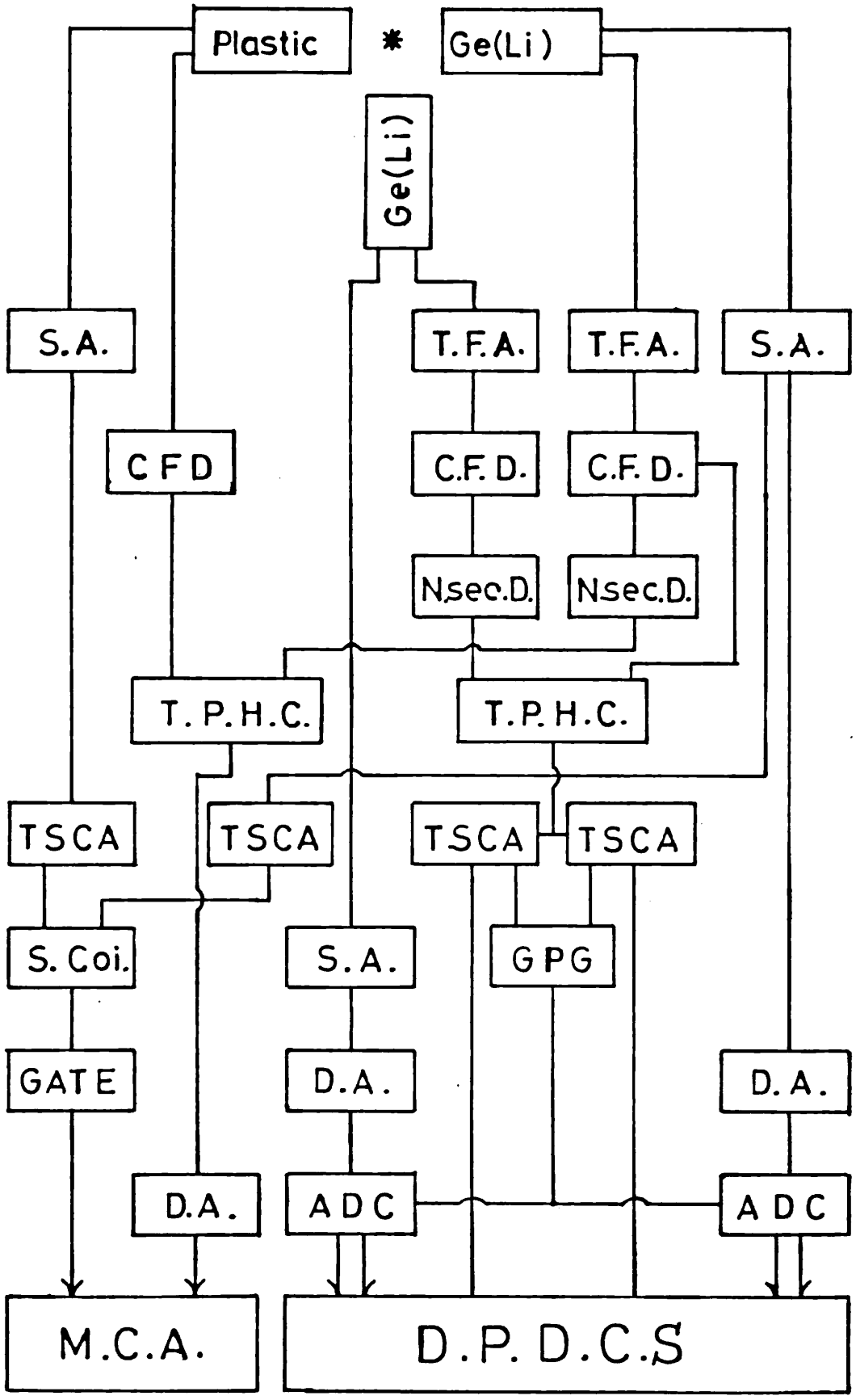

Fig. (3.11) A Block Diagram of the Energy-time Spectrometer.

ADC(NS - 628).

The two ADCs were coupled to the WRITE interface of the DPDC system. The data was written on the magnetic tape, which can be read into the memory unit (NS - 630) via the read-out unit onto the teletype.

With the DPDC system in the WRITE mode, the total spectrum was recorded in a single run and written onto the magnetic tape (ON line).

In the READ mode, coincidence data is produced from the total spectrum by setting the digital window on the region of interest for the required gate.

This records only that part of the spectrum which is in coincidence with the gate.

The background (B.g.)and the chance coincidence can be subtracted from the coincidence spectrum by using the subtraction mode of the memory unit (NS - 630).

The chance coincidence with a particular energy gate can be obtained and subtracted by setting the toggle switch on CHANCE mode of the READ unit in the magnetic tape interface unit, and using the subtraction mode of the memory unit, now reading the spectrum again from the magnetic tape onto the memory unit, the resulting spectrum will be the coincidence spectrum with the particular gate CORRECTED for chance.

The background coincidence is subtracted by resetting the gate to a slightly different energy (but of the same width of the energy gate) and by using the subtraction mode of the memory unit, thus reading the spectrum again from the magnetic tape. The resulting spectrum is the coincidence spectrum with the particular gate CORRECTED for background.

The spectrum obtained is the CORRECTED coincidence spectrum for

both chance and background.

A block diagram of the DPDC system arrangement is shown in Fig. (3.12.)

A general view of the apparatus is shown in Fig. (3.13.)

3.7. System Performance:

1. Time Spectrometer:

The time spectrometer was checked using two isotopes, ^{60}Co and ^{22}Na. The prompt timing spectrum of ^{60}Co is shown in Fig. (3.14). The fast part of the timing spectrum was gated by the line at 1.33 MeV (Fig. 3.6). The energy output of the preamplifier of the Ge(Li) detector was fed into the main spectroscopy amplifier. The decay time constant of this amplifier was set at 2μsec, that is to optimize the signal-to-noise ratio. The bipolar output of the amplifier was fed to the timing single channel analyser (TSCA) which was used to select the 1.33 MeV peak. The output of the (TSCA) was fed to one of the channel inputs of the slow coincidence unit. The energy information selected by the plastic detector came from the output of another TSCA which window was set at the Compton plateau of the 1.33 MeV peak ($\sim$1.08 MeV). This output was fed into the other channel of the slow coincidence unit. The resolving time of the unit was 2.3μ sec., this time was chosen because it provides the best true-to-chance ratio (See Equation 3.5.). The output of the coincidence unit was used to open the gate of the MCA. The delay amplifier was used to provide about 4μsec. delay between the fast timing signal from the TPHC and the gating signal of the slow coincidence unit.

The spectrum was accumulated for four weeks. The full width at half maximum (FWHM) was 4.81 $\pm$ 0.14 n sec. which represents the resolution

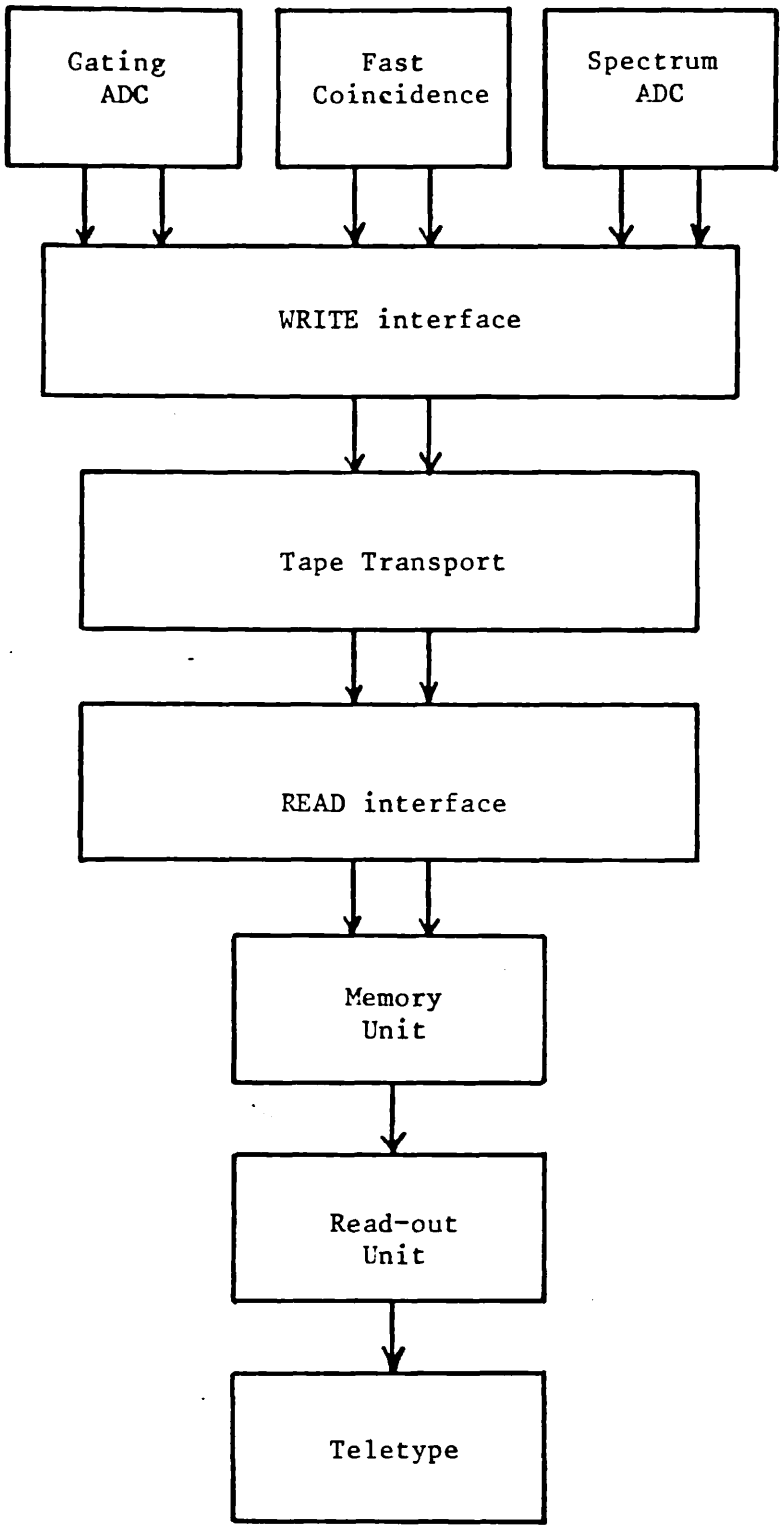

Fig. (3.12) Block diagram of the DPDC system arrangement

Fig. (3.13) General view of the apparatus

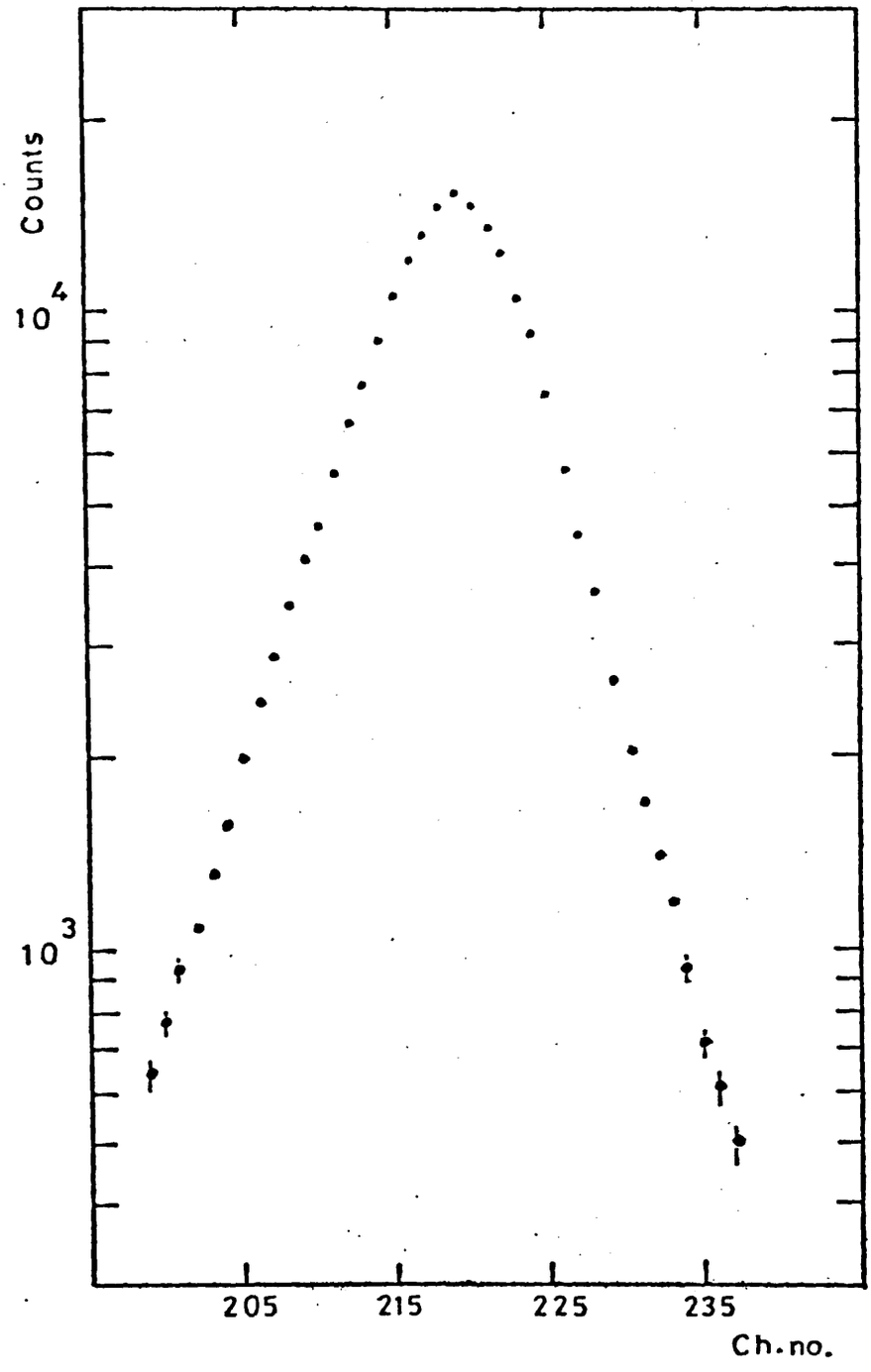

Fig. (3.14) Prompt time distribution curve for ^{60}Co. (370 p sec/ch.)

of the system. The FWTM was 10.36 $\pm$ 0.30 n sec. These values are the best for the apparatus used.

The positron annhilation half-life was measured using ^{22}Na isotope. The Ge(Li) detector was used to select the 511 keV peak in the spectrum of ^{22}Na, while the plastic detector was chosen to select the Compton plateau of this line.

The window of the TSCA (1) was set on the 511 KeV peak, while the window of the TSCA (2) was set on the Compton plateau, and the two output signals obtained from these TSCAs were fed into the inputs of the slow coincidence unit. The output signal from this unit was used to open the gate of the MCA, i.e. gating the fast part of the timing spectrum (see Fig. 3.6.).

The timing distribution spectrum is shown in Fig. (3.15), and the value measured for the positron annihilation is 1.66 $\pm$ 0.04 n sec.

In Table (3.2.), a comparison between the result obtained in this work and the results of other authors is shown. The value obtained in the present work agrees with the value reported by Ref. 89.

Fisi et al.[88] reported short half-life and this value could agree with the value presented here if their reported error is higher than they had estimated.

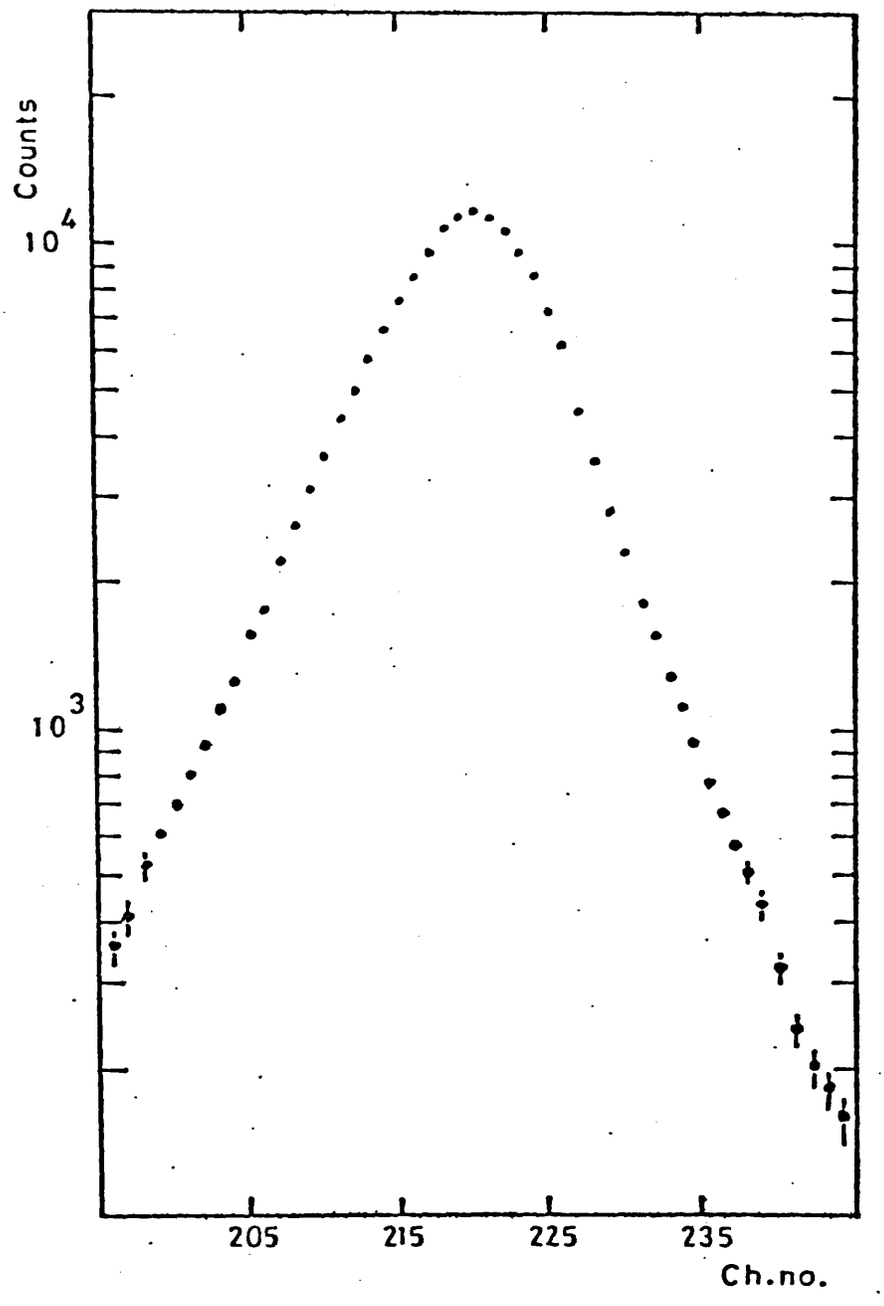

Fig. (3.15) Lifetime spectrum of Positron
(370 p sec/ch.)

Table 3.2.

Positron half-life in Lucite sample

(values are in n sec.)

Present work	Fisi et al.[88]	Wilson et al.[89]
1.66 ± 0.04	1.55 ± 0.01	1.7 ± 0.2

2. The DPDC system:

The DPDC system performance was checked using a well-known decay scheme of $^{110}Ag^{m}$. The preliminary check was made by studying the coincidence data resulting from taking two energy gates. $^{110}Ag^{m}$ decays to ^{110}Cd by emitting β^- particles and 67% of this β^- decay populates the level at 2927 keV (see Ref. 90).

Most of the transitions in ^{110}Cd nucleus are in coincidence with the 658 keV line, since this transition depopulates the first excited state to the ground state in this nucleus. Therefore one of the two gates used in the check was the 658 keV line. The second gate was the 764 keV line, since this transition depopulates the high level at 2927 keV to the state at 2163 keV. Thus the investigation of the decay scheme can be made by considering these two gates.

In each gate, chance coincidences were subtracted from the uncorrected spectrum by setting the toggle switch on the READ unit at CHANCE mode and reading out the spectrum from the magnetic tape, while the memory unit (NS - 630) was set at subtraction mode.

The background was subtracted by moving the region of interest (the digital window on the READ unit) to the right side of the gating peak (but with the same width as the energy gate). Then, reading out the uncorrected spectrum from the magnetic tape, while the memory unit (NS - 630) was switched to subtraction mode. (See Sec. 3.6.).

The spectrum obtained now is the coincidence spectrum with this gate corrected for chance coincidences and for the background.

The coincidence spectra are shown in Figs.(3.16.a),(3.16.b),...

The coincidence results are shown in Table (3.3). Computer program SAMPO[66] was used to analyse the singles and coincidence data.

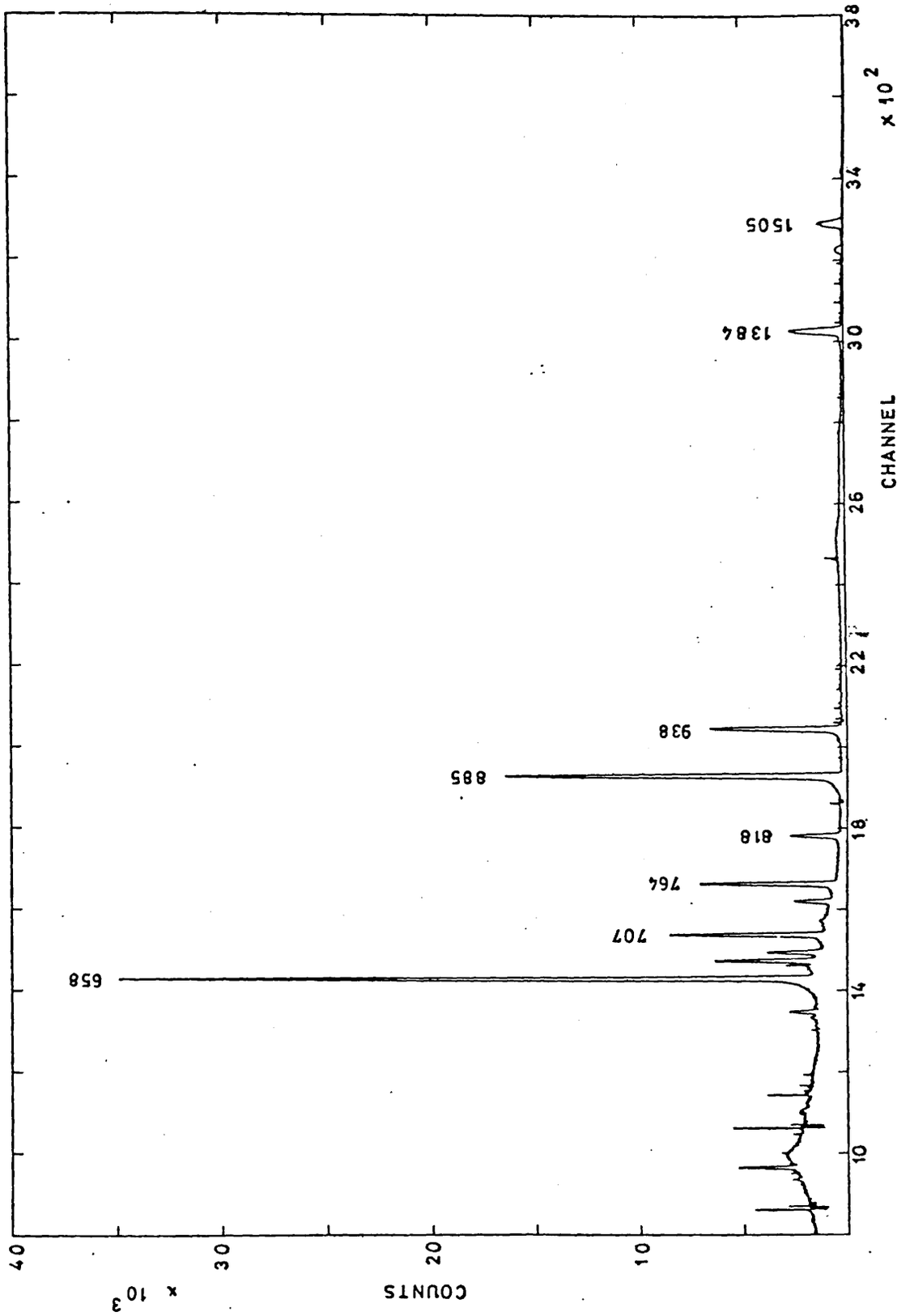

Fig.(3.16.a) Ag - 11C Total spectrum

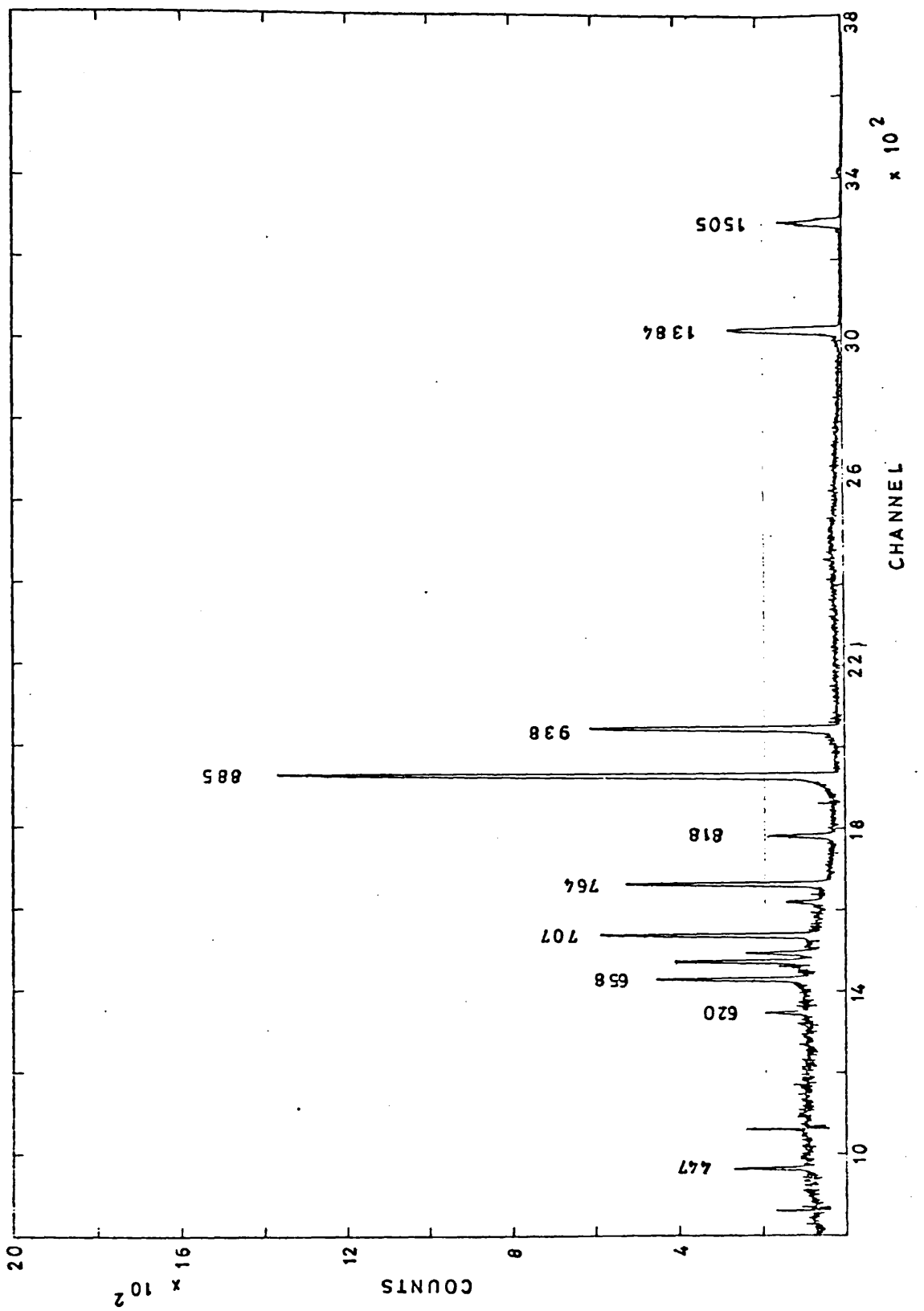

Fig.(3.16.b) Ag - 110 uncorrected spectrum in coincidence with 658 keV.

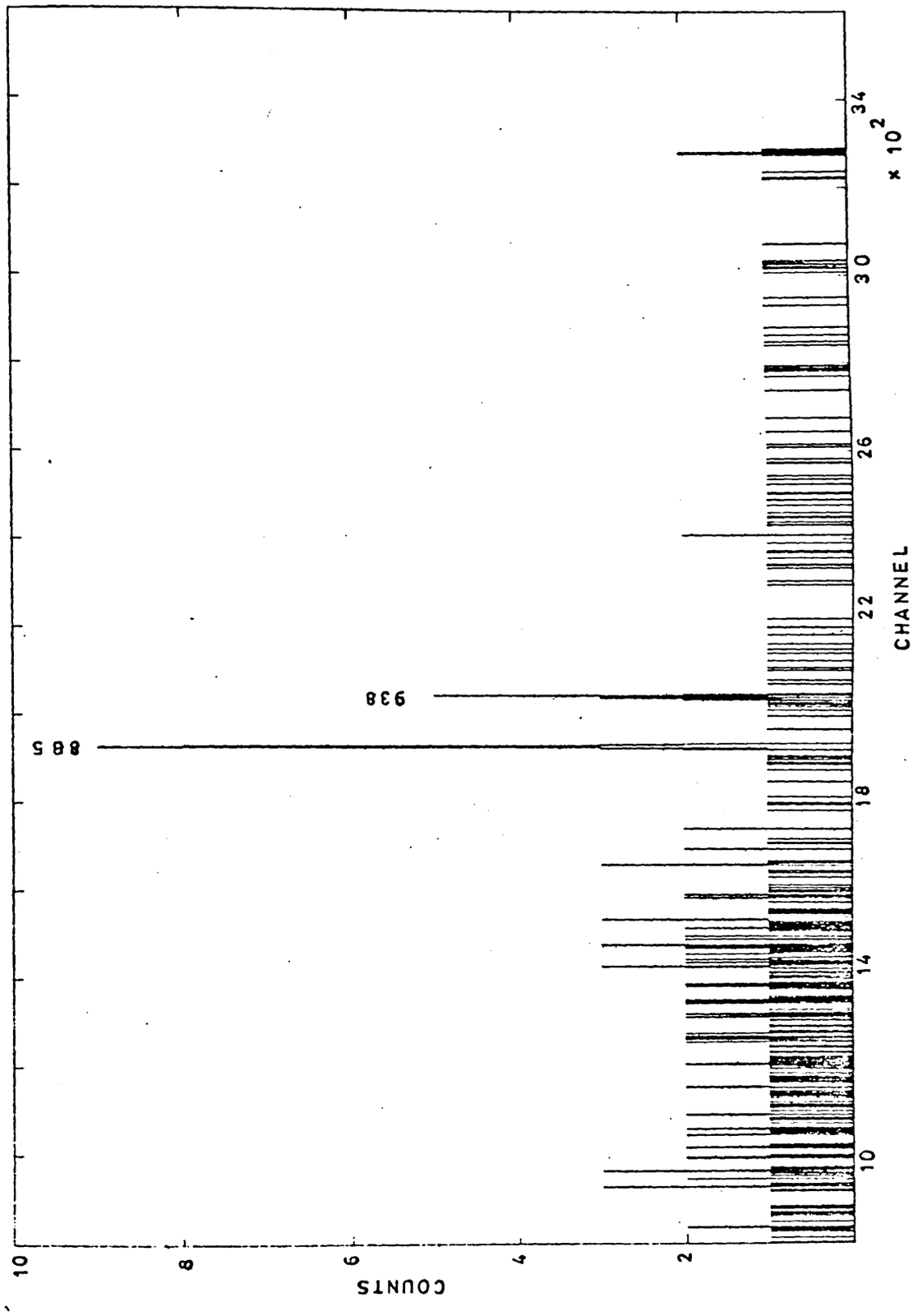

Fig.(3.16.c) Ag - 110 chance spectrum in coincidence with 658 keV.

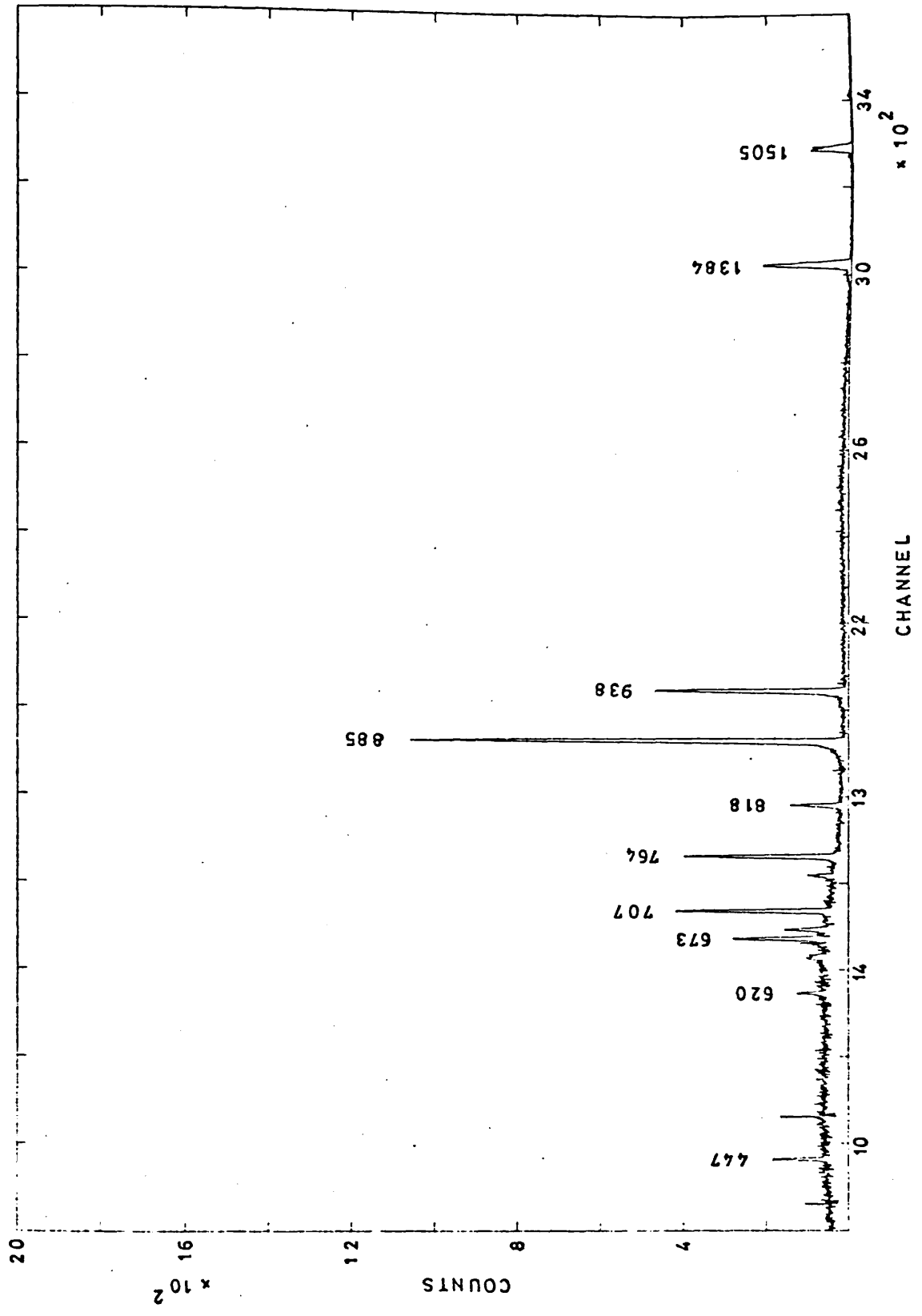

Fig.(3.16.d) Ag-110 corrected spectrum in coincidence with 658 keV.

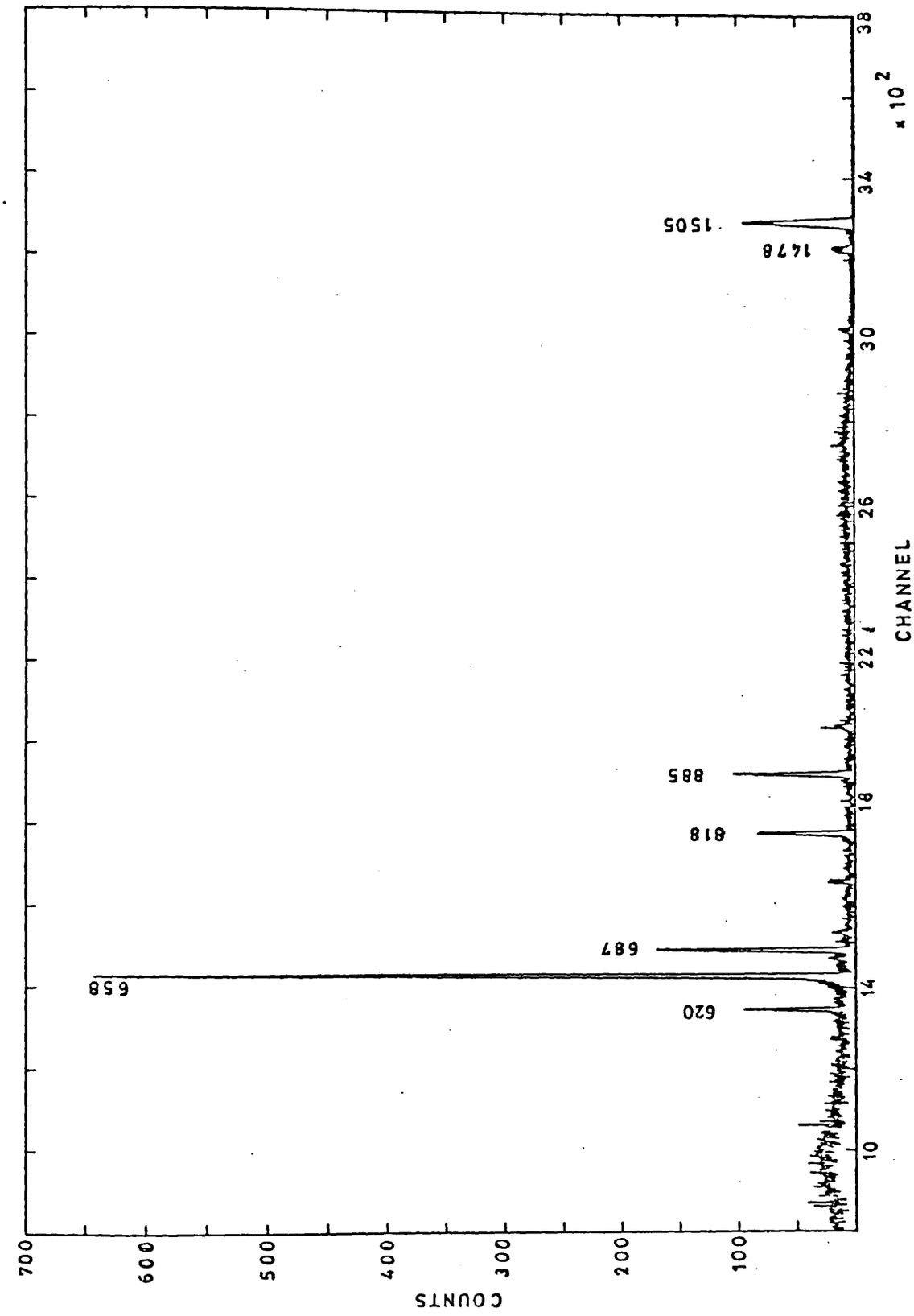

Fig.(3.16.e) Ag-110 uncorrected spectrum in coincidence with 764 keV.

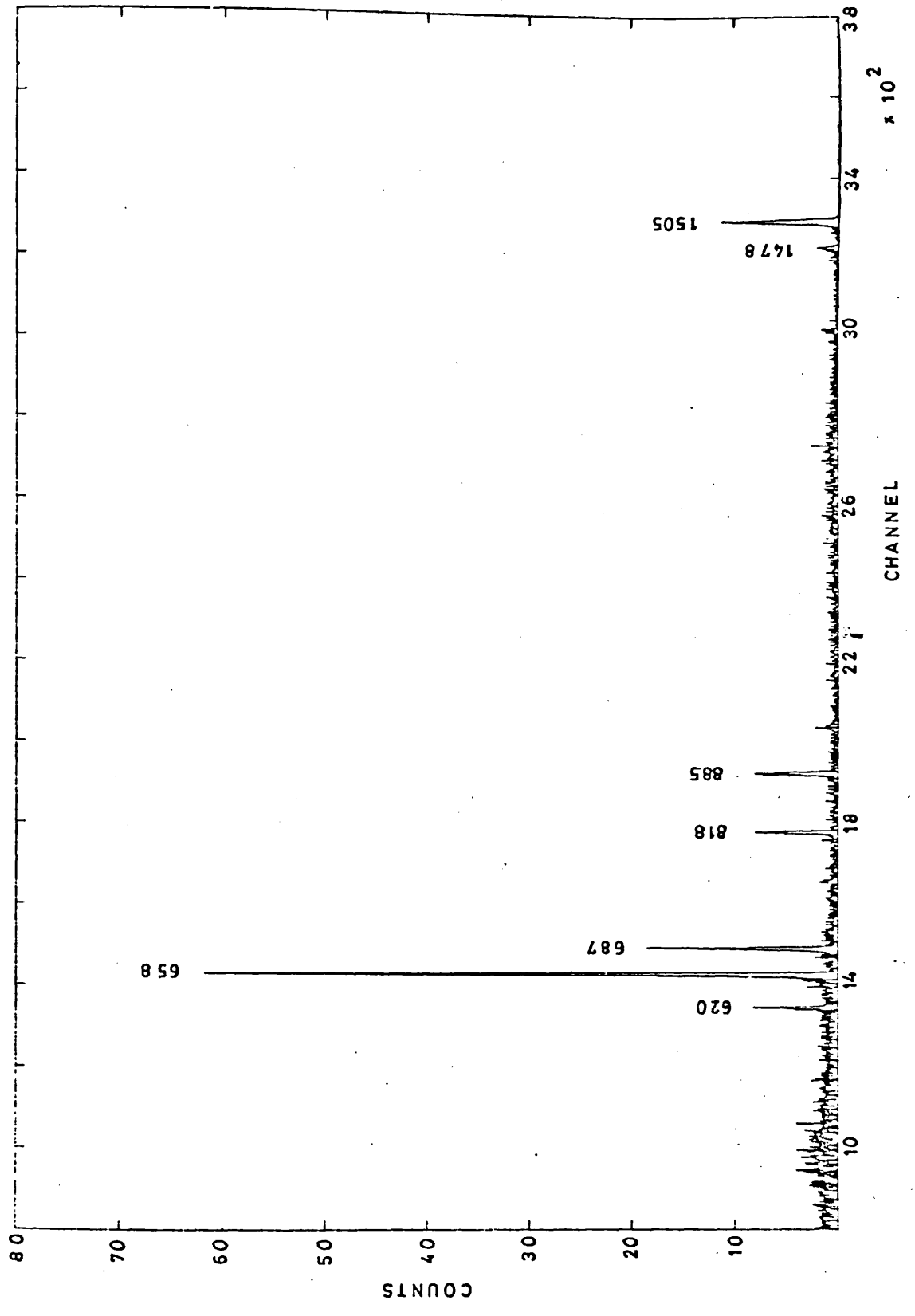

Fig.(3.16.f) Ag - 110 background spectrum in coincidence with 764 keV.

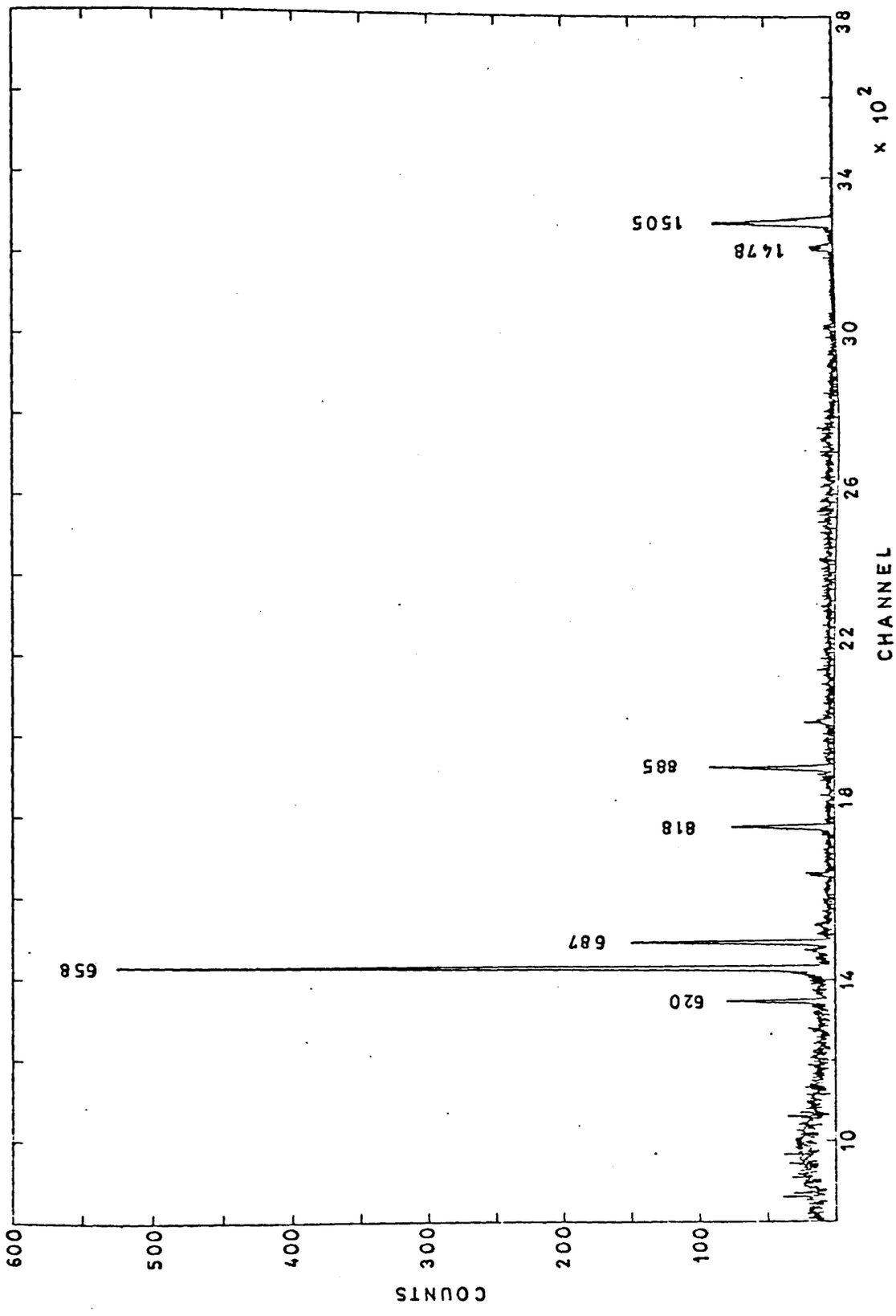

Fig.(3.16.g) Ag – 110 corrected spectrum in coincidence with 764 keV.

Table 3.3.

Coincidence Results of ^{110}Ag

Energy (keV)	Singles Intensity	Coincidence Intensities	
		658 keV	764 keV
446.97 (02)	4.36 (06)	62.21 (2.05)	-
620.38 (02)	3.01 (05)	43.95 (3.71)	59.53 (3.16)
657.75 (01)	100 (1.00)	-	511.3 (17.1)
677.60 (01)	11.06 (12)	194.7 (10.3)	-
686.99 (01)	7.07 (12)	88.36 (6.90)	164.0 (6.4)
706.65 (01)	17.36 (17)	305.3 (13.0)	-
744.22 (02)	4.96 (06)	43.16 (1.42)	-
763.90 (02)	23.88 (26)	311.5 (11.2)	-
817.96 (01)	7.69 (08)	100	100
884.63 (02)	77.72 (86)	1118.0 (41.3)	111.7 (5.4)
937.45 (02)	36.91 (39)	587.7 (21.9)	21.12 (2.27)
1384.30 (03)	27.14 (28)	498.6 (19.9)	-
1475.72 (03)	4.40 (07)	-	101.9 (8.9)
1504.97 (03)	14.39 (17)	27.42 (9.05)	469.5 (13.1)
1562.18 (03)	1.45 (02)	20.03 (0.66)	-

The Table shows the main lines in the β^- decay of $^{110}Ag^m$ to ^{110}Cd.

We notice from this table that the coincidence intensity for the peaks which are in strong coincidence with the gating peaks exceed their relative single intensities. The coincidence intensities were arbitrary normalized to the 818 KeV transition to be 100%.

In view of the above coincidences and singles results, a decay scheme of ^{110}Cd was built and shown in Fig. (3.17). This decay scheme agrees with the decay scheme shown in Ref. 90. This confirms the coincidence data reported in this work and supports the good performance of the DPDC system.

3.8. Source Preparations:

The radioactive sources used during the course of this work were prepared by neutron irradiation in the core tubes of the nuclear reactor of University of London in Silwood Park (see Chapter 1).

^{152}Eu was prepared by irradiation of the Europium oxide enriched to 97% in masses, at Europium 151, 0.5 mg. of the powder element was irradiated for 6 hours, then the source was kept for one week before taking any measurement. This allows any short life activity to be eliminated. The source was packed in a polythene thin tube.

The source strength was about 9 μci. This was chosen to give about 1500 C/sec. at a detector-to-source distance of 25 cm.

^{152}Eu undergoes two branches of decays. It decays by β^- to ^{152}Gd and by EC and β^+ to ^{152}Sm. Thus the singles spectra of the decay of ^{152}Eu contains the transitions of the two nuclei. However, it is difficult to distinguish between these transitions, but the coincidence technique was used to separate the transitions belonging to each nucleus.

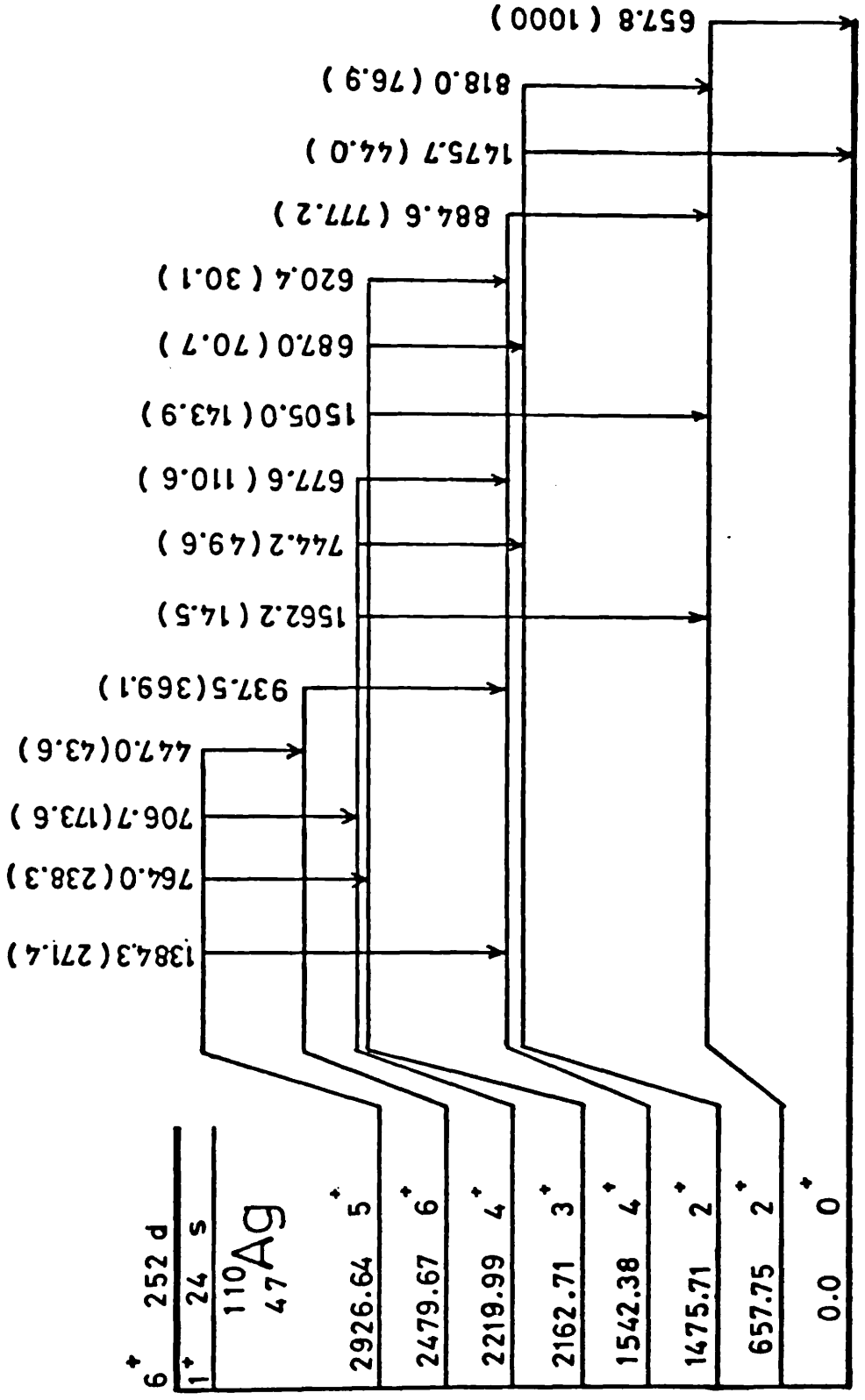

Fig.(3.17) Decay scheme of ^{110}Cd

Fifteen gates were taken to establish the separation, and it was found that four gates were enough to build the decay scheme of ^{152}Gd nucleus, while eleven gates were used to construct the decay scheme of ^{152}Sm. Hence according to this data the new transitions which were seen in this work can belong to one nucleus or the other.

To study the decay scheme of ^{182}W, the β^- decay of ^{182}Ta was investigated. ^{182}Ta was prepared through the (n,γ) reaction. 4mg. of natural ^{181}Ta in a form of thin wire was irradiated for about 6 hours in the core tube of the reactor of University of London. The source was left for one week before taking any experimental data, to allow the short life activities to die away.

The source was packed in a polythene thin tube and its activity was about 10μci which allowed a count rate below 2000 C/sec. at 25 cm. detector-to-source distance.

CHAPTER 4.

STUDIES OF THE ^{152}Gd ISOTOPE

4.1. Introduction:

The decay scheme of ^{152}Gd nucleus is established by considering the β^- - decay of ^{152}Eu (half-life = 13 years). This isotope emits several prominent and well-separated gamma-ray lines, hence used as calibration source for Ge(Li) detectors.

The ^{152}Gd nucleus itself has special importance, since it is considered as spherical nucleus with N = 88[32,42,91]. The energy spectrum is expected to be rather like a harmonic vibrator (see Chapter 2).

Barrette et al.[92] considered that the spectra of this nucleus show more rotational than vibrational characteristics, i.e., it can be described as a deformed nucleus. Riedinger, Johnson and Hamilton[93] preferred to consider the low lying states as resulting from quasirotations, and quasivibrations than to treat them as members of one-, two-, and three-phonon vibrational excitations about spherical equilibrium shapes. Toth, Faler and Rasmussen[94] classified a second 2^+ state at 930 keV and another 0^+ state at 1048 keV as members of a three-phonon vibrational band. Ghomov et al.[95] treated the third 2^+ state at 1109 keV, the second 0^+ state, and a possible 4^+ level as members of a three-phonon band. The work of Gono, Ishihara and Sakai[96] on the conversion electrons emitted in the $^{150}Sm(\alpha,2n)^{152}Gd$ and $^{153}Eu(p,2n)^{152}Gd$ reactions on the other hand indicate the rotation nature of the levels in ^{152}Gd. The results of that work indicate the presence of a rotational band up

through spin of 10, with the 344 and 755 keV states taken as the first and the second members of this band. Another β-band of levels built on the 615 keV state was reported. Bloch, Elbek and Tjom[97] found that the inelastic scattering cross-sections of 12 MeV deutrons for the 615, 930 and 1280 keV levels are similar to those for the 0^+, 2^+ and 4^+ members of the β -bands in deformed nuclei. Thus describing this band as quasi-β band. Baker et al.[98] calculated a ratio of B(E2) values for interband transitions in ^{152}Gd by considering it as an adiabatic rotor.

Conflicting values for energies and intensities emitted by ^{152}Eu were reported by many workers[92,93,98-104] and at the same time new transitions were suggested. Sharma et al.[99] gave a complete list of energies and intensities including those transitions seen by Riedinger et al.[93] and Barrette et al.[92]. Both workers reported new transitions, but they did not agree with each other. Baker et al.[98] reported another fourteen new transitions, some of which were determined from coincidence data. None of these were seen by other workers, while some of the transitions seen in Ref.99 were missing from the Baker et al.[98] list. Yoshizawa et al.[100] have reported a set of data starting from energies above 270 keV with a cutoff energy at 1528 keV.

In this work, all the energies reported in Ref. 99 were observed. Two new transitions reported in Ref. 100 and Ref. 105 were seen, but some of the uncertain transitions reported in the latter were not. Therefore the new level at 1047 keV was ruled out. Sixteen new transitions were seen and seven new energy levels have been suggested. These were confirmed from the coincidence data. The 511 keV transition which was reported in Refs. 99 and 93 but could not be

be placed in the decay schemes reported there, was placed in the present decay scheme. Spins and parities of some levels have been adjusted together with their log ft values and the branching ratios.

4.2. Results:

4.2.1. Singles spectra:

The Ge(Li) detector (no. 1, Table 3.1. in Chapter 3) was used to measure the singles spectra of γ-rays from the decay of ^{152}Eu. Source preparations and the experimental set-up were discussed in Chapter 3. Fig. (4.1) shows the singles spectra of ^{152}Eu. The resulting intensities calculations are given in Table (4.1.). Since the ^{152}Gd nucleus arises from β^- - decay of ^{152}Eu while ^{152}Sm arises mainly from electron capture (EC) and some β^+ decay of ^{152}Eu, a column in this table was introduced to specify the transition corresponding to certain nuclei. Some of these transitions are found to be belonging to both nuclei, these transitions are given to Sm and Gd.

The uncertainties in intensities are about 1%. These are due to uncertainties in the peak area and the errors in the efficiency calibration (see Chapter 3). The relative intensities reported in this work is compared with those of other authors. Good agreement between the values reported in this work and the values reported in the work of others is noticed. But the values reported in Ref. 93, are generally lower than those reported in this work and Refs. 92 and 99.

4.2.2. Coincidence spectra:

The $\gamma - \gamma$ coincidence spectra were written on three magnetic

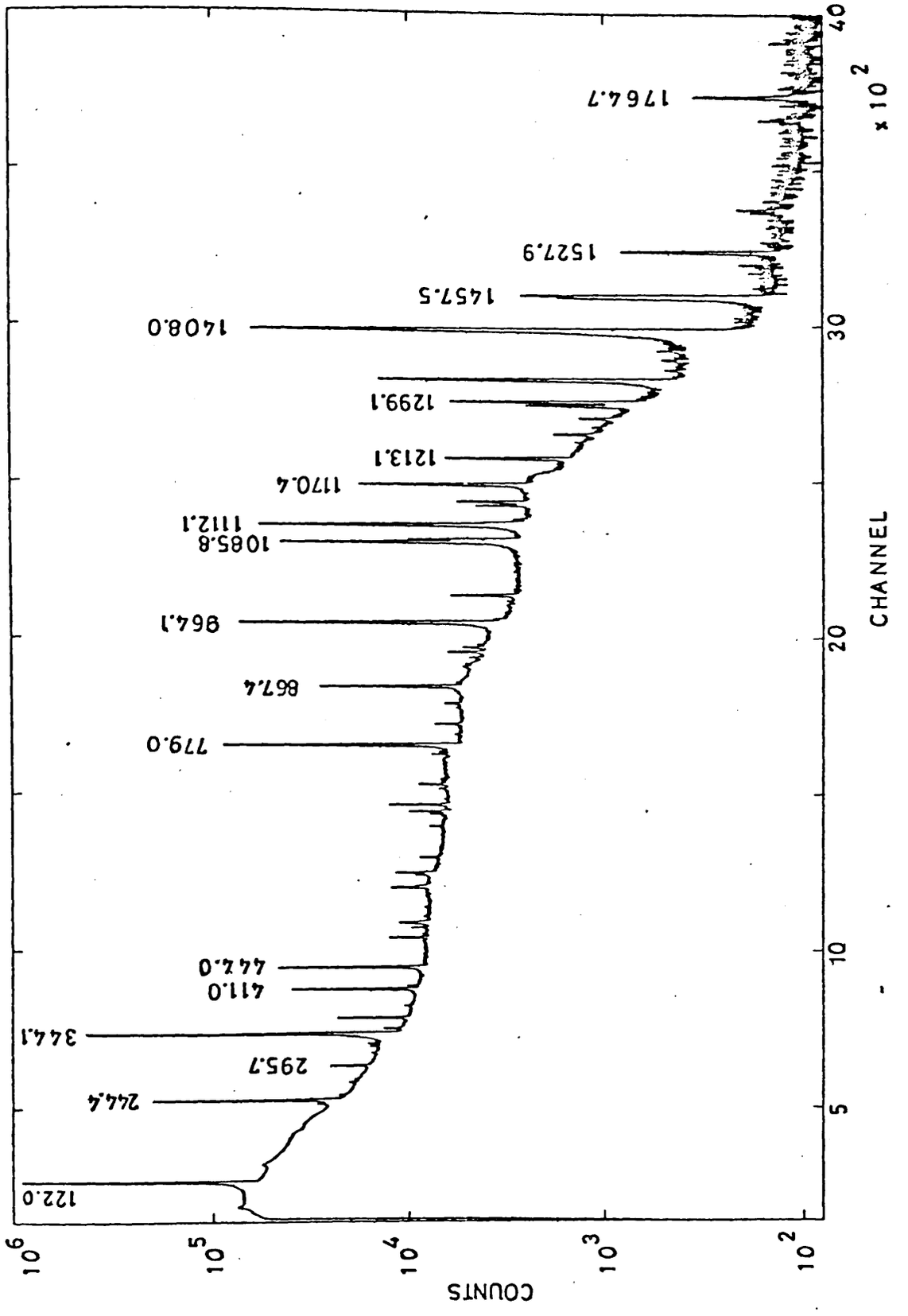

Fig.(4.1.) Single spectrum of ^{152}Eu

TABLE 4.1.

RELATIVE INTENSITIES OF γ -RAYS EMITTED FROM THE DECAY OF ^{152}Eu

Energy (keV)	Nucleus	Intensity related to I(344) = 100				
		Present Work	Ref. 99	Ref. 98	Ref. 92	Ref. 93
121.97(01)	Sm	103.8(1.0)	109.7(2.2)	112.79(3.7)	103.7(3.1)	108(5)
148.11(07)	Sm	0.05(02)	0.12(01)	0.02	0.06(02)	-
167.83(23)	Gd	0.04(01)				
186.03(34)	Gd	0.03(02)				
192.84(01)	Sm&Gd	0.024				
195.09(32)	Sm&Gd	0.08(02)				
203.11(01)	Sm	0.01(-)				
207.69(32)	Sm	0.023(020)	0.03(01)	0.02(009)	0.05(03)	
209.11(09)	Gd	0.083(03)	0.02(01)	0.03(02)	0.06(03)	
212.25(16)	Sm	0.09(02)	0.08(02)	0.076(023)	0.08(02)	0.067(029)
237.41(01)	Sm	0.045(020)	$\leq$ 0.01		0.04(02)	
239.63(01)	Sm	0.054(020)	$\leq$ 0.01		$\leq$ 0.02	
244.43(01)	Sm	28.51(63)	27.91(50)	28.38(93)	27.94(80)	28.2(1.4)
251.58(02)	Sm	0.25(01)	0.28(01)	0.28(04)	0.29(05)	0.26(04)
270.72(05)	Sm&Gd	0.314(020)	0.32(02)	0.28(03)	0.28(05)	0.28(04)
275.20(10)	Sm	0.13(02)	0.17(02)	0.12(01)	0.12(03)	0.11(03)
284.98(70)	Sm	0.02	$\leq$ 0.01	< 0.025	$\leq$ 0.03	
295.66(01)	Sm	1.77(05)	1.61(04)	1.59(05)	1.63(11)	1.51(09)
315.11(06)	Gd	0.24(02)	0.24(02)	0.16(03)	0.15(03)	0.17(03)
324.73(06)	Gd	0.26(02)	0.28(02)	0.27(04)	0.30(05)	0.26(03)
329.19(04)	Sm	0.49(03)	0.49(03)	0.45(05)	0.48(08)	0.44(04)
344.12(01)	Gd	100.00	100	100	100	100
351.81(02)	Gd	0.53(02)	0.08(02)	0.06(01)	0.06(02)	
367.66(01)	Gd	3.25(03)	3.24(07)	3.15(11)	3.23(12)	3.15(18)
378.75(16)	Gd	0.05(01)				
391.73(19)	Sm	0.05(01)				
411.03(01)	Gd	8.43(06)	8.23(17)	8.26(21)	8.40(30)	1.05(40)
415.95(01)	Sm	0.39(03)	0.40(02)	0.39(04)	0.40(05)	0.38(04)
443.91(01)	Sm	11.71(10)	11.66(06)	11.6(8)	11.8(4)	11.2(6)
453.53(03)	Gd	0.05(01)				
462.91(05)	Gd	0.07(02)				
482.34(19)	Sm&Gd	0.11(03)	0.13(01)	0.10(02)	0.09(02)	0.11(02)
488.66(02)	Sm	1.54(02)	1.52(02)	1.49(05)	1.52(10)	1.48(09)
493.51(14)	Sm&Gd	0.16(02)	0.14(02)	0.17(03)	0.12(03)	0.09(04)
497.01(11)	Gd	0.037(017)	0.04(01)	0.03(01)	< 0.04	
503.47(11)	Gd	0.49(03)	0.56(02)	0.55(03)	0.56(06)	0.55(03)
511.12(08)	Gd	0.50(03)	0.29(02)			0.29(14)
520.27(08)	Gd	0.22(02)	0.22(02)	0.24(03)	0.21(03)	0.18(04)
522.86(20)	Sm	0.05(02)	$\leq$ 0.01	0.06(03)	0.04(02)	

TABLE 4.1

RELATIVE INTENSITIES OF γ-RAYS EMITTED

FROM THE DECAY OF ^{152}Eu continued

Energy (keV)	Nucleus	Intensity related to I(344) = 100				
		Present Work	Ref. 99	Ref. 98	Ref. 92	Ref. 93
526.87(16)	Gd	0.08(03)	0.05(02)	0.06(01)	0.04(02)	
534.25(03)	Gd	0.21(02)	0.18(02)	0.16(04)	0.14(04)	0.16(04)
556.96(09)	Sm	0.06(05)	0.04(02)	0.07(02)	0.09(02)	
564.05(02)	Sm	1.78(07)	1.80(05)	1.86(07)	1.92(15)	1.87(15)
566.32(08)	Sm	0.24(06)	0.53(03)	0.45(04)	0.44(10)	0.41(10)
586.27(02)	Gd	1.73(03)	1.77(04)	1.73(07)	1.78(11)	1.62(21)
616.11(02)	Sm	0.04(01)	0.03(02)	0.04(02)	0.05(02)	
621.63(21)	Sm	0.06(03)				
644.00(11)	Sm	0.07(02)	0.03(02)	0.023(007)	0.05(03)	
656.58(02)	Sm	0.55(03)	0.51(03)	0.53(04)	0.58(07)	0.56(05)
661.91(26)	Gd	0.09(02)				
665.40(01)	Sm	0.06(03)	0.03(02)	0.013(006)	0.035(015)	
671.19(15)	Sm	0.13(03)	0.05(02)	0.085(030)	0.07(04)	0.046(021)
674.69(02)	Sm	0.763(032)	0.74(03)	0.58(09)	0.58(08)	0.66(08)
678.65(01)	Gd	1.85(03)	1.80(05)	1.71(11)	1.80(11)	1.61(12)
688.73(01)	Sm	3.12(09)	3.18(08)	3.13(20)	3.09(16)	3.03(L7)
696.88(21)	Gd	0.08(02)				
712.91(02)	Gd	0.36(03)	0.38(03)	0.31(07)	0.36(06)	0.27(07)
719.35(06)	Sm	1.33(03)	1.3(4)	1.19(13)	1.28(12)	1.11(10)
727.66(12)	Sm	0.24(04)	0.04(01)	0.034(007)	$\leqslant$ 0.03	
764.92(03)	Gd	0.804(037)	1.12(03)	0.69(09)	0.71(03)	0.64(11)
768.90(06)	Sm	0.43(03)	0.32(03)	0.27(03)	0.31(05)	0.29(08)
778.96(01)	Gd	48.75(39)	48.74(90)	46.76(53)	48.81(1.1)	46.6(2.3)
795.13(11)	Gd	0.22(03)	0.15(02)	0.16(07)	0.11(05)	0.15(04)
800.61(17)	Gd	0.11(02)				
805.19(04)	Sm	0.10(02)		0.061(02)		
810.46(03)	Sm	1.21(05)	1.21(04)	1.17(05)	1.22(08)	1.08(09)
822.50(05)	Sm	0.08(02)				
825.67(13)	Sm	0.13(02)				
834.94(14)	Gd	0.15(02)				
838.77(01)	Sm	0.08(03)	$\leqslant$ 0.01	0.06(03)	0.06(03)	
841.60(03)	Sm	0.64(03)	0.61(03)	0.60(09)	0.06(07)	0.59(08)
867.42(01)	Sm	15.83(30)	15.83(40)	15.06(27)	15.67(38)	15.0(7)
884.67(06)	Sm	0.10(03)				
901.28(13)	Sm	0.21(04)	0.27(03)	0.28(06)	0.30(05)	0.23(07)
919.43(03)	Sm	1.66(04)	1.67(05)	1.49(05)	1.61(19)	1.47(11)
926.26(26)	Sm	1.00(03)	1.04(04)	0.95(09)	1.02(10)	0.91(08)
930.69(10)	Gd	0.32(03)	0.28(03)	0.27(04)	0.26(05)	0.24(05)
938.44(11)	Gd	0.20(03)				
942.75(21)	Sm	0.09(03)				
957.40(30)	Sm	0.15(07)	0.05(02)	0.11(03)	0.05(03)	
964.09(02)	Sm	54.82(48)	54.95(1.1)	53.08(1.4)	54.0(1.4)	52.6(2.6)

TABLE 4.1

RELATIVE INTENSITIES OF γ-RAYS EMITTED FROM THE DECAY OF ^{152}Eu continued.

Energy (keV)	Nucleus	Intensity related to I(344) = 100				
		Present Work	Ref. 99	Ref. 98	Ref. 92	Ref. 93
969.32(27)	Gd	0.22(08)				
973.79(02)	Gd	0.07(01)	0.05(01)	0.08(01)	0.035(015)	
990.19(09)	Gd	0.14(03)	0.14(02)	0.12(04)	0.10(05)	0.13(04)
1005.18(02)	Sm	2.76(03)	2.8(1)	2.34(16)	2.44(25)	2.37(24)
1010.85(53)	Sm	0.02(02)				
1050.20(13)	Sm	0.13(02)				
1085.83(02)	Sm	39.52(70)	38.7(1.0)	37.12(67)	39.5(1.2)	37.2(2.2)
1089.77(02)	Gd	6.72(11)	6.7(2)	6.16(29)	6.6(6)	6.24(50)
1112.05(02)	Sm	51.67(47)	51.2(1.0)	49.28(67)	50.6(1.4)	49.6(2.5)
1147.23(05)	Sm	2.84(15)				
1170.40(02)	Sm	0.19(03)	0.20(02)	0.13(03)	0.13(03)	0.13(03)
1206.89(02)	Gd	0.03(02)	0.03(02)	0.03(01)	0.05(03)	
1213.08(03)	Sm	5.37(04)	5.24(11)	5.26(20)	5.5(2)	5.11(27)
1249.90(03)	Sm	0.75(03)	0.75(03)	0.65(05)	0.69(06)	0.62(07)
1260.96(04)	Gd	0.13(02)	0.15(02)	0.13(03)	0.13(03)	0.12(03)
1293.03(04)	Sm	0.85(04)	0.39(02)	0.37(06)	0.37(32)	0.38(07)
1299.06(03)	Gd	6.40(73)	6.22(15)	6.15(34)	6.42(32)	6.01(31)
1309.40(36)	Gd	0.04(01)				
1314.50(02)	Sm	0.008	0.03(01)	0.014(005)	0.015(007)	
1348.15(02)	Gd	0.10(01)	0.07(01)	0.063(008)	0.07(01)	0.045(018)
1363.46(06)	Sm	0.10(01)	0.11(01)	0.098(012)	0.10(01)	0.084(024)
1377.57(10)	Sm	0.13(01)				
1389.39(03)	Sm	0.02	$\leq$ 0.01	0.025(005)	0.02(01)	
1407.98(03)	Sm	83.25(1.60)	77.9(1.5)	76.2(2.2)	80.78(2.10)	77.6(3.9)
1457.47(03)	Sm	1.97(04)	1.92(04)	1.87(10)	1.92(15)	1.91(10)
1527.81(03)	Sm	0.97(02)	0.99(03)	1.14(07)	1.00(06)	1.30(07)
1538.24(59)	Sm	0.010(008)	0.009(003)	0.008(002)		0.0054(0022)
1605.56(03)	Gd	0.03(01)	0.04(01)	0.029(006)	0.03(01)	0.027(006)
1607.98(03)	Sm	0.019(010)	$\leq$ 0.02	0.021(005)	0.180(006)	0.023(005)
1643.01(03)*		0.003	0.004(002)			0.019(004)
1646.80(03)	Sm	0.025(010)	0.03(01)	0.024(005)	0.022(005)	0.026(005)
1661.87(03)	Sm	0.030(001)				
1728.83(03)	Gd	0.04(001)				
1764.65(05)	Gd	0.41(01)				
1768.19(03)	Sm	0.05(02)	0.03(01)	0.033(004)	0.032(005)	0.033(003)

* Cannot be placed in the decay scheme

tapes, then analysed off-line by the computer program SAMPO[66]. To establish the decay scheme of ^{152}Gd, four energy gates were taken to show the coincidence between these gates and the rest of the spectrum. These were 344, 411, 586 and 779 keV. The first level in ^{152}Gd is excited at 344 keV and most of the transitions are in cascade with the transition 344 keV which depopulates this level to ground. Hence, to establish the decay scheme of this nucleus, the energy gate at the 344 keV line has to be taken.

Barratte et al.[92] took only this gate to build up their decay scheme. In this work, another three gates were taken, hence more coincidence data is provided to confirm the existence of the levels in the decay scheme. The energy gate at 586 keV was taken to investigate the existence of the two new transitions at 193 and 195 keV which depopulate the 1123(3^-) and 1318(2^+)keV levels to 930(2^+) and 1123(3^-) keV levels, respectively (see Fig. 4.4.). The 779 keV gate was taken to provide coincidence support for the new transition 168 keV which depopulates the new level at 1719(2^+) keV to the 1551 (4^+) keV level. Thus, the above gates were chosen because they are strong peaks and at the same time depopulate three different levels. The intensity of the 1090 keV line is quite high, but this γ -ray is very close to the 1086 keV line, hence there is always a possibility for mixing with ^{152}Sm nucleus if we gate with the 1090 keV line.

Table (4.2.) shows these coincidence results. The first row shows the energy gates, the first column shows the energy transitions depopulating energy levels in ^{152}Gd. The symbols VS, S, W, VW stand for very strong, strong, weak and very weak, respectively. These entries show the strength of the observed γ -rays relative to the other γ -rays in the total spectrum. The total spectrum is shown in

TABLE 4.2.

γ- γ COINCIDENCE RESULTS FROM THE DECAY OF ^{152}Eu.

Energy (keV)	GATES (keV)			
	344	411	586	779
167.83	W	S	-	-
186.03	W	S	W	S
192.54	W	-	S	-
195.09	W	W	S	W
209.11	W	VW	-	-
270.72	W	-	-	-
315.11	S	-	-	-
324.73	W	-	-	-
344.12	-	VS	VS	VS
351.81	-	-	S	-
367.66	S	VS	-	-
378.75	W	-	W	-
411.03	VS	-	-	-
453.53	S	-	-	-
462.91	W	-	-	-
482.34	W	-	-	-
493.51	W	-	-	-
497.01	W	-	-	-
503.47	VS	-	VS	
511.12	S	-	-	-
520.27	S	W	W	VW
526.87	S	W	-	-
534.25	W	-	-	-
586.27	VS	-	-	-
661.91	W	-	-	-
678.65	VS	VS	-	-
696.88	S	-	-	-

TABLE 4.2.

$\gamma - \gamma$ COINCIDENCE RESULTS FROM THE DECAY of ^{152}Eu cont.

Energy (keV)	GATES (keV)			
	344	411	586	779
712.91	W	-	S	-
764.92	W	-	-	-
775.96	VS	-	-	-
795.13	W	S	-	-
800.61	VW	-	-	-
834.94	W	-	W	-
938.44	VW	-	-	-
973.79	VS	-	-	-
990.19	W	-	-	-
1089.77	VS	-	-	-
1206.89	W	-	-	-
1260.96	W	-	-	-
1299.06	S	-	-	-
1348.15	S	-	-	-

Fig.(4.2.). The coincidence spectra are shown in Figs. (4.3.a.), (4.3.b.), (4.3.c.) and (4.3.d.).

4.3. Decay scheme and level properties:

The decay scheme (Fig. (4.4.)) was established on the basis of the coincidence results of four gates (Table 4.2.) and the energy sum relations (Table 4.3.). On the left of the Fig, are shown the energy levels, spins, parities, β^- - feeding branching ratios (B.R.) and the log ft. values, respectively. The number at the base of the arrow indicates the energy of the transition, while between brackets is shown the relative intensity of the transition which was normalized to the intensity of the 344 keV energy as 1000. The new levels and transitions observed in this work are shown as dotted lines.

Table (4.4.) shows the B.R.s, the log ft. values for the β^- - decay of ^{152}Eu and the deduced spins and parities. The B.R.s were calculated from the balance between the decay and the feeding γ-rays for each level. The values reported here agree with those reported in Refs. 92, 93 and 105 (within the reported errors). The value reported in Refs. 92 and 105 for the 1109(2^+) keV level was twice the value reported here. In Ref. 93, the value reported was (0.097%) which is close to the value given in this work (Table 4.4.). In this work, as well as in Ref. 93, the 1109 keV single transition was not seen, for if it exists it will be masked by the strong peak at 1112 keV, hence the B.R. of this work is low. However, this difference in B.R. did not affect the log ft. value very much and the deduced spin and parity are not affected. The energy level at 615(0^+) keV could not be given a B.R. from direct balance between decay and feeding γ-rays, but the

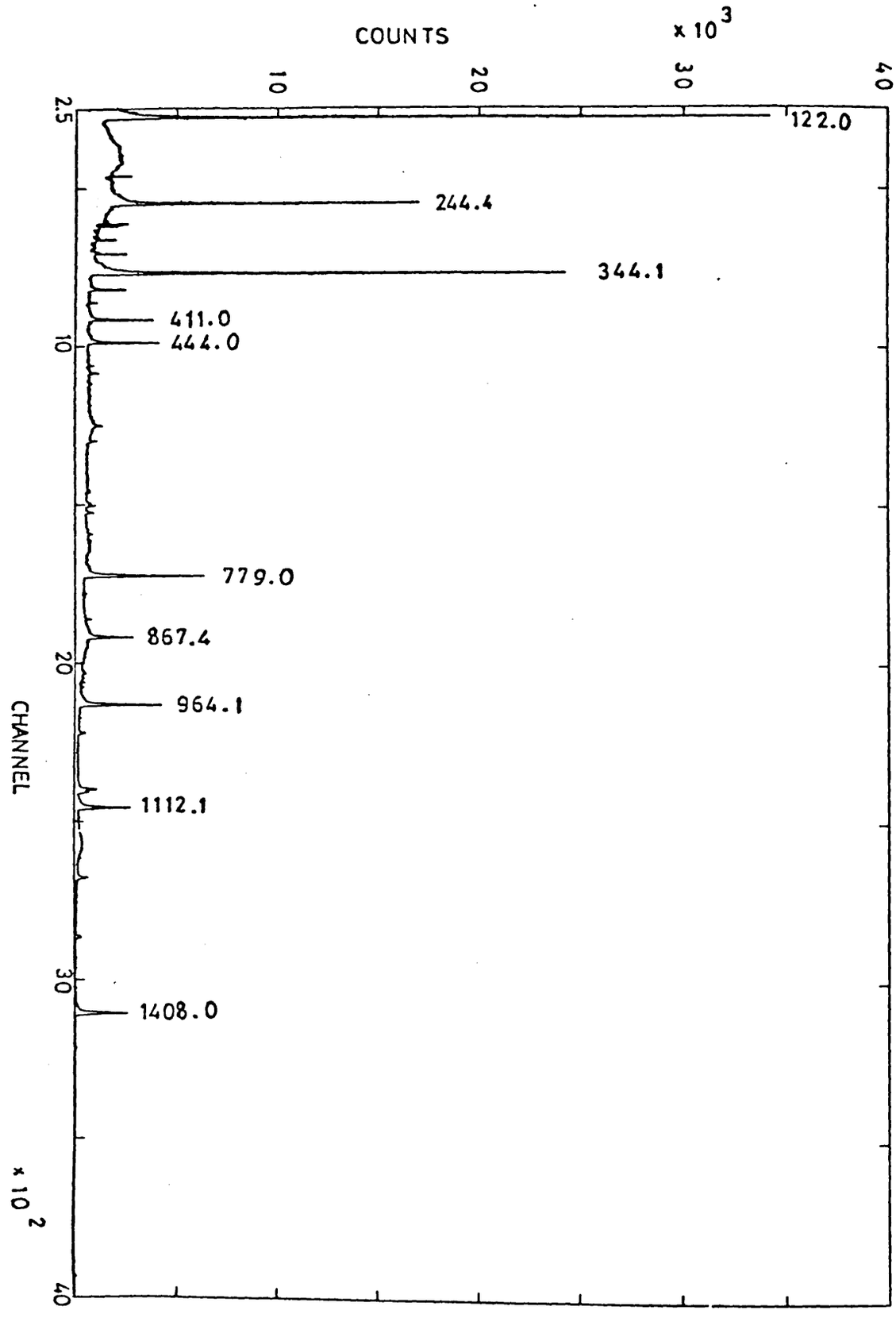

Fig. (4.2.) ^{152}Eu Total spectrum.

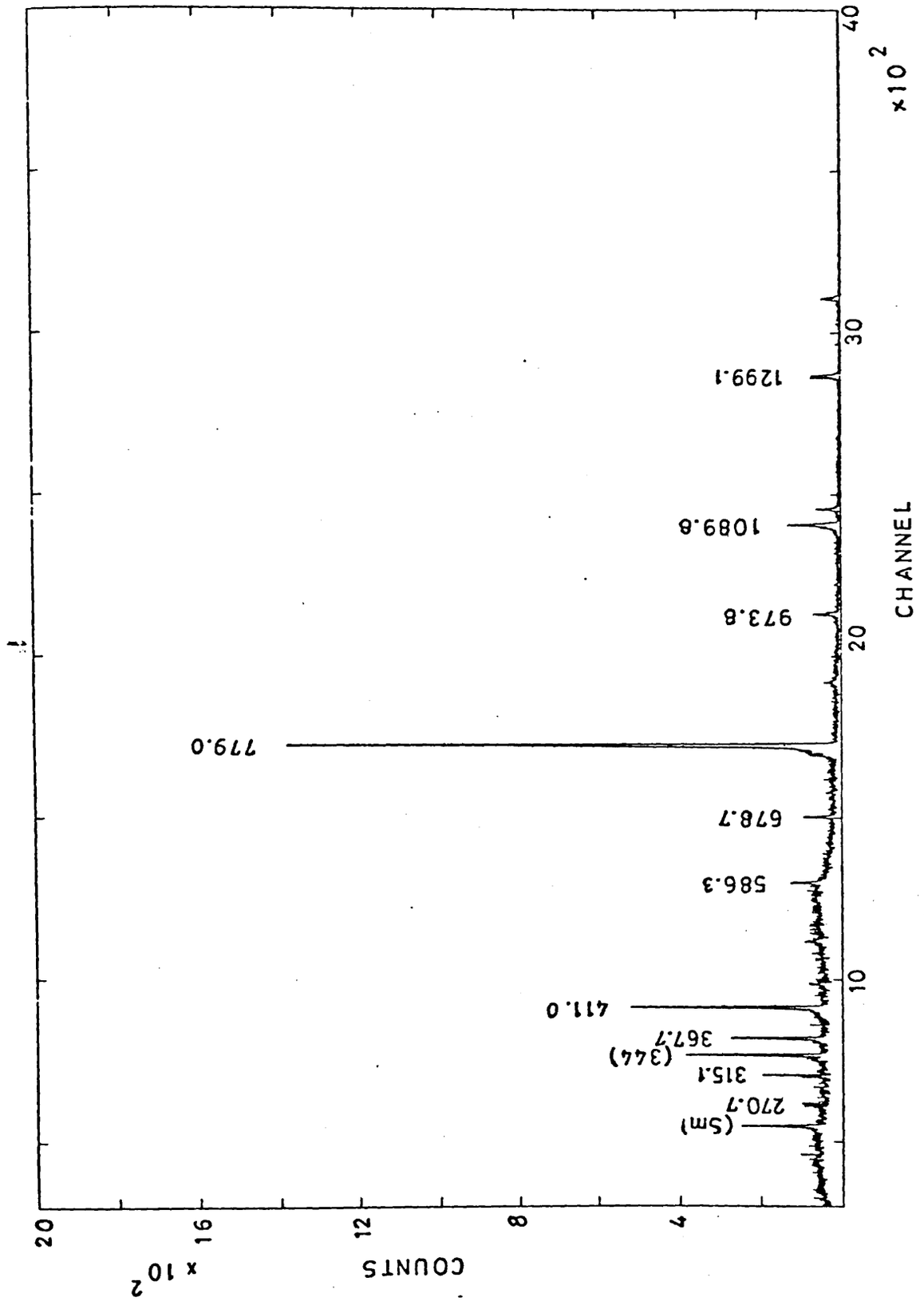

Fig. (4.3.a.) ^{152}Eu spectrum in coincidence with 344 keV.

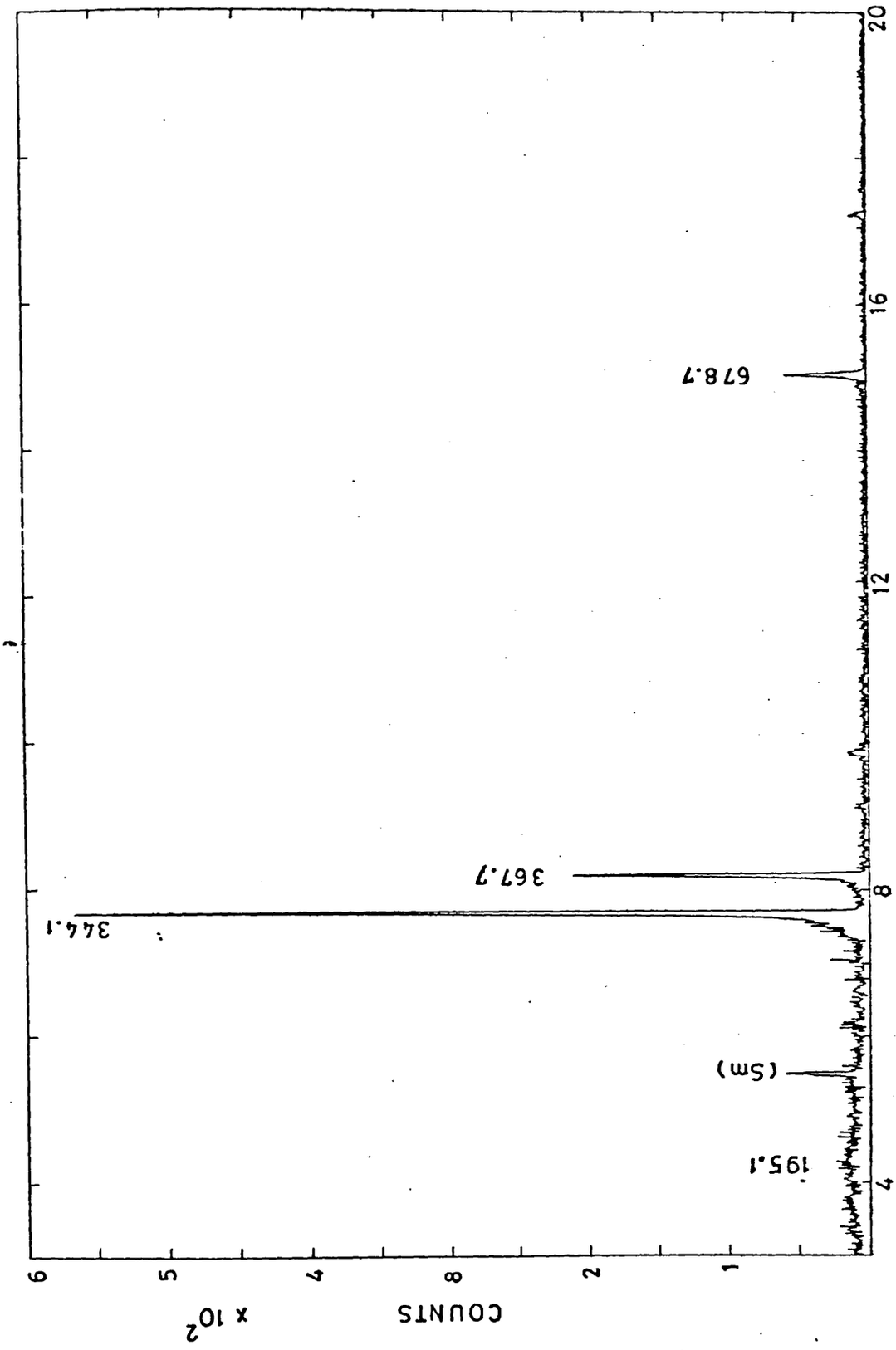

Fig. (4.3.b.) ^{152}Eu Spectrum in coincidence with 411 keV.

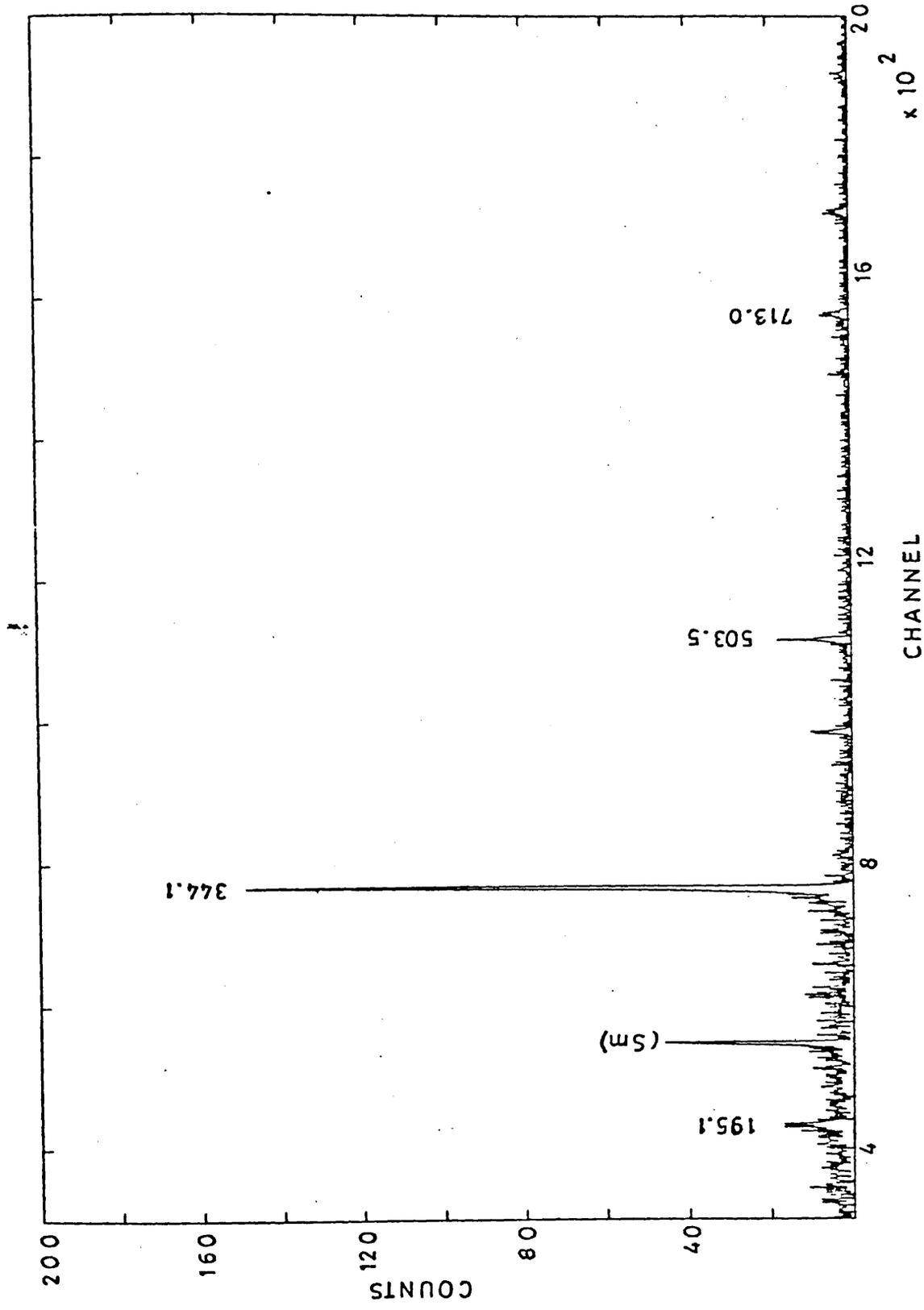

Fig.(4.3.c.) ^{152}Eu spectrum in coincidence with 586 keV.

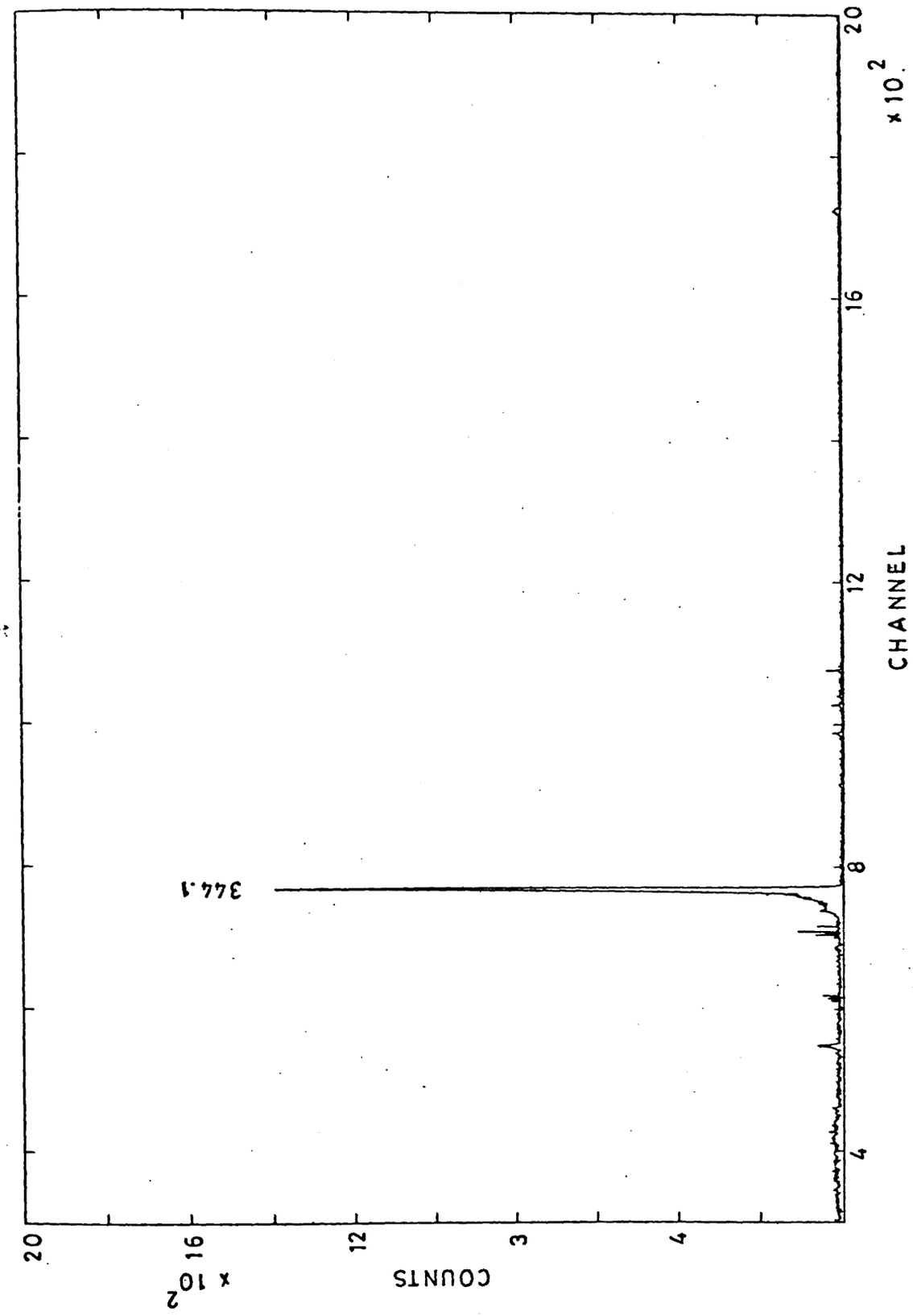

Fig. (4.3.d.) ^{152}Eu spectrum in coincidence with 779 keV.

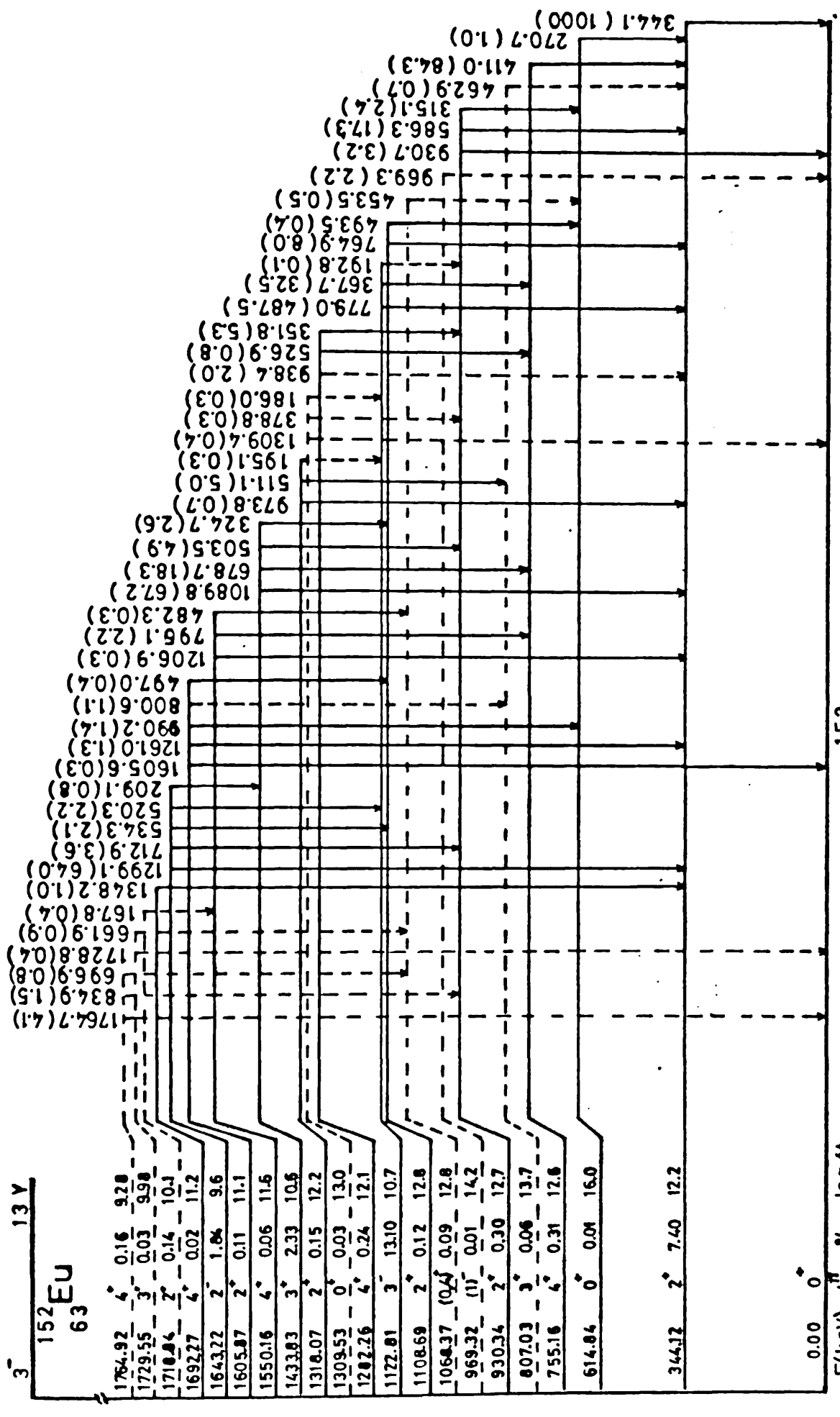

Fig. (4.4) Decay scheme of ^{152}Gd

TABLE 4.3.

ENERGY RELATIONS FOR ^{152}Gd

ENERGY OF TRANSITION (keV)	ENERGY SUM (keV)	ENERGY LEVEL (keV)
344.12	344.12	344.12
270.72 + 344.12	614.84	614.84
411.04 + 344.12	755.16	755.16
462.91 + 344.12	807.03	807.03
315.11 + 270.72 + 344.12	929.95	930.34
586.27 + 344.12	930.39	
930.69	930.69	
969.32	969.32	969.32
453.53 + 270.72 + 344.12	1068.37	1068.37
493.51 + 270.72 + 344.12	1108.35	1108.69
764.92 + 344.12	1109.04	
192.61+315.11+270.72+344.12	1122.56	1122.81
367.66 + 411.03 + 344.12	1122.81	
778.96 + 344.12	1123.08	
351.81 + 586.27 + 344.12	1282.20	1282.26
526.87 + 411.03 + 344.12	1282.02	
938.44 + 344.12	1282.56	
186.03 + 778.96 + 344.12	1309.11	1309.58
378.75 + 586.27 + 344.12	1309.14	
503.47 + 462.91 + 344.12	1310.50	
195.09 + 778.96 + 344.12	1318.17	1318.07
511.12 + 462.91 + 344.12	1318.15	
973.79 + 344.12	1317.91	
324.73 + 764.92 + 344.12	1433.77	1433.83
503.47 + 586.27 + 344.12	1433.86	
678.65 + 411.03 + 344.12	1433.80	
1089.77 + 344.12	1433.89	
482.34 + 453.53 + 270.72 + 344.12	1550.71	1550.66
795.13 + 411.03 + 344.12	1550.28	
1206.89 + 344.12	1551.01	
497.00 + 764.92 + 344.12	1606.04	1605.87
800.61 + 462.91 + 344.12	1607.64	
990.19 + 270.72 + 344.12	1605.03	
1260.96 + 344.12	1605.08	
1605.56	1605.56	

TABLE 4.3.

ENERGY RELATIONS for ^{152}Gd continued.

ENERGY OF TRANSITION (keV)	ENERGY SUM (keV)	ENERGY LEVEL (keV)
209.11 + 1089.77 + 344.12	1643.00	
520.27 + 778.96 + 344.12	1643.35	
534.25 + 764.92 + 344.12	1643.29	1643.22
712.90 + 586.27 + 344.12	1643.29	
1299.06 + 344.12	1643.18	
1348.15 + 344.12	1692.27	1692.27
167.83 + 1206.89 + 344.12	1718.84	1718.84
661.91 + 453.53 + 270.72 + 344.12	1730.28	1729.55
1728.83	1728.83	
696.88 + 453.53 + 270.72 + 344.12	1765.25	
795.13 + 969.32	1764.45	1764.92
834.94 + 586.27 + 344.12	1765.33	
1764.65	1764.65	

TABLE 4.4.

SUMMARY OF THE LEVEL PROPERTIES IN ^{152}Gd

Energy Level (keV)	E_{β^-} (keV)	ΣI_γ feed	ΣI_γ decay	B.R. %	log ft.	deduced J^π
344.12	1475.08	73.72	103.00	7.40	12.16	2^+
614.84	1204.36	0.33	0.07	0.01	16.00	0^+
755.16	1064.04	5.39	8.59	0.81	12.57	4^+
807.03	1013.09	1.15	0.12	0.06	13.67	3^+
930.34	888.86	112	2.32	0.30	12.72	2^+
969.32	849.88	0.25	0.30	0.01	14.15	$(1)^-$
1068.37	750.83	0.20	0.05	0.09	12.80	$(0,4)^+$
1108.69	710.51	0.30	0.80	0.12	12.81	2^+
1122.81	696.39	0.28	52.07	13.10	10.68	3^-
1282.26	536.94	-	0.96	0.24	12.06	4^+
1309.58	509.62	-	0.14	0.03	12.93	0^+
1318.07	501.13	-	0.60	0.15	12.16	2^+
1433.83	385.37	0.08	9.30	2.33	10.57	3^+
1550.66	268.54	0.04	0.28	0.06	11.59	4^+
1605.87	213.33	-	0.44	0.11	11.08	2^+
1643.22	175.91	-	7.27	1.84	9.64	2^-
1692.27	126.93	-	0.10	0.02	11.19	4^+
1718.84	100.36	-	0.56	0.14	10.05	2^+
1729.55	89.65	-	0.13	0.03	-9.98	3^+
1764.92	54.28	-	0.66	0.16	-9.28	4^+

spin and parity of this level are well determined to 0^+. This means that the B.R. of this level must be < 0.01 because this value will give log ft. a value of about 16, which agrees with the deduced spin and parity. The B.R. given to the new level at 1068 $(0,4^+)$ keV, was suggested in view of the deduced spin and parity $(0,4^+)$, the calculated value is 0.09%. The new level at 807 keV was given a B.R. equals 0.06, since this value is the difference between the 27% of the total β^- - decay of ^{152}Eu [90] and the sum of the B.R. of all levels in ^{152}Gd. This B.R. gives log ft. value equals 13.67. The β^- - decay selection rules[106], when applied to this level suggested second forbidden transition $(J^\pi = 1^-)$, but if we consider this β^-transition to be first forbidden $(J^\pi = 3^+)$, this assignment will agree with the spin and parity deduced for this level using the calculations of the IBM model. If this is the case, this new level could have more transitions depopulating it, hence increasing its B.R., decreasing log ft. to the first forbidden transition and making 3^+ more favourable. The log ft. values were calculated according to the relations given in Ref. 90, the end point energies of the β^- decay were calculated using the given Q-value in the same reference (Q = 1.8192 MeV). The deduced spins and parities were worked out according to the β^- - decay selection rules.

Table (4.5.) shows experimental and theoretical K-shell conversion coefficients for β^- - decay of ^{152}Eu (αk). The β^-electron intensities were taken from Ref. 107 and the relative intensities of the γ- transitions were taken from the singles measurements reported in the present work. The experimental (α_k) values were normalized to the theoretical α_k of 344 keV transition, which is considered pure E2 transition. The theoretical (α_k) were taken from Ref. 21. Good agreement between theoretical and experimental (α_k) values is shown in Table (4.5.). This

TABLE 4.5.

K-SHELL INTERNAL CONVERSION CO-EFFICIENTS FOR ^{152}Gd

E_γ (keV)	$J_i^\pi \rightarrow J_f^\pi$	Experimental α_K (x10^4)	Theoretical α_K (x10^4)			Deduced multi-polarity
			E1	E2	M1	
270.72	$0^+ \rightarrow 2^+$	875 (337)	180	640	1100	E2
315.11	$2^+ \rightarrow 0^+$	188.61(120.02)	140	395	730	E2
344.12	$2^+ \rightarrow 0^+$	300	100	300	580	E2
367.66	$3^- \rightarrow 4^+$	58.88(7.68)	80	250	500	E1
411.03	$4^+ \rightarrow 2^+$	172.99(14.82)	62	180	360	E2
503.47	$3^+ \rightarrow 2^+$	132.9(45.0)	38	105	205	E2
586.27	$2^+ \rightarrow 2^+$	264.93(48.16)	28	74	145	E0/E2
678.65	$3^+ \rightarrow 4^+$	45.53(6.83)	21	54	104	E2
764.92	$2^+ \rightarrow 2^+$	46.64(15.54)	16.5	42	77	E2
778.96	$3^- \rightarrow 2^+$	16.23(1.70	16	40	74	E1
1299.06	$2^- \rightarrow 2^+$	7.81(1.95)	6.2	13.8	24	E1

enables correct multipolarity for the given transitions to be assigned, these deduced multipolarities were written in the last column of Table (4.5.).

4.4. Nuclear model calculations:

4.4.1. Collective vibrations:

As ^{152}Gd nucleus is considered a spherical nucleus, it should show vibrational spectra. The results of calculations based on theoretical considerations, discussed in Chapter 2 are given in Table (4.6.). Column 3 shows the vibrational calculations based on the spherical shape assumption of ^{152}Gd nucleus. Column 4 gives the IBM calculations based on SU(5) limit, column 5 shows the pairing plus quadrupole (PPQM) calculations as given in Ref. 108, while the last column shows calculations based on variable moment of inertia (VMI) model as given in Ref. 109. From the table it is seen that vibrational and IBM calculations show degenerate states (see Chapter 2) and give more information about the nucleus than the other two models. Fig. (4.5) shows the experimental and the theoretical (vibrational) energy levels as determined in this work (see the degeneracy of the levels). The details of level structure are discussed below:-

- The ground state band ($344(2^+)$, $755(4^+)$, $1068(0,4^+)$ and $1109(2^+)$keV):

The theoretical energy of the first excited state, i.e., the one-phonon excitation was normalised to the experimental value 344.12 keV (2^+), the energy of the second excited state is 688 keV (4^+). This is in poor agreement with the experimental 755 keV(4^+). The spin of this level was confirmed from the α_k value of the 411 keV

TABLE 4.6.

THE ENERGIES OF LEVELS IN ^{152}Gd FOUND EXPERIMENTALLY COMPARED WITH VIBRATIONAL AND IBM (FOR POSITIVE PARITY) AND WITH VALUES FROM OTHER NUCLEAR MODELS

J^π	Energy band	Energy (keV)				
		Experiment	Vibration	IBM	PPQM Ref. 108	VMI Ref. 109
2^+	g	344.12	344.12	344.12	361	341.9
0^+	β	614.84	614.84	614.84		
4^+	g	755.16	688.24	755.16		769.7
3^+		807.03		834.38		
2^+	β	930.34	958.96	930.34	1180	
$(1)^-$		969.32				
$(0,4)^+$	g	1068.37	1032.36	1233.11		
2^+	g	1108.69	1032.36	1108.69	1717	
3^-		1122.81				
4^+	β	1282.26	1303.08	1312.76		1267.2
0^+	β	1309.58	1303.08	1312.76		
2^+	β	1318.07	1303.08	1312.76		
3^+		1433.83				
4^+		1550.66		1480.68		
2^+	β	1605.87	1647.20	-		
2^-		1643.22				
4^+	β	1692.27	1647.20			
2^+		1718.84		1762.11		
3^+		1729.55		1762.11		
4^+		1764.92		1762.11		

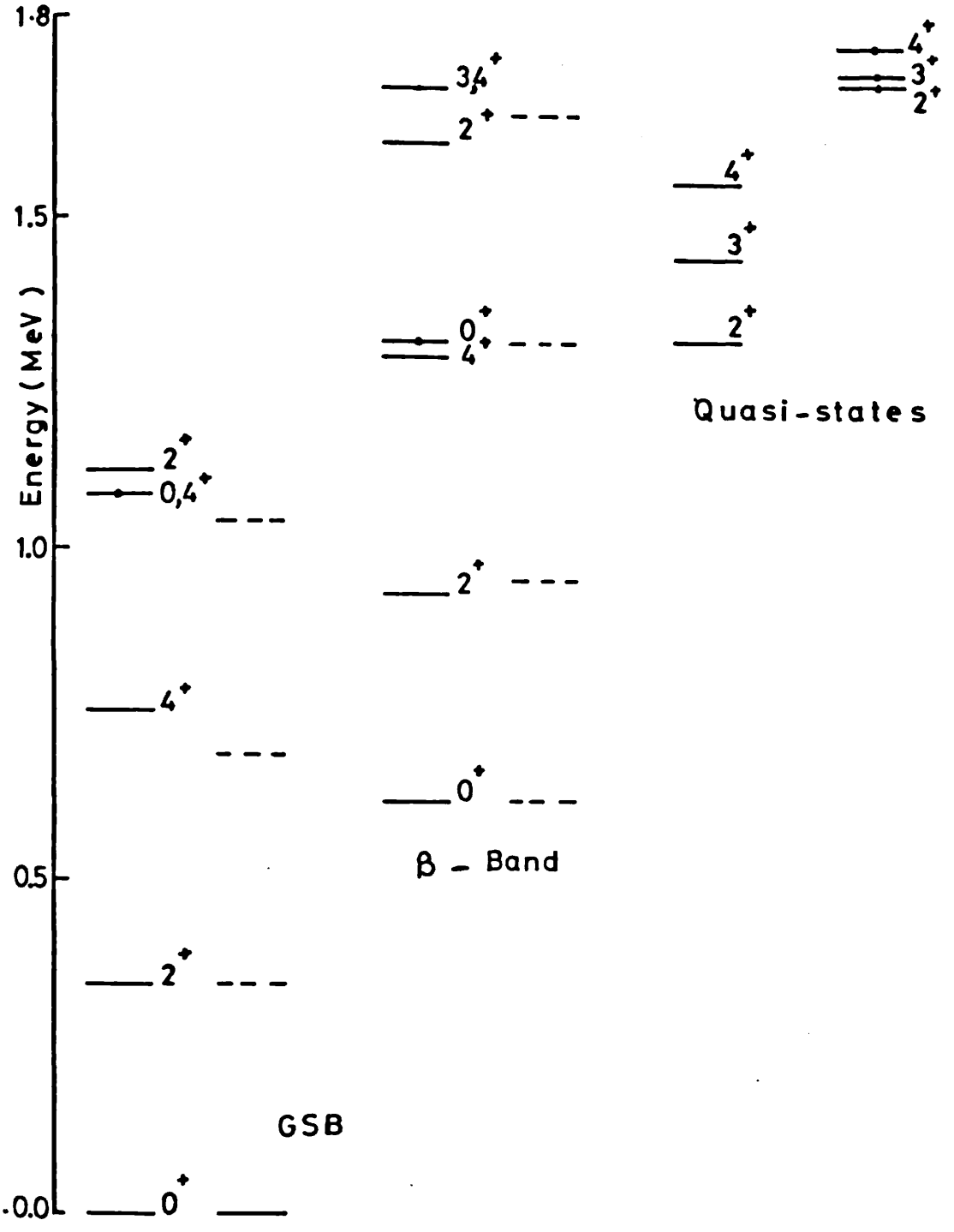

Fig. (4.5.) Experimental and theoretical vibrational (dotted lines) energy levels in ^{152}Gd. New levels are marked with a dot in the middle.

transition depopulating this level (Table 4.5.) to the first excited state. The calculated log ft. value for this level gives another support for the 4^+ assignment for it (Table 4.4.). The three phonon excitation is expected at 1032 keV (Table 4.6). This state may be five-fold degenerate with spins 0,2,3,4 and 6. We have two experimental levels at this excitation state, namely the new level at 1068 keV ($0,4^+$) and the 1109 keV (2^+) level. Both are in agreement with the theory. The spin of the 1068 keV level could be either 0^+ or 4^+, since this level is considered as one of the degenerates of the above three phonon state with $J^\pi = 6^+$.

The variable moment of inertia (VMI) calculations show good agreement with experiment, while the PPQM expectations are in less agreement with experiment than vibrational and IBM calculations performed in this work. Since the PPQM was built on the dynamic deformation theory[93] which allows rotational degrees of freedom for the ^{152}Gd nucleus, this supports the assumption that this nucleus is spherical i.e., having vibrational spectra.

The new level at 1068 keV was introduced in view of observation of three new transitions, 454, 662 and 697 keV. The 1068 keV decays to the 0^+ member of the β-band (615 keV level) by the 454 keV transition. The gate 344 keV shows strong coincidence between this gate and the 454 keV transition (see table 4.2.), this supports the existence of the new level at 1068 keV. The new transition 662 keV is in weak coincidence with the 344 keV gate (Table 4.2.). This supports the new level at 1730 (3^+) keV, since this level decays to the new level at 1068 keV through the 662 keV gamma-ray (see Fig. 4.4.). The transition 697 keV is in strong coincidence with the 344 keV gate (see Table 4.2.), but this transition depopulates a new level

at 1765 (4^+) keV to the new level at 1068 keV, this provides evidence for the existence of these new levels. The spin and parity of the level at 1109 keV is confirmed from log ft. values (Table 4.4.) and from the (α_k) values (TAble 4.5.). The transition 765 keV depopulates this level to the first excited state (344 keV level), the multipolarity of this transition is E2, which supports the 2^+ assignment for this level.

- The β -band:

This band is consisted fromthe levels 615(0^+), 930(2^+), 1282(4^+), 1310(0^+), 1318(2^+), 1606(2^+) and 1692(4^+) keV. A β -band could occur in the spectra of vibrational nuclei[110], this band started with a(0^+) level and the band is built on this level. The 615 keV level was suggested as the starting level for this band. The first excited state is expected at 959 (2^+) keV (see Table 4.6.), while the second excited state is expected at 1303(4^+) keV. This state is degenerate with three spins (0^+, 2^+ and 4^+). The level at 1282 keV is 4^+, this spin is confirmed from log ft. values (Table 4.4.). The new level at 1310 keV is (0^+), this is supported from the log ft. values (Table 4.4.). This level was suggested because three new transitions were observed. These are 186, 379 and 1309 keV. The first energy was seen to be in strong coincidence with both gates 411 and 779 keV (Table 4.2.), while this transition was seen in weak coincidence with the 344 and 586 keV gates. These coincidence data support the existence of the new level at 1310 keV. The new transition 379 keV is in weak coincidence with the two gates 344 and 586 keV (Table 4.2.), while the transition 1309 keV depopulates the 1310 keV level directly to ground. This supports the positive parity of this level and its existence (see Fig.

4.4.). Thus the two 1282 (4^+) and 1310 (0^+) keV levels are in good agreement with theoretical second excited state at 1303 keV (Table 4.6.).

The third degenerate state for the 1303 keV is the 1318 keV (2^+) level. This agrees with theoretical value. The spin and parity of this level is supported from log ft. values (Table 4.4.). The new transition 195 keV depopulates this level to the negative parity level at 1123 (3^-) keV, this is confirmed from coincidence data. This transition is seen in strong coincidence with the 586 keV gate, which means that the 193 keV new transition exists. (see Fig 4.4.). The other three gates show weak coincidence with these two new transitions (Table 4.2.). The two transitions 193 and 195 keV were seen in both nuclei ^{152}Gd and ^{152}Sm. This was proved from coincidence data (see Chapter 5). The transition 511 keV was reported in Refs. 93 and 99, but could not be placed in their decay scheme. This transition is in strong coincidence with the 344 keV gate, hence this 511 keV transition depopulates the 1318 keV level to the new level at 807(3^+) keV. This proves the existence of this new level. The 1318 keV level may be considered as a member of a quasi-particle γ-like band together with the levels 1434 (3^+) and 1551(4^+) keV.

The third excited state is expected at 1647 (6^+) keV with five degenerates. The level at 1606(2^+) keV was assigned 2^+, this was confirmed from log ft. values (Table 4.4.). The new transition 801 keV depopulates this level to the new level at 807(3^+) keV. This was confirmed from coincidence data, since this transition was seen in very weak coincidence with the 344 keV(Table 4.2.). The level at 1692 (4^+) keV is considered one of the degenerates of the 1647 keV state, since good agreement with this value is seen, the (4^+) assignment agrees

with the log ft. values (Table 4.4.). In Ref. 98, this level was assigned 2^+, but if this assignment is correct, then the 1606 keV level should be either 0^+ or 3^+, but these values do not agree with the log ft values reported for this level (Table 4.4.), therefore the remaining choice is the 2^+ assignment for the 1606 keV level and 4^+ for the 1692 keV level as given above.

4.4.2. The Interacting Boson Model (SU(5) limit):

The theory was discussed in Chapter 2. Here the results and the theoretical parameters of the model are given. These were determined by normalizing theory to four known experimental levels. These levels are the 344 keV (2^+), 755 keV(4^+) of the ground band and the 615 keV (0^+), the 930 keV(2^+) levels of the β -band. The parameters are (see Eqs. 2.14 and 2.15):

α = - 39.409 keV

β = 12.550 keV

γ = 13.291 keV

ϵ = 344.12 keV

C_o = - 73.401 keV

C_2 = -119.156 keV

C_4 = 66.920 keV

The results of the calculations are shown in Table (4.6) and in Fig. (4.6). Theoretical levels are shown as dotted lines in Fig. (4.6). We see good agreement with experimental values especially for the β and and the Z-bands. The different bands of the model are discussed below:

- The Y-band (ground band):

This band is consisted from the levels 344 keV (2^+), 755 keV (4^+)

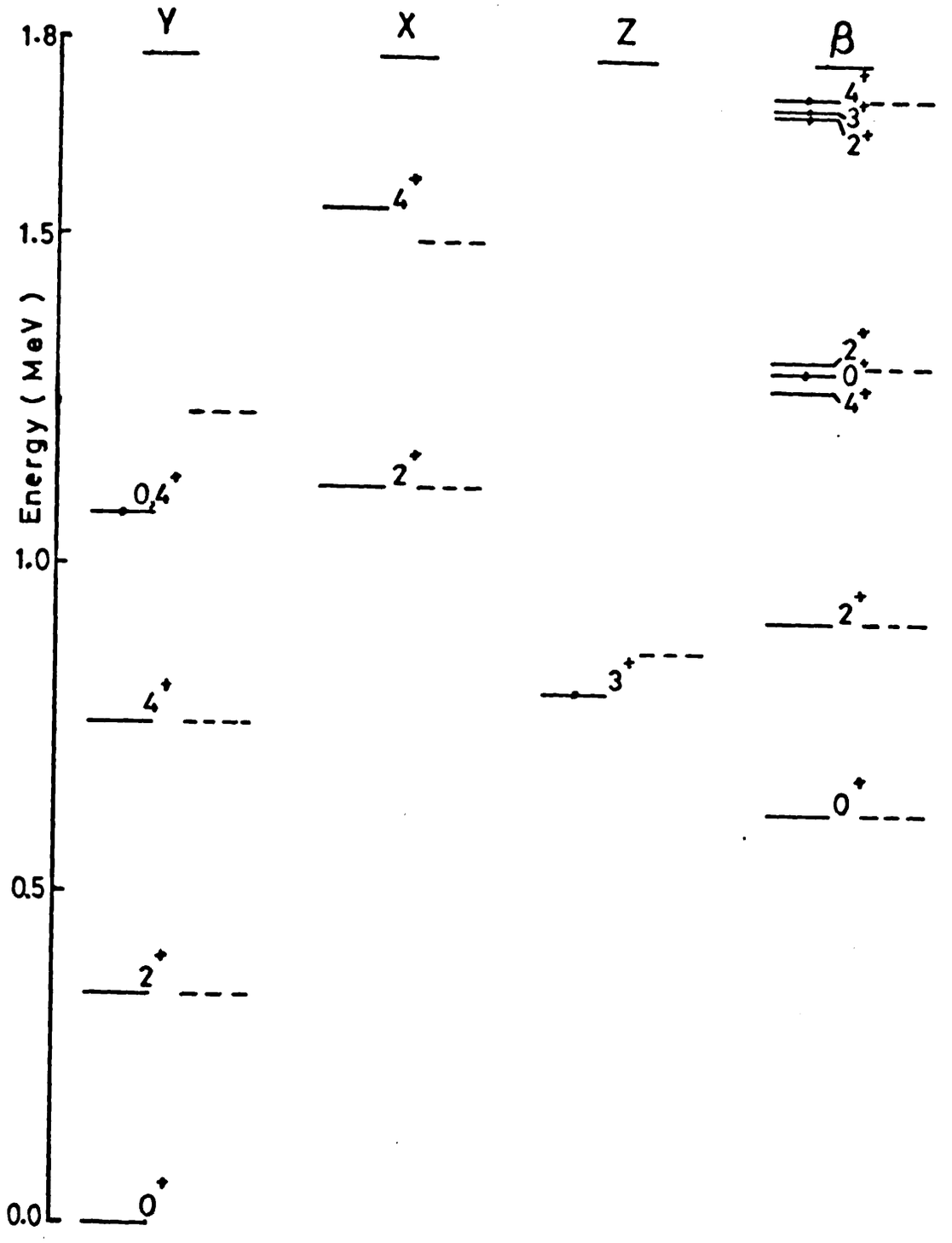

Fig. (4.6). Experimental and theoretical IBM (dotted lines) energy levels in ^{152}Gd. New levels are marked with a dot in the middle.

and 1068 keV ($0,4^+$). The 1068 keV level is one of the degenerates of the $J^\pi = 6^+$ level[111]. The value calculated for this level is 1233 keV. This value is in poor agreement with experiment, this might indicate that either we have large oscillation about the equilibrium spherical shape or we have other configuration for the nucleus at this state. But the collective vibration calculations gave good agreement with the experimental value for this level, thus one may conclude that the IBM might have breaking of symmetry at this level.

- The X-band (levels 1109 (2^+), 1551 (4^+) keV):-

In this band theory was normalized to the 1109 keV experimental level. Theory expectation gave 1481 keV for the 1551 (4^+) keV level (Table 4.6). This value is in poor agreement with experiment, but this level could not be predicted using the vibrational theory (see Section 4.4.1) which indicates a rather complicated structure at this state. Thus, while vibrational model of Bohr and Mottelson[31] failed to interpret this level, the SU(5) limit of the IBM (see Chapter 2) succeeded in predicting it.

- The Z-band (807(3^+) keV):

This new level could not be placed in any band of the vibrational spectrum. In this band, the first excited state is 3^+ (see Reference 42), and the theoretical calculations give 834 keV (see Table 4.6.). This agrees with the experiment. The log ft. values (Table 4.4.) support the 3^+ assignment for this level. The new transition 463 keV is in weak coincidence with the 344 keV gate. This supports the existence of the 807 keV level.

- The β-band:-

This band is consisted from the Levels: 615, 930, 1282, 1310, 1318, 1719, 1730 and 1765 keV. The spin and parity of the 615 (0^+) keV level were confirmed from the α_k values (Table 4.5), where the 271 keV transition which depopulates this level to the 344 keV member of the ground state band is E2 multipole transition. The 930 keV level was assigned the (2^+) value on the bases of α_k values (Table 4.5.) and the log ft. values (Table 4.5). The 315 keV transition depopulates this level to the 615(0^+) keV level. This transition is of E2 multipolarity, hence this supports the (2^+) assignment for the 930 keV level. The 586 keV transition is mixed transition (E0 and E2), since high values of α_k indicates the existence of E0 multipolarity (see Table 4.5) together with the E2 multipolarity. The direct transition to ground state (931 keV transition) supports the 2^+ assignment of the 930 keV level (see Fig. 4.4.)

The 1310 (0^+) keV level is considered one of the degenerates of the 4^+ expected state which equals 1313 keV (Table 4.6). This agrees with the previous experimental value (1310 keV). The second degenerate for the above state is the level at 1318 (2^+) keV, which again agrees with the expected value. The third degenerate is the level at 1282 (4^+) keV; this value agrees with theory (Table 4.6). The new transition 938 keV depopulates this level to the first excited state at 344 keV(2^+) and the coincidence data (Table 4.2) shows weak coincidence between this transition and the energy gate at 344 keV.

We notice that the IBM gives closer values to experiment than collective vibrations for this particular state and its degenerates (Table 4.6). The expectation of theory for the (6^+) state is 1762

keV, the last three levels of this band are considered as degenerates of this state, and the agreement with theory is obvious. This supports the existence of these new levels. We conclude that, while the collective vibration theory failed to predict these three levels, the IBM was able to predict these levels. These results are shown in Fig. (4.6).

4.5. Quasi-structure and negative parity levels:

(I) - The γ-like bands:-

The first band of these two bands is the band starting by the level 1318 keV (2^+), the other two levels are 1434 keV (3^+) and the 1551 keV (4^+). The energy difference between these levels is about 100 keV. This configuration is rather like quasi-band structure where the levels become closer to each other. This band could be referred to as resulting from two quasi-particle excitation, since the energy of the first excited state of this band is higher than that of the (4^+) ground band of the collective quadrupole states[42], i.e., is ≥ 1 MeV which equals twice the pairing gap energy.[31]

The second band is consisted of the new levels 1719 keV (2^+), 1730 keV(3^+) and 1765 keV (4^+). This is again γ-like band with smaller energy spacing than the previous band. This band again can be considered resulting from two quasi-particle excitation. One notes that while the simple vibration theory could not predict these levels, the IBM was able to predict them (except the level at 1434 keV) in the X and β bands of the model. This could support the spherical shape of ^{152}Gd.

The new transition 168 keV depopulates the new level 1719 (2^+) keV to the level 1551 (4^+) keV, the coincidence data show strong coincidence between the 168 keV transition and the 411 keV gate (Table 4.2). This supports the existence of this new level. The new transition 1729 keV depopulates the new level at 1730 (3^+) keV to ground. This supports the positive parity of this level. The two new transitions 835 and 1765 keV depopulate the new level 1765 (4^+) keV to

the 930 (2^+) keV and ground state respectively. Coincidence data show weak coincidence between the 835 keV transition and the two gates at 344 and 586 keV (Table 4.2). This confirms the existence of this level and its spin and parity. The spin and parity of the level at 1434 (3^+) keV are confirmed from log ft. values (Table 4.4) and from α_k values (Table 4.5). Since the two transitions which depopulate this level to 930 (2^+) keV level (503 keV) and to 755 (4^+) keV level (679 keV) are E2 of multipolarity. The 1551 (4^+) keV level is given this assignment (4^+) according to log ft. values (Table 4.4.) The levels of the last band, i.e., 1719, 1730 and 1765 keV are assigned their spins and parities according to the log ft. values (Table 4.4) and in view of the theoretical calculations of the IBM.

(2) - The negative parity levels:

(a) - The two levels at 969 keV (1^-) and 1123 keV (3^-):

The new level at 969 keV was suggested in view of the observation of the new transition 962 keV which depopulate this level to ground. The spin and parity of the 969 keV level were determined from the log ft. value (Table 4.4.). The log ft. value reported was 14.15; this value suggests second forbidden transition for the $3^{\pi} = 1^-$. This level together with the level 1123 keV (3^-) could form a new octupole band. The spin and parity of the 1123 keV (3^-) level were assigned from the log ft. values (Table 4.4) and from the α_k value (Table 4.5). The transition 779 keV depopulates this level to the first excited state of the ground band (Fig. 4.4), the experimental α_k for this transition is in excellent agreement with the theoretical value for E1 multipolarity. This proves the 3^- assignment to the 1123 keV level. The other transition is 368 keV which has E1 multipolarity.

which supports the 3^- assignment to this level. Thus these two levels form octopole band with spin sequence 1^- and 3^-.

(b) - The level at 1643 keV (2^-):

The spin and parity of this level were determined from both log ft. values (Table 4.4) and the α_k values (Table 4.5). The 1299 keV transition is E1 multipole transition. This was deduced from the excellent agreement between the theoretical and experimental α_k values, therefore we assign 2^- to this level.

4.6. Conclusion:

The ^{152}Gd nucleus was considered previously as a deformed nucleus, therefore showing rotational spectra as reported in Refs. 92 and 93. The rotational theory expects the ratio between the energies of the first two excited states (4^+ and 2^+) of the ground band to be 10/3 (see Chapter 2). The experimental value for this ratio for ^{152}Gd is 2.19, which is far from the rotational theory expectations.. The vibrational theory expectations yield 2 for this ratio (see Chapter 2). This shows that ^{152}Gd is very near to vibrational nuclei. The theoretical predictions based on the spherical nuclei (i.e. vibrational spectra) gave poor agreement with experiment for the ground band states (Table 4.6 and Fig. 4.5). But the degeneracy of the states as expected by the theory is seen and the new level at 1068 keV ($0,4^+$) is one of these degenerates. The β-band states show good agreement between experiment and theory. These data support the spherical shape of ^{152}Gd. The IBM vibrational limit (SU(5)) expectations agree with experimental data as seen in Fig. (4.6) and Table (4.6). This again supports the

vibrational behaviour of ^{152}Gd. This model has succeeded in including the three new levels at 1719, 1730 and 1765 keV in the β band of the model (Fig. 4.6). The VMI calculations (Table 4.6) show good agreement between theory and experiment. This model expects the ratio $E(4^+)/E(2^+)$ to be 2.23 in its vibrational limit. This value is very close to the experimental value of ^{152}Gd.

The SU(5) limit expected the ratio R (eq. 2.32) to be zero. The experimental value is 0.018 ± 0.002 which is close to the prediction of the IBM vibrational limit SU(5). Table (4.7) gives the reduced transition probability B(E2) for the 344 keV transition which depopulates the first excited state (2^+) to ground. The IBM expectation is about three times bigger than the experimental value, while the Weisskopf estimation ($B^W(E2)$) is smaller than the experimental value by about two orders of magnitude. Since this estimation is based on a single particle model (Chapter 2), this indicates that this state is not due to single particle excitation. Good agreement between the PPQM (Ref. 108) and experiment is seen, but the energy level calculations of this model show poor agreement with experiment (Table 4.6).

The possibility of having a rotational γ-like band in the spectrum of ^{152}Gd nucleus[112] arose from the existence of the three levels of 1318, 1434 and 1551 keV. The calculations of the theory yield wider spacing between these levels than experiment, i.e. no agreement with theory is seen. Another γ-like band is believed to exist as a result of the introduction of the three new levels at 1719, 1730 and 1765 keV. These two bands may be considered members of two quasiparticle states, since these levels started with energy > 1 MeV,

TABLE 4.7.

EXPERIMENTAL AND THEORETICAL B(E2) REDUCED TRANSITION PROBABILITY OF THE FIRST EXCITED STATE IN ^{152}Gd

Level energy (keV)	B(E2) e^2b^2			
	Experiment*	IBM	Single particle	PPQM Ref. 108
344.12	0.306(016)	1.0	0.0048	0.292

* This value was calculated using half-life of the 344 keV level reported in Ref. (8)

i.e. the pairing gap energy [31,42]. Table 4.8 shows the B(E2) ratios for some positive parity states, the theoretical values are calculated using the adiabatic rotor model. Disagreement between theory and experiment is seen, which indicates that these states are not pure rotational.

From the above considerations, ^{152}Gd nucleus is considered to be spherical nucleus showing vibrational spectra, but could have some kind of quasi-rotational spectra, since there is always a possibility of co-existence of the rotational motion with the vibrational motion.

To check that the β band starts from the level at 615 keV, the ratio B(E2, 494)/B(E2, 765) for the transitions from the ground band member at 1108 keV to the 615 keV level of the β band and to the 344 keV ground band member is 0.45 $\pm$ 0.06. This ratio supports the above assumption.

Seven new energy levels have been introduced together with sixteen new transitions which have been observed. The existence of these levels has been confirmed from coincidence data and theoretical calculations. The spins and parities for these levels have been assigned from log ft values and other possible information. In this work a new value for the B.R. of the 615 keV level was suggested (Table 4.). The 1551 keV level spin was confirmed to 4^+, the spin of the level 1692 keV was confirmed to new value 4^+. The spin of the level 1606 keV is confirmed to 2^+. The new level at 969 keV was assigned spin and parity 1^-, this level forms together with the level 1123 keV (3^-) an octopole band. The new energy 193 keV was reported in Ref. 105 and has been seen in this work and placed in the decay scheme according to coincidence data. The 511 keV transition was placed

TABLE 4.8

EXPERIMENTAL B(E2) BRANCHING RATIOS FOR TRANSITIONS FROM POSITIVE PARITY STATES IN ^{152}Gd COMPARED WITH ADIABATIC ROTOR (Ref. 98)

Transitions E_γ / E_γ'	Energy Level (keV)	$J_i \rightarrow J_f$ / $J_i \rightarrow J_f'$	B(E2) Ratio Experiment	Theory
315.10 / 586.27	930	$2_\beta \rightarrow 0$ / $2_\beta \rightarrow 2_g$	3.09 (26)	0.70
930.69 / 586.27	930	$2_\beta \rightarrow 0_g$ / $2_\beta \rightarrow 2_g$	0.018 (002)	0.70
351.81 / 526.87	1282	$4_\beta \rightarrow 2_\beta$ / $4_\beta \rightarrow 4_g$	49.9 (18.7)	1.1
1206.89 / 795.13	1551	$4 \rightarrow 2_g$ / $4 \rightarrow 4_g$	0.018 (012)	1.1

between the 1318 keV(2^+) level and the new level at 807 keV (3^+). This transition was reported in Refs. 99 and 93, but could not be placed in their decay schemes. This was confirmed together with the existence of this new level from coincidence data.

CHAPTER 5.

STUDIES OF THE ^{152}Sm ISOTOPE

5.1. Introduction:

The decay scheme of ^{152}Sm is established from the study of the electron caputre (EC) and β^+ decay of ^{152}Eu. Nuclei with N = 90 are believed to be slightly deformed, hence showing rotational like spectra. The ^{152}Sm nucleus lies on the edge of this deformation region[31,93] and hence many authors considered ^{152}Sm as transitional between spherical and deformed nuclei. This nucleus is at the very beginning of the deformed rare-earth region and as a consequence of its "softness", the β and the γ vibrational bands lie at lower excitation energies than the corresponding states of more rigid nuclei in the middle of the deformed rare-earth region.[92]

The B(E2) branching ratios show disagreement with rotation theory even if the mixing of the β and γ bands into the ground state band (first order effect) or the mixing of the β and γ bands into each other (second order effect) are allowed. This is a general feature for all the rotational nuclei clustering around the "transitional region"[113] and cannot be explained by the simple collective model of Bohr and Mottelson.[38] The level at 1293 keV is of special interest. Schick[114] suggested that this level may be the 2^+ member of the two-phonon β vibrational band. The results from two nucleon transfer reactions support this approach. In the (t,p) reaction on ^{150}Sm leading to states in ^{152}Sm, Hinds et al.[112] found evidence for 0^+ states: the ground state, the β vibrational band head and the 1091 keV (unseen). This suggests that we have "spherical" excitation

coexisting with rotational excitation. If this is true, one can expect interaction between spherical and deformed states in ^{152}Sm. In this work, the rotational collective model was applied to calculate the energy spectra, which were compared with experiment. Comparisons were also made with calculations based on the transitional limit between the spherical (vibrational) and the deformed (rotational) nuclear region.

The results of the study of the intensities of the γ-rays emitted in the decay of ^{152}Eu were given in the previous chapter. Table 4.1 shows that fifteen new transitions were observed in the case of ^{152}Sm (one of these was a confirmation of a transition reported only by Ref. 98). The existence of nine new energy levels was confirmed from coincidence data and energy band calculations. These levels were therefore introduced into the decay scheme of ^{152}Sm. Hence, some previously reported transitions could be replaced for the first time in the decay scheme. Spins and parities were evaluated for the new levels; for the remaining levels, values were either confirmed or assigned from several possibilities. The half-life of the first excited state was measured at the same time as the γ - γ coincidence data were being accumulated using the DPDC system.

5.2. Results:

5.2.1. Lifetime of the 122 keV level:

The details of the lifetime spectrometer were discussed in Chapter 3. The fast timing spectrum was gated by the 122 keV line which depopulates the 122 keV level to ground. The spectrum was collected over an interval of three weeks. The lifetime spectrum is shown in

Fig. 5.1. The slope method was used to analyse the spectrum and the value measured for the half-life of the level was 1.44 ± 0.04 n sec. Table 5.1 shows comparison between the half-life measured in this work and the values measured by other authors. Different technique was employed in this work by using plastic-Ge(Li) detectors. Fossan and Herskind[115]; and Kugal et al.[116] have used plastic-plastic detectors in their measurements. Good agreement between their values and the value measured here is achieved within the reported errors (Table 5.1). Richter et al.[117] have used a pulsed-beam technique in measuring the lifetime of the coloumb-excited state at 122keV, and a perfect agreement between their value and the value measured in this work is seen. El-asser et al.[118] have used an electron-electron spectrometer especially equipped for lifetime measurements. The value reported for the life-time is the smallest value given for this level, but this still agrees with the value measured in the present work, within the errors.

Table 5.1 shows that when plastic-plastic detectors are used, the measured half-life is lower than the values measured by other methods.

5.2.2. Singles and coincidence spectra:

In Chapter 4, the method of measuring the singles spectra following the decay of ^{152}Eu was described. These spectra were shown in Fig. 4.1 and the results were tabulated in Table 4.1. Although the most extensive coincidence measurements on the ^{152}Sm isotope were carried out by Baker et al., [98] the most complete analyses were reported by Barratte et al.[92] who only took two gates (122 and 689 keV) to establish the decay scheme. During the course of this work the eleven gates at 122, 244, 444, 489, 657, 689, 842, 867, 919, 964 and 1005 keV were taken to provide sufficient coincidence data to establish the decay

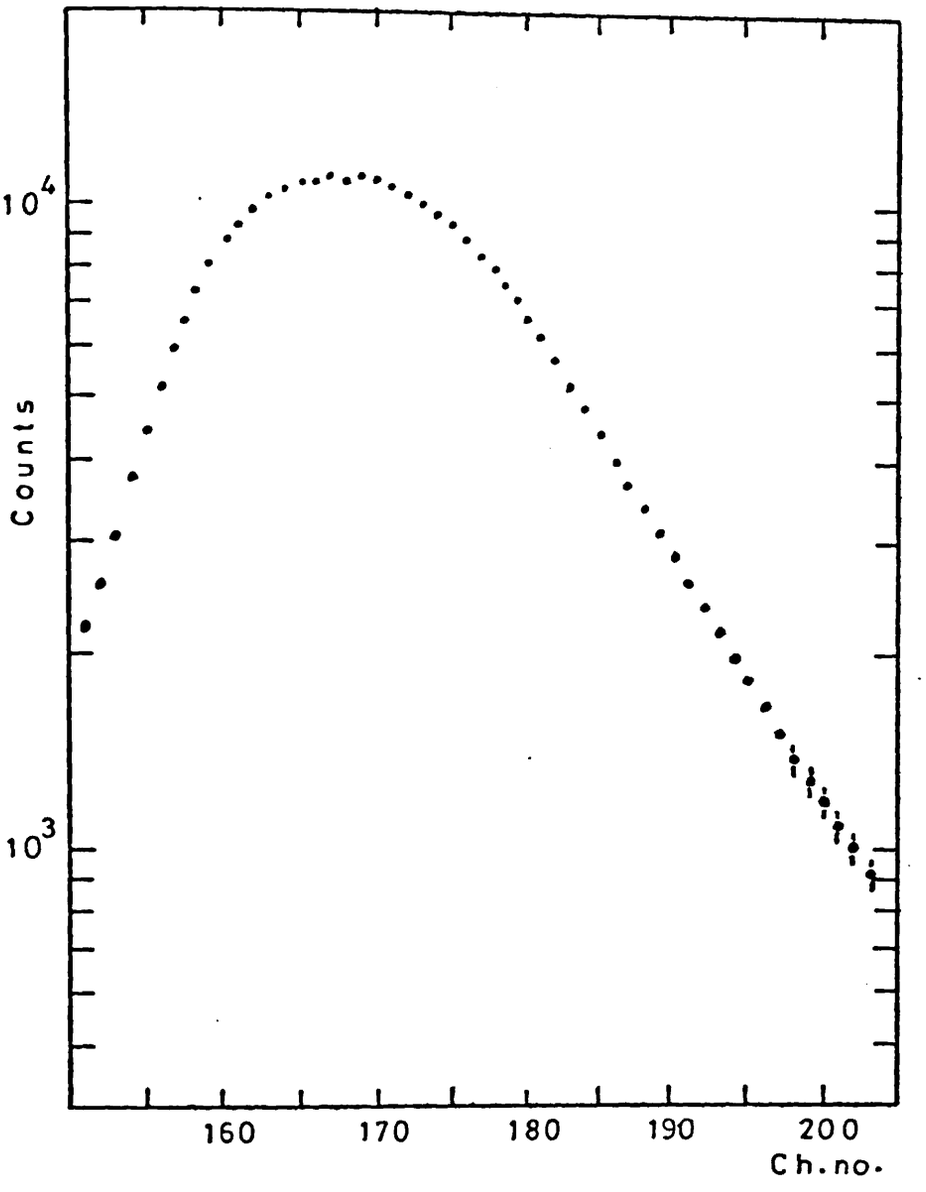

Fig. (5.1) Life time spectrum of the 122 keV level.

TABLE 5.1.

EXPERIMENTAL LIFETIME OF THE FIRST EXCITED STATE IN ^{152}Sm

Level (keV)	Lifetime (ns)				
	Present Work	Ref. 118	Ref. 117	Ref. 116	Ref. 115
122	1.44(04)	1.35(05)	1.44(03)	1.41(04)	1.37(04)

scheme. The 122 keV transition depopulates the first excited state to the ground state. This means that most of the transitions are in coincidence with this energy. Hence, the first step in coincidence investigations is to take this transition as a gating energy, especially as it leads to a very prominent and well-separated peak. The 444 keV energy was proved to be triplet, thus this gate provides vital coincidence data to investgate this assumption in addition to the fact that this line is prominent and well-separated peak (see Fig. 4.1.). The two gates 489 and 867 keV provide useful coincidence information for the levels which lie in the middle of the decay scheme. At the same time, the second gate gives coincidence data for the existence of the new transition 203 keV and the new level at 1437 (2^+) keV which decays by the 203 keV transition to the level at 1234 (3^+) keV. The 867 keV gate provides coincidence check for the two doublets 212 and 244 keV (see Fig. 5.3). The 919 keV gate provides coincidence check to the 193 keV transition which was suggested to belong to both nuclei ^{152}Gd and ^{152}Sm (see Chapter 4). The 1005 keV gate shows the coincidence between the higher levels in ^{152}Sm nucleus and the two lower states of the ground band.

The above gates were chosen rather than other gates in the spectrum because these provide large coincidence data and because these are well separated from other lines in the spectrum of ^{152}Eu and at the same time are quite strong peaks. The results of these measurements were given in Table 5.2. The symbols are the same as those used in Table 4.2 (Chapter 4). The coincidence spectra are shown in Figs.(5.2. a),(5.2.b),....

TABLE 5.2.

γ- γ COINCIDENCE RESULTS FROM THE EC DECAY OF ^{152}Eu.

TRANSITION (keV)	GATE (keV)										
	122	244	444	489	657	689	842	867	919	964	1005
121.97	-	VS	VS	W	VS	VS	VS	W	VS	VS	S
148.11	W	W	W	-	-	S	-	-	-	VS	-
192.54	S	S	-	-	-	-	-	-	VS	-	-
195.09	S	S	S	-	-	S	-	-	-	-	-
203.11	VW	W	W	-	-	W	W	W	W	S	-
207.69	VW	VW	W	-	-	W	-	-	-	-	W
212.25	S	S	W	-	-	W	W	S	W	S	-
237.41	W	W	W	-	-	W	VS	-	W	-	-
239.63	W	S	S	S	-	S	VS	S	S	S	-
244.43	VS	-	S	W	VS	S	VS	VS	W	W	VS
251.58	W	W	-	-	-	-	-	-	W	-	-
270.72	W	-	-	-	-	-	VS	-	-	-	-
275.20	S	S	VS	-	-	VS	-	-	-	-	-
284.98	W	W	W	-	-	VW	-	-	-	S	-
295.66	S	S	W	-	-	S	VW	S	VW	W	-
329.19	W	W	S	-	-	-	VS	-	-	-	-
391.73	VS	S	-	-	-	-	-	-	-	-	-
415.75	VS	S	VS	-	-	S	VW	S	S	S	-
443.91	VS	W	-	-	VS	S	-	-	-	VS	-
482.34	W	W	S	-	-	W	-	-	-	-	-
488.66	S	W	-	-	-	-	-	-	VS	-	-
493.51	S	VW	W	-	-	S	-	-	-	S	-
522.86	S	S	W	-	-	VW	VW	VW	VW	VW	-
556.96	W	W	VS	-	VS	W	-	-	-	-	-
564.05	S	W	W	-	-	S	-	-	-	VS	-
566.31	W	W	-	-	-	-	VS	-	-	-	-
616.11	W	W	-	-	-	-	W	-	-	-	-
621.63	W	-	-	-	-	-	-	-	-	-	-
644.00	W	W	VS	-	-	VW	-	-	-	S	-

TABLE 5.2.

γ- γ COINCIDENCE RESULTS FROM THE EC DECAY of ^{152}Eu. continued

TRANSITION	GATE (keV)										
(keV)	122	244	444	489	657	689	842	867	919	964	1005
656.58	VS	VS	VS	-	-	VW	-	-	-	-	-
665.40	W	W	-	-	-	-	-	-	-	-	-
671.19	VS	W	S	-	-	VW	-	-	-	W	-
674.69	W	VS	S	VS	-	S	-	-	-	-	-
688.73	VS	VW	VS	-	-	-	-	-	-	-	-
719.35	S	VS	VS	W	-	W	-	-	-	-	-
727.66	VS	S	-	-	-	-	-	-	S	-	-
768.90	W	W	VS	-	-	W	-	-	-	-	-
805.19	W	-	-	-	-	-	W	-	-	-	-
810.46	VS	W	S	-	-	-	-	-	-	-	-
822.50	S	-	-	-	-	-	-	-	-	-	-
825.67	W	-	-	-	-	-	-	-	-	-	-
838.77	S	S	W	-	-	W	-	-	-	-	-
841.60	VS	-	-	-	-	-	-	-	-	-	-
867.42	S	VS	-	-	-	-	-	-	-	-	-
884.67	VW	-	-	-	-	-	-	-	-	-	-
901.28	VW	-	W	-	-	-	-	-	-	-	-
919.43	S	S	-	W	-	-	-	-	-	-	-
926.26	VS	VS	-	-	-	-	-	-	-	-	-
957.40	W	S	S	-	-	VS	-	-	-	-	-
964.09	VS	-	Vs	-	-	-	-	-	-	-	-
1005.18	S	VS	-	-	-	-	-	-	-	-	-
1010.89	S	W	-	-	-	-	-	-	-	-	-
1085.83	-	-	VS	-	-	-	-	-	-	-	-
1112.05	VS	W	-	-	-	-	-	-	-	-	-
1147.23	S	-	-	-	-	-	-	-	-	-	-
1170.40	W	VS	-	-	-	-	-	-	-	-	-
1213.08	VS	VS	-	-	-	-	-	-	-	-	-
1249.90	S	-	-	-	-	-	-	-	-	-	-
1314.50	W	W	-	-	-	-	-	-	-	-	-

TABLE 5.2.

γ - γ COINCIDENCE RESULTS FROM THE EC DECAY of ^{152}Eu. continued

TRANSITION	GATE (keV)										
(keV)	122	244	444	489	657	689	842	867	919	964	1005
1363.46	W	W	-	-	-	-	-	-	-	-	-
1389.39	W	VW	-	-	-	-	-	-	-	-	-
1407.98	VS	-	-	-	-	-	-	-	-	-	-
1457.47	VS	-	-	-	-	-	-	-	-	-	-
1527.81	VS	-	-	-	-	-	-	-	-	-	-
1538.24	S	-	-	-	-	-	-	-	-	-	-
1607.98	VW	-	-	-	-	-	-	-	-	-	-
1646.80	VW	-	-	-	-	-	-	-	-	-	-

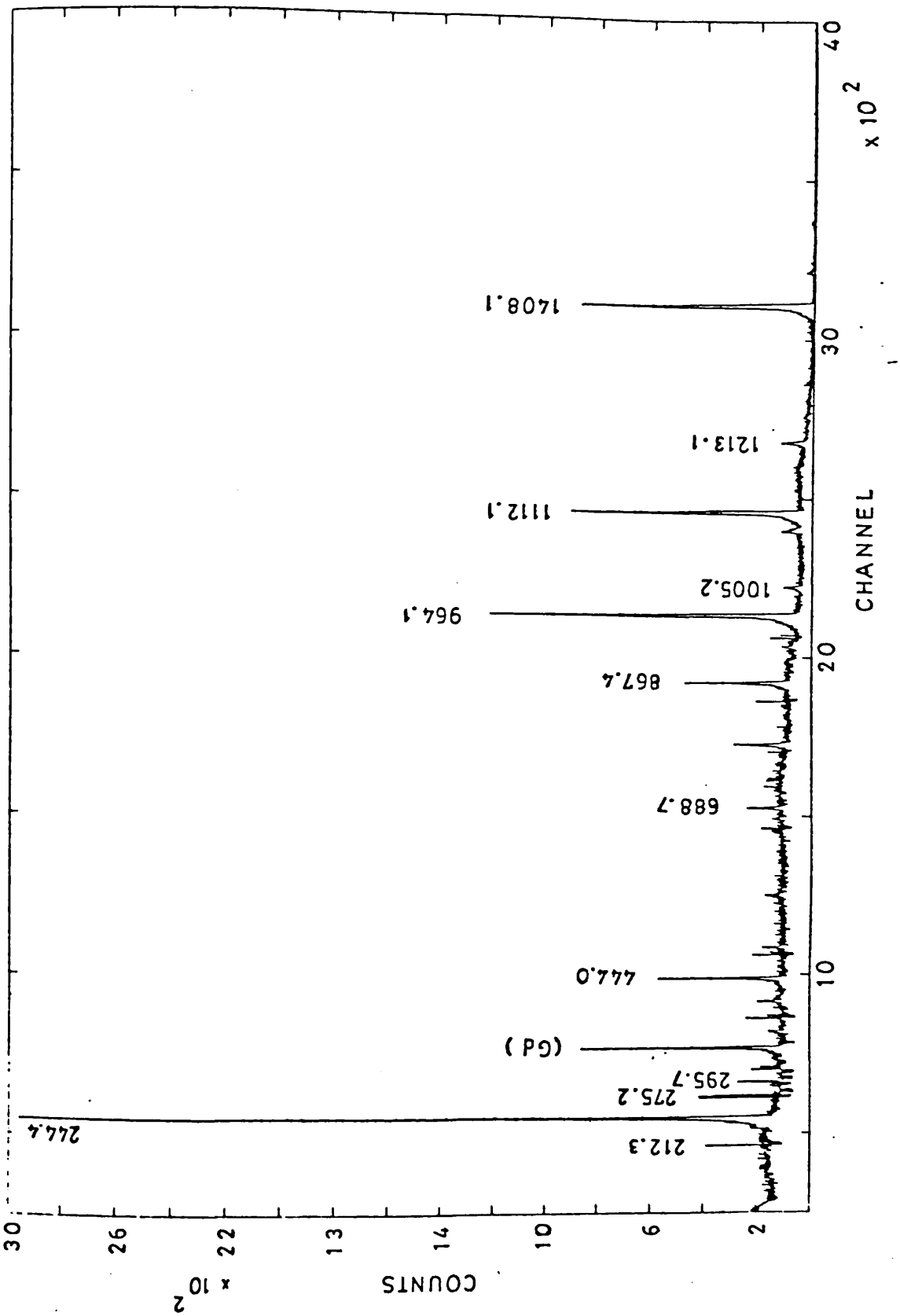

Fig. (5.2.a.) ^{152}Eu - spectrum in coincidence with 122 keV.

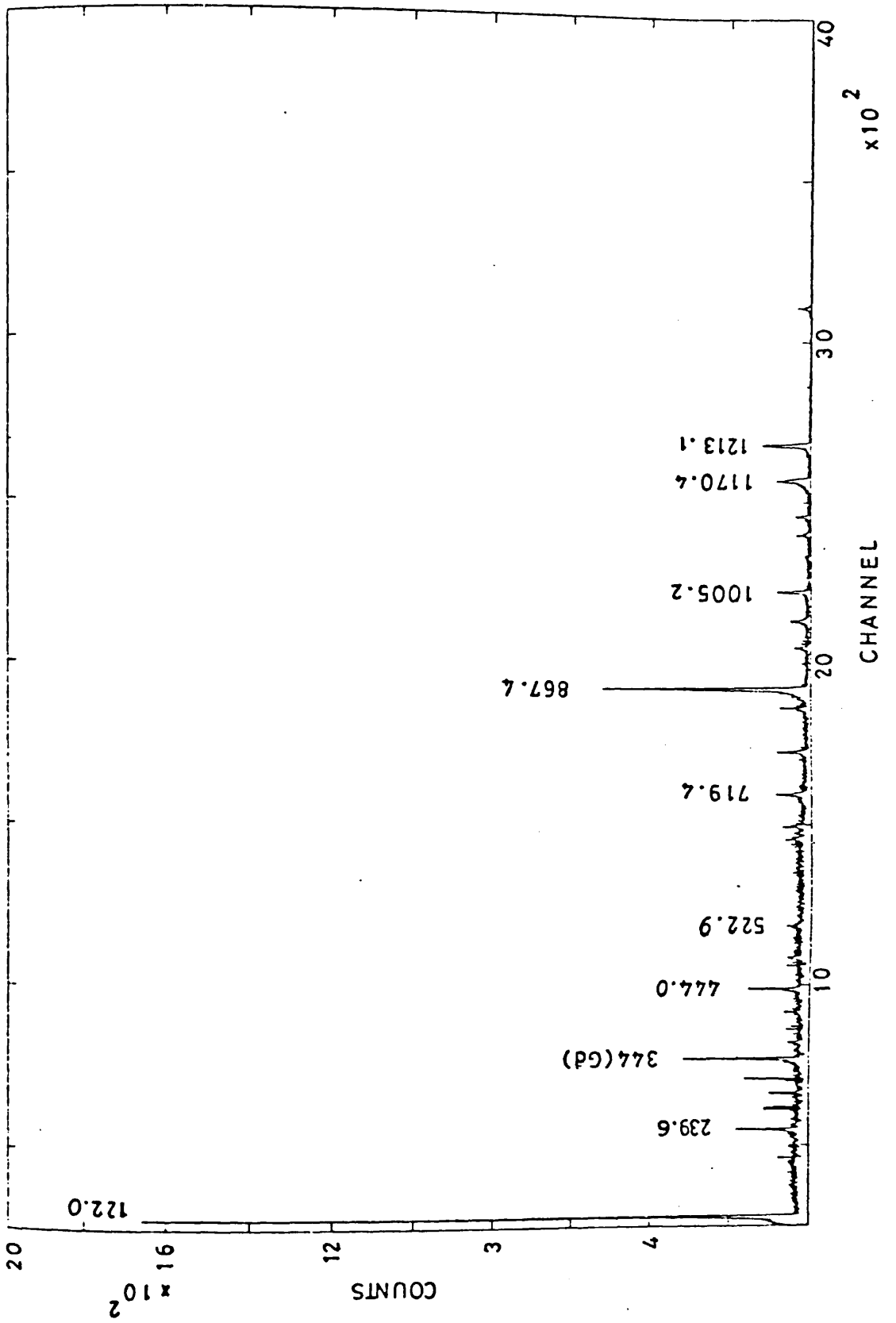

Fig. (5.2.b.) ^{152}Eu spectrum in coincidence with 244 keV.

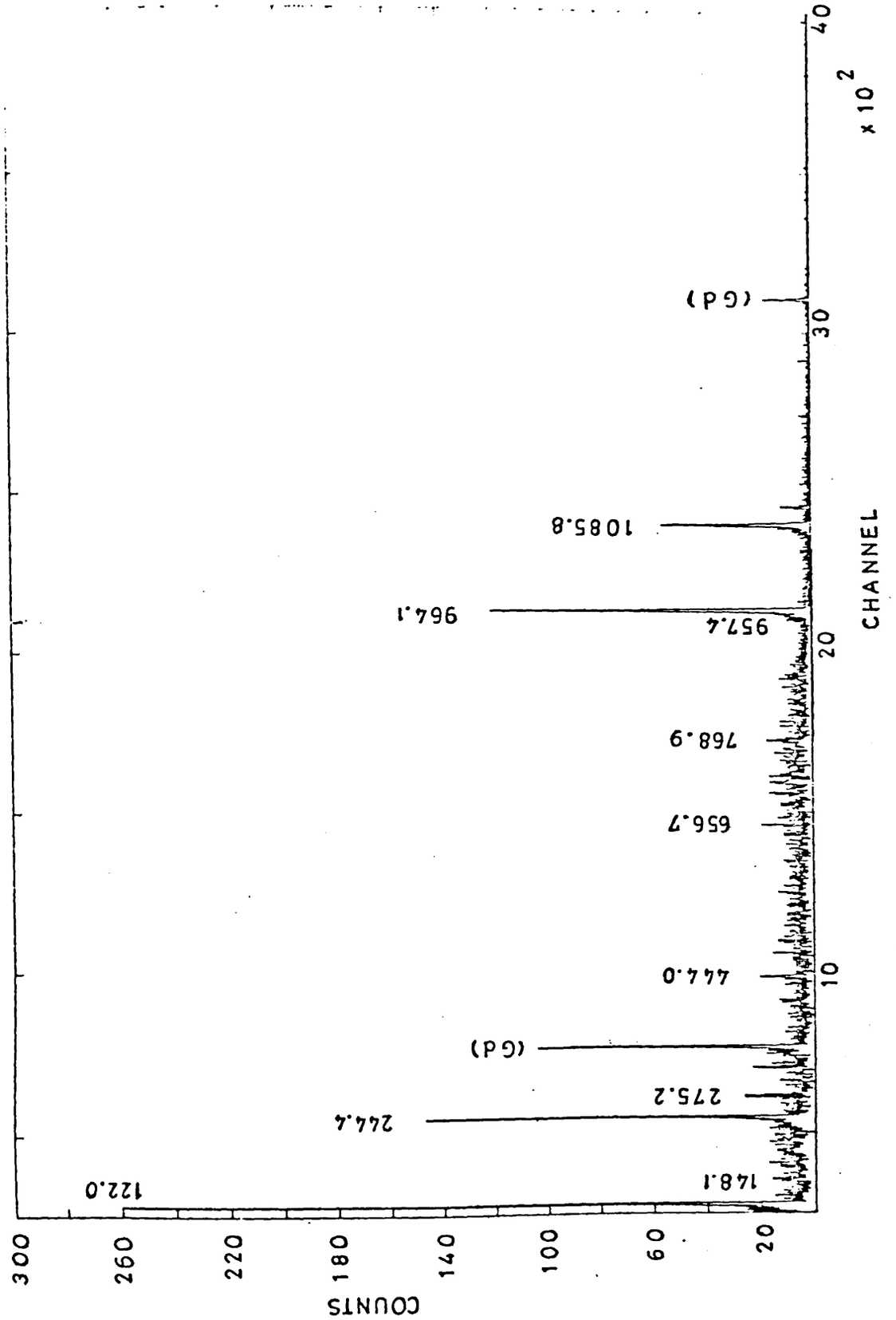

Fig.(5.2.c.) ^{152}Eu spectrum in coincidence with 444 keV.

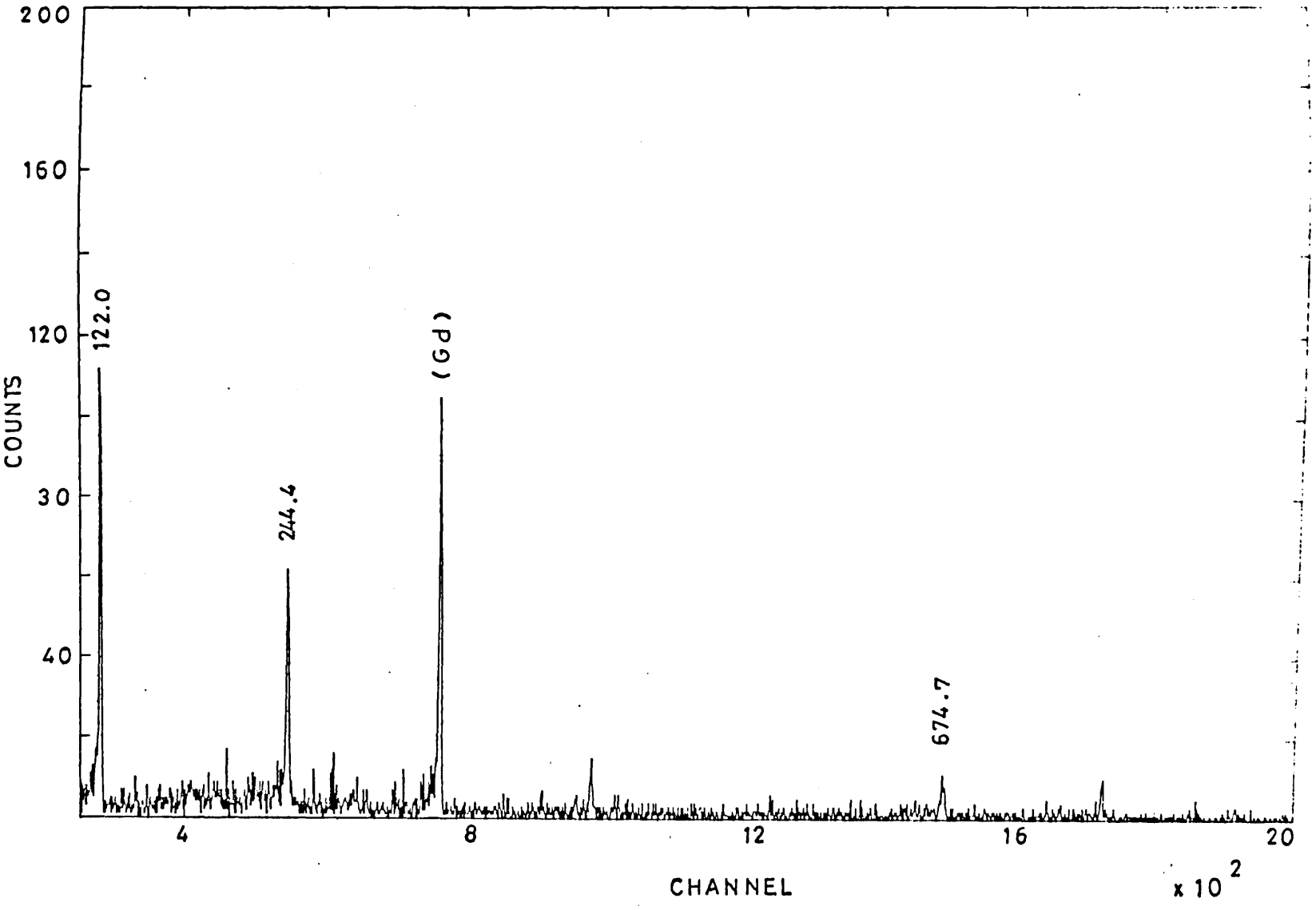

Fig. (5.2.d.) ^{152}Eu spectrum in coincidence with 489 keV.

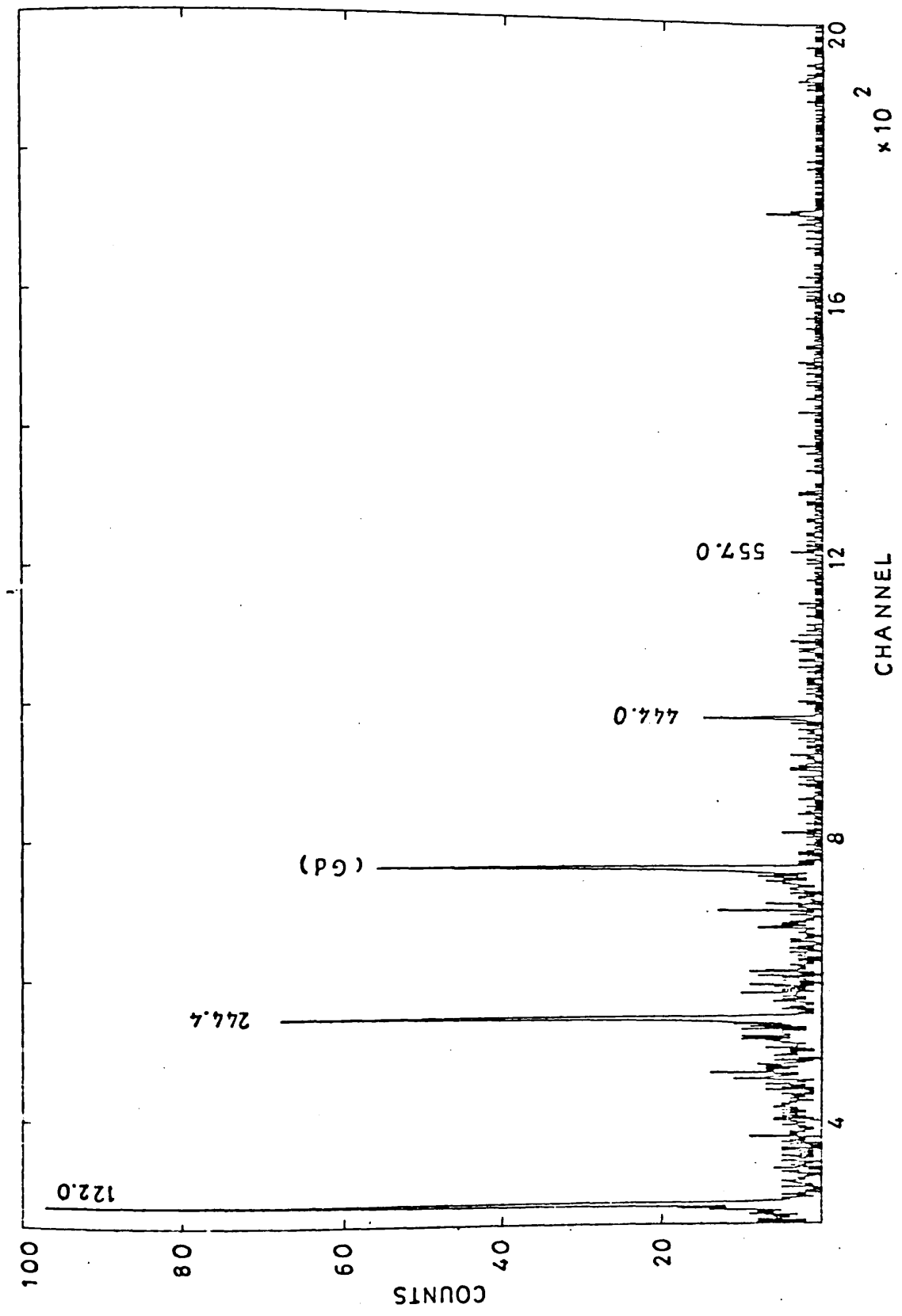

Fig. (5.2.e.) ^{152}Eu spectrum in coincidence with 657 keV.

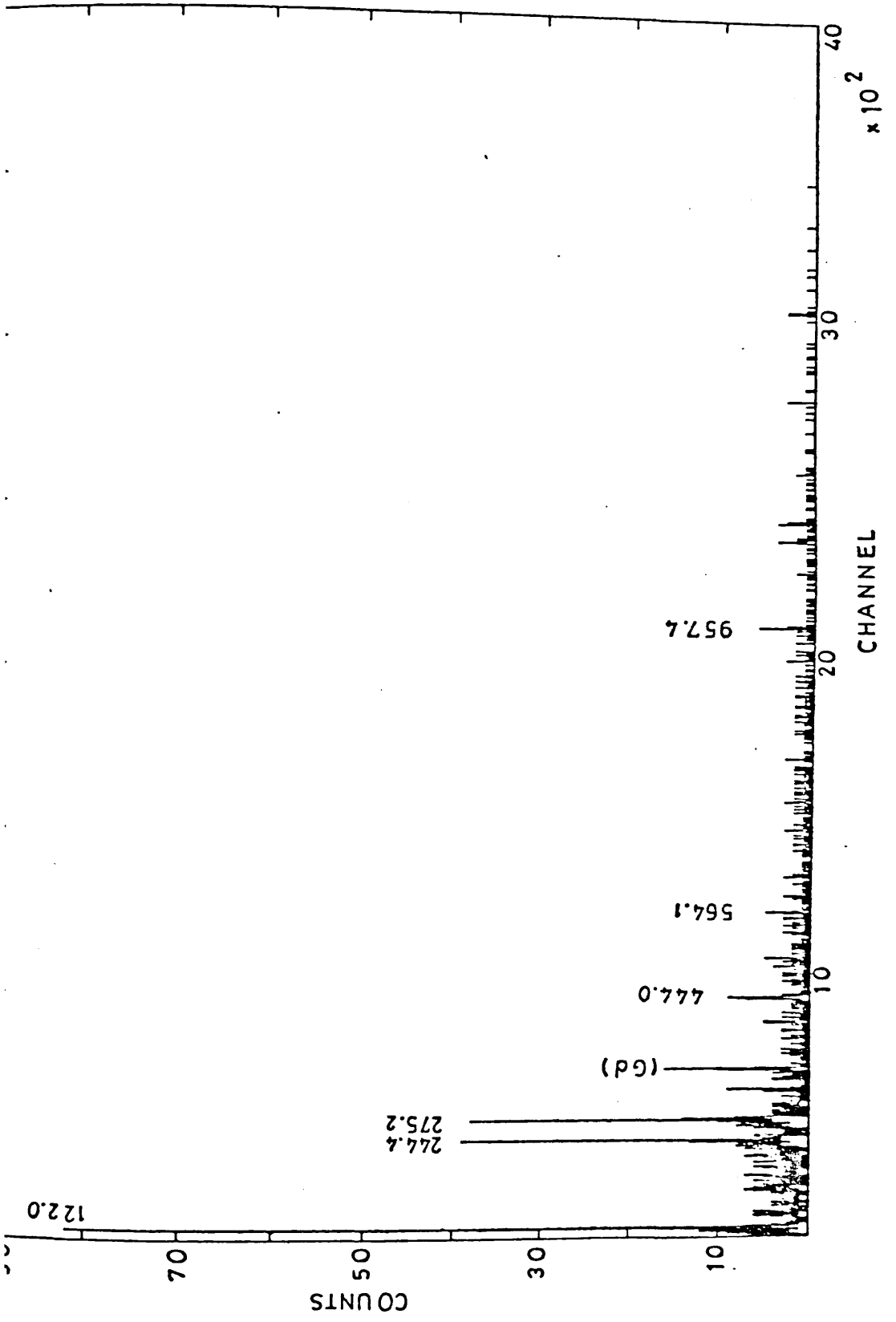

Fig. (5.2.f). ^{152}Eu spectrum in coincidence with 689 keV.

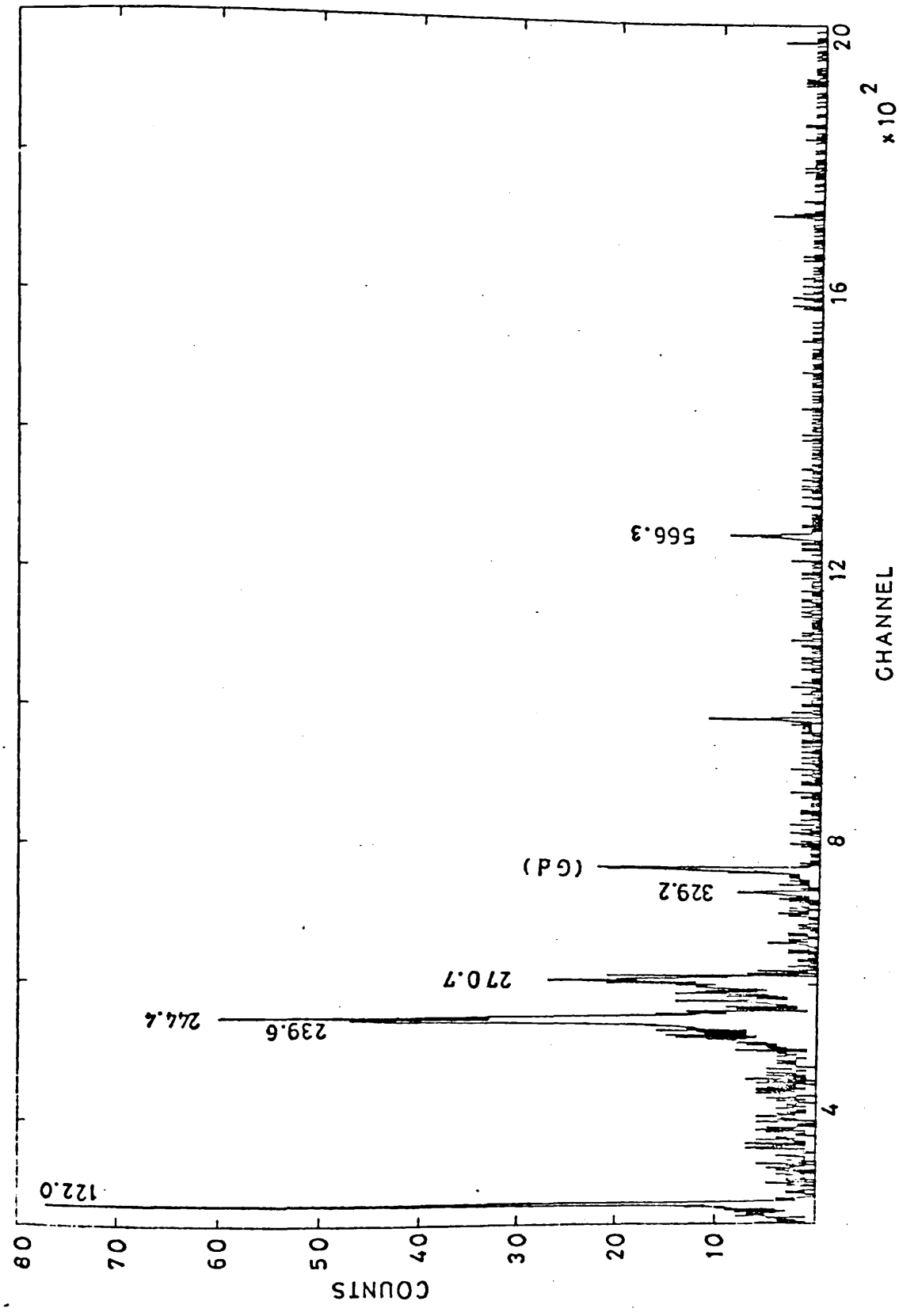

Fig. (5.2.g.) ^{152}Eu spectrum in coincidence with 842 keV.

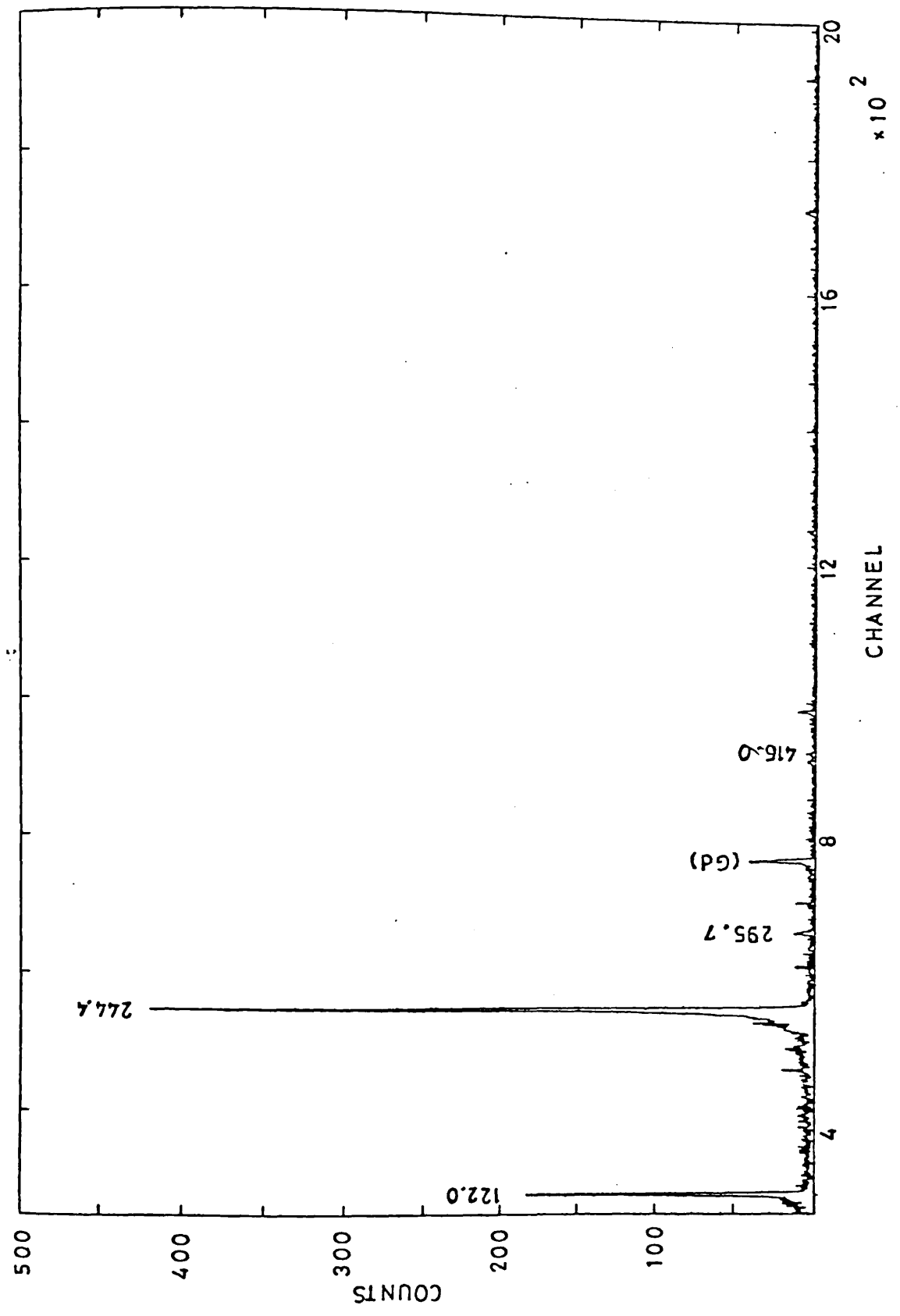

Fig. (5.2.h) ^{152}Eu spectrum in coincidence with 867 keV.

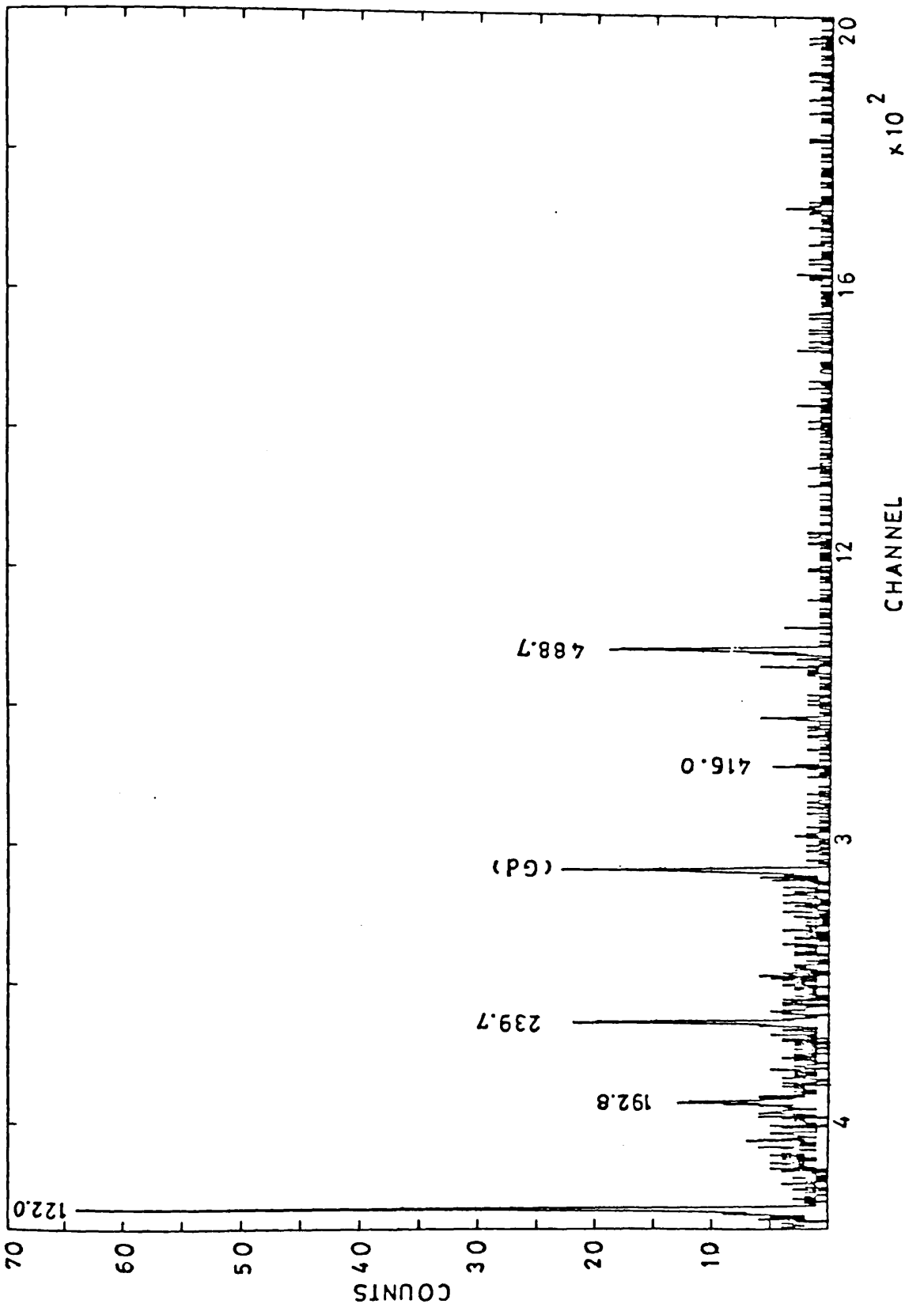

Fig. (5.2.i.) ^{152}Eu spectrum in coincidence with 919 keV.

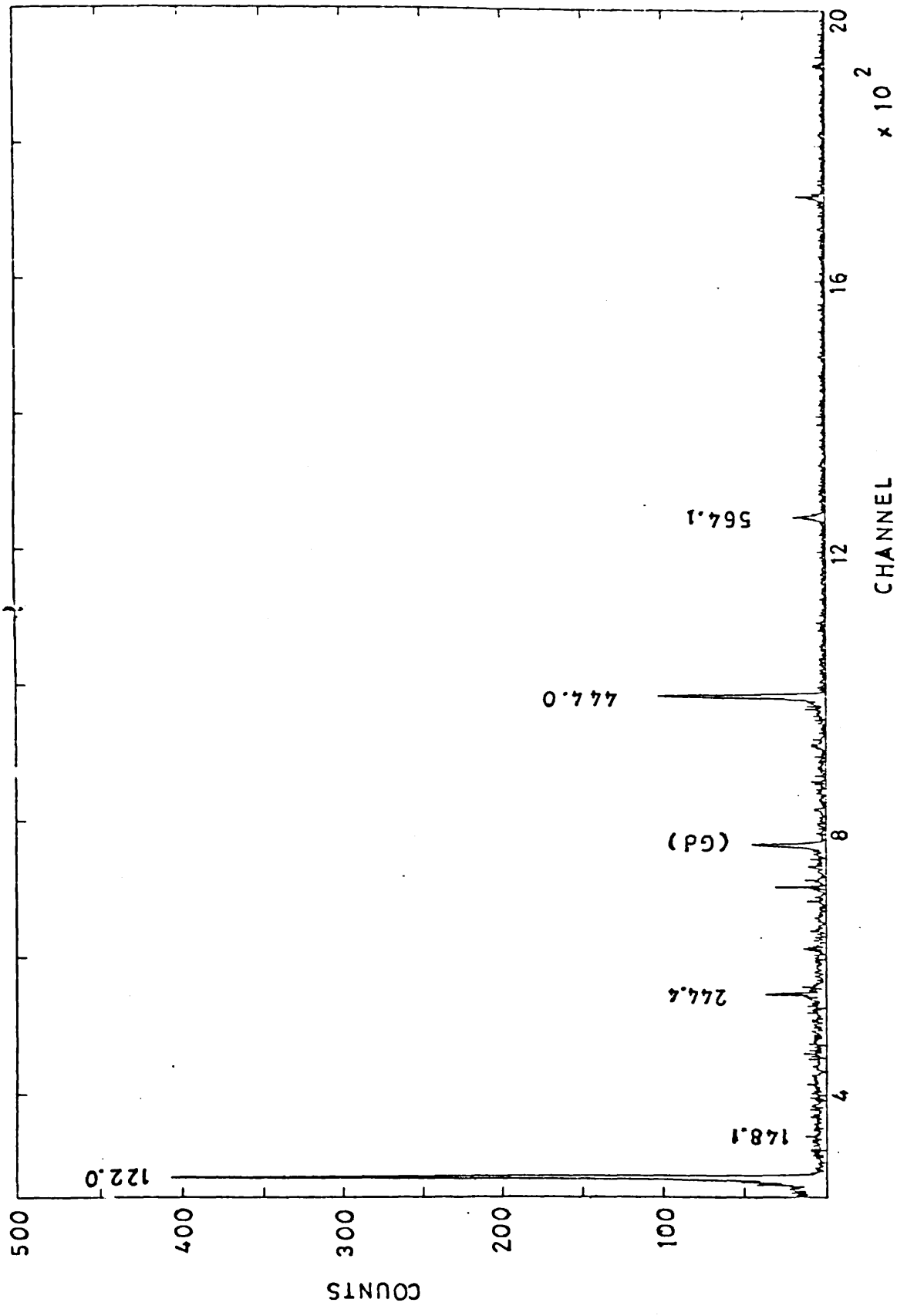

Fig. (5.2.j.) ^{152}Eu spectrum in coincidence with 964 keV.

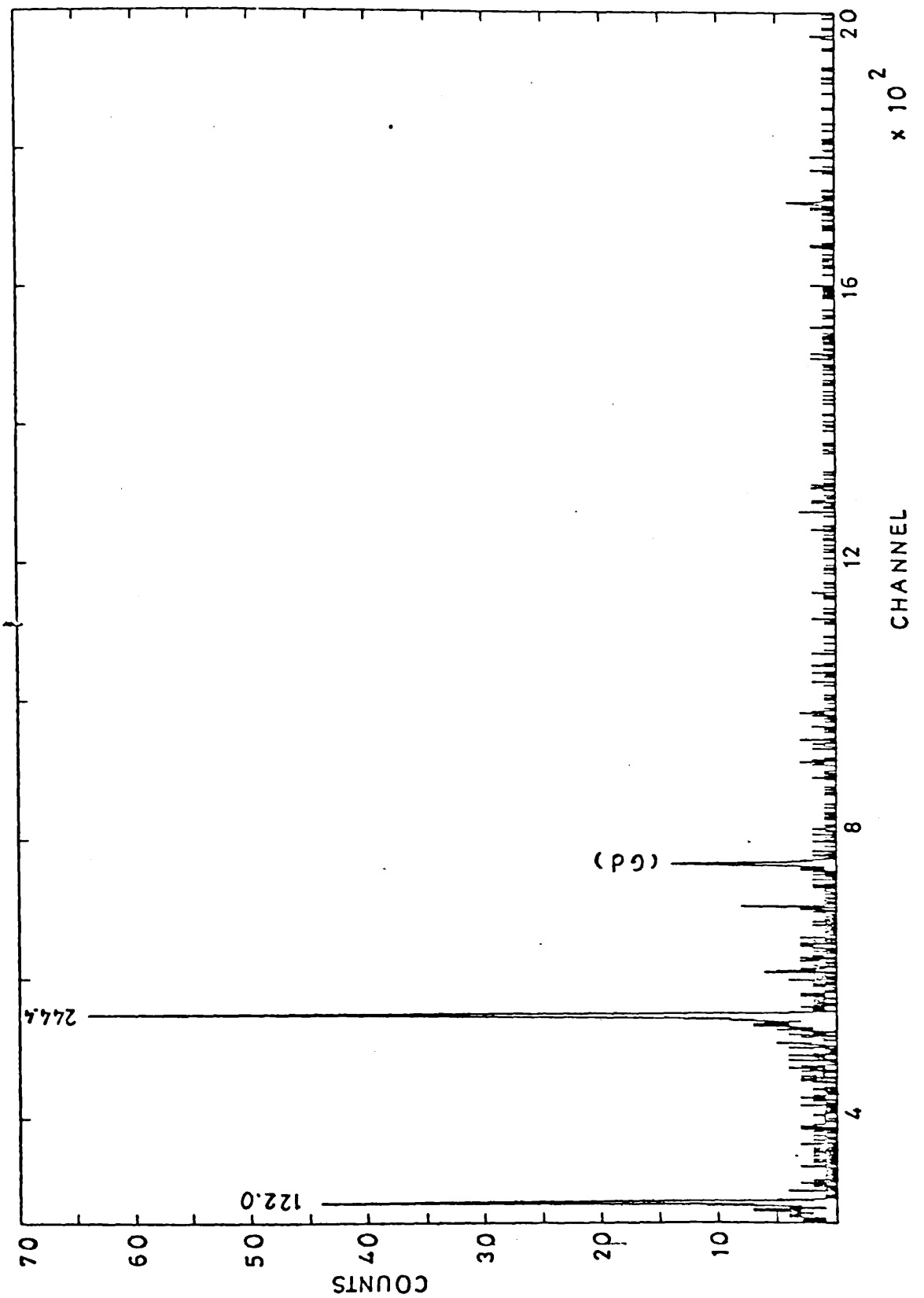

Fig. (5.2.k.) ^{152}Eu spectrum in coincidence with 1005 keV.

5.3. Decay scheme and level properties:

The decay scheme was established on the basis of the coincidence results of the eleven gates (Table 5.2) and the energy sum relations as given in Table 5.3. The decay scheme is shown in Fig. 5.3. On the right side of the Fig. are shown the log ft. values, the electron capture (E.C) feeding branching ratios (I_{EC}), the spins, the K quantum numbers, the parities and finally, the energy levels in keV. The number at the base of the arrow indicates the energy of the transition, while between the brackets is shown the relative intensity of the transitions normalized to the intensity of the energy 344 keV (of ^{152}Gd) as 1000. The new transitions and levels reported in this work are shown as dotted lines.

Table 5.4 shows the EC + β^+ branching ratios (B.Rs.) of the decay of ^{152}Eu, the log ft. values and the deduced spins and parities for the energy levels. The B.R.s were calculated from the balance between the decay and the feeding of the γ-rays for each level. These agree well with the values reported previously in Refs. 90, 92, 93 and 105, except for the two levels at 122 keV and 366 keV. For the 122 keV level, 13% was reported from Ref. 93, 1.6% from Ref. 105 and $\sim$1% from Ref. 90, while Barrette et al. (Ref. 92) did not give a value. The value calculated in this work was 0.23%. This value does not agree with the previous authors, but in this work tables of internal conversion coefficients (α_k) from Ref. 21 were used, whereas previously it was more common to use the values reported by Sliv and Band[119] which are about three times higher than Ref. 21. For the 366 keV level, Riedinger et al.[93] reported 1.7%, Barrette et al.[92] reported 0.7% and 0.8% was given in Ref. 105. The value calculated in this work is 0.74% consistent with Refs. 92 and 105. It seems that the

TABLE 5.3.

ENERGY SUM RELATIONS FOR ^{152}Sm

ENERGY OF TRANSITION (keV)	ENERGY SUM (keV)	ENERGY LEVEL (keV)
121.97	121.97	121.97
121.97 + 244.43	366.40	366.40
1371.42 - 665.40	706.02	706.60
1529.44 - 822.50	706.94	
1649.71 - 942.75	706.96	
1756.68 - 1050.20	706.48	
121.97 + 244.43 + 443.91	810.31	810.49
121.97 + 688.74	810.70	
810.46	810.46	
825.67	825.67	825.67
121.97 + 841.60	963.57	963.57
121.97 + 884.67	1006.64	1006.11
195.09 + 810.49	1005.58	
121.97 + 244.43 + 443.91 + 212.25	1022.56	1022.93
121.97 + 244.43 + 656.58	1022.98	
121.97 + 901 + 28	1023.25	
121.97 + 244.43 + 674.69	1041.69	1041.24
121.97 + 919.43	1041.40	
121.97 + 244.43 + 443.91 + 275.20	1085.51	1085.78
121.97 + 244.43 + 719.35	1085.75	
121.97 + 964.09	1086.06	
1085.83	1085.83	
1147.23	1147.23	1147.23
121.97 + 244.43+443.91+275.20+148.11	1233.62	1233.88
121.97 + 244.43 + 867.42	1233.82	
121.97 + 1112.05	1234.02	
121.97 + 244.43 + 674.69 + 192.58	1233.67	
121.97 + 841.60 + 270.72	1234.29	
121.97 + 244.43 + 674.69 + 251.58	1292.67	1292.69
121.97 + 841.60 + 329.19	1292.76	
121.97 + 1170.40	1292.37	
121.97 + 244.43 + 443.91 + 482.34	1292.65	
121.97 + 244.43 + 926.26	1292.66	
1293.03	1293.03	

TABLE 5.3.

ENERGY SUM RELATIONS FOR ^{152}Sm continued.

ENERGY OF TRANSITION (keV)	ENERGY SUM (keV)	ENERGY LEVEL (keV)
121.97+244.43+443.91+275.20+284.98	1370.49	
121.97 + 244.43 + 1005.18	1371.58	1371.31
121.97 + 1249.90	1371.82	
121.97 + 244.43 + 1010.85	1377.25	
1377.57	1377.57	1377.41
121.97 + 244.43 + 443.91 + 275.20 + 148.11 + 203.11	1436.73	1436.73
121.97+244.43+443.91+212.25+443.91	1466.47	
129.97 + 244.43 + 443.91 + 656.58	1466.89	1466.68
121.97+244.43+674.69+251.58+237.40	1530.07	
121.97 + 841.67 + 270.72 + 295.66	1530.02	
121.97+244.43+443.91+275.20+443.91	1529.42	
121.97+919.43 + 488.66	1530.06	1529.87
121.97 + 841.67 + 566.32	1529.96	
121.97 + 244.43 + 443.91 + 719.35	1529.66	
121.97 + 1407.98	1529.95	
121.97 + 244.43 + 1170.40	1536.80	1536.80
121.97 + 964.09 + 284.98 + 207.69	1578.73	
121.97 + 244.43 + 719.35 + 493.51	1579.26	
121.97 + 244.43 + 656.58 + 556.96	1579.94	
121.97 + 841.60 + 616.11	1579.68	1579.39
121.97 + 244.43 + 443.91 + 768.90	1579.21	
121.97 + 244.43 + 1213.08	1579.48	
121.97 + 1457.47	1579.44	
121.97+244.43+867.42+203.11+212.25	1649.18	
121.97 + 1112.05 + 415.95	1649.97	
121.97 + 964.09 + 564.05	1650.11	1649.62
121.97 + 244.43 + 443.91 + 838.77	1649.08	
121.97 + 1527.81	1649.78	
121.97 + 1538.24	1660.21	
1661.87	1661.87	1661.04
121.97 + 1112.05 + 203.11 + 244.43	1681.56	
121.97 + 884.67 + 674.69	1681.33	1681.26
121.97 + 244.43 + 1314.50	1680.90	
121.97 + 244.43 + 719.35 + 644.00	1729.75	
121.97 + 244.43 + 1363.46	1729.86	1729.85
121.97 + 1607.98	1729.95	

TABLE 5.3.

ENERGY SUM RELATIONS FOR ^{152}Sm, ctd .

ENERGY OF TRANSITION (keV)	ENERGY SUM (keV)	ENERGY LEVEL (keV)
121.97 + 964.09 + 671.19	1757.25	
121.97 + 244.43 + 1389.39	1755.79	1756.64
121.97 + 1112.05 + 522.86	1756.88	
121.97 + 1170.40 + 237.40 + 239.63	1769.40	
121.97 + 244.43 + 1010.85 + 391.73	1768.98	
1147.23 + 621.63	1768.86	
121.97 + 919.43 + 727.66	1769.06	
121.97 + 841.60 + 805.19	1768.76	1768.72
825.67 + 942.75	1768.42	
121.97 + 688.73 + 957.40	1768.10	
121.97 + 1646.80	1768.77	
1768.19	1768.19	

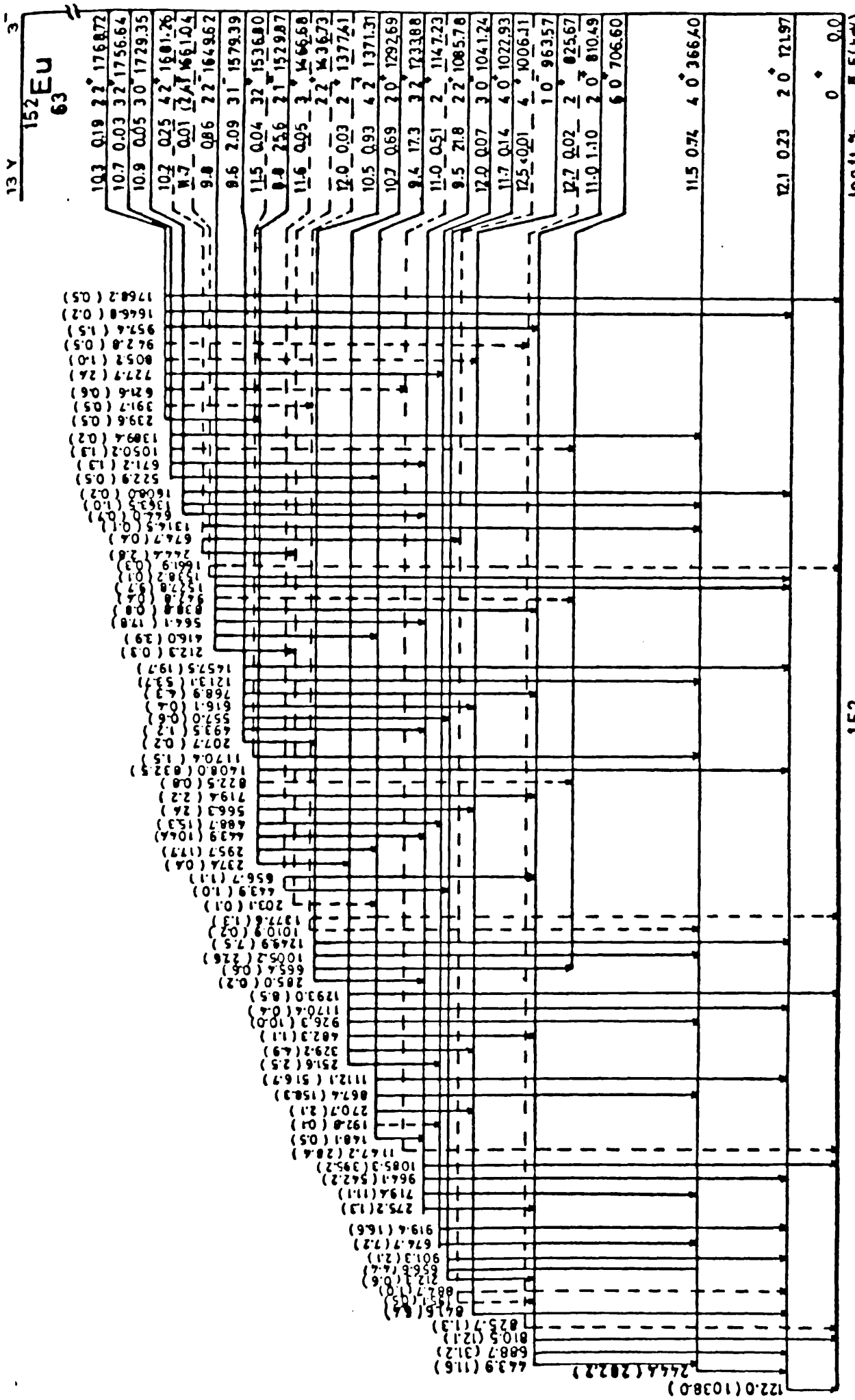

Fig. (5.3) Decay scheme of ^{152}Sm

TABLE 5.4.

SUMMARY OF THE LEVEL PROPERTIES IN ^{152}Sm

Energy Level (keV)	E_{CE} (keV)	ΣI_γ feed	ΣI_γ decay	B.R. %	log ft.	deduced J^π
121.97	1754.93	231.47	230.57	0.23	12.13	2^+
366.40	1510.50	31.04	28.18	0.74	11.53	4^+
706.60	1170.88	-	0.36	-	-	6^+
810.49	1066.41	5.50	1.30	1.10	11.00	2^+
825.67	1051.23	0.13	0.05	0.02	12.69	2^+
963.57	913.33	0.64	1.19	-	-	1^-
1006.11	870.79	0.15	0.04	0.002	12.50	4^+
1022.93	853.97	0.69	0.16	0.14	11.70	4^+
1041.24	835.66	2.38	2.08	0.07	11.97	3^-
1085.78	791.11	95.94	12.87	21.76	9.46	2^+
1147.23	729.67	2.84	0.86	0.51	10.99	2^+
1233.88	643.08	68.39	2.22	17.33	9.36	3^+
1292.69	584.21	2.71	0.06	0.69	10.66	2^+
1371.31	505.48	3.59	0.02	0.93	10.48	4^+
1377.41	499.76	0.15	0.05	0.03	11.98	2^+
1436.73	439.93	0.01	0.33	-	-	2^+
1466.68	410.06	0.21	-	0.05	11.60	3^+
1529.87	347.46	97.65	0.05	25.56	8.77	2^-
1536.80	340.10	0.15	-	0.04	11.50	3^+
1579.39	296.96	8.01	-	2.09	9.62	3^-
1649.62	227.19	3.31	-	0.86	9.76	2^-
1661.04	215.86	0.04	-	0.01	11.70	$(2,4)^+$
1681.26	196.00	0.95	-	0.25	10.20	4^+
1729.85	147.02	0.19	-	0.05	10.89	$(3)^-$
1756.64	120.22	0.33	-	0.08	10.68	3^-
1768.72	108.21	0.72	-	0.19	10.32	2^+

values from Ref. 93 are high.

The three levels at 707, 964 and 1437 keV could not be assigned a B.R. in the same way because the intensities of the feeding γ -rays was greater than the decay ones. The B.R. given for these three levels was 0.2% in agreement with log ft. calculations. The log ft. values were calculated using the relations given in Ref. 90; and end point energy of the conversion electrons was also taken from Ref. 90 (Q = 1.8769 MeV). The spins and parities of the levels were deduced according to the β -selection rules as given in Ref. 106. The theoretical α_k from Ref. 21 are compared with the experimental calculations in Table 5.5. The conversion electron intensities were taken from Ref. 107 and the γ -ray relative intensities (I_γ) were taken from this work. The experimental α_k were normalized to the pure E2 multipolarity of the first excited state (344 keV) in ^{152}Gd (see Chapter 4). In most cases there is excellent agreement with one of the predicted values for α_k and hence the multipolarity for the transition can be assigned with confidence. Thus, the spins and parities of the levels depopulated by these transitions can be compared with those deduced from log ft. values.

5.4. Collective rotation:

Nuclei with $N \geq 90$ are considered deformed, therefore having rotational spectra. In this section, ^{152}Sm is considered as a deformed nucleus and calculations based on rotational theory will be applied to it. The two parameters A and B from e.g.(2.6)(Chapter 2) were determined by fitting the experimental energies of the first two excited states of the ground band. The values calculated are:

TABLE 5.5.

K-SHELL INTERNAL CONVERSION COEFFICIENTS FOR ^{152}Sm

E_γ (keV)	$J_i^\pi \rightarrow J_f^\pi$	Experimental α_K ($\times 10^4$)	α_K(theory) $\times 10^4$			Deduced multi-polarity
			E1	E2	M1	
121.97	$2^+ \rightarrow 0^+$	6302(243)	1300	6600	8400	E2
244.43	$4^+ \rightarrow 2^+$	774(33)	200	800	1200	E2
295.66	$2^- \rightarrow 3^+$	82.3(16.6)	130	466	730	E1
443.91	$2^- \rightarrow 2^+$	47.7(3.3)	50	140	245	E1
488.66	$2^- \rightarrow 3^-$	119.8(20.8)	38	110	194	E2
564.05	$2^- \rightarrow 2^+$	35.1(16.1)	28	76	130	E1
566.32	$2^- \rightarrow 1^-$	208.3(101.0)	28	76	128	E2/M1
656.58	$4^+ \rightarrow 4^+$	558.3(108.3)	21	56	96	E0/E2
688.73	$2^+ \rightarrow 2^+$	347.2(28.4)	19	49	84	E0/E2
719.35	$2^+ \rightarrow 4^+$	45.03(15.9)	17	43	70	E2
810.46	$2^+ \rightarrow 0^+$	30.9(13.7)	14	34	57	E2
867.42	$3^+ \rightarrow 4^+$	26.3(2.6)	12	29	47	E2
964.09	$2^+ \rightarrow 2^+$	22.04(1.40)	9	23	37	E2
1005.18	$4^+ \rightarrow 4^+$	22.6(7.4)	9	21	34	E2
1085.83	$2^+ \rightarrow 0^+$	17.9(2.0)	8	17	28	E2
1112.05	$3^+ \rightarrow 2^+$	16.1(1.6)	7.6	16.8	27	E2
1213.08	$3^- \rightarrow 4^+$	22.5(6.0)	6.6	14	22	E1/M2
1407.98	$2^- \rightarrow 2^+$	4.1(0.3)	4.8	10.9	16	E1

A = 21.186 keV

B = -0.143 keV

The energy spectrum was calculated using these values; the results are given in Table 5.6 together with the energies found experimentally and also from different theoretical calculations. Fig. 5.4 shows the comparison between experimentally determined energy levels and those calculated by rotational theory. In general there is agreement. However, the bands consisted from negative parity levels show more departures from theory than other bands. This might be due to the existence of configurations of the nucleus differing from axial symmetry or arising from coupling between vibration and rotation interactions.

Differences for positive parity levels could also be due to departures from axial symmetry. These indicate some vibrational characteristics which suggest a transitional nature for the ^{152}Sm nucleus. The rotational theory for the ground state band supports the mainly rotational character and could allow some vibrational degree of freedom since $E(4^+)/E(2^+)$ is 3.33 and $E(6^+)/E(2^+)$ is 7.0, while experiment shows these ratios to be 3.02 and 5.8, respectively.

- The ground state band (122(2^+), 366 (4^+) and 707 (6^+) keV):

The spins and parities of these levels are well established in the view of the log ft. values (Table 5.4) and from the α_k coefficients (Table 5.5). Excellent agreement between experimental and theoretical value of α_k of the 122 keV transitions supports the 2^+ assignment of the 122 keV level. The experimental α_k for the 244 keV transition is in excellent agreement with theoretical α_k. This supports the E2 multipolarity of this transition, hence, the 4^+ assignment for the 366 keV

TABLE 5.6.

THE ENERGY OF LEVELS IN ^{152}Sm FOUND EXPERIMENTALLY COMPARED WITH ROTATION CALCULATIONS AND WITH VALUES FROM OTHER NUCLEAR MODELS

JK^{π}	Experiment	Energy (keV)					
		Rotor	IBM Ref 43	PPQM Ref 40	BET Ref 60	IBM Ref 50	VMI ref 109
20^{+}	121.97	121.97	110	114	121	101	121
40^{+}	366.40	366.40	340	314	346	316	369.9
60^{+}	706.60	636.96	681	585	706		712.3
20^{+}	810.49	810.49	854	855	835	935	
2^{+}	825.67	825.67					
10^{-}	963.57	963.57	990				
4^{+}	1006.11	1070.11					
40^{+}	1022.93	1054.93	1172	1039	1082	1222	
30^{-}	1041.24	1155.63	1030				
22^{+}	1085.78	1085.79	1039	1397	1050	1185	
32^{+}	1233.88	1197.43	1214	1559	1353	1333	
42^{+}	1371.31	1330.23	1357	1705	1441	1496	
2^{+}	1377.41	1377.41					
2^{+}	1436.73	1436.73					
3^{+}	1466.68	1488.78					
21^{-}	1529.87	1529.87	1450				
3^{+}	1536.80	1548.61					
31^{-}	1579.39	1641.08	1636				
22^{-}	1649.62	1649.62					
4^{+}	1681.26	1681.41					
32^{-}	1756.64	1761.35					

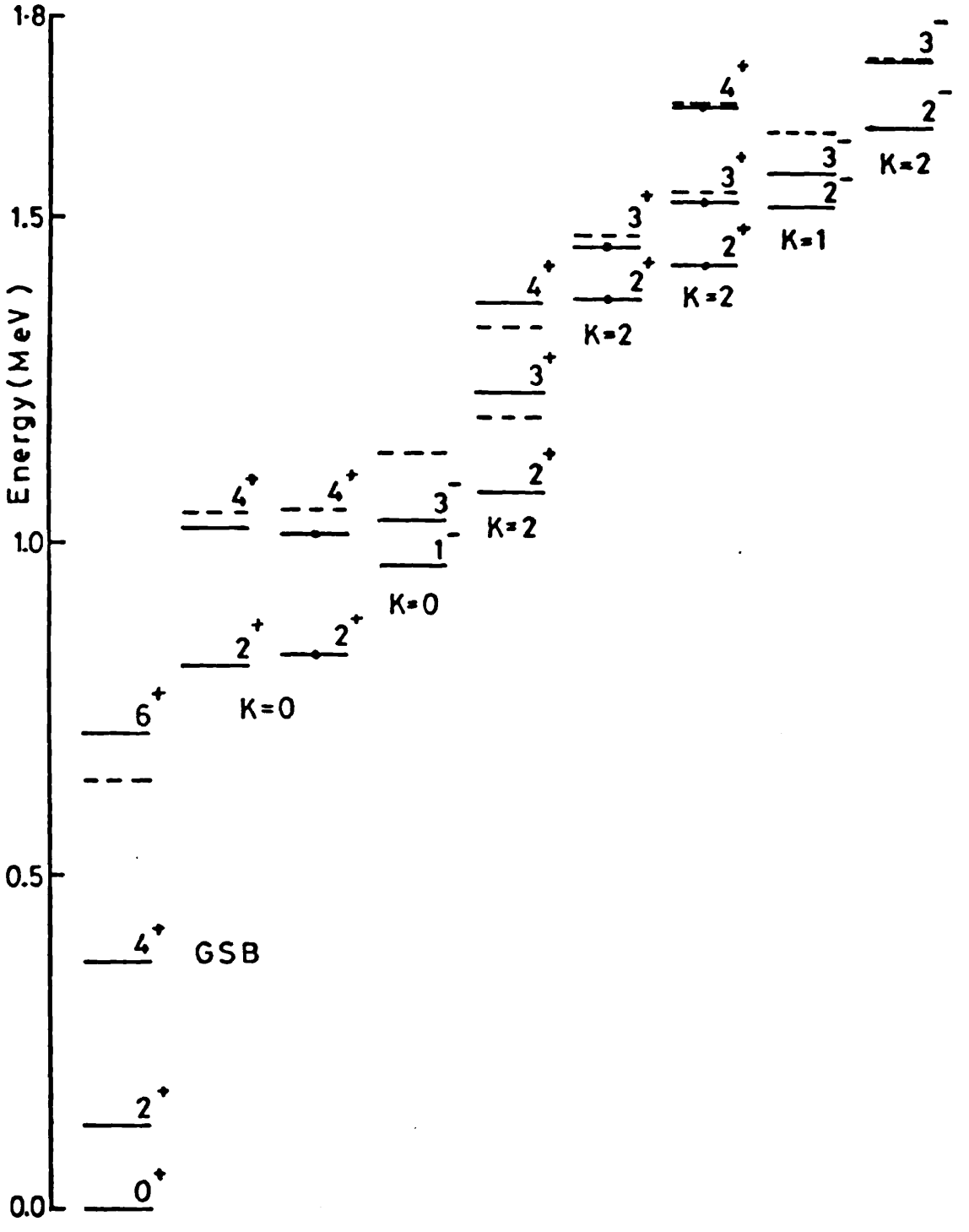

Fig. (5.4) Experimental and theoretical rotational (dotted lines) energy levels in ^{152}Sm. New levels are marked with a dot in the middle.

level is confirmed. The 707 keV level was assigned 6^+ since all theories (Table 5.6) predict a level of about 700 keV with $J^\pi = 6^+$.

The lowest two levels in this GSB were used to determine the parameters of the rotational theory (A & B). The calculated value for the 6^+ level is 637 keV which is better than the value reported in Ref. 40 which was based on pairing-plus-quadrupole model (PPQM). Closer agreement was achieved by the IBM in the transitional limit from SU(5) to SU(3) as reported in Ref. 43 and 50. The predictions of the VMI[109] for this band gave excellent agreement with experiment. The Boson expansion model (BET)[60,61] calculations show the best agreement with experiment for the 707 keV level, but this is not so for the 366 keV level. One concludes that in this band the interaction between the vibrational and rotational degrees of freedom is an important factor, i.e., it is necessary to allow transitional characteristic to be present.

- The β-band (810(2^+), 1023(4^+) keV levels:

The spins and parities of these levels were confirmed from log ft. values (Table 5.4) and from the α_k coefficients (Table 5.5). The 657 keV transition has high experimental α_k value, this suggested E0 multipolarity for this transition, since it depopulates the 1023 keV level to the ground band member 366 keV (4^+) level. This supports the 4^+ assignment to the 1023 keV level. The rotational theory calculations (Table 5.6, Fig. 5.4) show agreement with experiment if we assign 4^+ for this level, this means that this level together with the 810 keV level forms a β-band. Refs. 40 and 60 give another agreement with experiment.

Table 5.7 shows the B(E2) B.R. for transitions depopulating these

TABLE 5.7.

EXPERIMENTAL B(E2) RATIOS FOR TRANSITIONS DEPOPULATING POSITIVE PARITY STATES IN ^{152}Sm COMPARED WITH DIFFERENT NUCLEAR MODELS

Transition E_γ / E'_γ	Energy band	$J_i^\pi \rightarrow (J)^\pi_f$	B(E2) Ratios					
			Experiment	PPQM Ref 40	IBM Ref 43	BET (Ref 61)* A	BET (Ref 61)* B	BET Ref 60
443.91 / 688.73	β	$2^+ \rightarrow (4)^+_{(2)_g}$	3.36(10)	4.9	2.3	3.08	3.35	2.80
810.46 / 688.73	β	$2^+ \rightarrow (0)^+_{(2)_g}$	0.17(01)	0.11	.08	0.226	0.123	0.26
901.28 / 656.58	β	$4^+ \rightarrow (2)^+_{(4)_g}$	0.09(02)	0.008		0.213	0.152	0.32
212.25 / 656.58	β	$4^+ \rightarrow (2\beta)^+_{(4g)}$	38.6(8.8)	41.3		21.9	19.40	39.4
964.09 / 1085.83	γ	$2^+ \rightarrow (2)^+_{(0)_g}$	2.51(05)	2.33	1.0	1.06	0.786	1.06
964.09 / 719.35	γ	$2^+ \rightarrow (2)^+_{(4)_g}$	11.53(33)	19.7	1.6	5.26	2.39	9.14
275.20 / 964.09	γ	$2^+ \rightarrow (2\beta)^+_{(2g)}$	1.25(19)	0.96		2.78	7.00	2.64
1112.05 / 867.42	γ	$3^+ \rightarrow (2)^+_{(4)_g}$	0.94(02)	1.42	1.0	2.30	2.32	2.68
148.11 / 1112.05	γ	$3^+ \rightarrow (2\gamma)^+_{(2g)}$	23.09(9.23)	22.7		21.1	12.8	8.91
1249.90 / 1005.18	γ	$4^+ \rightarrow (2)^+_{(4)_g}$	0.091(004)	0.16		0.459	0.500	0.34

* A & B represent two different cases and correspond to adjusting parameters to produce best fit to the first (2^+) excited state.

levels, the agreement between thoery and experiment is not good for all transitions. For B(E2) ratios involving interband transition, the experimental and the theoretical B.R.s are in agreement, i.e. the ratios $B(E2, 4^+_\beta \rightarrow 2_\beta{}^+)/B(E2, 4^+_\beta \rightarrow 4^+_g)$ and $B(E2, 3^+_\gamma \rightarrow 2^+_\gamma)/B(E2, 3^+_\gamma \rightarrow 2^+_g)$ agree with the PPQM Ref. 40 and BET (Refs. 60 and 61). When band mixing is present as for the other ratios in Table 5.7, poor agreement between theory and experiment is seen. This band mixing could arise from coupling between the rotational and the intrinsic motion of the nucleus, which would support a transitional nature of ^{152}Sm.

- The new levels ($826(2^+)$ and $1006(4^+)$ keV):

The evidence for these new levels arose initially from the observation of the four new transitions at 195, 826, 855 and 943 keV. The coincidence data summarized in Table 5.2 show that the new transition at 195 keV occur in strong coincidence with the three energy gates at 122, 244 and 444 keV suggesting that it depopulates a level at 1006 keV to the known level at 810 keV. Additional support is given by the weak coincidence between the 122 keV gate and the new transition 885 keV which could depopulate a new level at 1007 keV to the first excited state at 122 keV. Further evidence comes from the strong coincidence between a 444 keV gate and the 675 keV transition (now assumed doublet) which would have the 195 keV transition as an intermediate cascade from a new level at 1006 keV. This doublet is taken to be about 5% of the original transition from the 1041 keV to the 366 keV level. The 675 keV doublet which populates the 1006 keV level arose from another new level at 1681 keV.

The existence of a level at 826 keV is consistent with the observation of the new 943 keV γ-line from the known level at 1769 keV

followed by the 826 keV transition to the ground state. Such a depopulating transition would be expected to have an E2 multipolarity suggesting a $J^{\pi} = 2^{+}$ for the 826 keV level. The log ft. value (Table 5.4) confirms this assignment and is also consistent with $J^{\pi} = 4^{+}$ for the 1006 keV level. These levels could not be fitted into the known band structure of ^{152}Sm, but taking the 826 keV as a band head allows a 4^{+} state at 1070 keV, which may be consistent with the 1006 keV level since such a discrepancy is not unusual for a nucleus which is not purely rotational. These levels would form a new β band ($K^{\pi} = 0^{+}$) similar to the adjacent β band (Fig. 5.4) formed from the 1023 and 810 keV levels. The ratio $B(E2, 4_{\beta} \rightarrow 2_{\beta})/B(E2, 4_{\beta} \rightarrow 2_{g})$ has the large value of 958 $\pm$ 374 which is characteristic of the enhancement for inter β-band transitions over β-ground state band transitions.

- The levels 964(1^{-}) and 1041 (3^{-}) keV:

Barratte et al.[92] have suggested spin and parity (1^{-}) for the level at 964 keV and the predictions of the IBM agree with this assumption but for a level at 990 keV (Table 5.6). If the spin of this level is 1^{-} a 3^{-} state will be expected by the rotational theory at 1156 keV, which is larger than the experimental value of 1041 keV. The spin and parity of this level are deduced from log ft. values to be 3^{-} (Table 5.4). The IBM calculations give 1030 keV for this level, which is better than the rotational value (Table 5.6). This discrepancy between experiment and rotational theory is expected, because symmetry breakings, such as caused by Coriolis coupling can easily arise for negative parity bands. Table 5.8 shows that the deduced value for the K-quantum number could be either 0 or 1, and that the agreement between

TABLE 5.8.

EXPERIMENTAL B(El) RATIOS FOR TRANSITIONS DEPOPULATING THE NEGATIVE PARITY STATE AT 1041 keV IN ^{152}Sm COMPARED WITH DIFFERENT NUCLEAR MODELS.

Transition E_γ/E'_γ	$J_i \rightarrow (I)^\pi_{(J)_f}$	B(El) Ratio				Deduced Ki
		Experiment	IBM Ref. 43	Rotor (Ref. 92) Ki = 0	Ki = 1	
$\frac{919.43}{674.69}$	$3 \rightarrow (2)^+_{(4)_g}$	1.06(06)	.86	0.75	1.33	0,1

experiment and IBM in the transitional limit is better than that with rotational theory.

The γ -band (1086(2^+), 1234(3^+) and 1371(4^+) kev):

The 1086 keV level was assigned (2^+) in view of the log ft. value (Table 5.4). The perfect agreement between theoretical and experimental (α_k) for the 1086 keV transition (Table 5.5) confirms the E2 multipolarity for this transition. The 1086 keV transition depopulates the 1086 keV level to ground, this together with the E2 multipolarity for the 1086 keV transition supports the (2^+) assignment for this level. The transition 719 keV depopulates this level to the level at 366(4^+) keV level, this transition is E2 multipole (Table 5.5). This supports the (2^+) assignment for the 1086 keV level. Another support for this assignment came from the α_k value for the 964 keV transition which depopulates this level to the first excited state 122 (2^+) keV (Table 5.5). The spin and parity of the level 1234 keV were confirmed from log ft. value (Table 5.4) and from the α_k values of the two transitions 867 and 1112 keV. The first transition depopulates this level to the level 366 (4^+) keV. This transition is E2 multipole (Table 5.5), while the second transition depopulates this level to the level at 122 (2^+) keV is another E2 multipole (Table 5.5) (see Fig. 5.3). The third level 1371 keV is assigned 4^+ according to the log ft. value (Table 5.4) and supported by the α_k value of the transition 1005 keV which depopulates this level to the state 366 (4^+) keV, since excellent agreement between theoretical and experimental α_k value (Table 5.5) indicates that this transition is E2 multipole. The theoretical expectations (Table 5.6) give another support for the spin sequence of these levels (2,3 and 4). The best theoretical values are

given by IBM (Ref. 43), and by rotational theory calculated in this work. Poor agreement with experiment is given by the theoretical calculations of the BET (Ref. 60) and PPQM (Ref. 40). Table 5.7 shows the B(E2)B.R.s for transitions depopulating these levels in the above band which was taken as γ band. It was mentioned (in the discussion of the β band with levels 810 and 1006 keV) that good agreement between theory and experiment is seen for transitions within the band (especially for PPQM and BET), while for transitions between different bands poor agreement is seen. The new transition 193 keV depopulates the 1234 keV level to the level at 1041 keV. This was proved from coincidence data, since the energy gate 244 keV shows strong coincidence with this transition (Table 5.2 and Fig. 5.2). This supports the existence of this transition and that it belongs to ^{152}Sm as well as ^{152}Gd (see Chapter 4).

- The new levels 1377 (2^+) and 1467 (3^+) kev:

The new level 1377 keV was introduced because two new transitions 1011 and 1378 keV were seen in the singles data during the present work (Table 4.). The coincidence spectra (Table 5.2 and Fig. 5.2) show strong coincidence between the 122 keV gate and the 1011 keV transition, while weak coincidence is seen between this transition and the 244 keV gate. This supports the existence of this level. The spin and parity of this level (2^+) were deduced from log ft. value (Table 5.4). This assignment is supported by the decay of this level to the ground state through the transition 1378 keV. The second level 1467 keV was suggested because the two transitions 443 and 657 which depopulate this level to the levels 1041 and 810 keV are triplet and doublet respectively. Coincidence data (Table 5.2 and Fig 5.2) show weak coincidence between 444 keV gate and the transitions 657 and 901 keV. This supports the

assumption that the 444 keV transition is doublet. The 567 keV gate shows very strong coincidence with 444 keV transition. This supports the doublet of the 444 keV line and the doublet of the 567 keV transition and the existence of the level at 1467 (see Fig. 5.3). The spin and parity of this level is deduced from log ft. values (Table 5.4). The two levels 1377 and 1467 could form a γ-like band, since the rotational theory calculations agree with experimental value for the 1467 keV (see Table 5.6). This supports the spin and parity assignments for these levels.

- The new band (1437(2^+), 1573(3^+) and 1681(4^+) keV):

The level 1437 decays by the new transition 203 keV to the level at 1234 keV which is a member of a γ-band. The intensity of this transition is weak (Table 4.) but the coincidence data prove its existence since strong coincidence between this transition and the 964 energy gate is seen (see Table 5.2 and Fig. 5.2). Two energeis populate this level, the 212 keV and the 244 keV doublet (see Fig. 5.3.) The log ft. value cannot be determined for this level because the decay-feeding γ-ray rule cannot be applied here, but theoretical calculations support the 2^+ assignment (Table 5.6). The second level 1537 keV was introduced because strong coincidence was seen between the 244 keV gate and the 1170 keV transition (both of these are doublets) (see Table 5.2). The log ft. value (Table 5.4) support the 3^+ assignment for this level. This value was suggested according to the agreement between theoretical and experimental energy levels (Table 5.6). The level 1681 keV was suggested in view of the coincidence data, since strong coincidence between the energy gate 689 keV and the transition 675 keV (doublet) was seen (Table 5.2). This level

decays to the level at 1437 keV by the 244 keV doublet transition and to the level at 366 keV by the transition 1315 keV (Fig. 5.3). This transition was reported previously[92,99] but could not be placed in the decay schemes. The coincidence data (Table 5.2) show weak coincidence between this transition and the two gates 122 and 244 keV, since the intensity of this transition is weak (Table 4.1),one can consider that these data support the existence of the new level at 1.681 keV. The log ft. value (Table 5.4) supports the 4^+ assignment for this level together with the theoretical calculations (Table 5.6). These three levels form a γ-like band with the spin sequence 2,3 and 4.

- The levels 1530(2^-) and 1579(3^-) keV:

The 1530 keV level was assigned 2^- in view of the log ft. value (Table 5.4) and from the α_k coefficients of the transitions depopulating this level (Table 5.5). To deduce the K_i-quantum number for this band of levels, the B(EL)B.R. were calculated and compared with theory (Table 5.9), K_i was given 1 or 2 for transition depopulating the 1530 keV level, while K_i is 1 for transitions depopulating the other member of the band (1579 keV level), thus we conclude that K_i is 1. The agreement between theory and experiment is not very good. In this particular case, the theoretical B.Rs of the transitions depopulating these levels to the ground state band disagree with experiment. This may suggest that ^{152}Sm near this region is rather transitional nucleus than rotational. The spin and parity of the 1579 keV level (3^-) are determined from log ft. value (Table 5.4) and the α_k coefficient of the 1213 keV transition which depopulates this level to 366 keV level (Table 5.5). The theoretical calculations for the energies of this band are in poor agreement with experiment

TABLE 5.9.

RELATIVE EXPERIMENTAL B(EL) RATIOS FOR TRANSITIONS

FROM NEGATIVE PARITY STATES IN ^{152}Sm COMPARED WITH THEORY

E_γ (kev)	Initial level keV	$J_i \rightarrow (JK)_f$	EL	B(EL) experiment	Theoretical B(EL) ratio for different K_i (Ref 92)				Deduced K_i
					0	1	2	3	
566.32	1530	2 → 10	E2	0.075(018)		0.25	4.00		1,2
488.66		2 → 30	E2	1.0		1.00	1.00		1,2
443.91		2 → 22	E1	1.0		1.00	1.00		1,2
295.66		2 → 32	E1	0.57(02)		2.00	0.50		2
1457.47	1579	3 → 20	E1	0.21(01)	0.75	1.33			0
1213.08		3 → 40	E1	1.0	1.0	1.0			0,1
768.90		3 → 20	E1	0.31(02)	0.22	0.22			0,1
556.96		3 → 40	E1	0.12(09)	0.29	0.16			1
564.05	1650	2 → 22	E1	1.83(07)		0.50	2.00		2
415.95		2 32	E1	1.0		1.00	1.00		2
1607.98	1730	3 → 20	E1	0.12(06)	0.75	1.33			(0)
1363.46		3 → 40	E1	1.00	1.00	1.00			
671.19	1757	3 → 22	E1	1.23(28)		0.11	0.71	2.86	2
522.86		3 → 32	E1	1.00		1.00	1.00	1.00	2

(Table 5.6), but, as was mentioned before, we expect breaking of symmetry for the negative parity bands. The new transition 823 keV was inserted in the decay scheme according to energy balance only. This transition depopulates the level at 1530 keV to the level at 707 keV, which has no gamma rays depopulating it; thus it is difficult to check the coincidence evidence for this transition.

- The levels 1650 keV (2^-) and 1757 keV(3^-):

The spin and parity of the 1650 keV level are confirmed as 2^- assignment from both log ft. values (Table 5.4) and the α_k coefficients of the 564 keV transition which depopulates this level to the 1086 keV level (Table 5.5). The K_i in this level is determined from Table (5.9), the value assigned is 2. The second level (1757 keV) was assigned 3^- in view of the log ft. values (Table 5.4) and the B(El) B.R. (Table 5.9). The theoretical calculations[c] of the energy spectrum show excellent agreement with experiment (Table 5.6) for this band. The theoretical prediction was based on the spins 2 and 3 for these two levels. This proves this spin assignment. The new transition 943 was seen in singles data (Table 4.1). This transition is assumed to be doublet, one of the doublets depopulates the level at 1650 keV to the level at 707 keV. No coincidence data can be obtained (Fig. 5.3). thus energy balance only was used to insert this energy.

Another new transition (1050 keV) depopulates the level at 1757 keV to the 707 keV level, again energy balance was used to insert this transition, since no coincidence data can be obtained.

5.5. The interacting boson model (IBM):

The theoretical background was discussed in Chapter 2. Here, the

results of the calculations of the transitional limit from SU(5) to SU(3) will be given.[43] In this model ^{152}Sm was treated as belonging to the transitional region between spherical and deformed nuclei. The energy values taken from Ref. 43 are given in Table (5.6). The agreement with experiment is poor, but the model succeeded in predicting a large number of levels including the negative parity states.

In the SU(5) vibrational limit (Chapter 2), the ratio $E(4^+)/E(2^+)$ is 2/1[42] while in SU(3) rotational limit, $E(4^+)/E(2^+)$ is 10/3 and $E(6^+)/E(2^+)$ is 7. In the case of ^{152}Sm, $E(4^+)/E(2^+)$ is 3.02 and $E(6^+)/E(2^+)$ is 5.79. These values lie between the two limits, the SU(5) and the SU(3) and closer to SU(3) limit. For ground band state and the γ-band state, closer agreement between experiment and theory is achieved than for the β-band.

Fig. 5.4 shows closer agreement between theory and experiment for these bands. Since these calculations were based on rotational theory, then one assumes that these bands have more tendency towards rotational properties than vibrational ones. The two levels 964 and 1041 keV show poor agreement with rotational theory, but closer agreement is achieved with the transitional limit (Table 5.6). One may conclude that this band possesses more vibrational properties than rotational ones. The transitional theory calculations[43] for B(E2) of the first excited state of ^{152}Sm is 0.59 e^2b^2. The calculations of SU(3) limit (Chapter 2) gives B(E2) = 1.05 e^2b^2, while the SU(5) limit gives 0.29 e^2b^2 for B(E2) of this state. This shows that ^{152}Sm lies between these two limits.

Table 5.10 shows the experimental and the different theoretical values for the B(E2) of the 122 keV transition. Good agreement between theory and experiment is achieved, especially the PPQM[40] and the BET[60,61].

TABLE 5.10

EXPERIMENTAL REDUCED TRANSITION PROBABILITY B(E2)

FOR THE 122 keV TRANSITION IN ^{152}Sm COMPARED WITH THEORY

$J_i^\pi \rightarrow J_f^\pi$	B(E2) e^2b^2						
	Experiment	PPQM Ref. 40	IBM Ref. 43	Single Particle	BET (ref. 61) A	B	BET Ref. 60
$2^+ \rightarrow 0^+$	0.649(041)	0.648	0.596	0.0048	0.697	0.651	0.673

Table 5.11 gives the Q_2 experimental and theoretical values and good agreement between these is seen.

Table(5.8) shows the B(El) B.R. for transitions depopulating the negative parity state at 1041 keV, closer value to experiment is given in the case of the transitional limit of IBM. This supports the transitional tendency in ^{152}Sm nucleus. The ratio R (equation 2.32, Chapter 2) was calculated. For β -band transition to ground, $R = 0.17 \pm 0.01$, while for γ -band transition to ground, $R = 0.39 \pm 0.01$. This proves the transitional nature of ^{152}Sm nucleus between the two limits, i.e., vibrational (with R = 0) and rotational (with R = 7/10).

5.6. Other levels:

- The new level 1147 keV(2^+) was suggested since the single transitions 1147 keV and the 622 keV were observed (see Fig. 5.3). Since this level decays directly to the ground state, 2^+ was suggested for it. The log ft. value (Table 5.4) supports this assignment.

- The 1 293 keV (2^+) level:

The spins and parity of this level are confined to (2^+) from the log ft. value (Table 5.4) and from the fact that this level decays to the ground state (1293 keV). Table 5.12 shows the B(EL) B.R. for transitions depopulating this level. The B(El) B.R. agrees with experiment ($K_i = 0$), while poor agreement with experiment for B(E2) B.R. for $K_i \neq 1$ is seen. The other B(E2) B.Rs. do not agree with experiment then ($K_i = 0,1$). This shows strange nature for this level, which could be excited in transitional mode of excitation between vibrational and rotational degrees of freedom. There is always possibility

TABLE 5.11

ELECTRIC QUADRUPOLE MOMENT Q FOR THE FIRST EXCITED STATE IN ^{152}Sm COMPARED WITH THEORY

Energy level (keV)	Q eb				
	Experiment	PPQM Ref. 40	BET(Ref. 61) A	BET(Ref. 61) B	IBM Ref. 43
121.97	- 1.631(100)	- 1.64	- 1.72	- 1.68	- 1.56

TABLE 5.12

RELATIVE EXPERIMENTAL B(EL) RATIOS FOR TRANSITIONS FROM POSITIVE PARITY STATES IN ^{152}Sm COMPARED WITH THEORY

E_γ (keV)	Initial level (keV)	$J \rightarrow (JK)^\pi_f$	EL	B(EL) ratios				
				Experiment	Theory for different K_i from Ref. 92			Deduced K_i
					0	1	2	
1293.03	1293	$2 \rightarrow 0^+_g$	E2	0.055(002)	0.012	0.048	0.012	
1170.40		$2 \rightarrow 2^+_g$	E2	0.004(001)	0.017	0.017	0.017	
926.26		$2 \rightarrow 4^+_g$	E2	0.35 (01)	0.031	0.054	0.008	0
482.34		$2 \rightarrow 2^+_\beta$	E2	1.0	1.0	1.0	1.0	
329.19		$2 \rightarrow 1^-$	E1	0.87 (07)	0.67	1.50		
251.58		$2 \rightarrow 3^-$	E1	1.0	1.0	1.0		
1768.19	1769	$2 \rightarrow 0^+_g$	E2	1.75 (22)	0.70	0.28	0.70	0,2
1646.80		$2 \rightarrow 2^+_g$	E2	1.0	1.0	1.0	1.0	

for predominantly spherical states (vibrational) co-exist with deformed states (rotational). This assumption was supported by two nucleon transfer reactions in the work of Hinds et al.[112] and McLatchie et al.[120].

- The new level 1661 keV ($2,4^+$)

This level was introduced in the decay scheme according to the observation of the new transition 1662 keV, which depopulates this level to the ground state, hence suggests $J^\pi = 2^+$. The log ft. value (Table 5.4) suggests 2^+ or 4^+ spins and parity. Hence, one assigned the unconfirmed spin and parity ($2,4^+$) for this level.

The 1538 keV transition was reported previously by many workers [93,95,99] but they could not be able to place it in their decay schemes. In this work this transition was inserted between this new level (1661 keV) and the 122 keV(2^+) member of the ground state. This was confirmed from the coincidence data (Table 5.2). This proves the existence of the 1661 keV level.

- The 1730 keV (3^-) level:

The spin and parity of this level were assigned according to log ft. value (Table 5.4). Table 4.9 shows B(El) B.R. for transitions depopulating this level. The theoretical values were calculated considering 3^- assignment, the agreement with experiment is poor, but as mentioned previously, for these octupole levels, one expects poor agreement with experiment $K_i = 0$).

- The 1769 (2^+) keV level:

This level is well established since eight transitions depopulate

it. Four of these are the new transitions 392, 622, 805 and 943 keV. The coincidence data (Table 5.2 and Fig. 5.2) show strong coincidence between the 392 keV transition and the two gates 122 and 244 keV. This would support the new level at 1377 keV (see Fig. 5.3). Transitional 622 keV is in weak coincidence with the gate 122 keV. This would support the new level at 1147 keV. The new transition 805 keV was reported to the first time in Ref. 98. In this work, it was inserted between this level and the level at 946 keV. This was supported from the coincidence data (Table 5.2) which show that this transition is in weak coincidence with both gates at 122 and 842 keV. The transition 943 is believed to be doublet. This doublet depopulates the level 1769 keV to the new level 826 keV. The energy balance was used only to insert this transition between these two levels, since no coincidence data can be obtained (Fig. 5.3). The spin and parity of this level were assigned according to log ft. value (Table 5.4). The direct decay of this level to ground support the (2^+) assignment.

Table 5.12 supports this assignment, since the B(E2) B.Rs were calculated assuming that this level is 2^+. For (K = 0,2), the agreement between experiment and theory is not good, but these calculations were based on the rotational theory, then one may conclude that ^{152}Sm is rather translational at this state.

5.7. Conclusion:

The ^{152}Sm nucleus has been considered as a deformed nucleus showing rotational characteristics but allowing some vibrational degrees of freedom. The expectations of the rotational theory for the

energy levels show reasonable agreement with experiment (Fig. 5.4). The transitional calculations of the IBM[43] show smaller values for the (GSB) than experimental ones, while for the β -band the experimental values are lower than the theoretical values. For γ -band, these predictions are lower than the experimental values, exactly like the rotational theory calculations. In the negative parity band ($K^{\pi} = 1^{-}$), the two experimental values lie in between the theoretical values.

From these considerations it is clear that the ^{152}Sm nucleus is transitional, but that the energy spectrum is more rotational than vibrational.

In the case of B(EL) ratios, the agreement between experiment and theory is poor if no correction is made for possible rotation - vibration interactions. For an axially symmetric rotor, the intrinsic and the rotational motions of the nucleus do not disturb each other[33], therefore no correction should be made and no vibration and rotation coupling is present. If band mixing is allowed between the β- or the γ-vibrational bands into the (GSB), the B(EL) ratios can be corrected. These reactions were given in the work of Lipas[121] and Mikhailove[122]. Table 5.13 shows the B(EL) ratios for the transitions from β- or γ - bands to the (GSB). Ref. 38 gives the predictions of the adiabatic symmetric rotor model without mixing between the bands, while Ref. 123 shows the predictions of Bohr & Mottelson model (assuming a symmetric rotor as given in Refs. 33 and 38), but with mixing corrections. Ref. 92 gives the predictions of the rotor model using the corrections made by Mikhailove (Ref. 122). It is seen that when mixing corrections are made, the theoretical values get closer to experiment.

TABLE 5.13

EXPERIMENTAL B(E2) RATIOS FOR TRANSITIONS FROM β AND γ BANDS TO GROUND BAND IN ^{152}Sm COMPARED WITH THEORY

Transition $E_\gamma / E_{\gamma'}$	Energy band	$J_i \rightarrow \frac{(J)'}{(J)_g}$	B(E2) ratio			
			Experiment	Ref. 38 without mixing	Ref. 123 with mixing	Refs. 92 & 122
$\frac{443.91}{688.73}$	β	$\frac{2 \rightarrow 4}{2 \rightarrow 2}$	3.36(10)	1.8	5.36(61)	2.14(19)
$\frac{810.46}{688.73}$	β	$\frac{2 \rightarrow 0}{2 \rightarrow 2}$	0.17(01)	0.70	0.33(04)	0.25(10)
$\frac{443.91}{810.46}$	β	$\frac{2 \rightarrow 4}{2 \rightarrow 0}$	19.45(82)	2.60	16.20(3.80)	8.49(3.46)
$\frac{901.28}{656.58}$	β	$\frac{4 \rightarrow 2}{4 \rightarrow 4}$	0.09(02)	1.10		0.106(011)
$\frac{964.09}{719.35}$	γ	$\frac{2 \rightarrow 2}{2 \rightarrow 4}$	11.53(33)	20.00		0.57(04)
$\frac{964.09}{1085.83}$	γ	$\frac{2 \rightarrow 2}{2 \rightarrow 0}$	2.51(05)	1.43		1.69(09)
$\frac{1085.83}{719.35}$	γ	$\frac{2 \rightarrow 0}{2 \rightarrow 4}$	4.54(13)	14.00		0.34(02)
$\frac{867.42}{1112.05}$	γ	$\frac{3 \rightarrow 4}{3 \rightarrow 2}$	1.06(02)	0.40		2.70(-)
$\frac{1005.18}{1249.90}$	γ	$\frac{4 \rightarrow 4}{4 \rightarrow 2}$	10.93(45)	2.94		3.54(91)

In general, it is difficult to evaluate the band mixing, especially for nuclei clustering around the transitional region.[113] It was noticed that there is general disagreement between the experimental and the theoretical B.Rs for the members of $K^{\pi} = 1^{-}$ band (Table 5.9) which could be due to Coriolis coupling between these negative parity γ-bands.

The 1293 keV level could be a member of K = 0 band (Table 5.12). The ratio B(E2, 482)/B(E2, 1170) is 250 $\pm$ 79, supports this assumption, therefore this level could be a member of another β-band. The k-quantum numbers of the other levels were confirmed by comparing the experimental and theoretical B.Rs of the transitions depopulating them. The new level at 1006 keV is proved to belong to a β-like band, since B(E2, 195)/B(E2, 884) is 958 $\pm$ 374.

Nine new energy levels have been inserted, together with fifteen new transitions and the existence of the levels by theoretical calculations (Table 5.6). The spins and parities of these levels were assigned in view of their log ft. values and from other possible information. Two old transitions, reported to be previously by other workers have been placed into the decay scheme. These are 1315 keV and 1538 keV (Fig. 5.3). The transition 1643 keV could not be placed in the decay scheme. The transition 805 keV was reported by Baker et al.[98] and was seen in the present work and was placed in the decay scheme according to coincidence spectra. The transition 192 keV was reported in Ref. 105 and was placed in the decay of ^{152}Gd. Here, clear evidence from coincidence data indicates that this transition belongs to both nuclei (see Chapter 4).

Barratte et al.[92] reported that the 1681 keV transition is arising

from the decay of $^{152}Eu^{m}$, hence they assigned (1^-) for this level.

In this work, this level is inserted in the decay scheme according to singles and coincidence data reported here. The spin and parity of this level is assigned 4^+, this was suggested in view of the log ft. value (Table 5.4) and from theoretical predictions of the rotational model. This level was well established as a member of the γ-like band consisting fromthe new two levels 1437 keV (2^+) and 1537 keV (3^+) together with this level (Fig. 5.4).

CHAPTER 6.

STUDIES OF THE ^{182}W ISOTOPE.

6.1. Introduction:

The decay scheme of ^{182}W was established by observing the γ-rays emitted after the β^- decay of ^{182}Ta. ^{182}Ta is used as a calibration source for Ge(Li) detectors, since it emits two sets of gamma energies, the low energy portion (< 300 keV) and the high energy portion (> 900 keV). Two detectors were used to measure the singles spectra for ^{182}Ta. The low energy portion was measured by pure Ge detector, while the high energy portion was measured by Ge(Li) detector.

Extensive measurements have been made on the γ-rays resulting from β^- decay of ^{182}Ta[124-129]. These authors have used different techniques and reported different portions of the single spectra of this isotope. Roney and Sale[124] have employed a coaxial Ge(Li) detector to measure singles and intensities in ^{182}Ta. They reported prominent γ-rays starting from 100 keV, but their cutoff energy was 1290 keV. They have reported six energies seen in the present work and in Ref. 130.

U. Schotzig et al.[125] have used a large volume Ge(Li) detector and reported energies starting from 32 keV with a cutoff energy at 1290 keV. The 1274 keV transition was missing from their list together with other six more energies while they have reported the new energy 58 keV which was not seen before. The intensity reported for both energies (66 and 68 keV) was 161.7, which did not agree with any previous value. Geherk et al.[126] reported a list starting from 68 keV

with a cutoff energy at 1453 keV, but fifteen energies sees before were missing, in addition to that, disagreement between intensities reported in their work and in Ref. 128 was seen. R. Helmer[127] measured the γ-rays above 800 keV and N. Lavi[128] has reported a list starting from 68 keV with a cutoff energy 1387 keV, but a remarkable disagreement between intensities reported in his work and other authors' was seen.

J. Sapyta et al.[129] have carried out singles and coincidence measurements using planar and coaxial Ge(Li) detectors. Their list started from 85 keV transition with a cutoff at 1453 keV and some transitions were missed from this list. The reported errors in relative intensities were 10% for energies $<$ 400 keV and 7% for energies $>$ 400 keV. In their coincidence experiment, only two energy gates (100 and 229 keV) were taken to establish the decay scheme. A complete list of γ-energies and their intensities was reported in Ref. 130.

In the present work, the β^- decay of ^{182}Ta was reinvestigated and all energies reported in Ref. 130 were seen in addition to the observation of new fifteen transitions. Five new energy levels were inserted which were confirmed from coincidence data and other theoretical considerations and the spins and parities of them were assigned from log ft. values and other possible information. The spins and parities of some levels were confirmed and a new β^- branching ratio was assigned for the 100 keV level. The half-lives of three energy levels were measured using the plastic - Ge(Li) detectors technique.

The nuclear structure of ^{182}W nucleus was investigated by applying the geometric model, hence calculating the rotational theory parameters of the axial rotor. The SU(3) limit of the IBM was

applied and the parameters of the model were calculated. The investigations show that ^{182}W is a deformed nucleus therefore shows rotational spectra.

The negative parity states were investigated in view of a residual interaction arising from pairing plus a modified octopole - octopole force. The miscroscopic theoretical calculations using the residual pairing plus multipole forces performed by Neergard and Vogal[131] well reproduced the $K^{\pi} = 2^{-}$ state at 1290 keV. Although these calculations were more realistic in explaining the band mixing between octopole vibrational multiplet states, the experimental evidence found by Herzog et al.[132] suggested that the band mixing between the $K^{\pi} = 2^{-}$ and the $K^{\pi} = 3^{-}$ bands was not so strong as was expected. A disputed configuration, Ref. 132, predicted a more collective structure at this state. Ref. 131 predicted a low-lying octopole vibration in this energy region with $K^{\pi} = 2^{-}$ and a rather strong Coriolis coupling of this band to the $K^{\pi} = 3^{-}$ member of the octopole multiplet. The inelastic scattering cross section of deuterons measurements indicate that the $K^{\pi} = 2^{-}$ rotational band in ^{182}W is rather more pure than predicted theoretically.[133] It was suggested that there is some configuration mixing with $K^{\pi} = 3^{-}$ band.

6.2. Results:

6.2.1. Singles Spectra:

Ge(Li) detector (no. 1, Table 3.1.) was used to measure energies greater than 300 keV, while the pure Ge detector (no. 3, Table 3.1., Chapter 3), was used to measure soft γ-rays below 300 keV. In Chapter 3, source preparations and experimental arrangements were discussed.

The singles spectra of ^{182}Ta (half-life 115 days)[90] are shown in Fig. (6.1) and the results are given in Table (6.1). In the low energy portion of the spectrum, results from Ge and Ge(Li) detectors were combined together to provide precise energy and intensity values. The table also shows the relative intensities reported in present work together with those given in previous work for comparison, good agreement between the values reported in the present work and other workers' values is seen especially for the high energy portion. The uncertainties in the intensities of the present work are about 1%.

6.2.2. Coincidence Spectra:

The $\gamma - \gamma$ coincidence spectra were written on three magnetic tapes and six energy gates were taken to establish the decay scheme on the basis of the coincidences between these gates and the rest of the spectrum. These were 100, 299, 352, 1002, 1122 and 1289 keV energies. In each gate the B.G. and the chance coincidences were subtracted (See Chapter 3).

Most of the transitions were in coincidence with the 100 keV transition, since this transition depopulates the first excited state 100 keV (2^+) to ground. The second gate was taken to provide more coincidence data for transitions depopulating the second excited state (4^+) in the ground state band to the 100 keV level. This gate gives support to some of the new transitions observed in the singles measurements during the course of this work. The 352 keV transition depopulates the 682 keV (6^+) level, which is the highest member of the ground state band to the 330 keV level. The γ -ray feeding of this level is weak and in this work two new transitions were seen to feed this level (see Fig. 6.4.). Therefore, it was important to study the

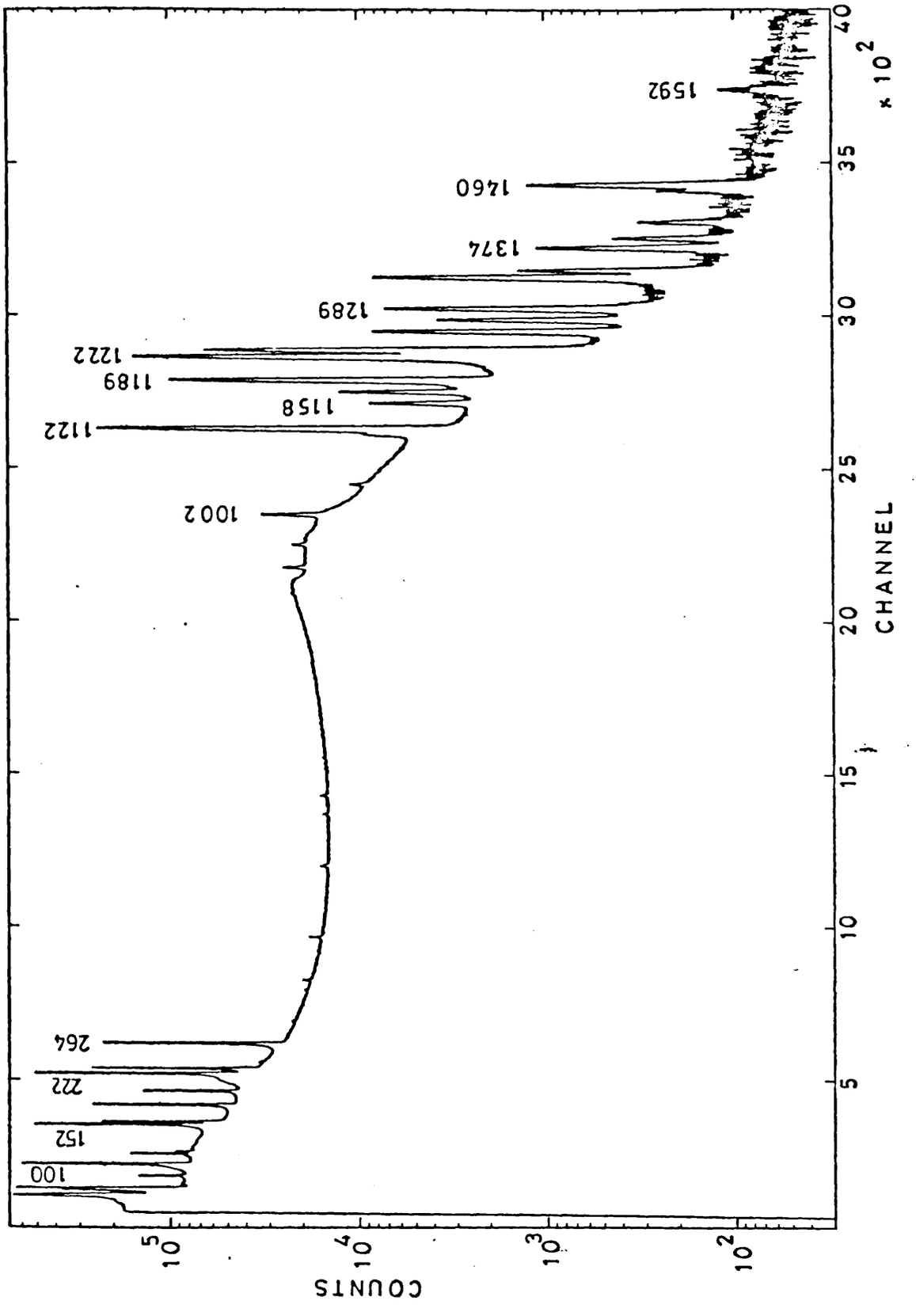

Fig.(6.1) Ta - 182 single spectrum

Table 6.1.

Relative intensities of γ-rays emitted from the decay of ^{182}Ta.

Energy (keV)	Intensity related to I (1122) = 100				
	Present work	Ref.124	Ref.125	Ref.126	Ref.130
32.25	1.40(02)		2.53(06)		1.8
43.16	0.80(01)		0.75(02)		0.70(04)
50.68	4.71(07)				
65.51	8.45(14)				8.0(4)
67.96	118.34(2.01)			122.0(6.0)	118.0(6.0)
75.12	0.30(01)				
84.76	6.81(26)		7.45(16)	7.8(4)	7.6(4)
100.0	40.50(64)	40.60(2.60)	40.33(94)	40.80(1.20)	40.2(1.10)
110.33	0.25(01)				0.26
113.58	5.47(08)	4.95(40)	5.29(19)	5.43(17)	5.5
116.30	1.22(02)	1.18(18)	1.26(05)	1.26(04)	1.27(80)
152.05	19.52(32)	19.59(80)	19.69(24)	20.50(60)	20.5(4)
156.20	7.26(11)	7.43(30)	7.46(11)	7.77(23)	7.8(2)
170.06	0.03(01)				
179.29	8.38(09)	8.88(66)	8.75(09)	9.10(28)	9.0(3)
198.33	3.91(04)	4.13(28)	4.09(05)	4.31(13)	4.4(2)
209.32	0.04(01)				
222.18	21.12(22)	21.75(56)	21.27(24)	21.9(7)	21.6(6)
229.43	10.33(13)	10.39(34)	10.32(11)	10.6(3)	10.4(3)
238.79	0.18(01)				
264.31	9.81(12)	10.36(52)	10.26(14)	10.5(3)	10.4(3)
320.60	0.04(01)				
338.80	0.07(01)				
352.39	0.24(01)				0.04(03)
473.21	0.03(01)				
610.11	0.37(02)				
892.87	0.14(04)				0.15(02)
911.90	0.32(04)				
928.61	1.85(03)	1.53(45)			1.79(09)
960.34	1.06(03)	0.92(47)			1.02(06)
1,002.25	5.99(06)	5.99(35)			5.98(03)
1,044.87	0.68(03)				0.69(08)
1,113.71	0.95(04)	1.18(07)			1.13(01)
1,121.66	100	100	100	100	100
1,157.82	2.72(06)				2.83(63)
1,180.79	0.10(03)				0.26(04)
1,189.29	46.90(45)	47.61(53)	46.59(33)	46.5(5)	47.0(5)
1,221.57	78.31(79)	78.14(93)	76.96(54)	77.8(8)	78.3(1)
1,231.14	33.20(22)	32.32(56)	32.81(23)	32.96(33)	33.1 (4)
1,257.40	4.27(02)	4.33(15)	4.25(02)	4.26(04)	4.33(07)
1,273.87	1.87(01)	1.66(18)		1.86(02)	1.9(4)
1,289.15	3.89(04)	4.06(22)	3.86(02)	3.86(05)	4.04(07)
1,342.58	0.72(01)				0.75(02)
1,373.61	0.60(01)				0.66(02)
1,386.89	0.20(01)				0.21(10)
1,409.45	0.10(01)				0.11(01)
1,452.73	0.09(-)				0.12(01)
1,460.29	1.54(01)				
1,592.18	0.05(01)				
1,620.36	0.03(-)				
1,711.93	0.02(-)				
1,762.99	0.18(04)				

coincidence between the 352 keV transition and the rest of the spectrum. The coincidence between the high energy transitions and the rest of the spectrum were studied by considering the last three gates 1002, 1122 and 1289 keV. The 1122 keV transition depopulates the first excited state in the γ - band to the 100 keV level, thus this gate provides the coincidence data which allows us to study the transitions between the members of this band and the members of other bands. The 1289 keV transition depopulates the first member of the octopole band ($K^{\pi} = 2^{-}$) to the ground, and choosing this transition as energy gate enables us to study the transitions from other bands to this band. The coincidence data taken in these six gates provide a required evidence for the existence of the new energy levels and transitions. These results are listed in Table (6.2), the symbols used are the same as those used in Chapters 4 and 5. A typical coincidence spectra are shown in Figs.(6.2.a.),(6.2.b.), . . .

6.2.3. Lifetime measurements:

The details of the lifetime spectrometer were discussed in Chapter (3). The half-lives of three nuclear levels were measured in this work. In the case of the 100 keV level, the fast time spectrum was gated by the 100 keV transition, the plastic detector gate was set to the Compton edge of the 100 keV peak, and the life-time spectrum was recorded and stored in the MCA memory for about four weeks. Fig. (6.3.a.) shows the lifetime spectrum for the 100 keV level and the value calculated was 1.38 ± 0.03 n.sec.

The half-life of the energy level at 1554 keV was measured by gating the fast time spectrum by the 264 keV line, since this peak is well separated from others in the spectrum and its intensity

γ - γ coincidence results from the decay of ^{182}Ta.

Transition	Gate (keV)					
	100.10	229.43	352.39	1,002.25	1,121.66	1,289.15
65.51	S	VW	S		S	
67.96	S	VW	S		S	
75.12	S	W				
84.76	W	W	W		S	W
100.10		W	S	W	VS	
110.33	VW	S			S	
113.58	W	W	VW	W	VS	
116.30	W	W				
152.05	S	W	VS		VS	
156.20	S	S	W	W	VW	
170.06	S	VW	VW			
179.29	S	W	S	W	S	S
198.33	W	VW			VS	VS
209.32	VS	W	VW	S	W	VW
222.18	VS	VS	VS	VS	W	S
229.43	S		VS	VS		
238.79	VS	S			S	
264.31	S	W	VS		VS	S
320.60	W	W				
338.80	S	W	VW	VW	VW	VW
352.39	S	S			W	
473.21	W	VW	VW		W	VW
610.11	W	W	W			
892.87	W	VS				
911.90	W	W	W			
928.61	W	VS				
960.34	W	VS				
1002.25	VS	VS				
1044.87	S	S				
1113.71	VW	VS				
1121.66	S					
1157.82	S	VS				
1180.79	VW	VS				
1189.29	S	W				
1231.14	W					
1273.87	W					
1289.15	VW					
1342.58	W					
1386.89	W					
1409.45	W					
1452.73	W					

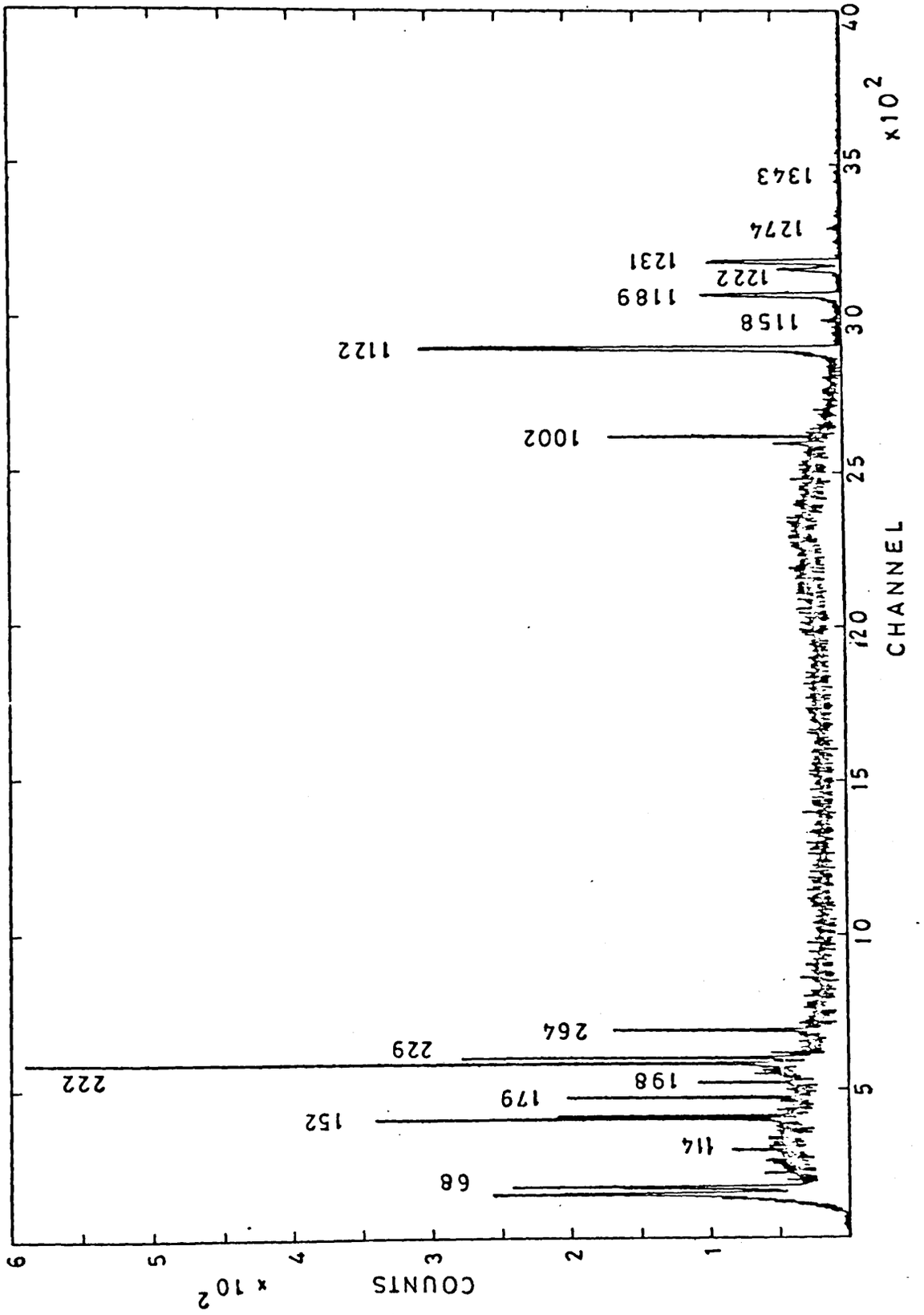

Fig.(6.2.a) Ta - 182 spectrum in coincidence with 100 keV.

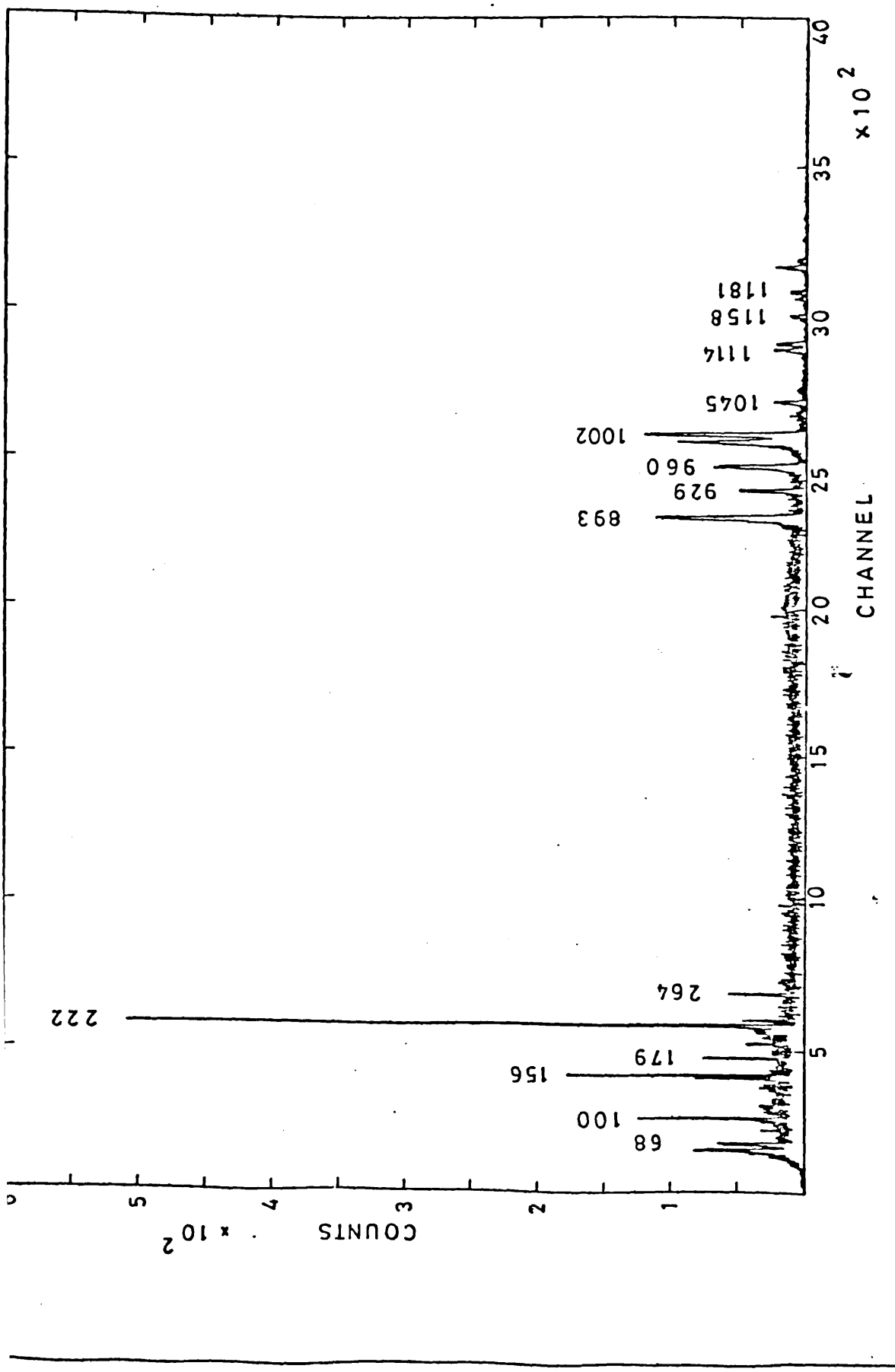

Fig.(6.2.b) Ta - 182 spectrum in coincidence with 229 keV.

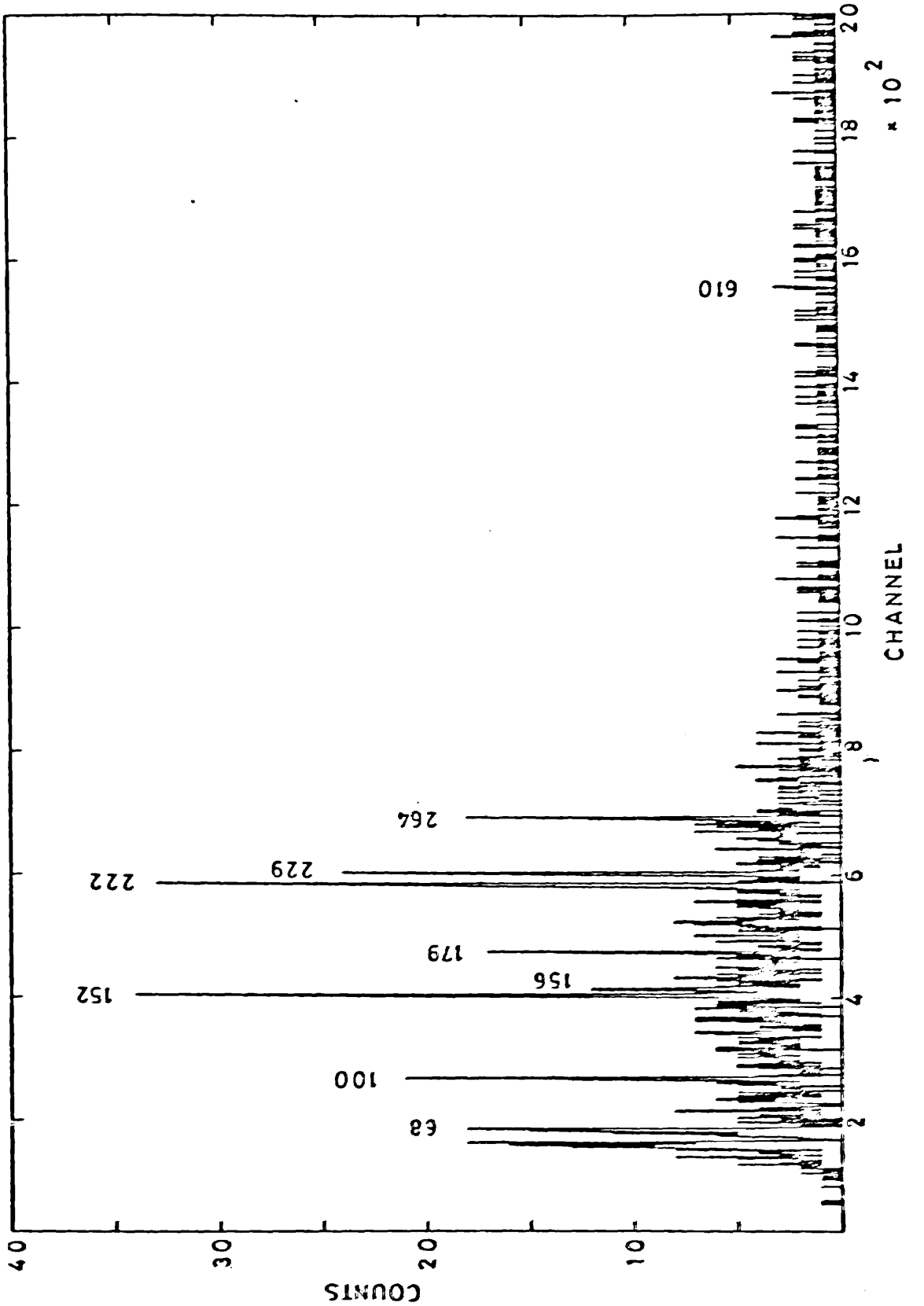

Fig.(6.2.c) Ta - 182 spectrum in coincidence with 352 keV.

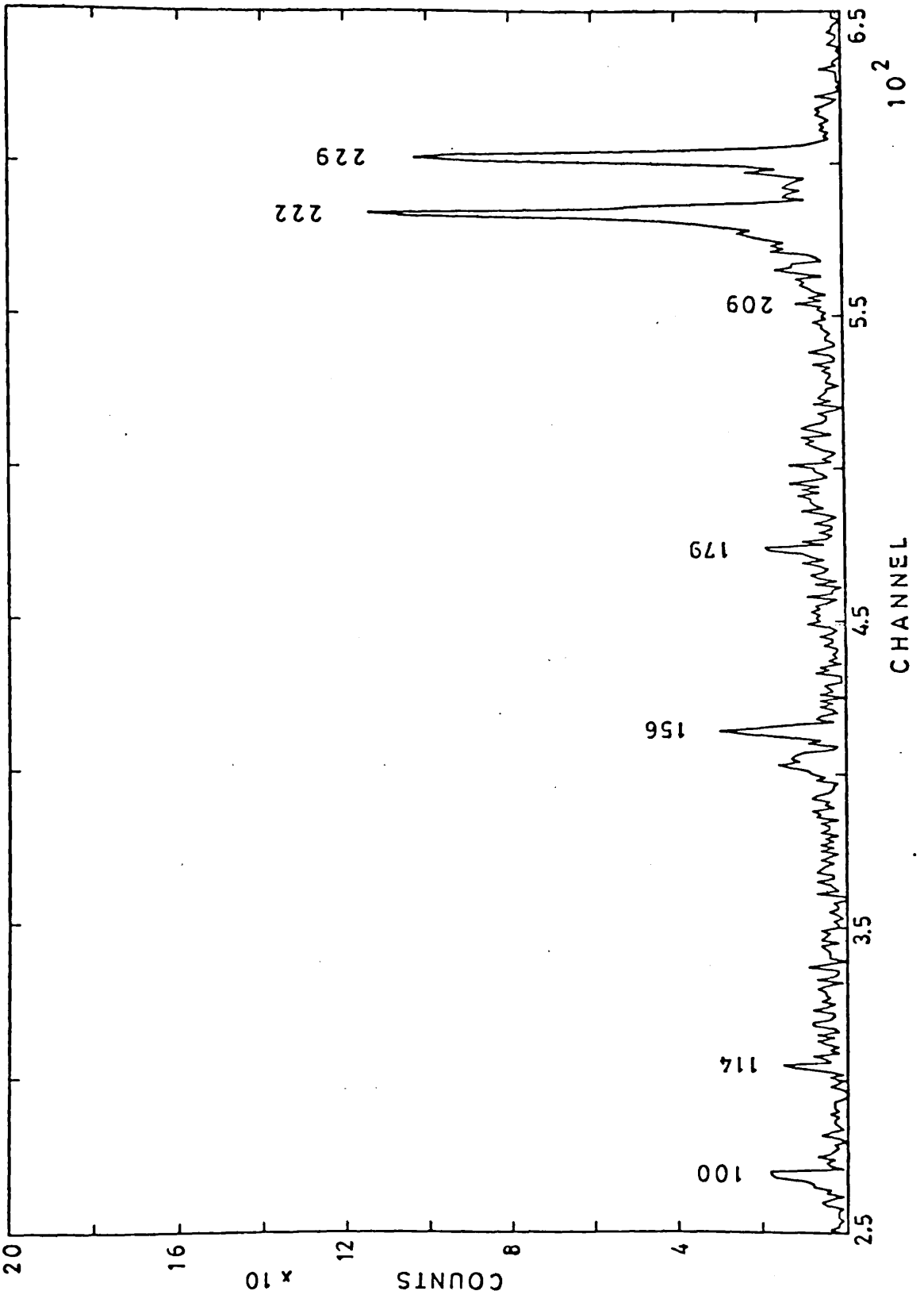

Fig.(6.2.d) Ta - 182 spectrum in coincidence with 1002 keV.

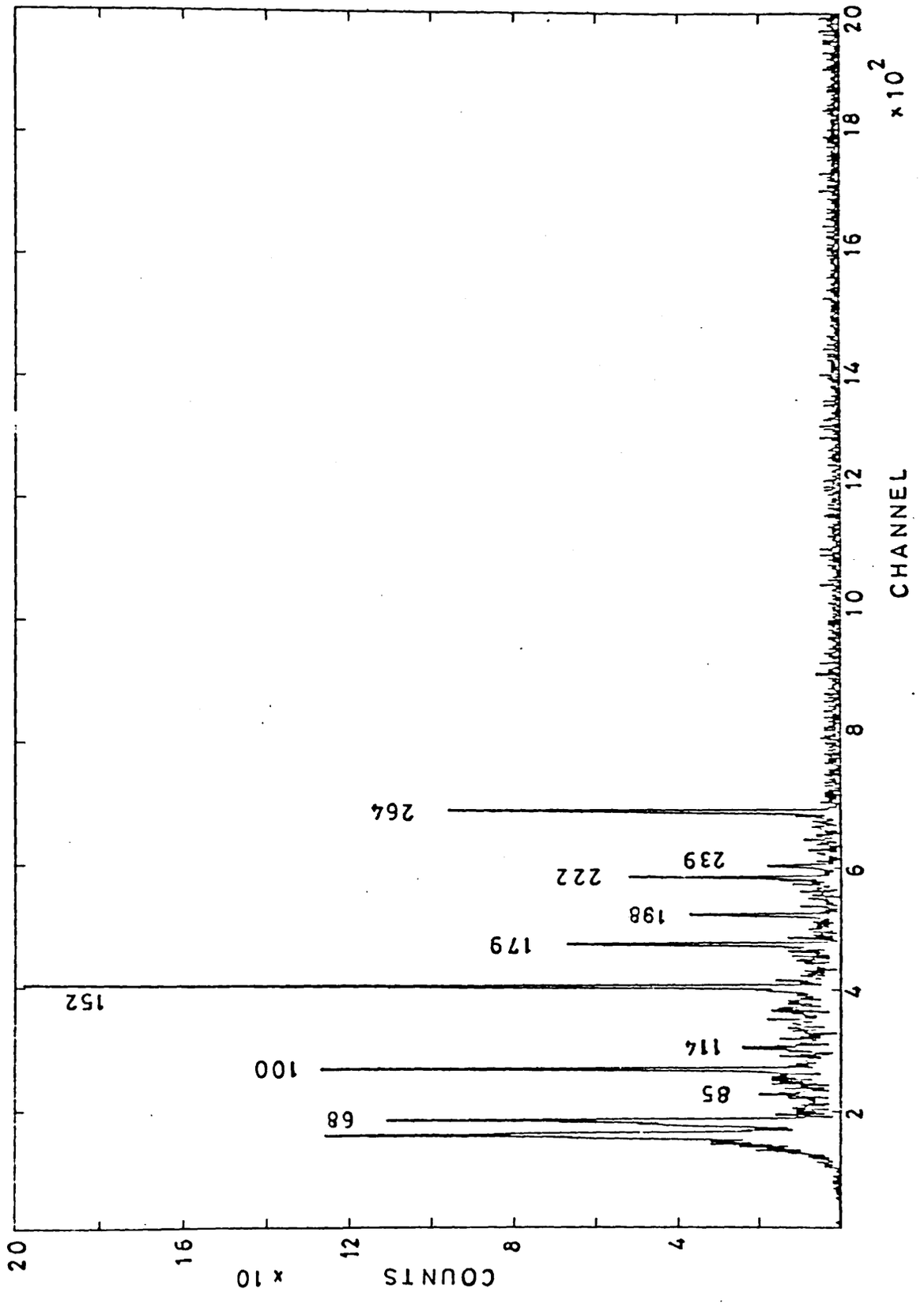

Fig.(6.2.e) Ta - 182 spectrum in coincidence with 1122 keV.

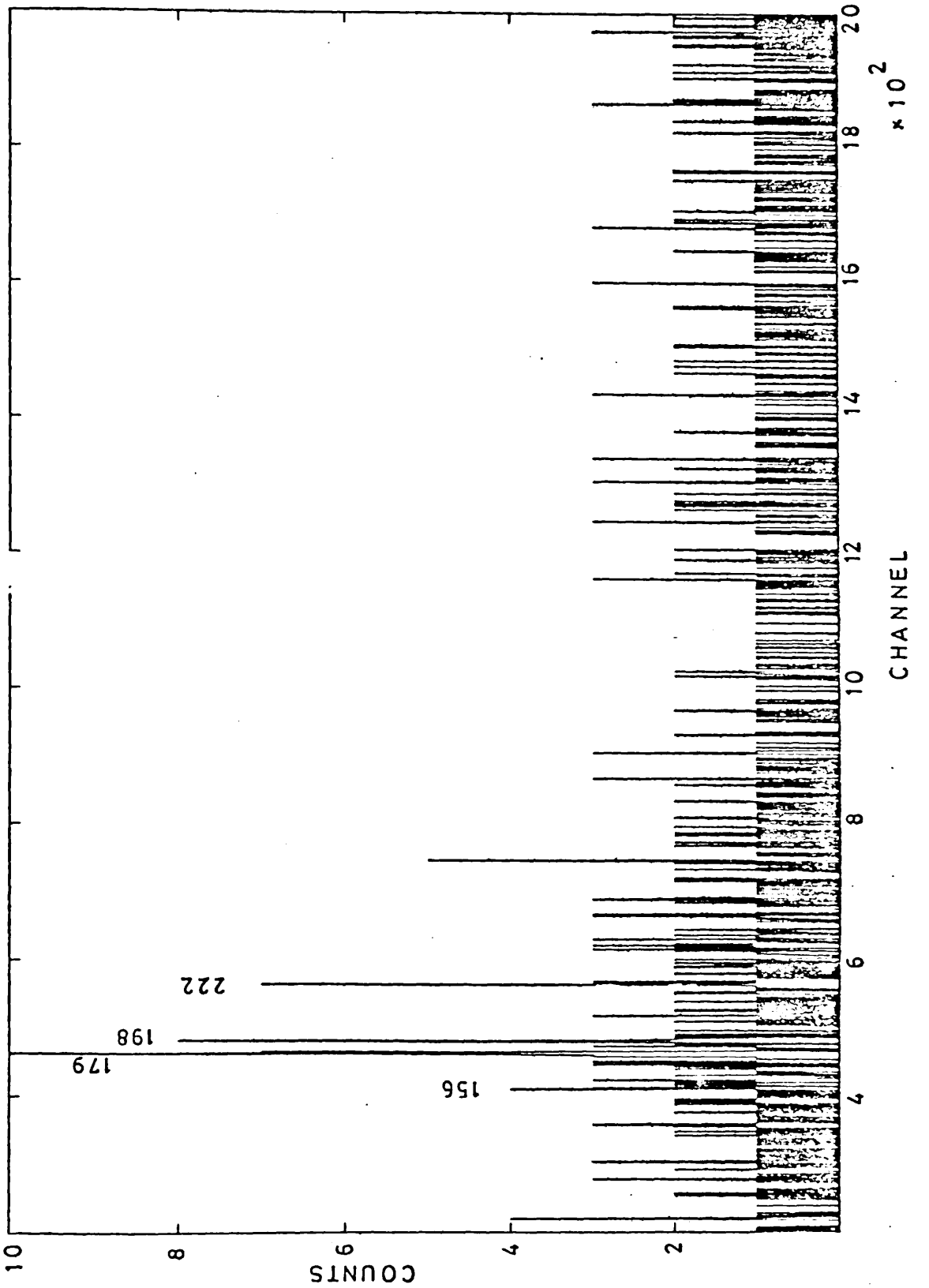

Fig.(6.2.f) Ta - 182 spectrum in coincidence with 1289 keV.

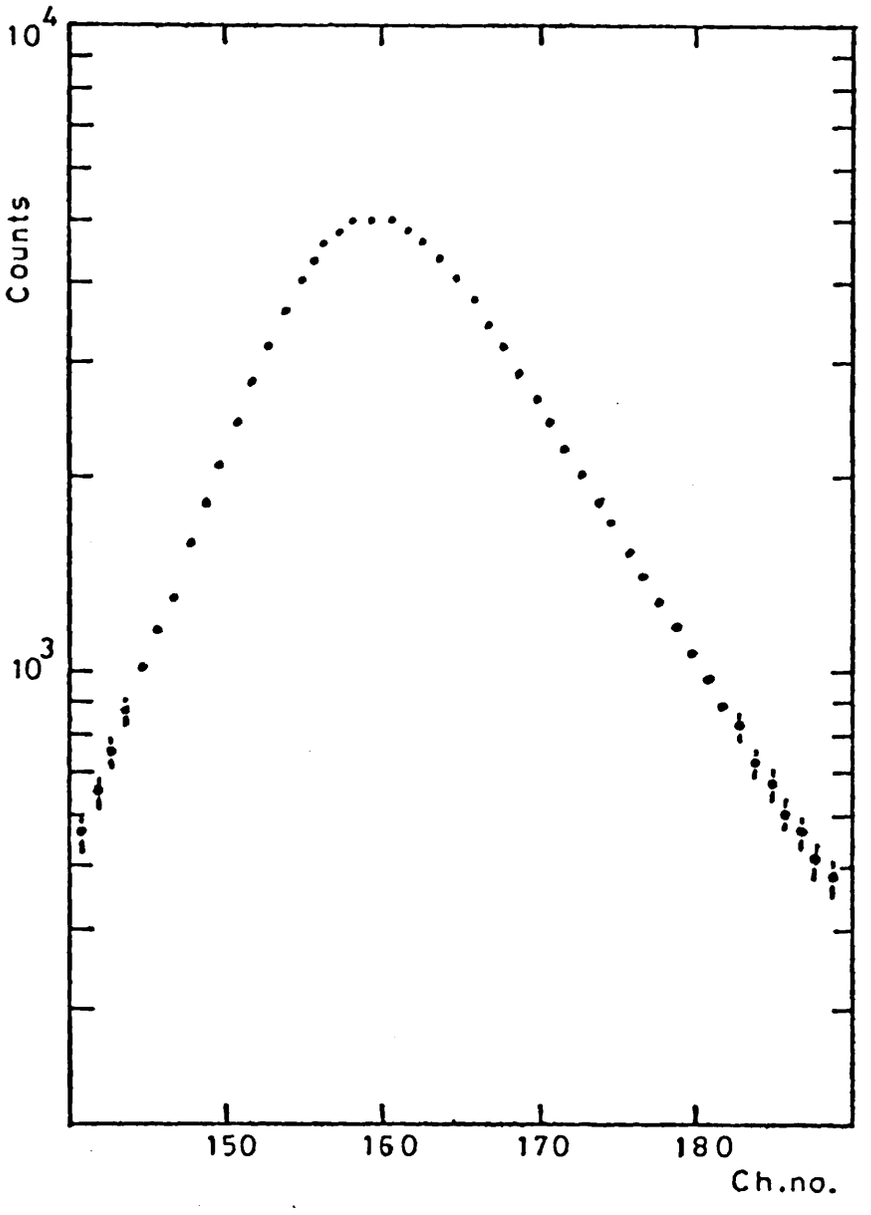

Fig. (6.3.a.) Lifetime spectrum of 100 keV level.

is quite suitable. The lifetime spectrum is shown in Fig. (6.3.b) and the value calculated was 1.35 $\pm$ 0.03 n.sec.

The third level (the 1289 keV) half-life was measured by gating the timing spectrum by the 68 keV line, making use of the superior resolution of the Ge(Li) detector. The TSCA lower level was adjusted just on the lower edge of the 68 keV peak, since this peak is very close to the 66 keV peak. However, the resultant spectrum is the sum of the half-lives of the two energy levels (1554 keV, coming from possible mixing due to a small fraction of the 66 keV peak contributing to 68 keV line and the 1289 keV level). (See Fig. 6.4.). The value calculated for both is 2.52 $\pm$ 0.06 n.sec., and the value for the 1289 keV is 1.17 $\pm$ 0.08 n.sec. The lifetime spectrum for this level is shown in Fig. (6.3.c).

The results obtained in this work are given in Table (6.3.) which also shows the values reported by other workers. In ref. 132, magnetic electron spectrometer especially equipped for lifetime measurements and plastic - plastic detectors for conversion electrons Ce - Ce coincidences were used. Ref. 134 used long lens electron - electron spectrometers especially equipped for the lifetime measurements. Ref. 135, used double magnetic lens spectrometer to measure Ce - Ce and β - Ce delayed coincidences. Ref. 136 used different technique, they have employed plastic and NaI(Tl) scintillators to measure the $\beta - \gamma$ delayed coincidences.

The value reported in this work for the half-life of the 1289 keV level agrees with those reported in Refs. 134 and 135 within the reported errors. The half-life reported here for the 1554 keV level agrees with those reported in Refs. 135 and 136 within the errors. The value reported in Ref. 134 is lower than those reported in the

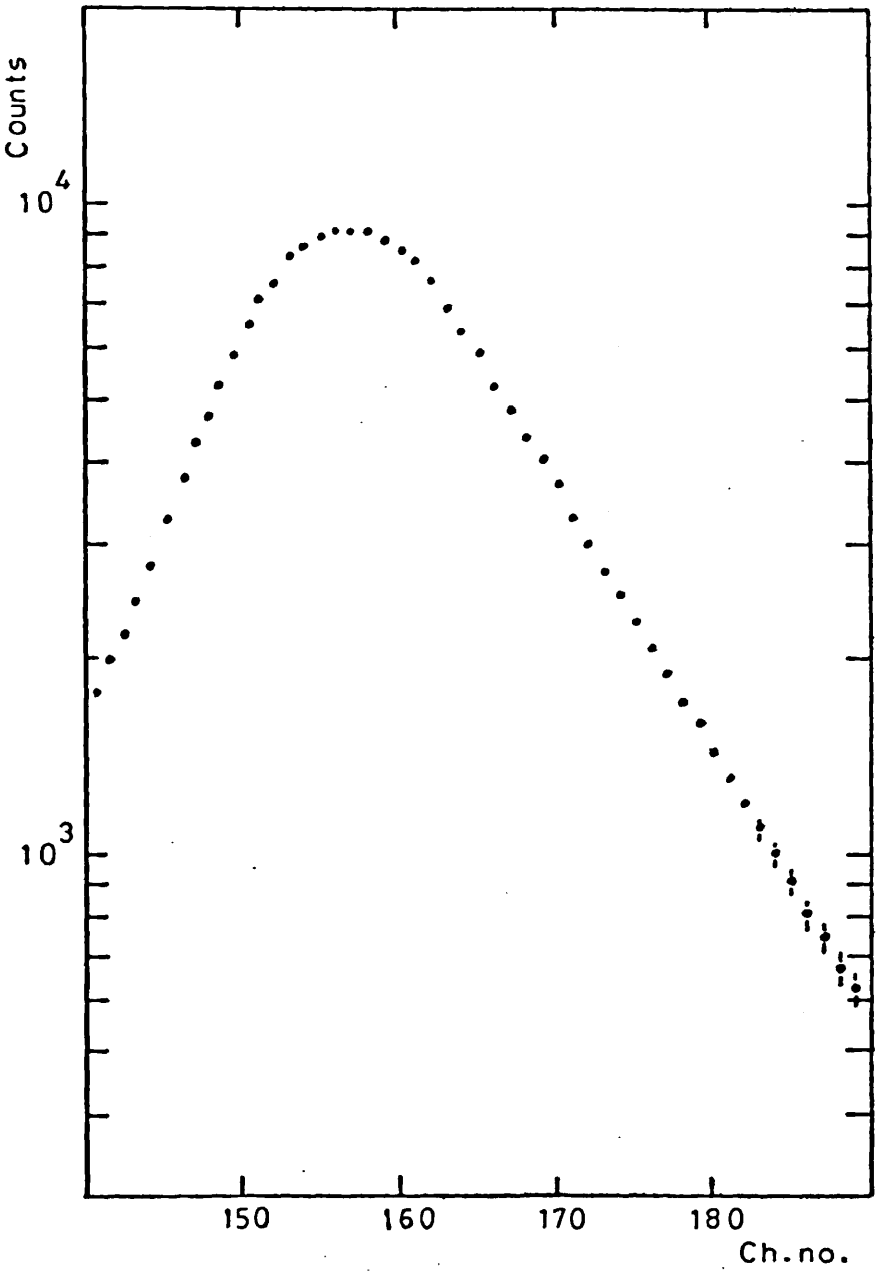

Fig. (6.3.b.) Lifetime spectrum of 1554 keV level.

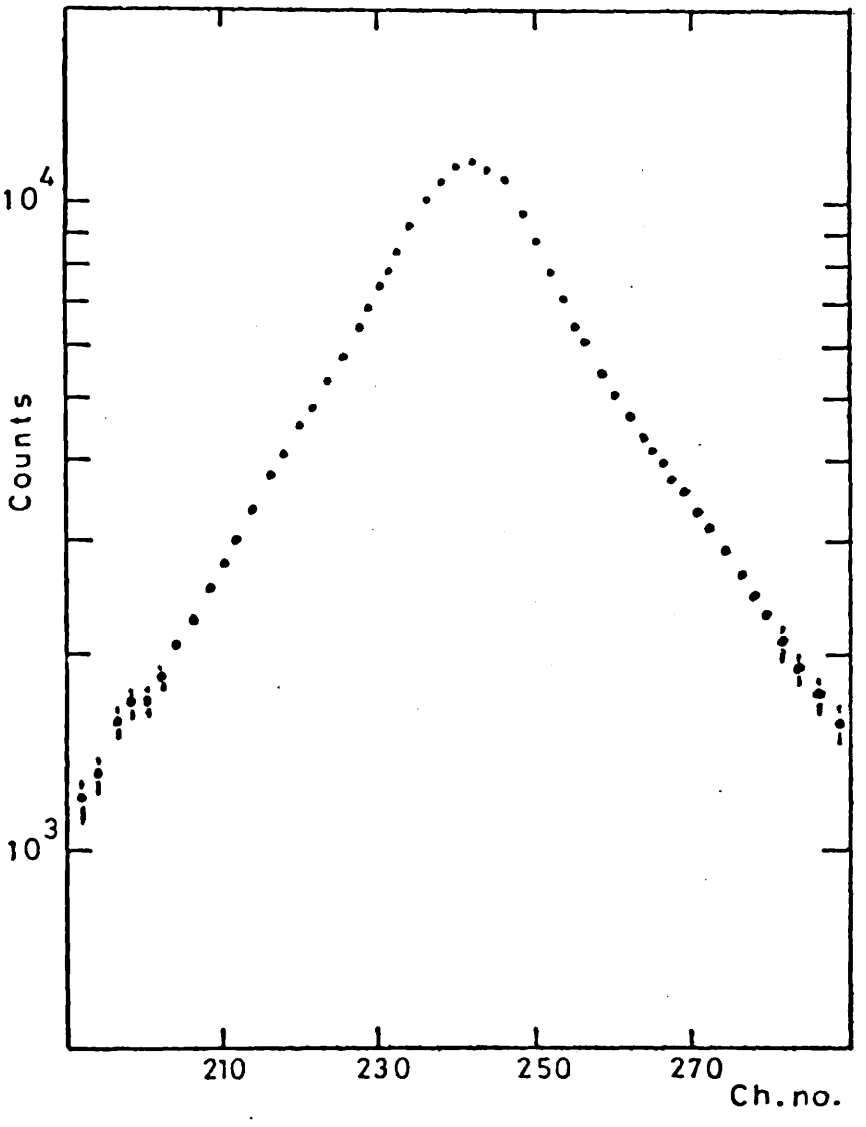

Fig. (6.3.c) Lifetime spectrum of 1289 keV level

Table 6.3.

Measured lifetimes for selected states in ^{182}W.

Level (keV)	Lifetime (ns)				
	Present work	Ref. 132	Ref. 134	Ref. 135	Ref. 136
100.10	1.38(03)		1.38(02)	1.48(03)	
1289.45	1.17(08)		1.12(02)	1.06(02)	1.00(05)
1553.57	1.35(03)	1.74(09)	1.23(02)	1.35(04)	1.30(07)

present work and in Refs. 132 and 135.

It is seem from the Table that the values reported in Ref. 136 are generally smaller than the values reported by other methods. That this is the case with scintillation counters, one concluded that when scintillators were used in lifetime measurements, the values reported are smaller than they should be. This may be due to the poor resolution of these detectors compared to Ge(Li) detectors, or due to their fast decay time which may affect the lifetime spectrum distribution.

6.3. Discussion:

6.3.1. Decay scheme:

The decay scheme of ^{182}W was established on the basis of the coincidence results of six energy gates (Table (6.2.)) and the energy sum relations as given in Table (6.4.). The decay scheme is shown in Fig. (6.4.). On the left side of the Fig. are shown the energy levels, the branching ratios (B.R.s) the log ft. values, spins, parities and the K quantum numbers. The numbers at the base of the arrow indicate the energy of the transition, while between the brackets is shown the relative intensity of the transition normalized to 1000 for the 1122 keV transition. The new transitions and levels are shown as dotted lines.

The experimental and theoretical K-shell internal conversion coefficients $\alpha(K)$ are shown in Table (6.5.). The conversion election intensities (I_β) were taken from Refs. 137 and 138, while the γ-ray intensities (I_γ) were taken from this work. In the low energy portion of the spectrum, the experimental $\alpha(K)$ of the 100 keV transition from the first excited state to ground was normalized to the theoretical $\alpha(K)$ for pure E2 multipolarity.

In the high energy portion, the experimental $\alpha(K)$ of the

Table 6.4.

Energy sum relations

Energy of Transition keV	Energy Sum keV	Energy Level keV
100.10	100.10	100.10
100.09 + 229.42	329.51	329.51
100.09 + 229.42 + 352.38	681.89	681.89
100.09 + 1121.66 1221.57	1221.75 1221.57	1221.66
100.09 + 1157.81 100.09 + 229.42 + 928.61 1257.40	1257.90 1258.12 1257.40	1257.80
100.09 + 229.42 + 960.34 100.09 + 1189.28 1289.14	1289.85 1289.37 1289.14	1289.45
100.09 + 1231.14 100.09 + 229.42 + 1002.24 75.12 + 1257.40 75.12 + 1157.81 + 100.09 1289.14 + 43.15	1331.23 1331.75 1332.52 1333.02 1332.29	1332.16
100.09 + 1273.87 100.09 + 229.42 + 1044.86 152.04 + 1121.66 + 100.09 1373.60 152.04 + 1221.57	1373.96 1374.37 1373.79 1373.60 1373.61	1373.86
100.09 + 1342.57 100.09 + 229.42 + 1113.71	1442.66 1443.22	1442.94
100.09 + 1121.66 + 238.79 1460.28	1460.54 1460.28	1460.41
100.09 + 1386.88 100.09 + 156.20 + 1002.24 + 229.42 198.32 + 67.95 + 1221.57	1486.97 1487.95 1487.84	1487.58
100.09 + 229.42 + 1180.79 100.09 + 1409.44 50.67 + 1460.28	1510.30 1509.53 1510.95	1510.26
100.09 + 1452.72 264.31 + 1289.14 222.18 + 43.15 + 1289.14 110.33 + 1342.57 + 100.09 100.09 + 1386.88 + 65.51	1552.81 1553.45 1554.47 1552.99 1552.48	1553.57

Table 6.4. continued

Energy of Transition keV	Energy Sum keV	Energy Level keV
100.09 + 229.42 + 352.38 + 911.90 1592.18	1593.79 1592.18	1592.98
1620.36 110.1 + 1409.44 + 100.09	1620.36 1619.63	1620.36
1711.93 338.80 + 1373.86	1711.93	1712.29
1762.99 170.06 + 911.90 + 352.38 + 329.51 209.32 + 1452.72 + 100.09 320.60 + 1342.57 + 100.09 473.20 + 1289.14	1762.99 1763.85 1762.13 1763.26 1762.34	1762.91

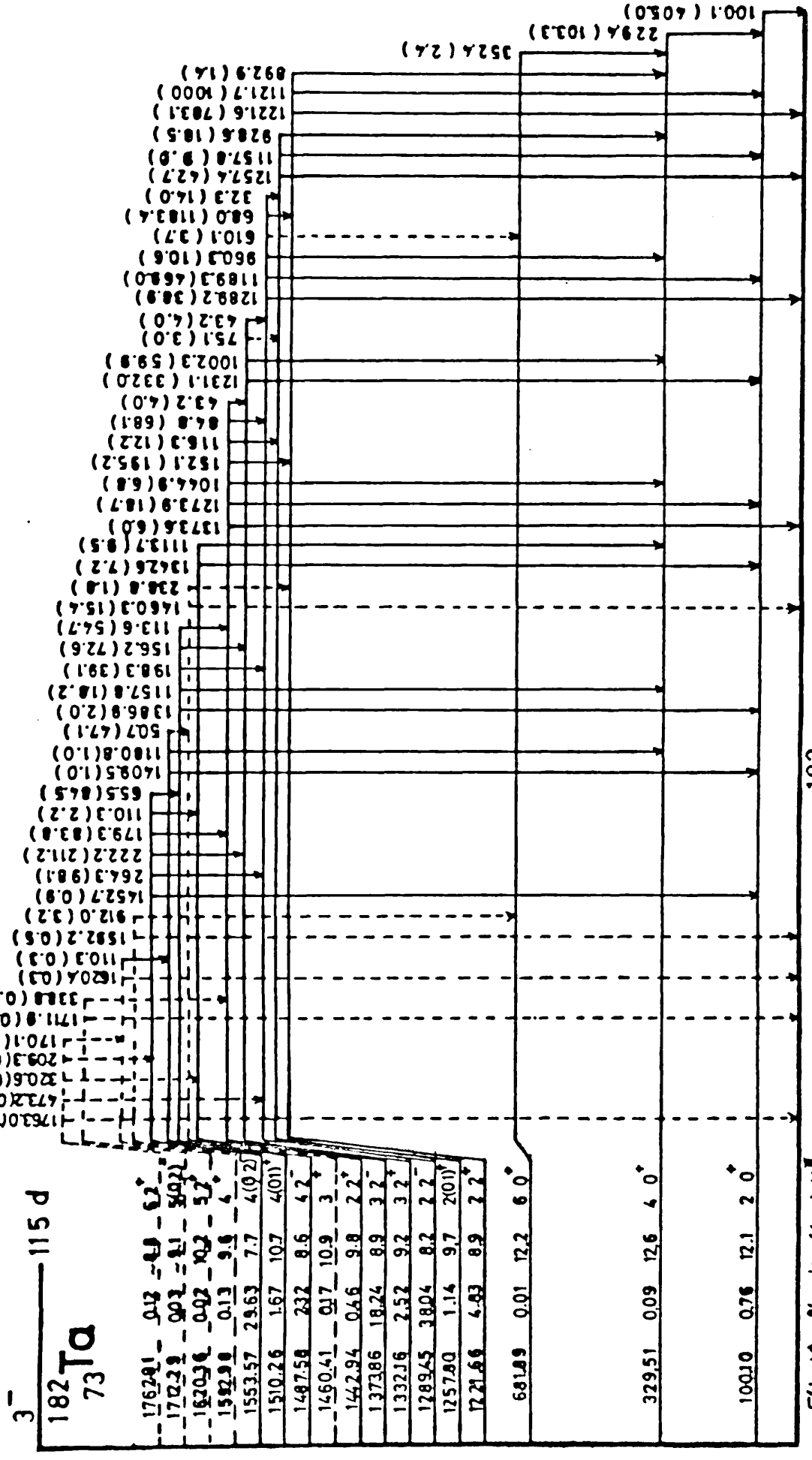

Fig. (6.4.) Decay scheme of $^{182}_{W}$

Table 6.5.

K-shell internal-conversion coefficients for ^{182}W.

E_γ (keV)	$I_i^\pi \rightarrow I_f^\pi$	Experimental $\alpha(K)$		Theoretical $\alpha(K)$					Adopted Multi-polarity
				E1	E2	M1	E3	M2	
84.76	$3^- \rightarrow 2^-$	64.33	(5.47)	47.63	10.83	68.01	15.14	570.0	M1
100.10	$2^+ \rightarrow 0^-$	8.73		3.07	8.73	41.14	1.88	30.54	E2
113.57	$4^- \rightarrow 3^-$	26.49	(2.80)	2.36	6.82	28.01	18.03	180.0	M1
116.30	$3^- \rightarrow 2^+$	2.05	(50)	2.11	6.23	27.04	17.03	170.0	E1
152.04	$3^- \rightarrow 2^+$	1.09	(10)	1.10	3.42	14.04	9.86	72.0	E1
156.20	$4^- \rightarrow 3^-$	1.08	(17)	1.00	3.20	11.50	9.40	64.0	E1
179.28	$4^- \rightarrow 3^-$	5.22	(45)	0.70	2.30	7.80	6.80	41.00	M1/E2
198.32	$4^- \rightarrow 2^+$	1.85	(16)	0.54	1.75	5.50	5.10	29.00	E2
222.18	$4^- \rightarrow 3^+$	0.42	(03)	0.40	1.29	3.95	3.70	18.00	E1
229.42	$4^+ \rightarrow 2^-$	1.38	(12)	0.37	1.15	3.70	3.30	17.00	E2
264.31	$4^- \rightarrow 2^-$	0.82	(07)	0.02	0.74	2.55	2.20	9.50	E2
† 892.87	$2^+ \rightarrow 4^+$	4.61	(1.31)	1.85	4.60	15.10	9.80	28.50	E2
928.61	$2^+ \rightarrow 4^+$	3.87	(06)	1.70	4.20	10.00	9.10	25.00	E2
960.34	$2^- \rightarrow 4^+$	8.36	(23)	1.60	4.00	9.60	8.60	23.00	E3
1002.24	$3^+ \rightarrow 4^+$	3.48	(03)	1.50	3.70	8.60	7.80	20.00	E2
1044.86	$3^- \rightarrow 4^+$	4.34	(19)	1.40	3.40	7.60	7.00	18.00	E1/M2
1113.71	$4^+ \rightarrow 4^+$	4.05	(16)	1.30	3.00	6.40	6.20	15.00	E2/M1
1121.66	$2^+ \rightarrow 2^+$	2.97		1.30	2.90	6.00	6.00	14.80	E2
1157.81	$2^+ \rightarrow 2^+$	4.77	(10)	1.20	2.80	5.60	5.60	13.80	E2/M1
1189.28	$2^- \rightarrow 2^+$	3.85	(03)	1.10	2.70	5.40	5.40	13.00	E1/E3/M2
1221.57	$2^+ \rightarrow 0^+$	2.50	(1.10)	1.10	2.50	4.90	5.00	11.20	E2
1257.40	$2^+ \rightarrow 0^+$	2.46	(01)	1.00	2.40	4.70	4.80	11.10	E2
1273.87	$3^- \rightarrow 2^+$	2.89	(01)	1.00	2.30	4.60	4.80	11.10	E1/M2
1289.14	$2^- \rightarrow 0^+$	10.61	(11)	0.90	2.30	4.40	4.70	11.00	M2
1342.57	$4^+ \rightarrow 2^+$	2.27	(03)	0.90	2.20	4.20	4.40	9.80	E2
1373.60	$3^- \rightarrow 0^+$	4.26	(07)	0.90	2.00	3.70	4.20	8.90	E3
1386.88	$4^- \rightarrow 2^+$	4.54	(02)	0.80	1.90	3.70	4.00	8.50	E3
1409.44	$3^+ \rightarrow 2^+$	2.93	(29)	0.80	1.90	3.50	3.90	8.00	E2/M1
1452.77	$4^- \rightarrow 2^+$	3.91	(04)	0.80	1.80	3.40	3.70	7.70	E3

† For the remainder of the table all $\alpha(K)$ values are to be multiplied by 10^3

1222 keV line was normalized to the theoretical α (K) for pure E2 multipolarity, since this state forms the first excited state of the γ - rotational band. The theoretical α_K values were taken from Ref. 21. The comparison between theoretical and experimental α (K) values enables us to deduce the transition multipolarity, hence it is possible to assign spins and parities to the concerned levels. Good agreement between the experimental and theoretical α_K is seen in Table (6.5.).

The β^- B.R. were calculated from the balance between the decay and feeding of the γ -rays for each level. The end point energies of the β^- electron were taken from Ref. 90 (Q value is 1811.3 keV). The spins and parities of the levels were deduced according to the β - selection rules as given in Ref. 106. The three levels 330, 682 and 1460 keV, could not assign any B.R. on the basis of feed-decay γ -ray rule, hence 0.17% for these three levels was assigned (Ref. 125 assign this value for the two former levels together with the 100 keV level).

6.3.2. Nuclear model calculations:

a. Single particle Model:

The single particle estimation calculated by Weisskopf [7] was used to calculate the absolute reduced transition probability $B^W(\sigma L)$. These theoretical calculations were compared with the experimental values. The experimental $B(\sigma L)$ were calculated for the three levels whose half-lives were measured in this work. Table (6.6) shows the experimental and theoretical $B(\sigma L)$. Good agreement between the experimental values measured in this work and those of Ref. 8 is seen.

The two transitions 264, 960 keV are believed to be due to a single particle excitation, since good agreement between their

Table 6.6.

Experimental and Weisskopf single particle absolute transition probabilities B (σL) calculated for selected transitions from the energy levels whose lifetimes were measured in this work

Level (keV)	Transition (keV)	Multi-polarity (σL)	B (σL) (e^2b^2) This work[a]	Ref.8.[b]	[ ] powers of 10 Single Particle
100.10	100.10	E2	0.82 [0]	0.84 [0]	6.12 [-3]
1289.45	32.24	E1	0.96 [-6]	1.2 [-6]	2.07 [-2]
	67.95	E1	7.17 [-6]	7.4 [-6]	2.07 [-2]
	610.11[c]	M4	4.86 [7]		5.78 [-6]
	960.34	E3	6.63 [-3]	> 7 [-3]	1.96 [-3]
		M2	22.40 [-5]	<6.7 [-5]	52.99 [0]
	1189.28	E1	2.15 [-10]	3.1 [-10]	2.07 [-2]
		M2	8.40 [-3]	6.2 [-3]	52.99 [0]
		E3	2.39 [-2]	2.3 [-2]	1.96 [-3]
	1289.14	M2	2.42 [-3]	2.6 [-3]	52.99 [0]
1553.57	110.33[c]	E1	1.10 [-8]		2.07 [-2]
	222.18	E1	7.50 [-8]	8.5 [-8]	2.07 [-2]
	264.31	E2	3.97 [-3]	4.5 [-3]	6.12 [-3]
	1452.72	E3	7.46 [-5]	5.4 [-5]	1.96 [-3]

[a] Errors are about 5%

[b] Errors are 20%

[c] New transitions

experimental B(σL) values and the Weisskopf estimation is seen. In this work we suggested that the 960 keV transition is pure E3, (α_K values support that as seen in Table(6.5.)). The agreement between experiment B(E3) and the Weisskopf estimation of B(E3) supports the E3 multipolarity.

In Ref. 90, mixing with M2 multipolarity was reported for this transition. The B^W(M2) disagrees with the experimental B(M2), which means that, since the 960 keV is due to a single particle excitation (B(E3)), then B^W(M2) - if it is mixed - should agree with experiment. One concludes that unless experimental evidence from angular correlation is seen this transition is pure E3 multipolarity.

If it is proved experimentally that there is mixing, then the M2 component could rise from another configuration of the nucleus i.e. collective degrees of freedom.

b. Collective Rotation:

The ^{182}W nucleus is considered deformed nucleus. Nuclei possessing a nonspherical shape show a rotational spectra.[139] In axially symmetric deformation nuclei, the general formula which describes the energy spectrum is given in Chapter 2. (Eq. 2.6.). Here the results will be reported. The two parameters of the theory (A & B) are:

$$A = 16.593 \text{ keV}$$

$$B = -0.015 \text{ keV}$$

The whole spectrum was calculated using these values, the results are given in Table (6.7.) together with the experimental values and other

Table 6.7.

The energies of levels in ^{182}W found experimentally compared with rotational and IBM (for positive parity) and with values from other nuclear models

J	K^{π}	Energy (keV)						
		Experiment	Rotor	IBM	Ref.59	Ref.140	Ref.41	Ref.109
2	0^+	100.1	100.1	100.1	111	104	100	100.0
4	0^+	329.5	329.5	333.7	346	314	328	329.2
6	0^+	681.9	671.0	700.7	680		673	678.9
2	2^+	1221.7	1221.7	1221.7	1164	936	1210	
2	$(0,1)^+$	1257.8	1257.8	1257.8	1539	1063	1260	
2	2^-	1289.5	1289.5					
3	2^+	1332.2	1319.6	1321.8	1298	1231	1320	
3	2^-	1373.9	1387.4					
4	2^+	1442.9	1448.6	1454.9	1442		1456	
3	$-^+$	1460.4	1460.4	1460.4				
4	2^-	1487.6	1516.4					
4	$(0,1)^+$	1510.3	1484.8	1491.0	1870		1543	
4	$(0,2)^-$	1553.6	1553.6					
4	$-^+$	1592.9	1589.5	1593.9				
5	2^+	1620.4	1607.2	1622.0	1637			
5	$(0,2)^-$	1712.3	1712.5					
6	2^+	1762.9	1794.7	1822.2	1817			

theoretical calculations. Fig. (6.5.) shows a comparison between the experimental and theoretical energy levels.

The ratio $E(4^+)/E(2^+)$ of the ground bond is 3.29, while the ratio $E(6^+)/E(2^+)$ is 6.81. These two ratios are in excellent agreement with the theoretical predictions of the symmetric rotor[33,139] (see Chapter 2). The general feature of the calculations of the rotational spectra is the good agreement between theory and experiment which indicates that ^{182}W is true deformed nucleus with axial symmetry.

c. The Interacting Boson Model (IBM)

The deformed nuclei are described by the SU(3) rotational limit of the model, the details of which are described in Chapter 2. Here the calculations are given. The two parameters of the model α & β (Chap. 2, Eq. 2.27) were determined by fitting the ground band 100 keV (2^+) and the γ - band 1222 keV (2^+) experimental states to theory, then:

$$\alpha = 16.68 \text{ keV}$$

$$\beta = 7.47 \text{ keV}$$

The experimental reduced transition probability B(E2) of the first excited state of the ground band (2^+) was used to normalize the theoretical calculations and hence to determine the constant α_2 (Chapter 2, Eq. 2.28), then

$$\alpha_2 = 0.104 \text{ eb}$$

These values will be used to produce the spectrum in the SU(3) limit and to calculate some important quantities for testing the model. The results are shown in Table (6.7.) and in Fig. (6.5.). Good agreement between theory and experiment is seen. The individual bands will be discussed below.

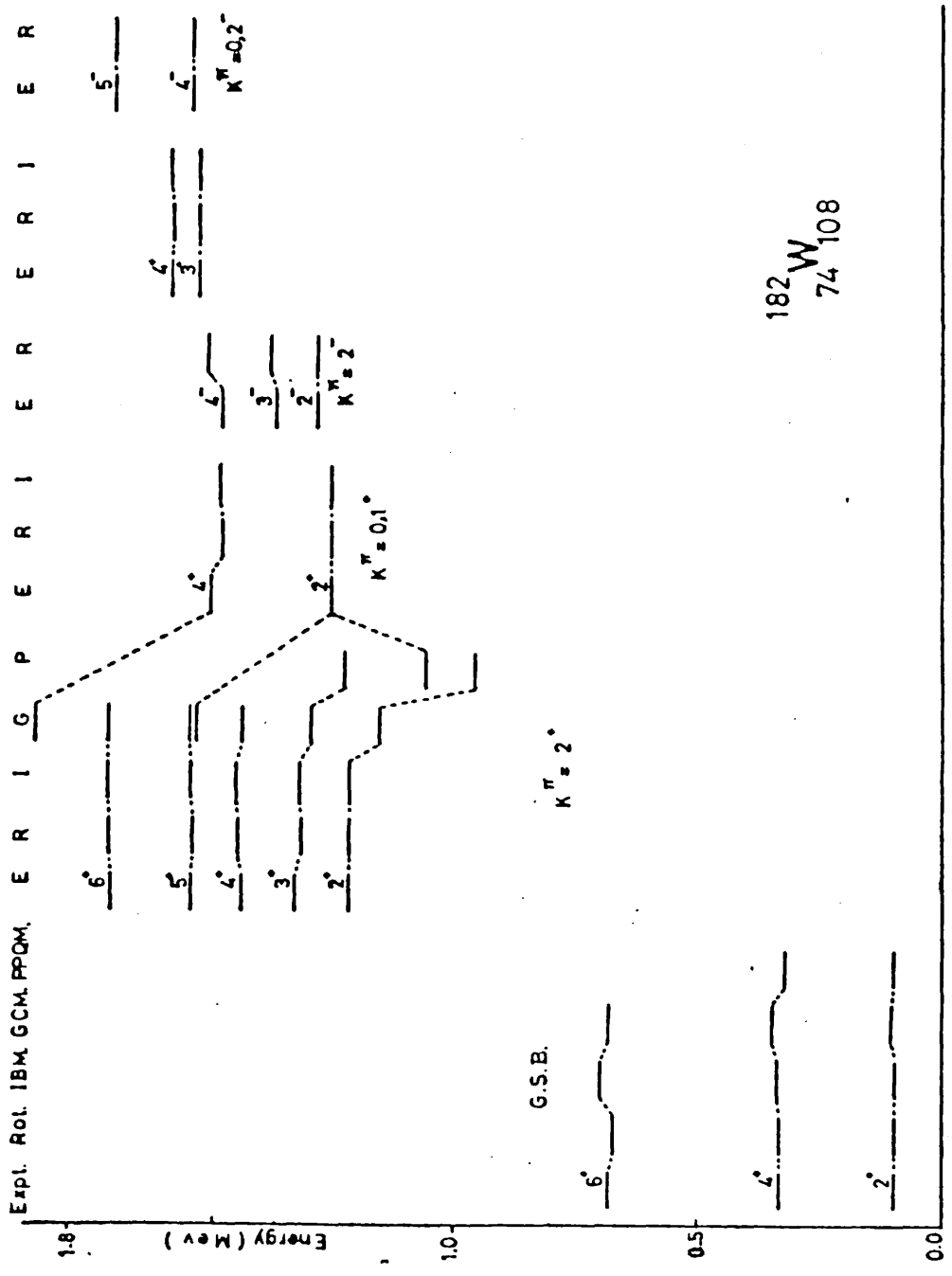

Fig.(6.5) Energy levels in ^{182}W.

6.3.3. Energy band structure:

- The ground state band:-

This band is consisted from the levels (100 (2^+), 330 (4^+) and 682 (6^+) keV.) The first two levels were used to determine the parameters of the rotational theory (A & B). The calculated value for the third level is 671 keV (Table 6.7.). This is in good agreement with the experimental value.

The IBM calculations predicted the values 334 keV for the experimental value 330 keV and 701 keV for the experimental value 682 keV. The first value is in excellent agreement with the experiment, while the prediction of the rotational theory is better than the IBM values (Table 6.7.) for the second. The prediction of the VMI[109] provides the best agreement with the experiment (Table 6.7.), but these calculations are given only for the ground state band. The spins and parities of these levels were confirmed from the α_K coefficients (Table 6.5) and from the log ft. values.

The B.R. of the 100 keV level is given a new value (0.76%) depending on the decay-feeding balance of the γ-rays. This value disagrees with that reported in Ref. 90 which was 0.05%. The B.R. for the other two levels were given the values 0.09% for the 330 keV level and 0.01% for the 682 keV level. This was in agreement with the assigned spins and parities as predicted from log ft. values. The experimental B(E2) values and the electric quadropole moment (Q) for the transitions depopulating these levels are shown in Table (6.8) together with different theoretical models. The best agreement between theory and experiment is achieved when IBM calculations are used.

Table 6.8.

Transition probabilities B(E2) and electric moments Q determined from experiment compared with IBM calculations and with values from the general collective model (Ref. 59), the pairing plus quadrupole model (Ref. 140), the rotational model (Refs. 7,141) and the pairing plus quadrupole model assuming axial symmetry (Ref. 142)

Level Energy (keV)	$J_i \rightarrow J_f$	B(E2) $-Q$ (e^2b^2) (eb)						
		Expt.	IBM	Ref.59	Ref.140	Ref.141	Ref.7	Ref.142
100.10	2→0	0.82 (02)	0.82	0.77	0.80	0.84		0.66
		1.83 (06)	1.83	1.77	1.79		1.85	
329.41	4→2	1.10[a]	1.15			1.20		
		2.26	2.33				2.36	
681.89	6→4	1.20[a]	1.24			1.32		
		1.47	2.56				2.59	

[a] Lifetime taken from Ref. (8)

- The γ -band ($K^{\pi} = 2^{+}$):

This band is consisted fromthe levels 1222 (2^{+}), 1332 (3^{+}), 1443(4^{+}), 1620 (5^{+}) and 1763 (6^{+}) keV. The last two levels are new levels. The K quantum number is assigned in view of the comparison between the experimental and the theoretical branching ratios $B(\sigma L)/B^{-}(\sigma L)$, which are shown in Table (6.9.). The rotational theory calculation for the energy spectrum is in good agreement with the experiment except for the last level, but they are still good enough for considering the validity of the theory. The IBM calculations are in agreement with the experiment, but again with poor agreement for the higher spins levels, (Table 6.7.). The spins and parities of the first three levels were assigned in view of the $\alpha(K)$ values (Table 6.5.) and from the log ft. values.

The spins and parities of the new levels (1620 and 1763 keV) were assigned in view of the agreement between theoretical predictions and experiments. Another support came from the log ft. values. In the IBM, the Ratio $R = B(E2, 2_2^+ \rightarrow 0_g^+)/B(E2, 2_2^+ \rightarrow 2_g^+)$ is 7/10. The experimental calculated value for R was 0.51 (01) and this supports the above assumption.

Another expectation of the model is that the transition between the β and γ bands and the ground band is absolutely forbidden (Chapter 2). The ratios: $B(E2, 3_\gamma^+ \rightarrow 2_\beta^+)/B(E2, 3_\gamma^+ \rightarrow 2_g^+)$ is 10684 ± 356 and $B(E2, 3_\gamma^+ \rightarrow 2_\beta^+)/B(E2, 3_\gamma^+ \rightarrow 4_g^+)$ is 21173 ± 706. (See Fig. 6.4.) support that assumption, i.e., the transition from the γ -band to the ground state band is extremely small compared with transitions to other β or γ bands. The transition 43 keV depopulates the level 1332 keV to the level 1289 (2^{-}) keV, this transition was considered previously to depopulate the level 1374 (3^{-}) keV to the level 1332 keV,

Table 6.9.

Experimental B(E2) branching ratios for transitions from positive parity states in ^{182}W compared with symmetric rotor (Ref. 129) and asymmetric rotor calculations (Ref. 143).

Transitions E_γ / E'_γ	Energy level (keV)	B(E2) ratios: Experiment present work		B(E2) ratios: Theory for different K_i			Deduced K_i
				K_i	Ref.129	Ref.143	
1221.57/1121.66	1221.66	0.51	(01)	2	0.70	0.52	2
892.87/1121.66		0.004	(001)		0.05	0.09	2
1002.24/1231.14	1332.16	0.50	(07)	2	0.40	0.80	2
1342.57/1113.71	1442.94	0.29	(02)	2	0.34	0.16	2
				1	12.19		
				0	1.10		
1157.81/1257.40	1257.80	1.14	(05)	2	1.43	1.92	
				1	0.36		
				0	1.43	1.41	0
928.61/1257.40		1.60	(03)	2	0.07	0.16	
				1	1.40		1
				0	2.57	2.58	
1157.81/928.61		0.71	(03)	2	20.0	11.50	
				1	0.31		
				0	0.56	0.55	0

but the coincidence data (Table 6.2.) show weak coincidence between the transition 156 keV and the energy gate 1122 keV, the only route for this is through the doublet 43 keV. Another support came from the weak coincidence between 156 keV and the 352 keV gate (Table 6.2. and Fig. 6.4.). The new 75 keV transition depopulates the level 1332 keV to the level 1258 (2^+) keV, this is supported by the strong coincidence between this energy and the gates 100 and 229 keV. (Table 6.2.). The transition 110 keV is doublet, since strong coincidence between this transition and the gate at 1122 keV is seen (Table 6.2., Fig. 6.2.) this supports the existence of the new level at 1620 keV. Since this level decays directly to ground (the transition 1620 keV, Fig. 6.4.) this suggests positive parity for this level.

The four new transitions 170, 209, 321 and 473 keV depopulate the new level 1763 keV to different levels in the decay scheme (see Fig. 6.4.), the coincidence data (Table 6.2.) support the existence of these transitions hence, the existence of this new level. This level decays to ground state by the transition 1763 keV (Table 6.1.), hence this supports the positive parity assignment for it.

- The $K^{\pi} = (0,1)^+$ band:

This band is consisted from the two levels 1258 (2^+) and 1510 (4^+) keV. The rotational theory calculations for this band show an agreement with experiment (Table 6.7.) while the IBM calculations show better agreement with experiment.

The K - quantum number for this band is assigned in view of the comparison between experimental and theoretical B(E2) B.R. as given in Table (6.9.). The spins and parities of these levels were confirmed from log ft. values and from α_K values (Table 6.5.).

Sapyta et al.[129] assigned the values (2,3,4) for the spin of the 1510 keV level. The above theoretical calculations for the energies of this band support the assumption of 4^+ for this level. The new transition 51 keV depopulates the level 1510 keV to the new level 1460 (3^+) keV. The coincidence data show strong coincidence between the transition 110 keV and 1122 keV gate (Table 6.2.). The only route for this is through the two new transitions 51 and 239 keV, this supports the new level at 1460 keV (see Fig. 6.4.).

— The ($K^{\pi} = 2^-$) band:

This band is consisted from the levels 1289 (2^-), 1374 (3^-), and 1488 (4^-) keV. The rotational theory calculations agree with the experiment. (Table 6.7.) But it was mentioned in Chapter 5 that the negative parity bands seem to have some kind of breaking symmetry. Although the calculations here for this band are still satisfactory, the agreement with the experiment is less than in the case of positive parity bands.

It was mentioned before that the transition 960 keV which depopulates the 1289 keV level to the 330 kev (4^+) level is of a single particle nature. This supports the idea of the broken symmetry in this band. The spins and parities of these levels are assigned in view of the log ft. values and from the α_K values (Table 6.5.). The K - quantum number for this band is assigned in view of the B(σ-L) B.R. as given in Table (6.10). The new transition 610 keV depopulates the level 1289 keV to the level 682 keV, this was supported from coincidence data, since the gates 100, 229 and 352 keV show weak coincidence with this transition (Table 6.2. and Fig. 6.2.).

Table 6.10.

Experimental B(σL) branching ratios for transitions from negative parity states in ^{182}W compared with the Bohr and Mottelson model (Ref. 144).

Transitions E_γ/E'_γ	Energy level (keV)	B(σL) ratios						Deduced K_i
		Experiment present work	Theory for different K_i from Ref. 144					
			0	1	2	3	4	
1289.14/1189.28	1289.45	0.39 (04)		2.8	0.7			2
1044.86/1273.87	1373.86	0.62 (02)	1.33	0.75	0.75	0.75		2
43.15/152.04		1.81 (16)	8.75	8.75	1.4	0.35		2
179.28/264.31	1553.57	2.95 (26)		6.86	2.24	0.14	0.56	2
65.51/179.28		3.01 (26)	3.16	0.58	0.16	8.7	0.35	0

— The new levels 1460 (3^+) and 1593 (4^+) keV:

These new levels were suggested in this work, the theoretical calculations of both rotational and IBM show excellent agreement with the experiment (Table 6.7.), this supports their existence and at the same time confirms their spin and parity assignment. The log ft. values support these assignments.

The new transition 239 keV depopulates the level at 1460 keV to the level 1222 keV, this was supported from the coincidence data, since strong coincidence was seen between this transition and the gates 100, 229 and 1122 keV, this supports the existence of this level. The new transition 912 keV (Table 6.1.) depopulates the level 1593 keV to the state 682 keV, this was supported from the coincidence data. Table (6.2.) shows weak coincidence between this transition and the three gates 100, 229 and 352 keV, this gives another support for the existence of this level.

— The band $K^{\pi} = (0,2)^-$

This band is consisted from the two levels 1554 (4^-) and 1712 (5^-) keV. The second level is the new level suggested in this work. The rotational theory calculations show excellent agreement with experiment. This seems rather strange, since it was mentioned before that in the negative parity bands, the breaking of the symmetry is expected and that the agreement with experiment is not good.

The transition 264 keV which depopulates the 1554 keV level to the 1289 keV(2^-) level is showing a single particle configuration. This supports the assumption of the breaking symmetry in the negative parity bands. The spin and parity of the new level were determined according to the above theoretical calculations and from log ft. values.

The spin and party of the 1554 keV level were confirmed from log ft values and from the α_K coefficients (Table 6.5.). The K - quantum number for this band was assigned in view of B(E2) B.R. as given in Table (6.10). The new transition 339 keV depopulates the level 1712 keV to the level 1374 keV. The strong coincidence between this transition and the energy gate 100 keV (Table 6.2. and Fig. 6.2.) supports this and the existence of this new level.

6.4. Conclusion:-

The half-lives of three energy levels were measured by the delayed coincidence method using plastic - Ge(Li) detectors. The values obtained using this system agree with those reported by other workers who used different techniques within the quoted errors (Refs. 134, 135, Table 6.3.). The value reported for the half-life of the 1554 keV level in Ref. 132 does not agree with any value reported previously, one may suggest that a mixing of energy happens in that measurement because of the use of the plastic detectors. The half-lives measured in the present work were used to calculate the absolute reduced transition probabilities for transitions depopulating these levels to other levels, hence the nuclear structure of these levels can be investigated (Table 6.6.)

The whole energy range of the ^{182}Ta spectrum (32 - 1763 keV) was covered. Fifteen new transitions have been observed for the first time together with another ten transitions which were reported in Refs. 90 and 130. Five new energy levels were introduced and their existence was supported from coincidence data. The spins and parities of these new levels have been assigned from both log ft values and the comparison between the experimental data and the predictions of the rotational model and the IBM.

Two of the new levels (1620 and 1763 keV) were fitted to a γ - band, while another level (1712 keV) was fitted with the level at 1554 keV to form another band with $K^{\pi} = (0,2)^{-}$. The two levels (1460 and 1593 keV) were suggested to form a new band. (see Fig. 6.5.). The spin of the level 1510 keV was confirmed to 4^{+}. The new B.R. was assigned for the 100 keV level using the γ -ray balance between the

decaying and the feeding transitions (0.76%).

Nuclei which lie in the mass range $155 < A < 185$ are considered as strongly deformed and therefore possess rotational spectra. ^{182}W lies within this range, hence should show rotational characteristics. The rotational theory was applied on ^{182}W and the results are given in Table (6.7.). The SU(3) rotational limit of the IBM was applied and the results are given in the same table. The table shows the experimental values for the energy levels, together with five different theoretical nuclear models. The calculations of the pairing plus quadrupole model (PPQM) of Ref. 140 and the general collective model (GCM) as given in Ref. 59 are in good agreement with experiment for the low spin states. But no agreement with experiment can be seen at higher spin states, especially for the $K^{\pi} = (0,1)^{+}$ band.

The calculations of the IBM-1 are as good as the IBM-2 (Ref. 41) calculations (see Chapter 2) which assume a distinction between proton and neutron bosons. Excellent agreement is seen for the VMI (Ref. 109), but this model is applied only to the ground band states.

The agreement between both the rotational theory and the SU(3) limit of the IBM calculations with the experimental values of the energy levels supports the assumption that ^{182}W is a deformed nucleus and is very much like an axially symmetric rotor[33]. This is supported also by the validity of the rotational theory and the IBM, for the energy ratios $E(4^{+})/E(2^{+})$ and $E(6^{+})/E(2^{+})$ of the ground band states and the $B(E2, 2^{+}_{\gamma} \rightarrow 0^{+}_{g})/B(E2, 2^{+}_{\gamma} \rightarrow 2^{+}_{g})$ ratio. The assumption that the transition between the β and γ bands and the ground band is absolutely forbidden as stated in the SU(3) limit (Chapter 2) was investigated and supported by experiment.

The geometric model of Bohr & Mottelson, i.e., axial rotor[33,37,38] and the SU(3) limit of the IBM give results very close to each other and both agree with the experimental data (Table 6.7.). This is expected, since the SU(3) limit corresponds to an axially deformed shape (Chapter 2).

The observation of a single particle excitation in ^{182}W supports the theoretical prediction[31] of some kind of intrinsic motion in those nuclei which perform collective motion (e.g. rotation) (see section 6.3.2.).

REFERENCES

1. F.S. Goulding, Nucl. Instr. and Meth. 43(1966) 1.

2. G.T. Ewan, 1968, Semiconductor Spectrometers, in: Progress in Nucl. Techniques and Instrumentation, ed. F.J.M. Farley (North-Holland, Amsterdam) pp.67-157.

3. A.J. Tavendale, Nucl. Instr. and Meth. 84(1970) 314.

4. R.D. Baersch and R.N. Hall, IEEE Trans. NS-17(3), 1970, 235.

5. The Radiochemical Manual, ed. B. Wilson (Radiochemical Centre Amersham, 1966) second ed.

6. J. Blatt and V. Weisskopf; Theoretical Nuclear Physics (J. Wiley and Sons, Inc., New York, 1952).

7. H. Morinaga and T. Yamazaki, in Beam γ-ray spectroscopy (North Holland Pub. Co. 1976)

8. W. Andrejtscheff and K.D. Schilling and P. Mantrass, Atomic Data and Nucl. Data Tables, 16 no. 6 (1975) 516.

9. O. Hahn and L. Meitner, Z. Physik 29(1924) 161.

10. N. Tralli and G.H. Goertzel, Phys. Rev. 83(1951) 399.

11. M.E. Rose et al., Phys. Rev. 76(1949) 1883.

12. M.E. Rose et al., Phys. Rev. 83(1951)79

13. L. Sliv and I. Band, Tables of Gamma-ray conversion coefficient part I (K-Shell), part II(L-shell) Physico Technical Insitute, Academy of Science, 1956, Leningrad.

14. T. Green and M.E. Rose, Phys. Rev. 110(1958) 105

15. E. Church and J. Weneser, Nucl. Phys. 28(1961) 602.

16. R. Hager and E. Seltzer, Nucl. Data A4(1968a) 1, A4(1968b)397.

17. R. Hager and E. Seltzer, Nucl. Data A6(1969) 1.

18. H.C. Pauli and K. Alder, Z. Physik. 202(1967)2SS

19. H.C. Pauli, K. Alder and R. Steffen, The Electromagnetic Interaction in Nuclear Spectroscopy, ed. W.D. Hamilton (North Holland Pub. Co., Amsterdam, 1975).

20. M.E. Rose, α, β & γ -ray spectroscopy, ed. K. Siegbahn (North Holland Pub. Co., Amsterdam, 1965).

21. F. Rosel, H.M. Fries, K. Alder and H.C. Pauli, Atomic Data and Nuclear Data Tables 21 (1978) 325, 268, 258.

22. A. Bohr and B. Mottelson, Nuclear Structure Vol. 1 (W.A. Benjamin, Inc. Amsterdam, 1969).

23. O. Haxel, J. Jensen and H. Suess, Phys. Rev. 75(1949) 1766.

24. M.G. Mayer, Phys. Rev. 75(1949)1969

25. M. Mayer, J. Jensen and D. Kurath, α , β & γ -ray spectroscopy ed. K. Siegbohn (North Holland Pub. Co., Amsterdam, 1965). Vol. 1.

26. S.G. Nillson, Mat. Fys. Medd. Dan. Vid. Selsk 29 No. 1(1955)

27. J.P. Elliott, Proc. Roy. Soc. A 245 (1958) 128, 562.

28. A. De-Shalit and H. Feshbach, Theoretical Nuclear Physics Vol. 1, Nuclear Structure (J. Wiley & Sons. Inc., New York 1974).

29. A. Wapstra, Nijgh and Lieshout, Nuclear Spectroscopy Tables (North Holland Pub. Co., Amsterdam, 1959).

30. V.F. Weisskopf, Phys. Rev. 83(1951) 1073.

31. A. Bohr and B. Mottelson, Nuclear Structure Vol. II (W.A. Benjamin, Inc., Amsterdam, 1975).

32. A. Bohr et al., Rev. Mod. Phys. 28(1958) 433.

33. G. Alaga et al., Mat. Fys. Medd. 29, no. 9 (1955).

34. P.C. Sood, Nucl. Data A4 (1968) 281.

35. A. Arima and F. Iachello, Phys. Rev. lett. 35 (1975) 1069

36. F. Iachello, Interacting Bosons in Nuclear Physics ed. F. Iachello (Plenum Press, New York, 1979).

37. A. Bohr, Mat. Fys. Medd. Dan. Vid Selsk 26, no. 14 (1952).

38. A. Bohr and B. Mottelson, Mat. Fys. Medd. Dan. Vid. Selsk 27, no. 16 (1953).

39. G. Gneuss and W. Greiner, Nucl. Phys. A 171(1971) 449

40. K. Kumar, Nucl. Phys. A 231 (1974) 189

41. P. Duval and B. Barrette, Phys. Rev. C, 23 (1981) 492.

42. A. Arima and F. Iachello, Ann. Phys. 99 (1976) 253.

43. A. Arima and F. Iachello, Ann. Phys. 115 (1978) 325

44. A. Arima and F. Iachello, Ann. Phys. 111 (1978) 201.

45. M. Hamermesh, Group Theory (Addison Wesley, Pub. Co. Reading, Mass., 1962).

46. B. Wybourne, Classical Groups for Physicists (J. Wiley and Sons, New York, 1974).

47. O. Castanos, A. Frant, E. Chacon and M. Moshinsky, J. of Math. Phys. 20(1979) 35.

48. F.Iachello, and A. Arima, Phys. lett. 53B (1974) 309

49. F. Iachello, Proc. Int. Conf. on Nucl. Phys. and Spectroscopy Vol. 1 (Amsterdam, 1974).

50. O. Castanos et al., Phys. Lett. 88B(1979) 203.

51. T.Otsuka et al., Phys. Lett. 76 B (1978) 139.

52. A. Arima and F. Iachello, Ann. Rev. Nucl. Part. Sci. 31 (1981) 75.

53. T. Otsuka, Boson Model of Medium - Heavy Nuclei, Ph.D. thesis 1979, Un. of Tokyo, Japan.

54. J. Ginocchio and M. Kirson, Phys. Rev. Lett. 44 (1980) 1744.

55. M.A. Mariscotti, G.S. Goldhaber & B. Buck, Phys. Rev. 178 (1969) 1864.

56. R.M. Diamond, F.S. Stephen & W.T. Swiatecki, Phys. Lett. 11 (1964) 315.

57. B.R. Mottelson & J.G. Balatin, Phys. Rev. Lett. 5 (1960) 511.

58. K. Kumar & M. Baranger, Nucl. Phys. A 92 (1967) 608.

59. P.O. Hess et al., J. of Phys. G. Nucl. Phys. 7 (1981) 737.

60. T. Tamura, K. Weeks & T. Kishimoto, Phys. Rev. C 20 (1979) 307.

61. T. Kishimoto & T. Taumra, Nucl. Phys. A 270 (1976) 317.

62. T. Kishimoto & T. Tamura, Nucl. Phys. A 192 (1972) 264.

63. W.M. Gibson, G.L. Miller & P.F. Donovan, α, β and γ -ray spectroscopy, ed. K. Siegbahn (North Holland, Amsterdam, 1965) Vol. 1.

64. K. Debertin & U. Schotzig, Nucl. Instr. & Meth. 140 (1977) 337.

65. K. Debertin & U. Schotzig, Nucl. Instr. & Meth. 158 (1979) 471.

66. J. Routti & S. Prussin, Nucl. Instr. & Meth. 72 (1969) 125.

67. U.S.A. Atomic energy catalogue, 3 ed ed., Aerojet Nuclear Company, U.S.A. energy research and development and administration.

68. J. Routti, Lawrence Berkely Laboratory Report UCRL 19452 (1969)

69. The T.R.C. Set. Radiochemical Centre, Amersham, Buckinghamshire, U.K.

70. W. Meiling & F. Stary, Nanosecond Pulse Technique (Gordon & Breach, New York, 1968.)

71. J.H. Neiler & P.R. Bell, α, β and γ -ray spectroscopy, ed. K. Siegbahn (North Holland, Amsterdam, 1965) Vol. 1.

72. K. Lobner, The Electromagnetic Interaction in Nuclear Spectroscopy, ed. W. Hamilton (North Holland Pub. Co. Amsterdam, 1975).

73. G. Bertolini, Semiconductor Detectors, ed. G. Bertolini & A. Coche (North Holland, Pub. Co., Amsterdam, 1968).

74. Instruments for research and applied science, ORTEC Inc. 1980, p. 16

75. Radiation Spectroscopy and Analysis Instruments for Research and Industry Catalogue 1004, 1976.

76. R. Rougny et al., Nucl. Instr. Meth. 95 (1971) 333.

77. R.D. Barton & M.E. King, Nucl. Instr. & Meth. 100(1972) 165.

78. B. Johansson, Nucl. Instr. & Meth. 1 (1957) 274.

79. R.L. Chase, Rev. Sci. Inst. 39 (1968) 1318.

80. M. Moszynski & B. Bengston, Nucl. Instr. & Meth. 80 (1970) 233.

81. D.A. Gedcke & W.J. McDonald, Nucl. Instr. & Meth. 55 (1967) 377.

82. D.A. Gedcke & W.J. McDonald, Nucl. Instr. & Meth. 58 (1968) 253.

83. K. Kowalski, Nuclear Electronics (Springer-Verlage, New York, 1970)

84. A. Schwarzschild & E.W. Warburton, Ann. Rev. Nucl. Sci. 18 (1968) 265.

85. A.H. Wapstra, α, β and γ-ray Spectroscopy, ed. K. Siegbahn (North Holland, Amsterdam, 1965). p. 539.

86. R.E. Bell & H.E. Petch, Phys. Rev. 76 (1949) 1409.

87. M.Y. Suliman & R.N. Thomas, Nucl. Instr. & Meth. 166 (1979) 305.

88. R. Risi & A. Gainotti, Phys. Rev. 175 (1968) 383.

89. B. Wilson & L. Bostrom, Nucl. Instr. & Meth. 44 (1966) 65.

90. M. Ledereh & V. Shirley, Table of Isotopes, 7th ed. (J. Wiley & Sons, New York, 1978).

91. K. Kumar, The Electromagnetic Interaction in Nuclear Spectroscopy ed. W. Hamilton (North Holland Pub. Co., Amsterdam, 1975).

92. J. Barrette et al., Can. J. Phys. 49 (1971) 2462.

93. L.L. Riedinger et al., Phys. Rev. C 2 (1970) 2358.

94. K.S. Toth et al., Phys. Rev. 115 (1959) 158.

95. K. Ya Gromov et al., Nucl. Phys. A 99 (1967) 585.

96. Y. Gono et al., in proceedings of the international symposium on nuclear structure contributions, Dubna 1968 (International Atomic Energy Agency, Vienna, Austria, 1969).

97. R. Bloch et al., Nucl. Phys. A 91 (1967) 576.

98. K. Baker et al., Z. Physik 256 (1972) 387.

99. A. Sharma et al., J. Phys. Soc. Jap. 48 (1980) 1407.

100. Y. Yoshizawa et al., Nucl. Instr. & Meth. 174 (1980) 133.

101. K. Debertin, Nucl. Instr. & Meth. 158 (1979) 479.

102. R. Meyer, Lawrence Livermore Laboratory (1978) M-100.

103. R.J. Gehrke et al., Nucl. Instr. & Meth. 147 (1977) 405.

104. K. Debertin et al., PTB-Mitteilungen 85 (1975) 187.

105. C.M. Baglin, Nucl. Data sheets 30 (1980)1.

106. G. Friedlander, J. Kennedy & J. Miller, Nuclear and Radioactivity (J. Wiley & Sons, Inc., New York, 1964).

107. G. Malmsten et al., Arkiv Fur Fysik 33 (1966) 361.

108. K. Kumar & S.N. Gupta, Nucl. Phys. A304 (1978) 295.

109. M.A. Mariscott et al., Phys. Rev. 178 (1969) 1864.

110. M. Sakai, Nucl. Phys. A 104 (1967) 301.

111. R.F. Casten, Nucl. Phys. A 347 (1980) 173.

112. S. Hinds et al., Phys. Lett. 14 (1965) 48.

113. N.R. Johnson et al., Bull.Am. Phys. Soc. 16 (1971) 130.

114. W.C. Schick, Bull. Am. Phys. Soc. 15 (1970) 75.

115. D.B. Fossan & B Herskind, Nucl. Phys. 40 (1963) 24.

116. H.W. Kugal et al., Phys. Rev. 165 (1968) 1352.

117. F.W. Richter et al., Z. Physik 213 (1968) 202.

118. M.R. El-asset et al., Z. Naturforsch 27 a (1972) 1229

119. L.A. Sliv & I.M. Band, α, β and γ -ray Spectroscopy, App. 5, ed. K. Siegbahn (North Holland Pub. Co., Amsterdam, 1965).

120. W. Mclatchie et al., Phys. Lett. 30B(1969) 529.

121. P.O. Lipas, Nucl. Phys. 39 (1962) 468.

122. Mikhailove, V.M., 1966, IZV. Akad. Nauk. SSSR. Ser. Fiz. 30, 1334 (Transl. 1966 Bull Acad. Scie, USSR, Phys. Ser 30, 1392).

123. L. Riedinger & N. Johnson, Phys. Rev. Lett. 19 (1967) 1243.

124. W.R. Roney & W.A. Sale, Nucl. Instr. & Meth. 171 (1980) 389.

125. U. Schotzig et al., Nucl. Instr. & Meth. 169 (1980) 43.

126. R.J. Gehrek et al., Nucl. Instr. & Meth. 147 (1977) 405.

127. R.G. Helmer, Nucl. Phys. A 272 (1976) 269.

128. J.J. Sapyta et al., Nucl. Phys. A 139 (1969) 161.

130. M.R. Schmorak, Nucl. Data Sheets 14(1975) 559.

131. K. Neergard and P. Vogel, Nucl. Phys. A 145 (1970) 33.

132. P. Herzog et al., Nucl. Phys. A 187 (1972) 49.

133. C. Gunther et al., Nucl. Phys. A 172 (1971) 273.

134. A. Hoglund et al., Nucl. Phys. A 169 (1971) 49.

135. H. Abou-Leila et al., Nucl. Phys. A 158 (1970) 568.

136. W. Meiling & F. Stary, Nucl. Phys. 84 (1966) 534.

137. R.G. Helmer, Nucl. Phys. A 272 (1976) 269.

138. H. Danial et al., Nucl. Phys. 56 (1964) 147.

139. K. Alder et al., Rev. Mod. Phys. 28 (1956) 433.

140. K. Kumar & M. Baranger, Nucl. Phys. A 122 (1968) 273.

141. Ph. Hubert et al., Nucl. Phys. A 321 (1979) 213.

142. M.R. Gunye & A. Kumar, Phys. Rev. C 22 (1980) 869.

143. J.P. Davidson & M.G. Davidson, Phys. Rev. 138 (1965) B 316.

144. A. Bohr & B. Mottelson, Atomic energy 14 (1963) 225.